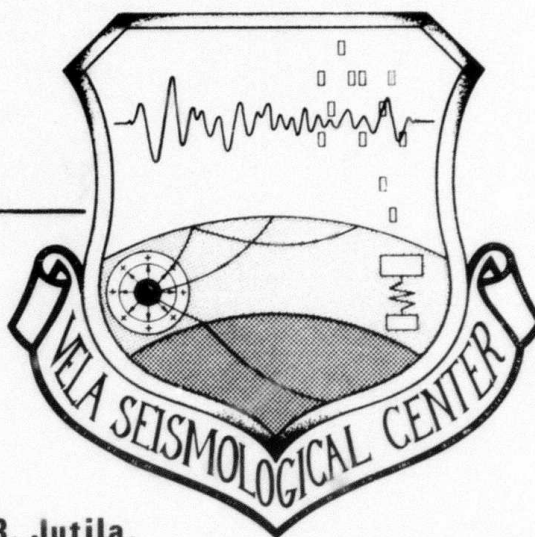


AD A120589

12

VSC-TR-82-14

**A STUDY OF SEISMIC WAVE
PROPAGATION AT REGIONAL
DISTANCES IN FIVE AREAS
OF THE WORLD**



Z.A. Der, A. O'Donnell, T.W. McElfresh, R. Jutila,
J.A. Burnett, M. Marshall, M. Silk and E. Gordon

Seismic Data Analysis Center
Teledyne Geotech
314 Montgomery Street
Alexandria, Virginia 22314

08 FEB 1982



APPROVED FOR PUBLIC RELEASE; DISTRIBUTION UNLIMITED.

DTIC FILE COPY

Monitored By:
VELA Seismological Center
312 Montgomery Street
Alexandria, VA 22314

82 10 21 008

Sponsored by
The Defense Advanced Research Projects Agency (DARPA)
DARPA Order No. 2551

Disclaimer: Neither the Defense Advanced Research Projects Agency nor the Air Force Technical Applications Center will be responsible for information contained herein which has been supplied by other organizations or contractors, and this document is subject to later revision as may be necessary. The views and conclusions presented are those of the authors and should not be interpreted as necessarily representing the official policies, either expressed or implied, of the Defense Advanced Research Projects Agency, the Air Force Technical Applications Center, or the US Government.

Unclassified

SECURITY CLASSIFICATION OF THIS PAGE (When Data Entered)

REPORT DOCUMENTATION PAGE		READ INSTRUCTIONS BEFORE COMPLETING FORM
1. REPORT NUMBER VSC-TR-82-14	2. GOVT ACCESSION NO. A120589	3. RECIPIENT'S CATALOG NUMBER
4. TITLE (and Subtitle) A STUDY OF SEISMIC WAVE PROPAGATION AT REGIONAL DISTANCES IN FIVE AREAS OF THE WORLD		5. TYPE OF REPORT & PERIOD COVERED Technical
7. AUTHOR(s) Z. A. Der R. Jutila M. Silk A. O'Donnell J. A. Burnett E. Gordon T. W. McElfresh M. Marshall		6. PERFORMING ORG. REPORT NUMBER SDAC-TR-81-12
9. PERFORMING ORGANIZATION NAME AND ADDRESS Teledyne Geotech 314 Montgomery Street Alexandria, Virginia 22314		8. CONTRACT OR GRANT NUMBER(s) F08606-79-C-0007
11. CONTROLLING OFFICE NAME AND ADDRESS VELA Seismological Center 312 Montgomery Street Alexandria, Virginia 22314		10. PROGRAM ELEMENT, PROJECT, TASK AREA & WORK UNIT NUMBERS VT 0709/B/PMP
14. MONITORING AGENCY NAME & ADDRESS (if different from Controlling Office) Defense Advanced Research Projects Agency 1400 Wilson Boulevard Arlington, Virginia 22209		12. REPORT DATE 02/08/82
		13. NUMBER OF PAGES 208
		15. SECURITY CLASS. (of this report) Unclassified
		15a. DECLASSIFICATION/DOWNGRADING SCHEDULE
16. DISTRIBUTION STATEMENT (of this Report) APPROVED FOR PUBLIC RELEASE; DISTRIBUTION UNLIMITED.		
17. DISTRIBUTION STATEMENT (of the abstract entered in Block 20, if different from Report)		
18. SUPPLEMENTARY NOTES		
19. KEY WORDS (Continue on reverse side if necessary and identify by block number) Attenuation L _g , P _n , S _n , P _g Seismic coda		
20. ABSTRACT (Continue on reverse side if necessary and identify by block number) Propagation and excitation of regional phases in southern Africa, the southwestern United States, the Pakistan-India region, South America, and the Kamchatka-Kuriles region were studied. Comparison of the shield areas of South America, Pakistan and southern Africa reveals no appreciable differences in the excitation and attenuation of regional phases in these areas. On the other hand, excitation and attenuation rates for all regional phases are markedly different in the southwestern		

Unclassified

Unclassified

SECURITY CLASSIFICATION OF THIS PAGE(When Data Entered)

United States. The mountainous areas of South America are characterized by highly variable propagation characteristics, with S₁ and L₁ being absent from many seismograms studied. Attenuation of S₁ and L₁ is especially severe along the southern Andes mountains in Chile and Argentina. For these areas, the value of regional phases for detection and discrimination is highly questionable. The Andes region is also characterized by highly unusual seismograms with scattered, emergent phases resembling lunar seismograms. These problems are present, though to a much lesser degree, in the mountainous areas surrounding India and Pakistan. These areas are also characterized by highly variable propagation efficiency and by spatial attenuation that is higher than that of the shield. Propagation from the Kamchatka-Kuriles area to nearby stations, which occurs over larger distances and may not be considered truly regional, is typically oceanic, with high frequency P_n and S₁ phases and the absence of other types of arrivals.

Using the coda method developed by Aki we have measured Q in the crust at a number of digital stations in various areas of the world, and we have found that Q increases rapidly with frequency in all areas.

Accession <input checked="" type="checkbox"/>	
NTIS <input checked="" type="checkbox"/>	
DTIC <input type="checkbox"/>	
Unannounced <input type="checkbox"/>	
Justification <input type="checkbox"/>	
By <input type="text"/>	
Distribution/ <input type="text"/>	
Availability Codes <input type="text"/>	
Dist <input type="text"/>	Special <input type="text"/>



Unclassified

SECURITY CLASSIFICATION OF THIS PAGE(When Data Entered)

**A STUDY OF SEISMIC WAVE PROPAGATION AT REGIONAL
DISTANCES IN FIVE AREAS OF THE WORLD**

SEISMIC DATA ANALYSIS CENTER REPORT NO.: SDAC-TR-81-12

AFTAC Project Authorization No.:	VELA T/9709/B/PMP
Project Title:	Seismic Data Analysis Center
ARPA Order No.:	2551
Name of Contractor:	TELEDYNE GEOTECH
Contract No.:	F08606-79-C-0007
Date of Contract:	27 October 1978
Amount of Contract:	\$2,191,475
Contract Expiration Date:	30 September 1983
Project Manager:	Robert R. Blandford (703) 836-3882

P. O. Box 334, Alexandria, Virginia 22313

APPROVED FOR PUBLIC RELEASE; DISTRIBUTION UNLIMITED.

ABSTRACT

Propagation and excitation of regional phases in southern Africa, the southwestern United States, the Pakistan-India region, South America, and the Kamchatka-Kuriles region were studied. Comparison of the shield areas of South America, Pakistan and southern Africa reveals no appreciable differences in the excitation and attenuation of regional phases in these areas. On the other hand, excitation and attenuation rates for all regional phases are markedly different in the southwestern United States. The mountainous areas of South America are characterized by highly variable propagation characteristics, with S_n and L_g being absent from many seismograms studied. Attenuation of S_n and L_g is especially severe along the southern Andes mountains in Chile and Argentina. For these areas, the value of regional phases for detection and discrimination is highly questionable. The Andes region is also characterized by highly unusual seismograms with scattered, emergent phases resembling lunar seismograms. These problems are present, though to a much lesser degree, in the mountainous areas surrounding India and Pakistan. These areas are also characterized by highly variable propagation efficiency and by spatial attenuation that is higher than that of the shield. Propagation from the Kamchatka-Kuriles area to nearby stations, which occurs over larger distances and may not be considered truly regional, is typically oceanic, with high frequency P_n and S_n phases and the absence of other types of arrivals.

Using the coda method developed by Aki we have measured Q in the crust at a number of digital stations in various areas of the world, and we have found that Q increases rapidly with frequency in all areas.

TABLE OF CONTENTS

	Page
ABSTRACT	2
LIST OF FIGURES	5
LIST OF TABLES	15
INTRODUCTION	17
RESULTS OF REGIONAL PROPAGATION STUDIES FOR FIVE REGIONS	19
SOUTHERN AFRICA	19
Structural Setting	19
Efficiency of Propagation and Amplitude-Distance Relationships	21
SOUTH AMERICA	40
Structural Setting	40
Efficiency of Propagation and Amplitude-Distance Relationships	45
Seismograms with Unusual Characteristics	68
PAKISTAN-INDIA REGION	75
Structural Setting	75
Efficiency of Propagation and Amplitude-Distance Relationships	77
SOUTHWESTERN UNITED STATES	90
Structural Setting	90
Efficiency of Propagation and Amplitude-Distance Relationships	98
Investigation of Discrimination Capability of Various Combinations of Regional Phases in the Southwestern United States	117
KAMCHATKA-KURILES	132
Structural Setting	132
Efficiency of Propagation and Amplitude-Distance Relationships	138

TABLE OF CONTENTS CONTINUED

	Page
COMPARISON OF AMPLITUDE-DISTANCE RELATIONSHIPS IN THE VARIOUS REGIONS STUDIED	146
STUDIES OF CRUSTAL Q USING CODAS OF REGIONAL EVENTS	150
STATION NOISE LEVELS	170
SUMMARY AND CONCLUSIONS	171
REFERENCES	173
APPENDIX A	A-1
Cumulative Noise Probability in South America, Southern Africa, the India/Pakistan Region, and the Kumchatka/Kurile Region	

LIST OF FIGURES

Figure No.	Title	Page
1	Southern African tectonics and seismicity. Culturally induced seismicity is not shown (after Swanson, 1978).	20
2	Trace amplitudes of P_n in southern Africa plotted against epicentral distance. The trace amplitudes were normalized to that of an earthquake with $m_b = 5$. Natural earthquakes are denoted as circles and rock bursts as triangles.	24
3	Trace amplitudes of P_g in southern Africa plotted against epicentral distance. The trace amplitudes were normalized to that of an earthquake with $m_b = 5$. Natural earthquakes are denoted as circles and rock bursts as triangles.	25
4	Trace amplitudes of S_n in southern Africa plotted against epicentral distance. The trace amplitudes were normalized to that of an earthquake with $m_b = 5$. Natural earthquakes are denoted as circles and rock bursts as triangles.	26
5	Trace amplitudes of the vertical component of L_g in southern Africa plotted against epicentral distance. The trace amplitudes were normalized to that of an earthquake with $m_b = 5$. Natural earthquakes are denoted as circles and rock bursts as triangles.	27
6	Trace amplitudes of the horizontal (transverse) component of L_g in southern Africa plotted against epicentral distance. The trace amplitudes were normalized to that of an earthquake with $m_b = 5$. Natural earthquakes are denoted as circles and rock bursts as triangles.	28
7	Logarithmic plots of A/T (amplitudes divided by periods reduced in the manner used to compute m_b) for various regional phases (after Swanson, 1978). These plots show that the A/T thus obtained can discriminate between natural earthquakes and rock bursts. All events were corrected to an earthquake with $m_b = 5$.	29
8	Histograms of the dominant periods of P_n for earthquakes and rock bursts in southern Africa.	30
9	Histograms of the dominant periods of S_n for earthquakes and rock bursts in southern Africa.	31

LIST OF FIGURES (Continued)

Figure No.	Title	Page
10	Histograms of dominant periods of L_g for earthquakes and rock bursts in southern Africa.	32
11	Histograms of m_b values for earthquakes and rock bursts in southern Africa.	33
12	Dominant period for P as a function of epicentral distance in southern Africa for earthquakes in the m_b range of 4-5.	35
13	Dominant period for P_g as a function of epicentral distance in southern Africa for earthquakes in the m_b range of 4-5.	36
14	Dominant period for S as a function of epicentral distance in southern Africa for earthquakes in the m_b range of 4-5.	37
15	Dominant period for L (vertical component) as a function of epicentral distance in southern Africa for earthquakes in the m_b range of 4-5.	38
16	Dominant period for L (horizontal component) as a function of epicentral distance in southern Africa for earthquakes in the m_b range of 4-5.	39
17	Tectonic features of South America (modified after Swanson, 1878).	41
18	Contour map of the Moho discontinuity beneath the Andes (after James, 1971).	42
19	Cross section of the Andes and the coastal region (after James, 1971).	43
20	Regions of high (squares) and low (stippled) attenuation in the upper mantle under South America (after Barazangi et al., 1975).	44
21	Sketches of regional seismogram envelope types in South America (after Chinn et al., 1980). Arrival velocities of some typical regional phases are marked on the figure.	46
22	Symbols used by Chinn et al (1980) for denoting various seismogram types from Figure 21 (after Chinn et al., 1980).	47

LIST OF FIGURES (Continued)

Figure No.	Title	Page
23	Propagation and the occurrence of various seismogram types along the western coast of South America. Symbols used are explained in Figure 22 (after Chinn et al., 1980).	48
24	Propagation and seismogram types for shallow events along various Andean paths (symbols are from Figure 22, after Chinn et al., 1980). These paths were associated with S_n phases.	49
25	Paths for which no S_n was observed. Symbols are explained in Figure 22 (after Chinn et al., 1980).	50
26	Efficiency map for S_n propagation from shallow events in South America. The efficiency criteria of Molnar and Oliver (1969) were used in constructing this map.	57
27	Efficiency of L_g phase propagation from shallow events. Criteria for classification are explained in the text.	58
28	Trace amplitudes of P_n in South America, plotted against epicentral distance. The trace amplitudes were normalized to that of an earthquake with $m_b = 5$. The various types of propagation paths are denoted by symbols shown in the legend.	60
29	Trace amplitudes of S_n in South America, plotted against epicentral distance. The trace amplitudes were normalized to that of an earthquake with $m_b = 5$. The various types of propagation paths are denoted by symbols shown in the legend.	61
30	Trace amplitudes of L_g (vertical component) in South America, plotted against epicentral distance. The trace amplitudes were normalized to that of an earthquake with $m_b = 5$. The various types of propagation paths are denoted by symbols shown in the legend.	62
31	Trace amplitudes of L_g (horizontal component) in South America, plotted against epicentral distance. The trace amplitudes were normalized to that of an earthquake with $m_b = 5$. The various types of propagation paths are denoted by symbols shown in the legend.	63

LIST OF FIGURES (Continued)

Title	Page
minant periods of P_n in South America, plotted against epicentral distance for shallow earthquakes in the m_b range of 4.5-5.5. The various types of propagation paths are designated with symbols shown in the legend.	64
minant periods of S_n in South America, plotted against epicentral distance for shallow earthquakes in the m_b range 4.5-5.5. The various types of propagation paths are designated with symbols shown in the legend.	65
minant periods of L_v (vertical component) in South America, plotted against epicentral distance for shallow earthquakes in the m_b range 4.5-5.5. The various types of propagation paths are designated with symbols shown in the legend.	66
minant periods of L_h (horizontal component) in South America, plotted against epicentral distance for shallow earthquakes in the m_b range 4.5-5.5. The various types of propagation paths are designated with symbols shown in the legend.	67
Sketches of regional seismogram envelope shapes for various paths.	69
Band pass filtered vertical traces for the 15 February 1979 event observed in La Paz, Bolivia.	72
Band pass filtered vertical traces for the 23 January 1977 event observed in La Paz, Bolivia.	73
Band pass filtered vertical traces for the 12 February 1979 event.	74
Simplified tectonic map of the region studied (after Tapponier and Molnar, 1979).	76
Seismicity map of the Pakistan-India region (after Wittmayer and Jacob, 1979).	78
Efficiency of S_n propagation (after Molnar and Oliver, 1969).	79
Plot of events and WWSSN stations used in this study.	80

Figure No.	(U) LIST OF FIGURES (Continued) Title	Page
44	Efficiency map of S_n determined in this study.	82
45	Efficiency of propagation for L_g .	83
46	Trace amplitudes of P_n in the Pakistan-India region plotted against epicentral distance. The trace amplitudes were normalized to that of an earthquake with $m_b = 5$. Various symbols explained in the legend ^b denote various types of propagation paths.	85
47	Trace amplitudes of P in the Pakistan-India region plotted against epicentral distance. The trace amplitudes were normalized to that of an earthquake with $m_b = 5$. Various symbols explained in the legend ^b denote various types of propagation paths.	86
48	Trace amplitudes of S_n in the Pakistan-India region plotted against epicentral distance. The trace amplitudes were normalized to that of an earthquake with $m_b = 5$. Various symbols explained in the legend ^b denote various types of propagation paths.	87
49	Trace amplitudes of L (vertical component) in the Pakistan-India region ^g plotted against epicentral distance. The trace amplitudes were normalized to that of an earthquake with $m_b = 5$. Various symbols explained in the legend denote various types of propagation paths.	88
50	Trace amplitudes of L (horizontal component) in the Pakistan-India region ^g plotted against epicentral distance. The trace amplitudes were normalized to that of an earthquake with $m_b = 5$. Various symbols explained in the legend denote various types of propagation paths.	89
51	Dominant periods of P_n waves from shallow earthquakes in the m_b range 4.5-5.5, plotted against epicentral distance.	91
52	Dominant periods of P_g waves from shallow earthquakes in the m_b range 4.5-5.5, plotted against epicentral distance.	92
53	Dominant periods of S_n waves from shallow earthquakes in the m_b range 4.5-5.5, plotted against epicentral distance.	93

LIST OF FIGURES (Continued)

Figure No.	Title	Page
54	Dominant periods of L_g (vertical component) waves from shallow earthquakes in the m_b range 4.5-5.5, plotted against epicentral distance.	94
55	Dominant periods of L_g (horizontal component) waves from shallow earthquakes in the m_b range 4.5.-5.5, plotted against epicentral distance.	95
56	Major tectonic provinces in the western United States.	96
57	Efficiency of S_n propagation in North America (after Molnar and Oliver, 1969).	99
58	Efficiency of S_n propagation from explosions.	100
59	Efficiency of S_n propagation from earthquakes.	101
60	Trace amplitudes of P_g in the southwestern United States plotted against epicentral distance. Nuclear explosion data are denoted by circles and earthquake data by triangles.	103
61	Trace amplitudes of P_g in the southwestern United States plotted against epicentral distance. Nuclear explosion data are denoted by circles and earthquake data by triangles.	104
62	Trace amplitudes of S_n in the southwestern United States plotted against epicentral distance. Nuclear explosion data are denoted by circles and earthquake data by triangles.	105
63	Trace amplitudes of L_g (vertical component) in the southwestern United States plotted against epicentral distance. Nuclear explosion data denoted by circles and earthquake data by triangles.	106
64	Trace amplitudes of L_g (horizontal component) in the southwestern United States plotted against epicentral distance. Nuclear explosion data denoted by circles and earthquake data by triangles.	107
65	Dominant period of P_g for earthquakes in the southwestern United States plotted against epicentral distance. The symbols denote various ranges of event magnitude.	108

LIST OF FIGURES (Continued)

Figure No.	Title	Page
66	Dominant period of Pn for explosions in the southwestern United States plotted against epicentral distance. The symbols denote various ranges of event magnitude.	109
67	Dominant period of P _g for explosions in the southwestern United States plotted against epicentral distance. The symbols denote various ranges of event magnitude.	110
68	Dominant period of Pg for earthquakes in the southwestern United States plotted against epicentral distance. The symbols denote various ranges of event magnitude.	111
69	Dominant period of L _g (vertical component) for earthquakes in the southwestern United States plotted against epicentral distance. The symbols denote various ranges of event magnitude.	112
70	Dominant period of L _g (vertical component) for earthquakes in the southwestern United States plotted against epicentral distance. The symbols denote various ranges of event magnitude.	113
71	Dominant period of Lg (horizontal component) for earthquakes in the southwestern United States plotted against epicentral distance. The symbols denote various ranges of event magnitude.	114
72	Dominant period of Lg (horizontal component) for explosions in the southwestern United States plotted against epicentral distance. The symbols denote various ranges of event magnitude.	115
73	Map of events analyzed and stations utilized for the southwestern United States.	120
74	Trace amplitude ratios of L _g (horizontal component) to P _g plotted against epicentral distance. Explosion and earthquake data are designated with circles and triangles respectively.	121

LIST OF FIGURES (Continued)

Figure No.	Title	Page
75	Trace amplitude ratios of L_g (horizontal component) to P_g plotted against event magnitude. Explosion and earthquake data are designated with circles and triangles respectively.	122
76	Trace amplitude ratios of L_g (vertical component) to P_g plotted against epicentral distance. Explosion and earthquake data are designated with circles and triangles respectively.	123
77	Trace amplitude ratios of L_g (vertical component) to P_g plotted against event magnitude. Explosion and earthquake data are designated with circles and triangles respectively.	124
78	Trace amplitude ratios of L_g (horizontal component) to P_n plotted against epicentral distance. Explosion and earthquake data are designated with circles and triangles respectively.	125
79	Trace amplitude ratios of L_g (horizontal component) to P_g plotted against event magnitude. Explosion and earthquake data are designated with circles and triangles respectively.	126
80	Trace amplitude ratios of L_g (vertical component) to P_n plotted against epicentral distance. Explosion and earthquake data are designated with circles and triangles respectively.	127
81	Trace amplitude ratios of L_g (vertical component) to P_g plotted against event magnitude. Explosion and earthquake data are designated with circles and triangles respectively.	128
82	Trace amplitude ratios of P_g to P_n plotted against epicentral distance. Explosion and earthquake data are designated with circles and triangles respectively.	129

LIST OF FIGURES (Continued)

Figure No.	Title	Page
83	Trace amplitude ratios of P_g to P_n plotted against event magnitude. Explosion and earthquake data are designated with circles and triangles respectively.	130
84	Seismicity map of the Kamchatka-Kuriles area.	133
85	Focal mechanism types and depth contours of the seismic zone (after Veith, 1974).	134
86	Major features of the Bering Sea region with the stations used in this study.	136
87	Major features of the Okhotsk Sea region. Crustal thickness map superposed.	137
88	Seismograms from shallow events in the Kamchatka-Kuriles area as recorded at ATAK at various epicentral distances.	139
89	Location of the events used for the study of the Kamchatka-Kuriles area.	142
90	Travel time curves for the oceanic P_n and S_n .	143
91	Trace amplitudes of P_n plotted against epicentral distance. The data points for the various stations are denoted by different symbols.	144
92	Trace amplitudes of S_n plotted against epicentral distance. The data points for the various stations are denoted by different symbols.	145
93	Illustration of the procedure for determining Q in the crust.	153
94	Q^{-1} as a function of frequency at OB2NV for the event of 12 Sep 77, O.T. = 13:59:22.3.	154
95	Q^{-1} as a function of frequency at OB2NV for the event of 12 Sep 77, O.T. = 12:14:02.3.	155
96	Q^{-1} as a function of frequency at OB2NV for the event of 12 Sep 77, O.T. = 06:17:42.6.	156
97	Q^{-1} as a function of frequency at OB2NV for the event of 08 Jun 77, O.T. = 13:09:07.4.	157

LIST OF FIGURES (Continued)

Figure No.	Title	Page
98	Q^{-1} as a function of frequency at OB2NV for the event of 11 Jun 77, O.T. = 14:18:20.5.	158
99	Q^{-1} as a function of frequency at OB2NV for the event of 17 Oct 76, O.T. = 05:38:11.9.	159
100	Q^{-1} as a function of frequency at OB2NV for the event of 09 Oct 76, O.T. = 02:09:28.1.	160
101	Q^{-1} as a function of frequency at ANMO for the event of 05 Mar 77, O.T. = 03:00:54.7.	163
102	Q^{-1} as a function of frequency at ANMO for the event of 09 Feb 76, O.T. = 03:07:22.0.	164
103	Q^{-1} as a function of frequency at ANMO for the event of 11 Oct 77, O.T. = 07:56:06.5.	165
104	Q^{-1} as a function of frequency at ANMO for the event of 08 Apr 76, O.T. = 15:21:37.9.	166
105	Q^{-1} as a function of frequency at ANMO for the event of 17 Jan 76, O.T. = 03:58:51.4.	167
106	Q^{-1} as a function of frequency at ANMO for the event of 08 Jun 77, O.T. = 13:09:07.4.	168
107	Q^{-1} as a function of frequency at ZOBO for event (26 Dec 78, O.T. = 01:40:33.3) in Argentina.	169

LIST OF TABLES

Table No.	Title	Page
I	ISC hypocenters for analyzed southern African event (after Swanson et al., 1979).	22
II	ISC hypocenters for analyzed South American earthquakes (after Swanson et al., 1979).	53
III	Additional South American earthquakes for which WWSSN data was analyzed.	55
IV	Additional South American earthquakes for which data at LRSM station LZ-BV was analyzed.	56
V	NEIS hypocenters for earthquakes in the Pakistan/India region.	81
VI	NEIS hypocenters for earthquakes and explosions in the southwest U.S.	118
VII	NEIS hypocenters for earthquakes in the Kamchatka/Kuriles region.	140
VIII	Events used in coda analyses.	161

INTRODUCTION

This report presents the results of studies of regional seismic wave propagation in five areas of the world: the southwestern United States, South America, southern Africa, the Pakistan-India region and the Kamchatka-Kuriles region. Due to the wide extent and the great geological variability of these regions, it was not possible to conduct a detailed study of all aspects of regional propagation. Fortunately, there have been some intensive studies in the past of some of these same regions. Therefore, we attempted to review the earlier studies and to incorporate the results into our study, at the same time filling some gaps. Further work is still needed to answer the many questions remaining and to solve problems that make detection, discrimination, and magnitude estimation difficult in these complex areas. All of the regions involve continental type of crustal phases except the Kamchatka-Kurile region which has quite complicated propagation paths to Japan and to island stations such as ADIS. These types of paths have not yet been studied with respect to regional propagation characteristics.

In this study, we confine ourselves to the analysis of shallow focus events with the assumption that deep events can be diagnosed and eliminated from consideration in discrimination by independent means. This assumption, of course, is not always true. In any region, there are two features of interest in a discrimination and detection context. The first is the relative excitation at the source of the various regional phases for various types of sources, and the second is the efficiency of propagation of each phase as reflected in the decay of amplitudes as functions of distance. The first, which depends on the crustal structure near the source, determines the possibility of discrimination at close range; the second also affects discrimination due to the changing ratios of the various phases, but it may have even greater effect on the detectability of the events if the largest regional phase L_g is blocked by regions of inefficient propagation.

We also attempted to summarize previous results, especially the magnitude determination criteria, in a manner that allows one to compare directly the results obtained by various workers. Unfortunately, it is extremely difficult to compare amplitude-distance formulas and magnitude formulas in various publications because of the varying scales, forms of mathematical expressions and criteria used. L_g amplitude distance relationships, for instance, are often given in the form Δ^{-n} or by Nuttli's formula with the characteristic decay exponent δ . The $\log(A/T)$ in the various formulas are often multiplied by factors different from unity even though the data are too scattered to justify such refinements. In other cases, we have found that the quality of the fits of the actual data to some magnitude formulas is clearly unsatisfactory, and we changed the formulas. The appropriate formulas are tabulated in a later section of the report, and the amplitude (A/T) versus distance curves for a standard event with $m_b = 5$ are also plotted on the same scale for direct comparison.

We have found in past work concerning body wave magnitudes that the standard procedure of correcting for magnification at the dominant period of the waveform and the successive division by period to obtain A/T tends to mask attenuation effects and also introduces period dependent adjustments that increase the data scatter. Therefore, we have used the trace amplitudes in our formulas and corrected for the instrument magnification at 1 Hz only. This is analogous to magnitude measures that use the "b" phase for body waves which tend to be more consistent than the standard m_b .

An important parameter that has a profound effect on the efficiency of the propagation of crustal phases is the effective Q_β in the crust. This quantity can be measured by coda analysis. In the latter part of this report, we shall present some results with respect to Q_β .

RESULTS OF REGIONAL PROPAGATION STUDIES FOR THE FIVE REGIONS

SOUTHERN AFRICA

Structural Setting

The area of southern Africa studied has been a stable shield-type region since the pre-Cambrian, and its regional phase propagation is expected to be uncomplicated and shield-like. We therefore find it convenient to start the discussion of the five regions with southern Africa and to compare the other, more complex, areas with it. The pre-Cambrian rocks of the shield are either exposed over much of the surface or covered with sediments. Most of the area is an elevated plateau, the southernmost part of which is a fold belt (the Cape fold belt). North of the Cape fold belt lies the Karroo Basin, containing sediments up to 7000 m thick of Mississippian to Jurassic age. North of these features lie typical shield areas with or without sedimentary cover: the Rhodesian and the Kaap-Vall cratons and the Kalahari desert. The latter is overlain by Cretaceous and Tertiary sediments. Figure 1 shows the location of these features.

A prominent tectonic feature of Africa is the extensive system of rift valleys from Ethiopia to the region of study along the eastern part of the continent. How far this system continues southward is debatable, but it appears that most of the region studied is outside of the rift system.

The seismic activity in the area is moderate. There is a belt of diffuse seismicity along the eastern part of the continent, while another region of more concentrated seismicity is associated with Lake Kariba. A unique feature of southern African seismicity is the presence of a large number of rock bursts associated with deep mining for gold in the area surrounding Pretoria. These artificial events, as we shall show later, are somewhat different from natural earthquakes.

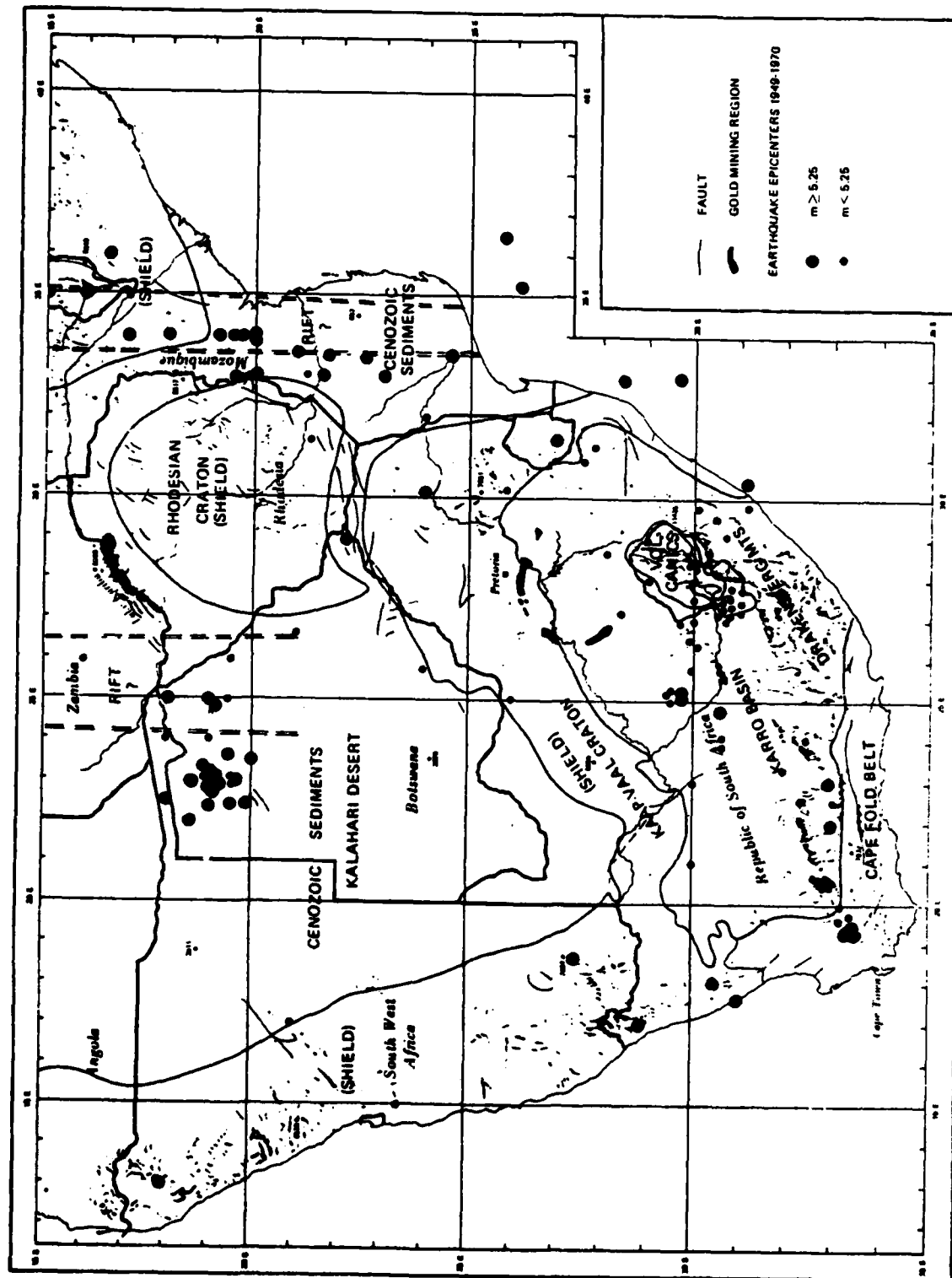


Figure 1. Southern African tectonics and seismicity. Culturally induced seismicity is not shown (after Swanson, 1978).

Efficiency of Propagation and Amplitude-Distance Relationships

In two previous studies Swanson and Goforth (1978) derived amplitude-distance relationships for regional phases in southern Africa in terms of the quantity A/T corrected for instrument response at the dominant period in the fashion customary for m_b . Because we believe that the trace amplitude is a better measure of magnitude for all kinds of events, we reformulated all amplitude-distance relationships for regional phases in terms of trace amplitudes correcting only for instrument magnification at 1 Hz. In order to normalize the trace amplitudes with respect to event magnitude, we subtracted from the ten base logarithms of trace amplitudes the difference between the event magnitude and five. This reduces the trace amplitudes to those of an event with $m_b = 5$. Table I lists the earthquakes and rockbursts we studied.

The reduced logarithms of trace amplitudes were then plotted against the logarithms of the epicentral distance. Such plots are shown in Figures 2 - 6 for the regional phases P_n , P_g , S_n , and the vertical and horizontal components of L_g . The S_n were also measured on the horizontal component. In all the plots, we have used triangles to denote the rock bursts and circles for the earthquakes. As expected for a homogeneous region with respect to the average properties of the crust and upper mantle, the plots show little scatter compared to the other regions investigated in this report. The data points for L_g , S_n and P_g are grouped tightly along a fairly well defined curve, while the scatter is considerably greater for P_n . There is no discernible difference between earthquakes and rock bursts with respect to the trace amplitudes.

Swanson and Goforth (1978) on the other hand, found that he could discriminate between earthquakes and rock bursts by means of magnitude measures derived in a similar way to the conventional m_b measurements using A/T as shown in Figure 7. Since the trace amplitudes are not different, the difference must be in the dominant periods of the waves from these two types of events. As seen in Figures 8, 9, and 10, which compare histograms of the dominant periods for S_n , P_n and L_g phases for

TABLE I

Hypocenters for Analyzed Southern African Event
(after Swanson et al., 1979).

Earthquakes

Origin Time <u>Hr:Min:Sec</u>	S Lat <u>deg</u>	E Long <u>deg</u>	Depth <u>km</u>	Mag <u>ISC</u>
01 07 16.3	24.42	27.4	32	4.7
18 12 32.4	23.67	30.26	0	4.3
05 21 06.1	29.52	29.37	18	5.0
11 43 03.0	28.10	25.60	33	4.4
19 03 51.0	30.08	25.80	33	4.0
23 26 19.1	29.53	25.65	48	4.9
18 32 52.6	29.45	25.20	33	4.7
17 35 21.6	31.752	25.37	0	4.1
12 03 44.0	30.74	23.80	34	4.9
01 00 10.0	33.17	23.60	25	5.5
21 45 19.0	33.41	21.80	33	5.2
20 03 25.9	33.28	19.24	37	6.0
11 40 45.0	32.90	19.80	33	4.3
05 01 22.1	33.18	19.52	33	5.1
19 02 35.5	33.13	19.61	33	5.3
01 42 56.0	33.30	19.70	33	4.5
11 38 16.5	32.90	19.87	33	4.3
20 46 52.9	33.36	19.40	33	4.5
05 06 09.0	33.18	19.72	45	5.1
19 08 21.8	33.17	19.47	33	6.1
13 54 06.0	17.92	14.00	52	4.6
17 52 46.8	20.455	16.574	11	4.1
09 42 19.4	18.54	26.39	33	5.2
02 33 11.0	19.50	23.73	33	4.1
12 17 08.2	18.57	26.43	33	4.8
15 24 55.9	19.32	23.93	20	5.1
13 13 57.0	19.54	23.41	18	4.6
15 49 29.6	18.07	25.88	33	4.6
02 50 58.2	16.64	28.26	33	5.5
06 05 41.1	16.86	28.05	33	4.9
02 12 11.6	16.642	28.044	33	3.9
05 22 22.7	16.71	27.91	33	4.3
09 36 26.8	16.67	28.07	14	5.3
02 36 53.8	15.72	34.59	13	5.1
10 36 36.8	23.67	33.00	28	5.0
15 22 38.0	20.00	33.40	7	4.8
23 21 47.9	21.308	33.368	33	4.2
23 27 50.9	21.377	33.546	33	3.9
21 35 43.9	21.20	33.27	33	4.4
23 15 30.9	23.55	37.44	33	4.3

TABLE I (cont.)

ISC Hypocenters for Analyzed Southern African Event
(after Swanson et al., 1979).

Rockbursts

<u>Event Code</u>	<u>Date YrMoDa</u>	<u>Origin Time Hr:Min:Sec</u>	<u>S Lat deg</u>	<u>E Lon deg</u>	<u>Depth km</u>	<u>Mag ISC</u>
RC 1	700101	14 35 23.2	26.17	28.18	33	4.3
RC 2	710127	20 53 01.1	25.97	28.17	13	4.5
RC 3	730327	00 48 07.9	26.16	28.17	41	4.1
RC 4	730805	05 05 31.5	26.26	27.30	33	3.9
RC 5	740121	15 15 53.8	26.10	28.17	25	4.7
RC 6	730206	09 50 46.0	26.02	28.12	33	4.0
RK 1	690420	20 53 33.0	26.80	27.20	33	4.1
RK 2	690830	15 52 29.1	26.77	26.80	14	4.3
RK 3	701031	02 42 11.6	26.78	26.85	33	4.5
RK 4	730814	13 01 03.5	26.76	26.70	33	3.8
RK 5	731219	03 06 59.0	26.75	26.99	33	4.8
RO 1	691031	22 09 51.0	27.95	26.86	1	4.1
RO 2	710802	16 52 24.1	27.91	26.93	1	4.8
RO 3	730906	20 13 35.7	27.832	26.84	33	4.4
RO 4	761208	08 38 25.2	27.91	26.71	33	5.2

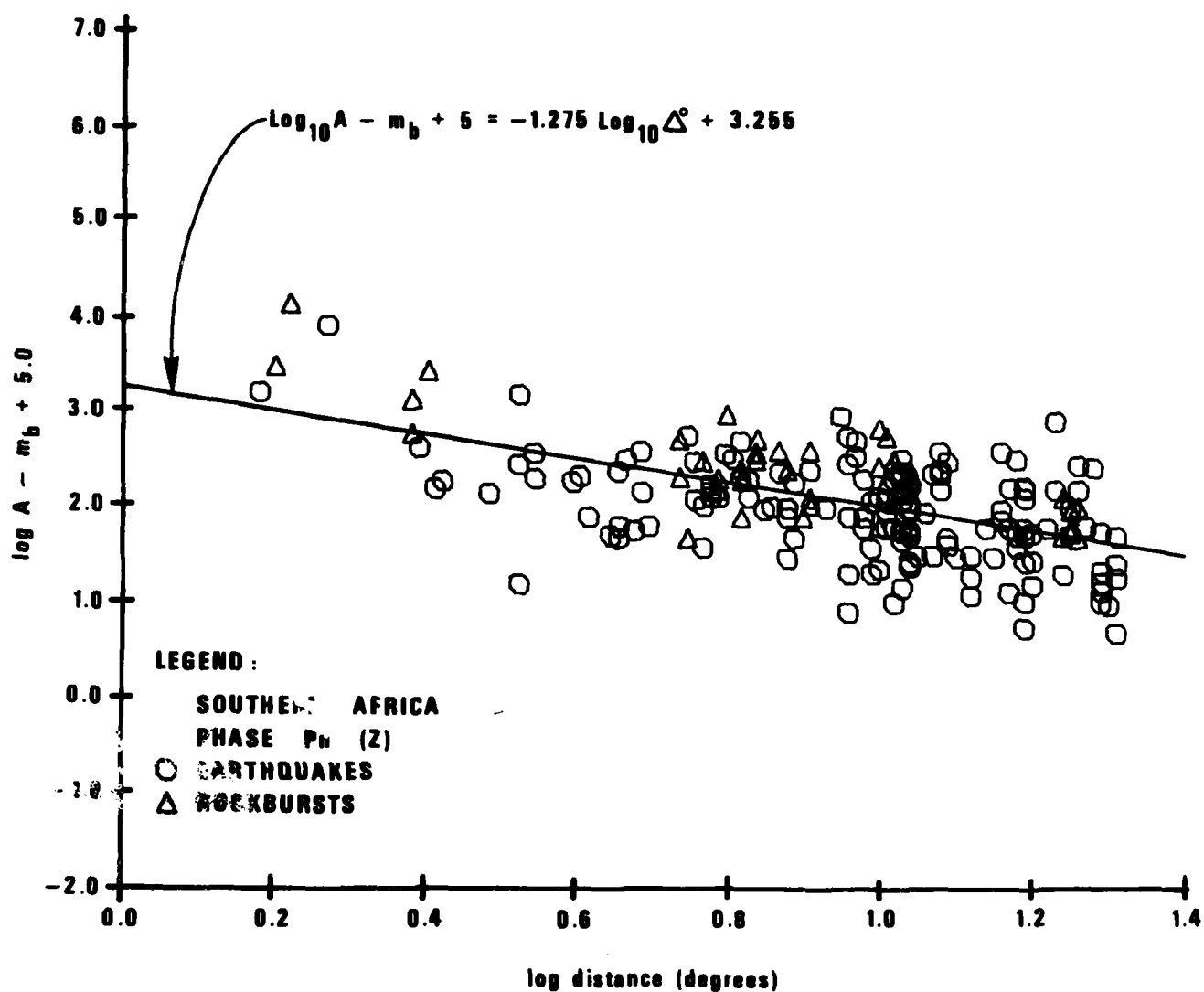


Figure 2. Trace amplitudes of P_n in southern Africa plotted against epicentral distance. The trace amplitudes were normalized to that of an earthquake with $m_b = 5$. Natural earthquakes are denoted as circles and rock bursts as triangles.

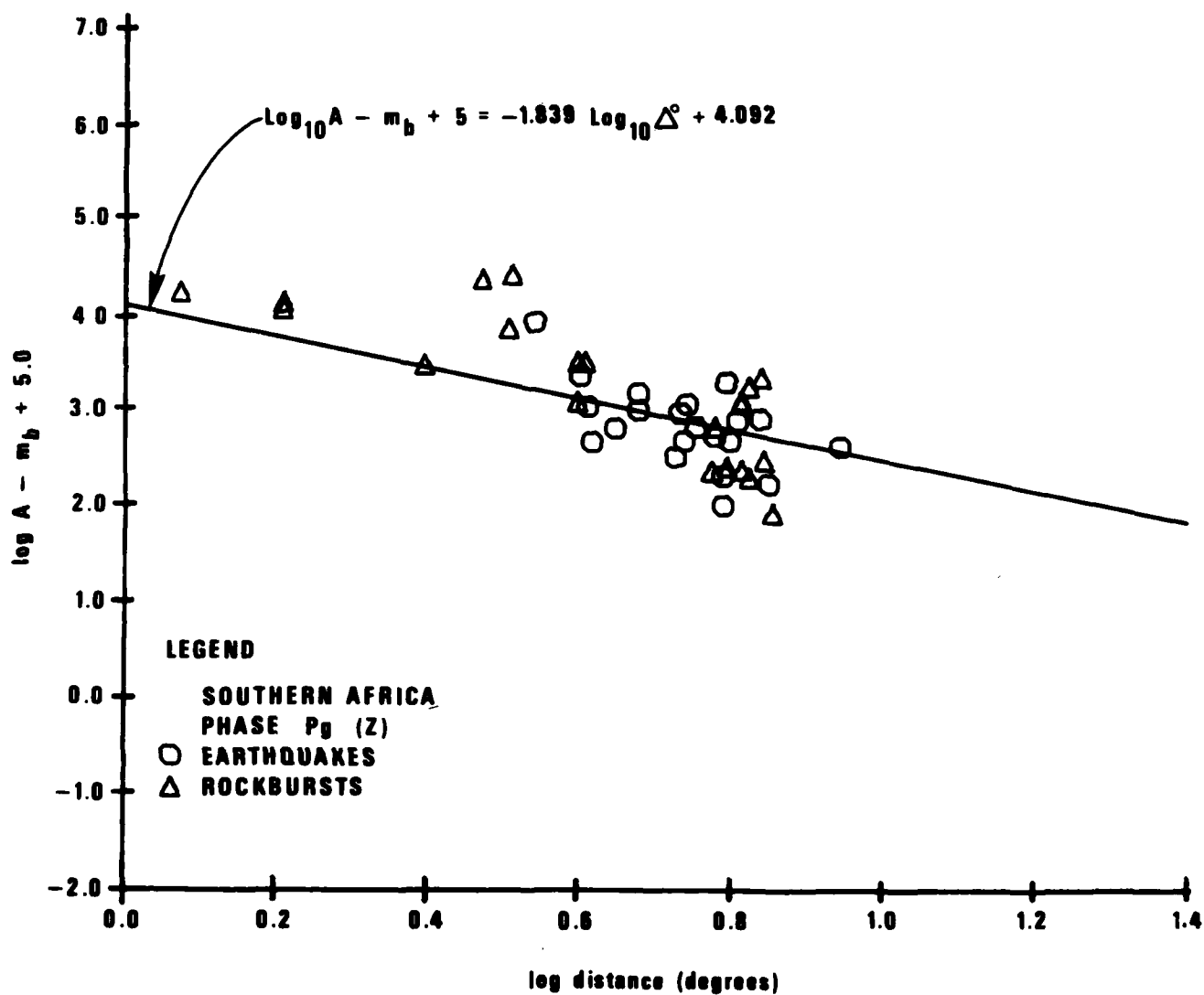


Figure 3. Trace amplitudes of P in southern Africa plotted against epicentral distance. The trace amplitudes were normalized to that of an earthquake with $m_b = 5$. Natural earthquakes are denoted as circles and rock bursts as triangles.

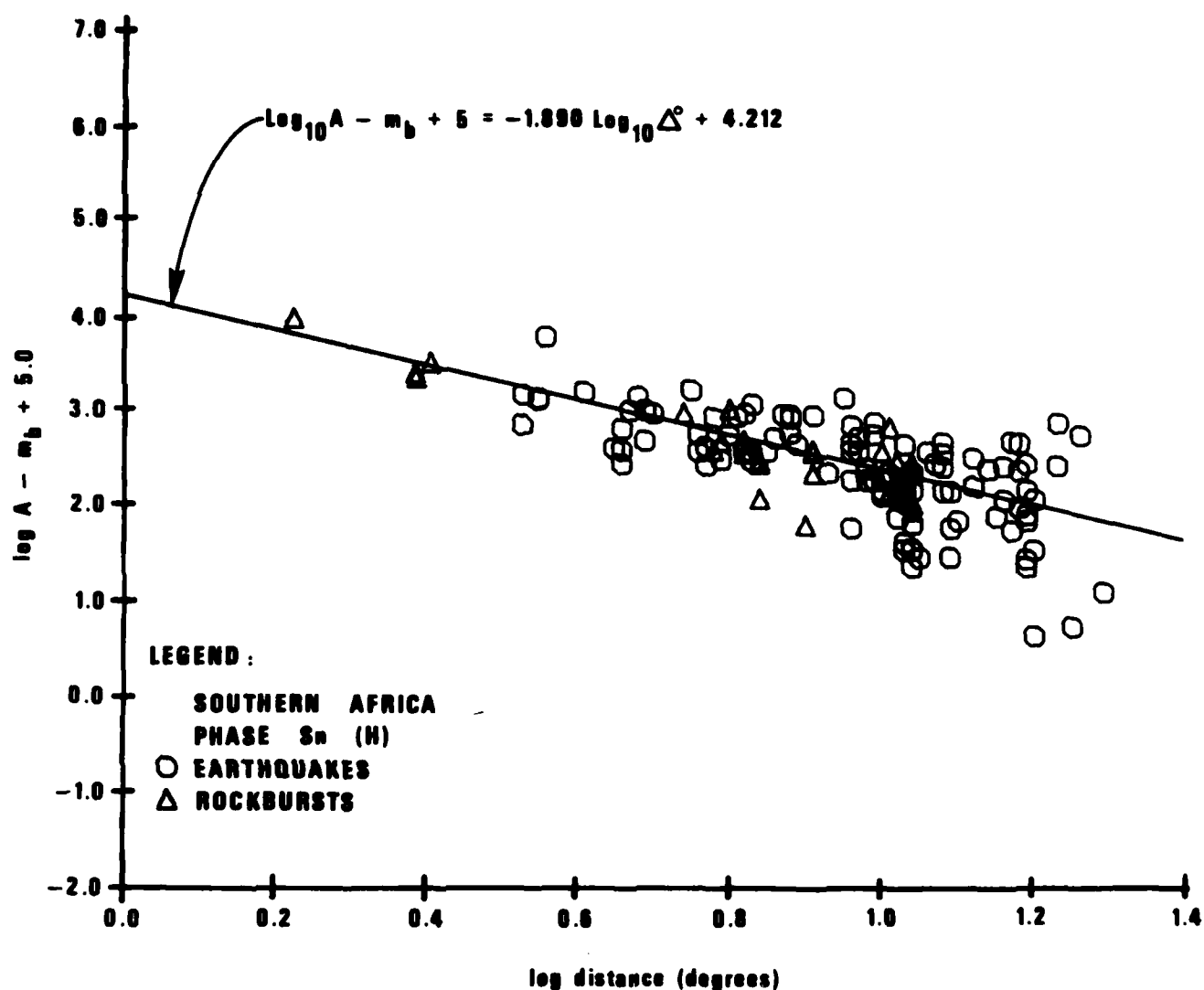


Figure 4. Trace amplitudes of S_n in southern Africa plotted against epicentral distance. ⁿThe trace amplitudes were normalized to that of an earthquake with $m_b = 5$. Natural earthquakes are denoted as circles and rock bursts as triangles.

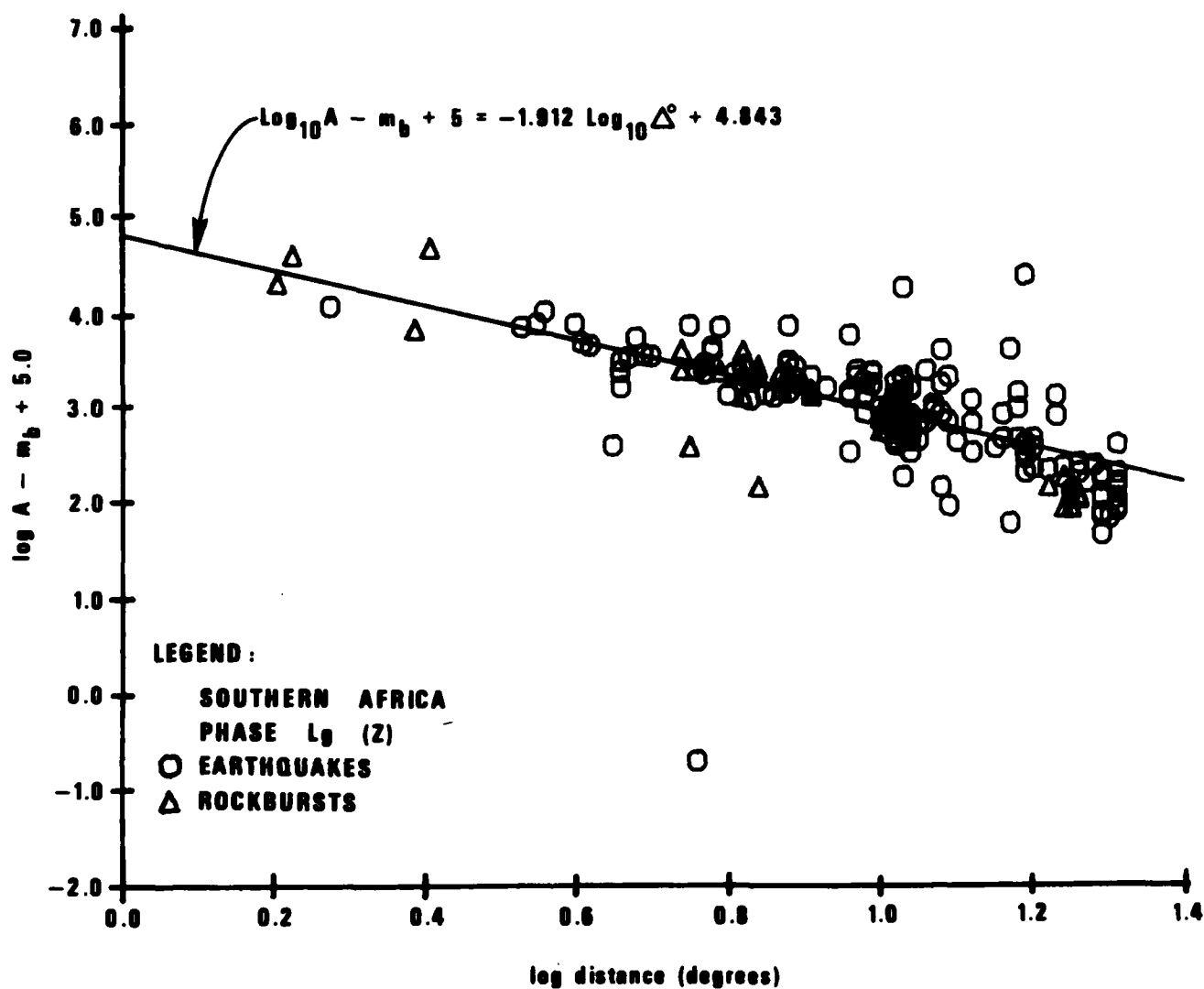


Figure 5. Trace amplitudes of the vertical component of L_g in southern Africa plotted against epicentral distance. The trace amplitudes were normalized to that of an earthquake with $m_b = 5$. Natural earthquakes are denoted as circles and rock bursts as triangles.

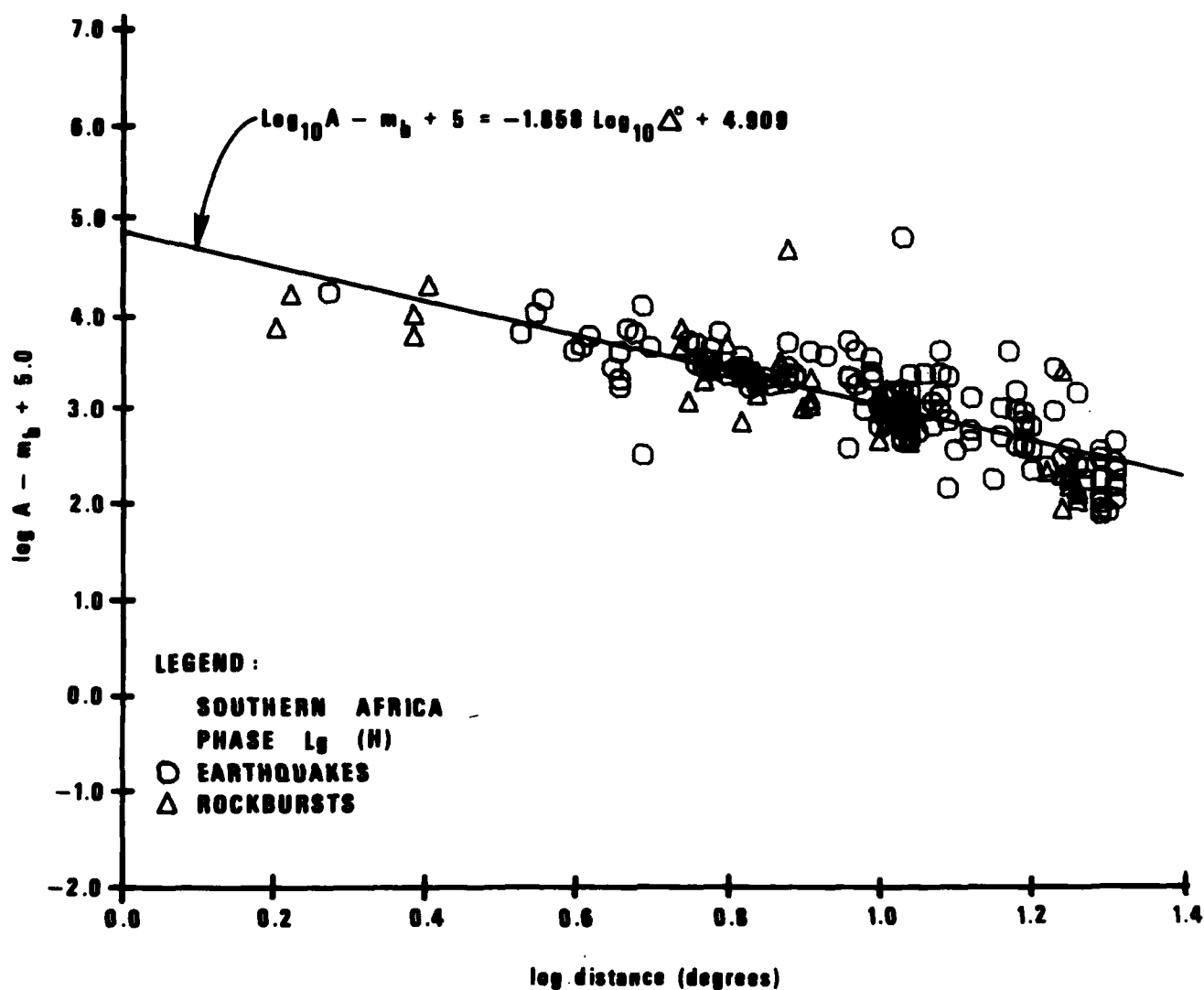


Figure 6. Trace amplitudes of the horizontal (transverse) component of L_g in southern Africa plotted against epicentral distance. The trace amplitudes were normalized to that of an earthquake with $m_b = 5$. Natural earthquakes are denoted as circles and rock bursts as triangles.

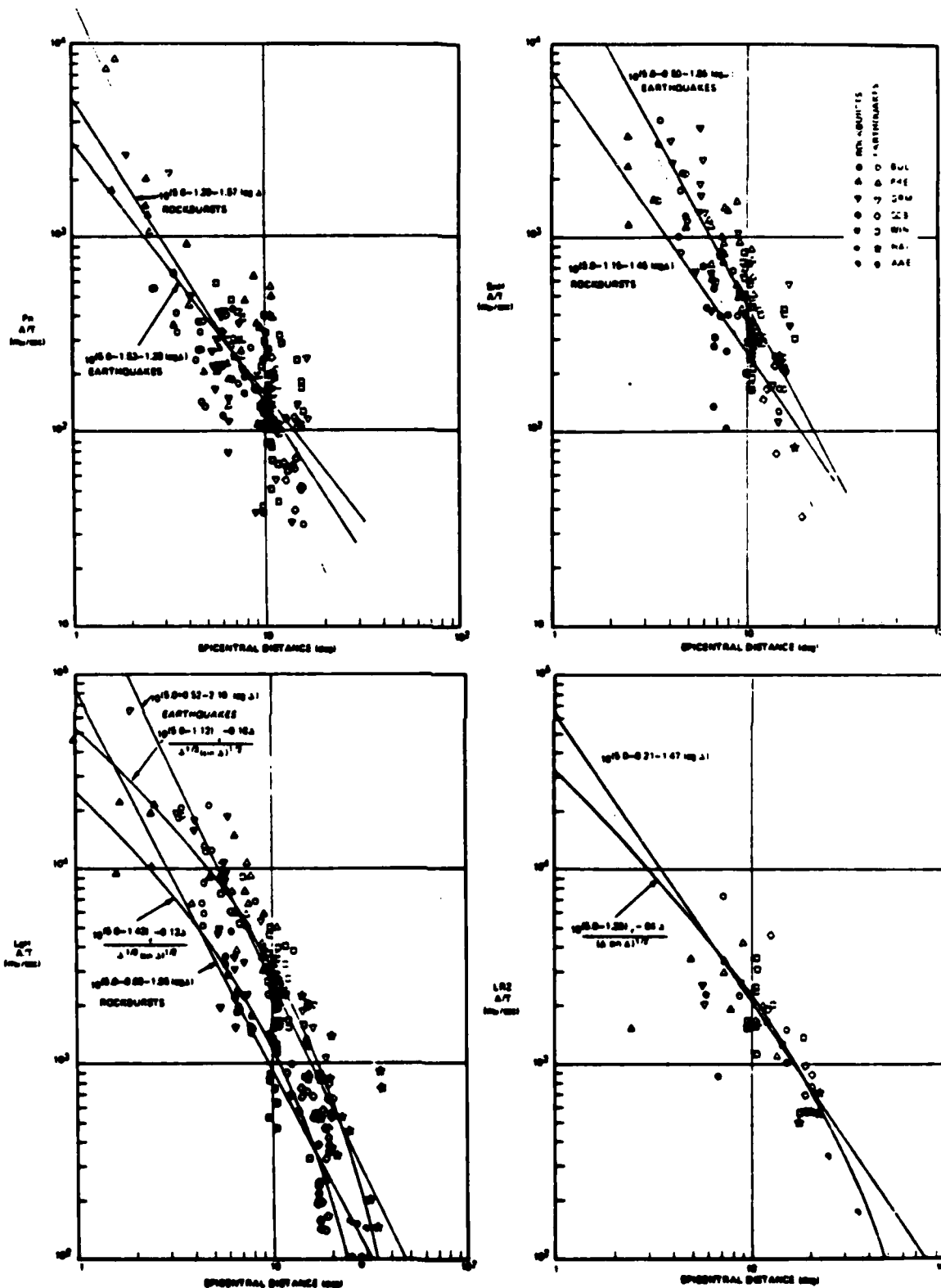


Figure 7. Logarithmic plots of A/T (amplitudes divided by periods reduced in the manner used to compute m_b) for various regional phases (after Swanson, 1978). These plots show that the A/T thus obtained can discriminate between natural earthquakes and rockbursts. All events were corrected to an earthquake with $m_b = 5$.

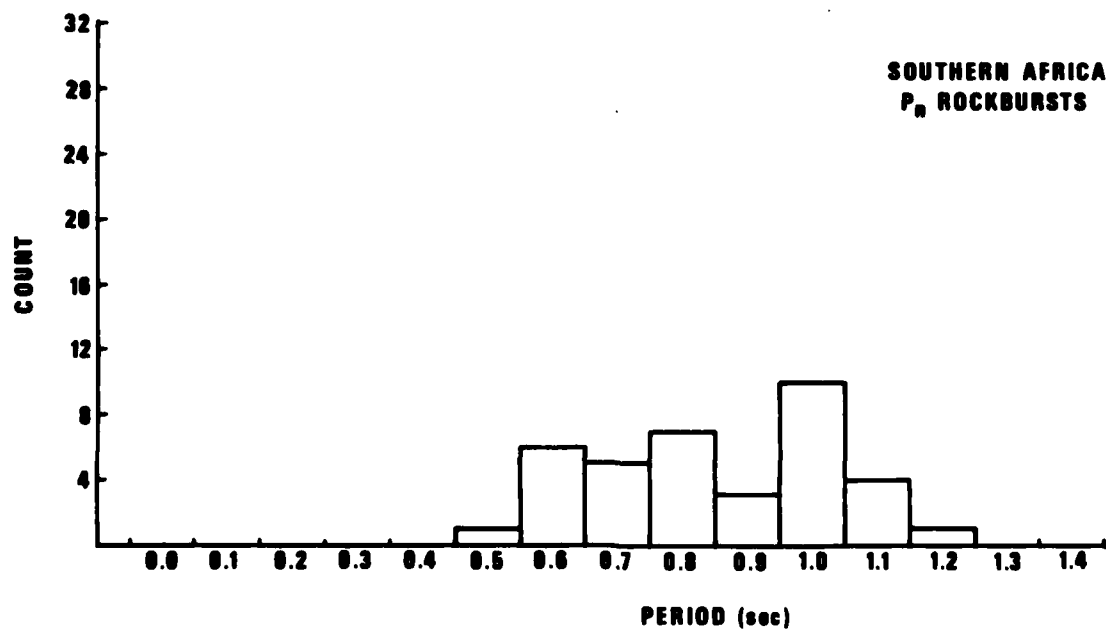
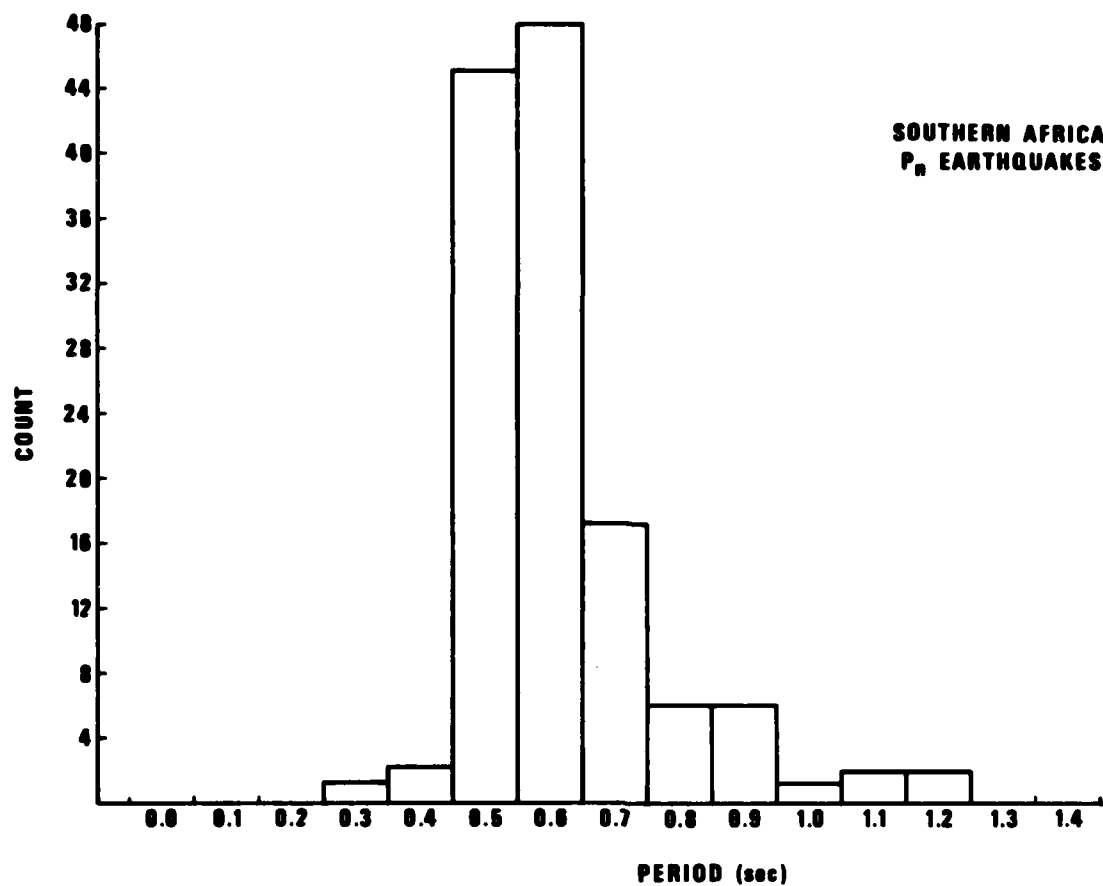


Figure 8. Histograms of the dominant periods of P_n for earthquakes and rock bursts in southern Africa.

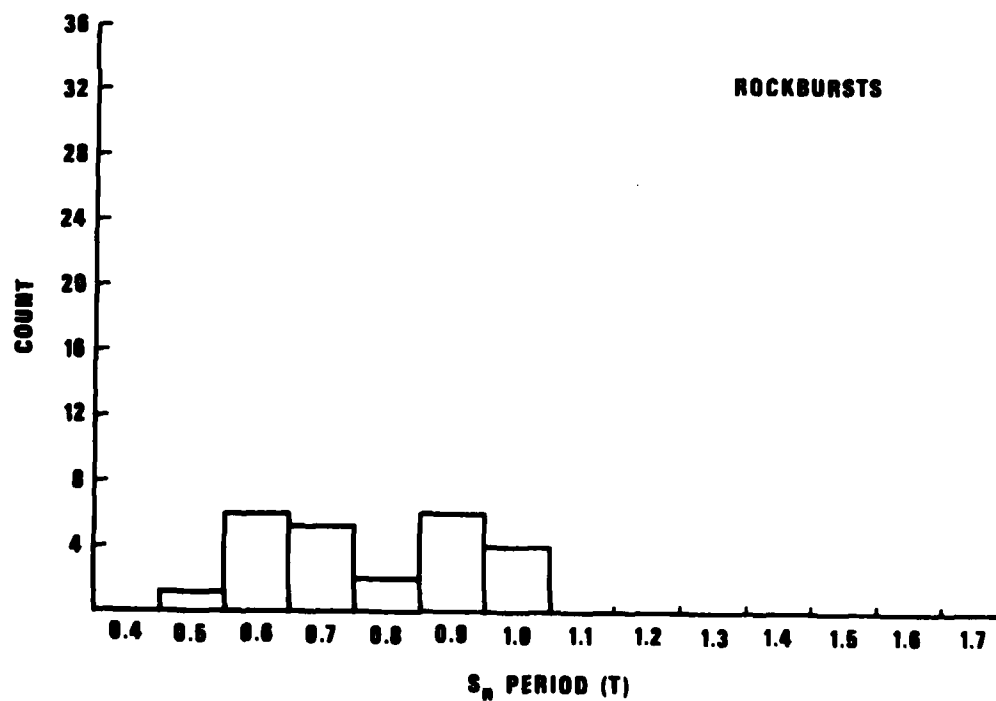
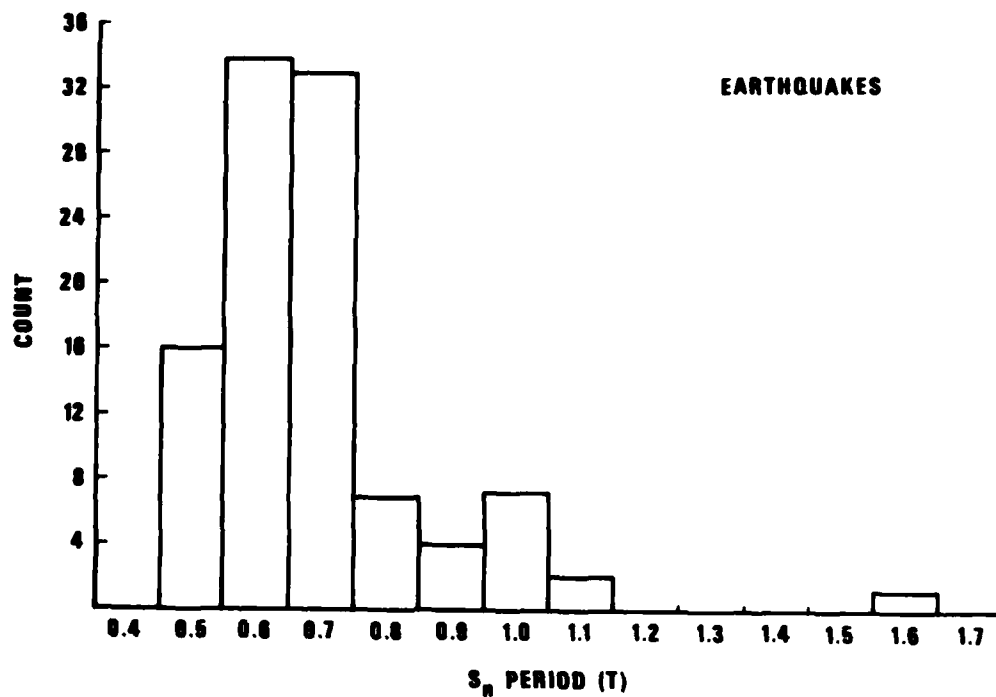


Figure 9. Histograms of the dominant periods of S_n for earthquakes and rock bursts in southern Africa.

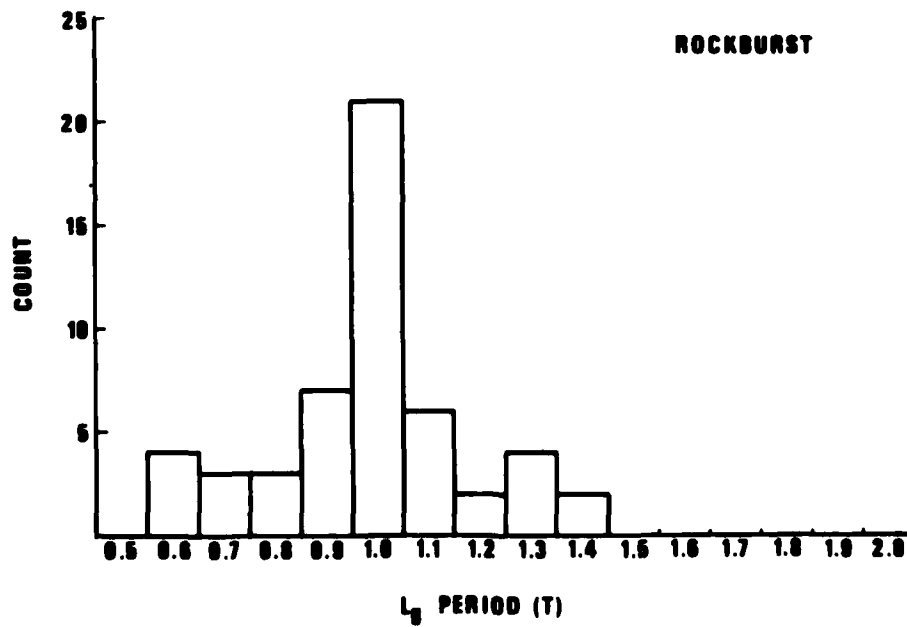
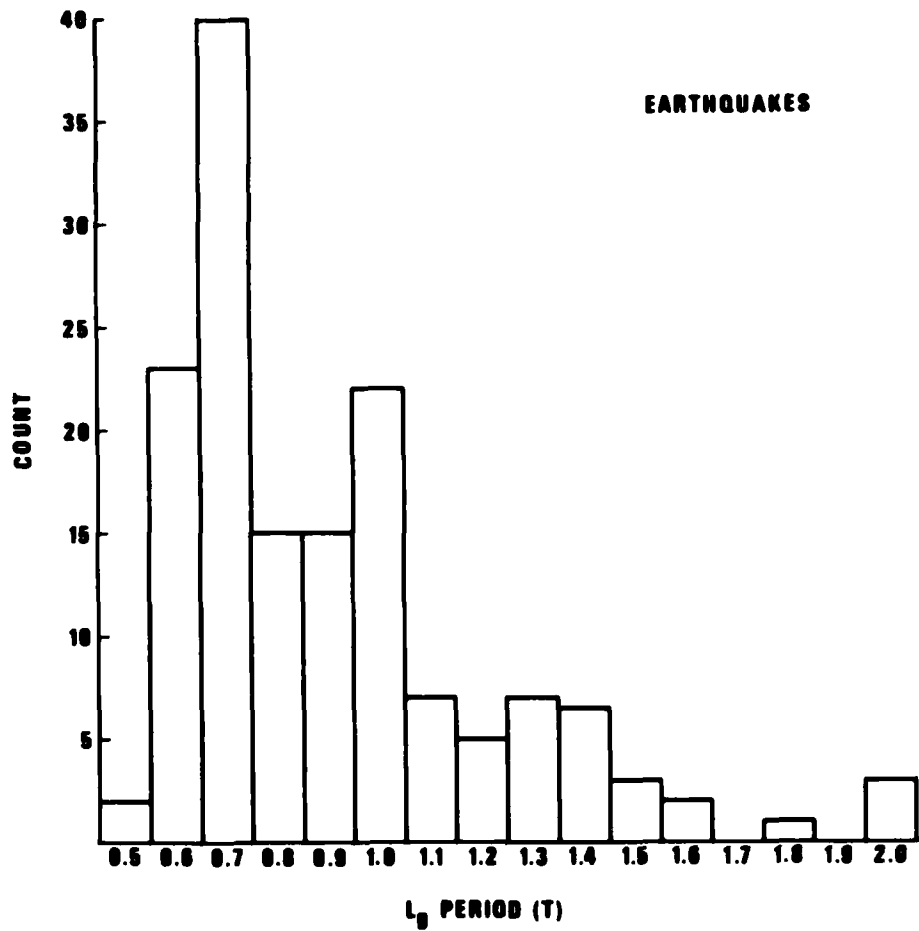


Figure 10. Histograms of dominant periods of L_g for earthquakes and rock bursts in southern Africa.

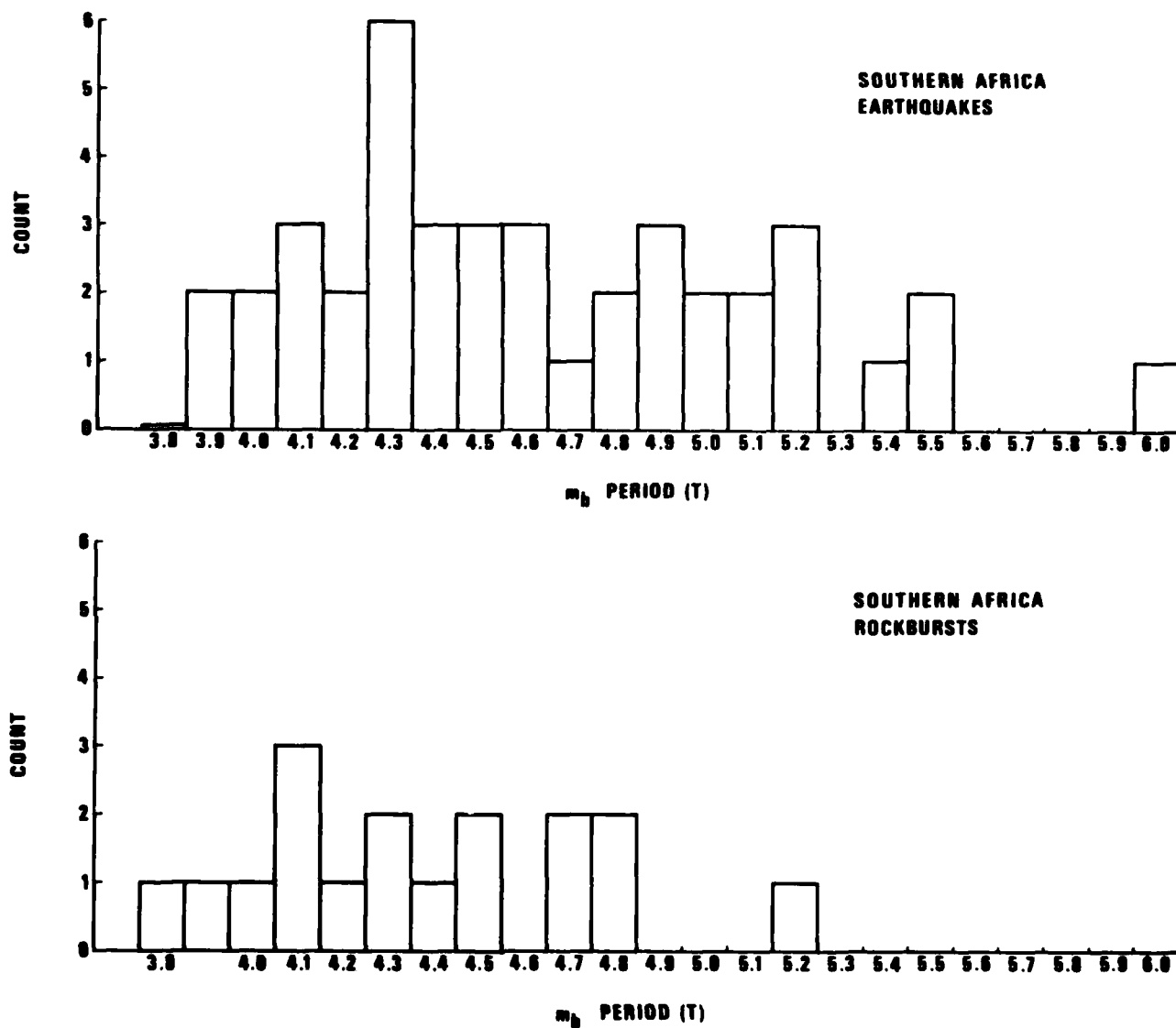


Figure 11. Histograms of m_b values for earthquakes and rock bursts in southern Africa.

earthquakes and rock bursts, this appears to be the case. The surprising fact is that rock bursts appear to have source functions which radiate less high frequency than do earthquakes. This is hard to believe because rock burst sources have much smaller dimensions, but the difference in stress drops may be one plausible explanation. While earthquakes at greater depth may have high stress drops in the interior of a shield, rock bursts usually occur at depths of the order of 2.5 km, and the associated stresses may not be as great. Figure 11 shows histograms of m_b values for earthquakes and rockbursts in Southern Africa.

Having examined the amplitude-distance relationships in southern Africa, let us consider now the distance dependence of the dominant periods of the observed waves. Since dominant periods also depend on event magnitude, we have restricted the magnitudes to a range of 4 to 5 m.u. in order to reduce the scaling effect and uncover the possible change of periods with distance. Figures 12 to 16 are plots of dominant periods of various regional phases versus distance. For P_n and S_n , Figures 12 and 14, the dominant periods are about the same and show no clear indications of change with distance. The dominant frequency for both types of waves is about 2 Hz. The lack of noticeable distance dependence for both P_n and S_n periods and the near equality of frequency content is diagnostic of a high Q crustal structure. The results are not conclusive for P_g , Figure 13, although the periods seem to be fairly constant with respect to distance for this phase also. For the vertical and horizontal components of L_g , Figures 15 and 16, there is a slight hint of dependence of periods on distance. These changes can be due to intrinsic Q in the crust or to scattering; we have no preferred explanation.

Consistent with the reasons given above, we chose to investigate the dominant periods separately from the wave amplitudes. Both amplitudes and periods can be interpreted in terms of physical concepts, but A/T reduced in the manner of the m_b calculations is relatively meaningless. The southern African amplitude and period data is the basis of comparison for the rest of the regions in this report. This is because southern Africa is a more homogeneous, high Q environment, according to all current geophysical data.

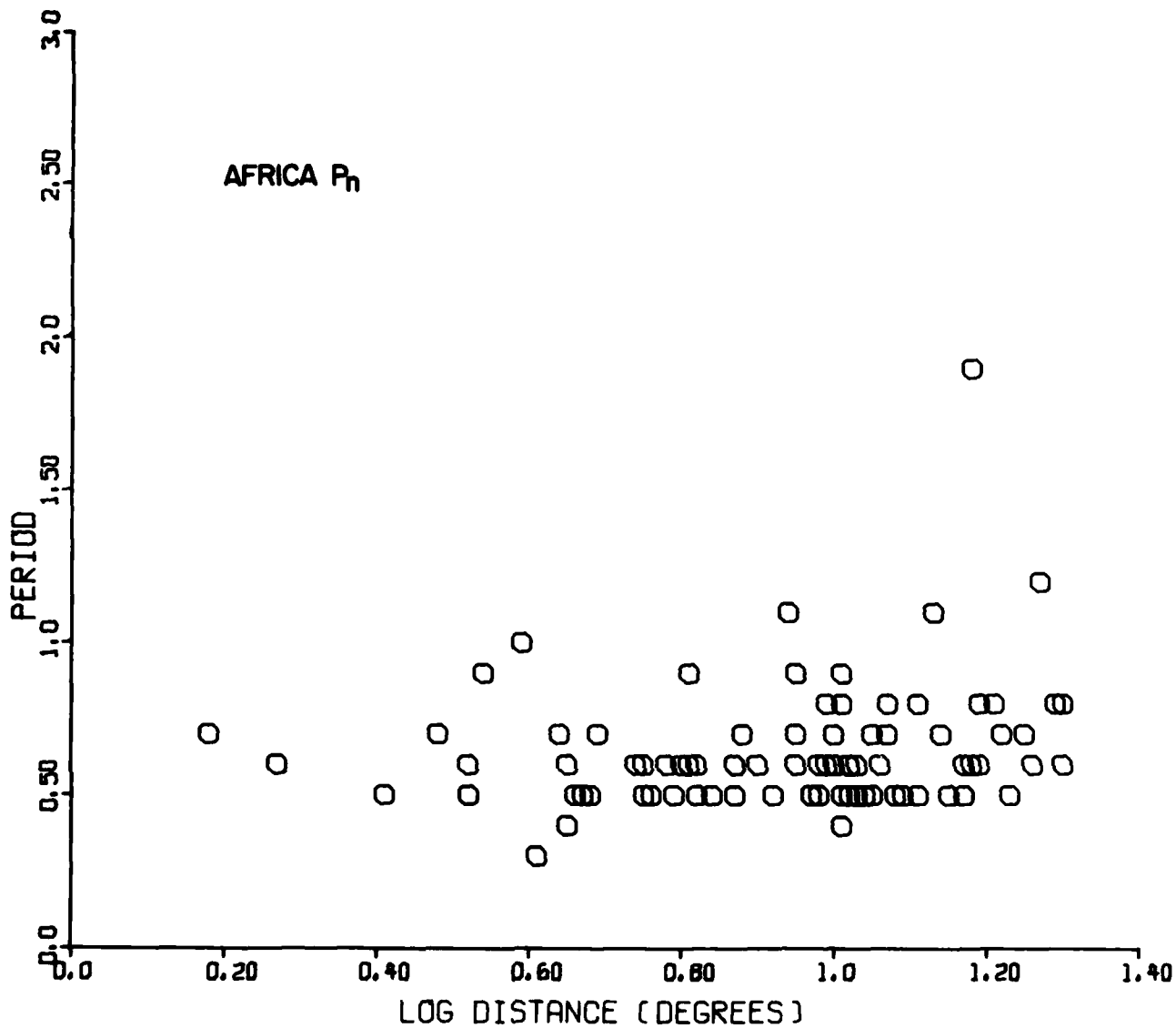
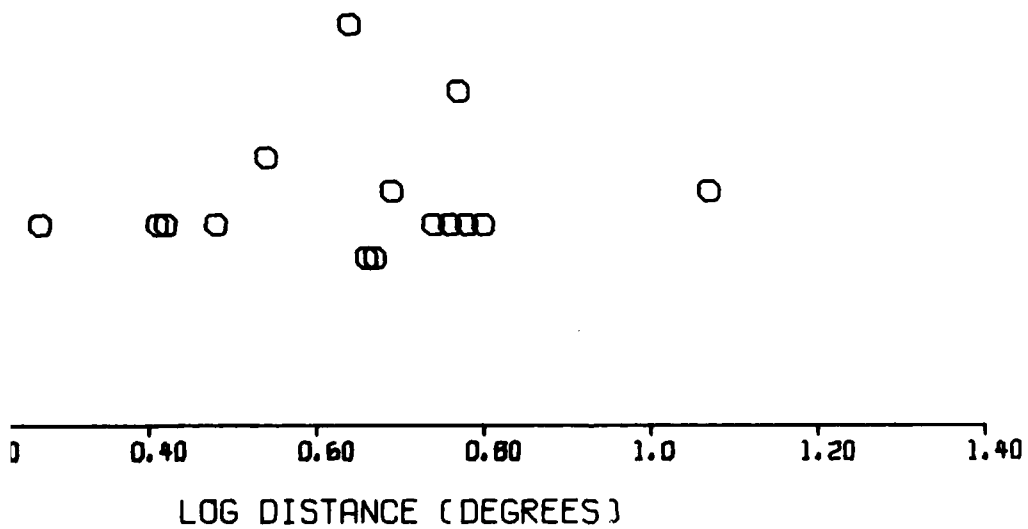


Figure 12. Dominant period for P_n as a function of epicentral distance in southern Africa for earthquakes in the m_b range of 4-5.

RICA P_g



dominant period for P_g as a function of epicentral distance
 southern Africa for earthquakes in the m_b range of 4-5.

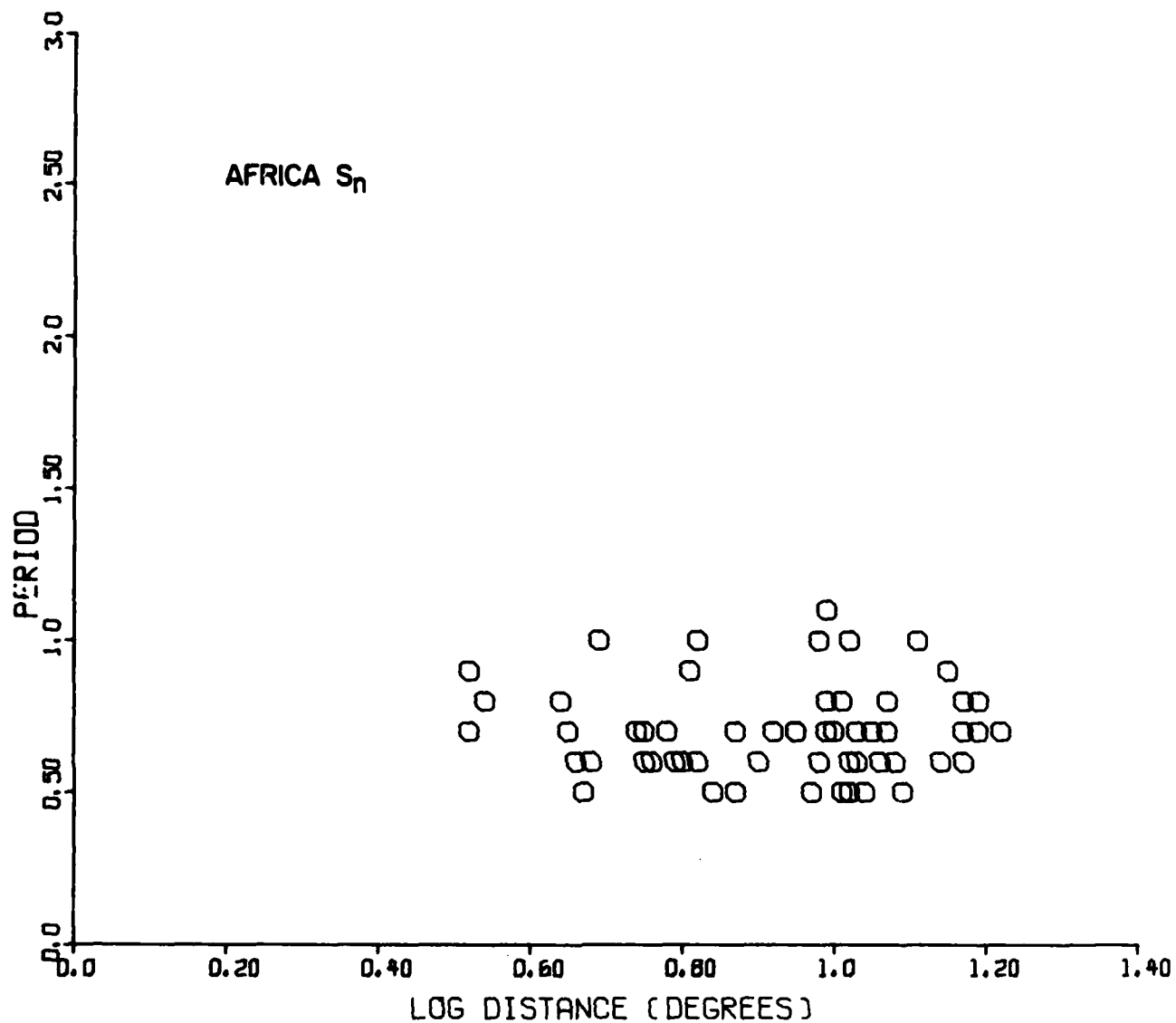


Figure 14. Dominant period for S_n as a function of epicentral distance in southern Africa for earthquakes in the m_b range of 4-5.

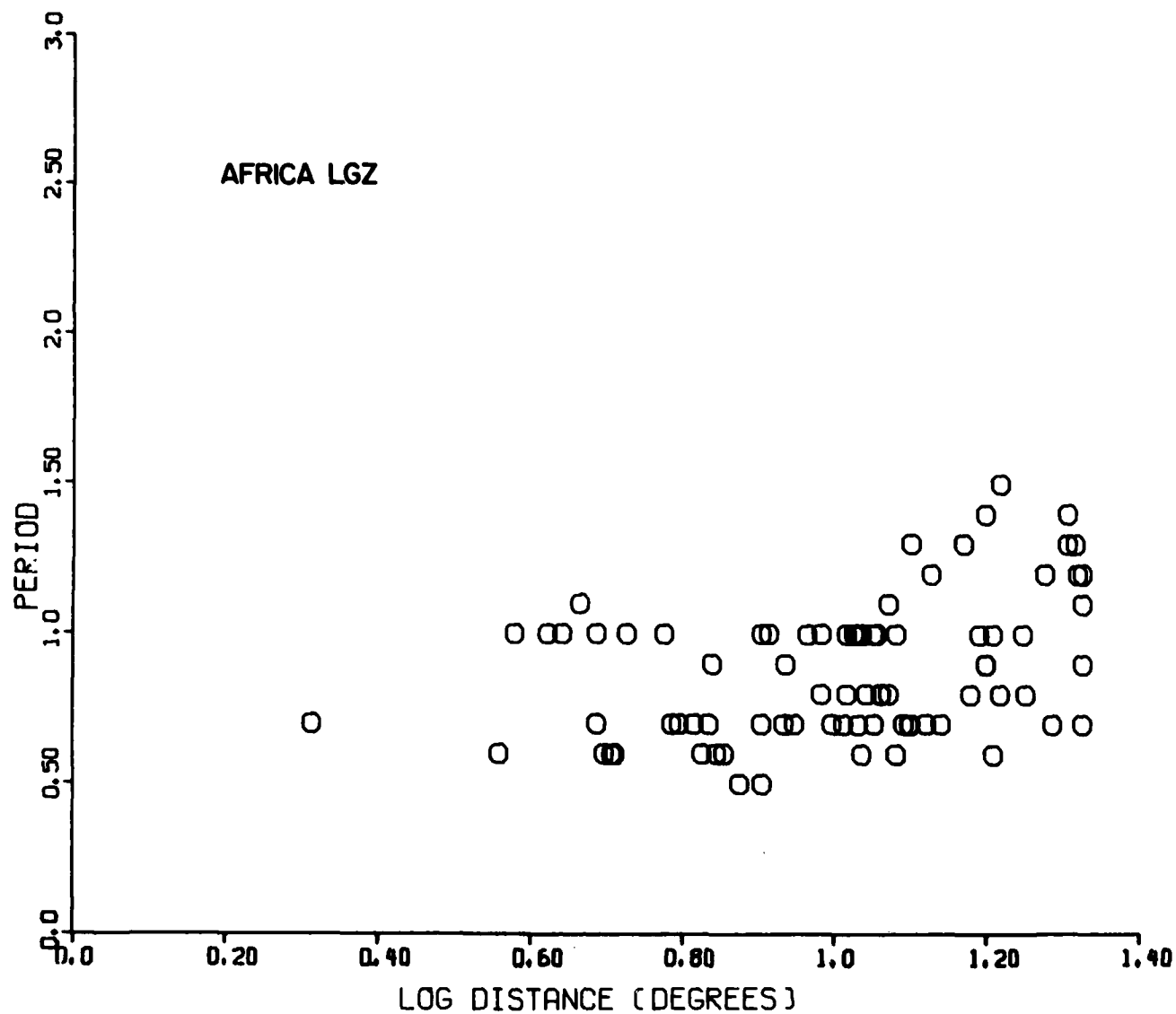


Figure 15. Dominant period for L_v (vertical component) as a function of epicentral distance in southern Africa for earthquakes in the m_b range of 4-5.

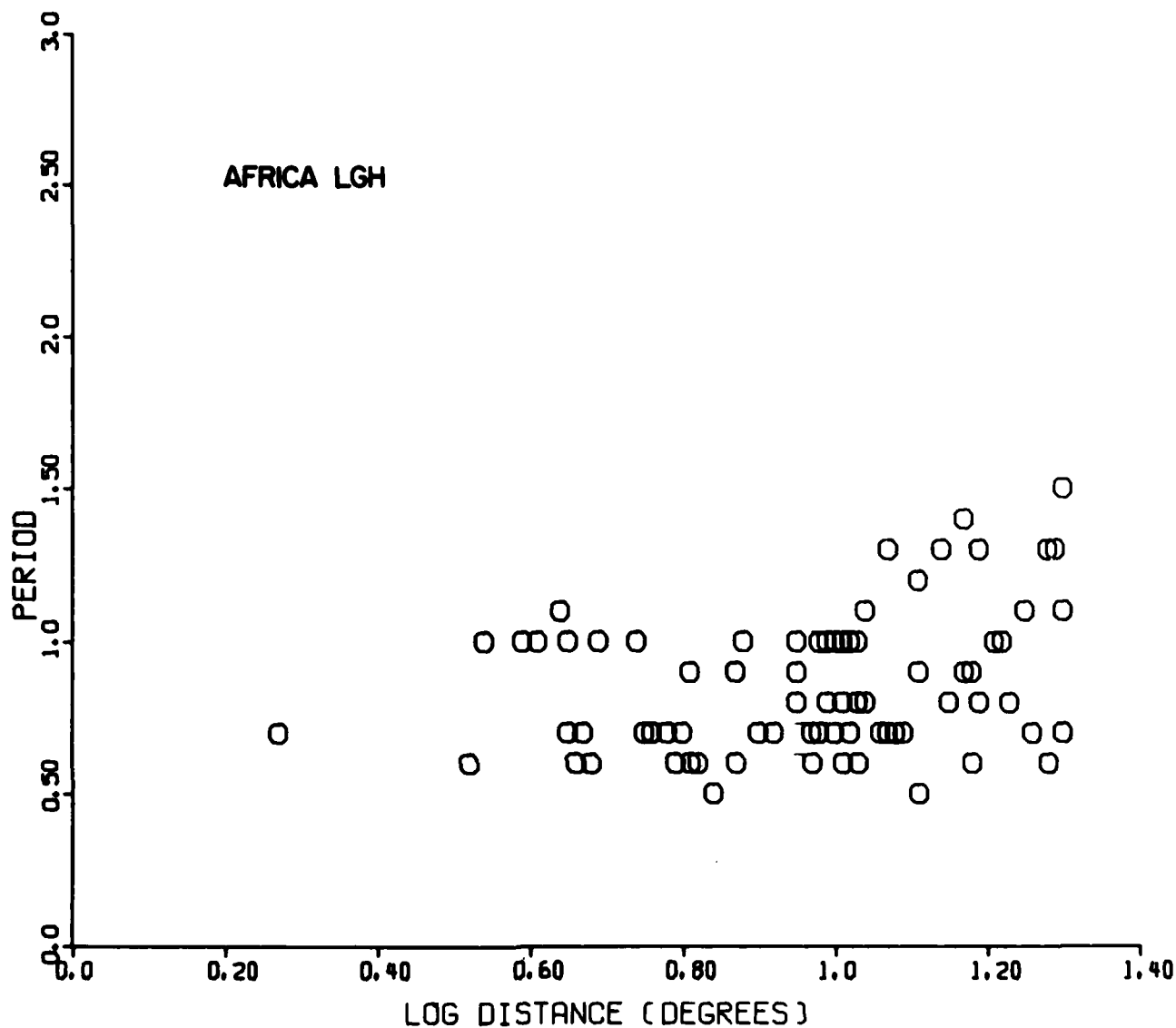


Figure 16. Dominant period for L_g (horizontal component) as a function of epicentral distance in southern Africa for earthquakes in the m_b range of 4-5.

SOUTH AMERICA

Structural Setting

The present day tectonic activity of South America is dominated by the plate subductions at the western boundary of the continent and the motion of the Caribbean plate relative to the South American plate. As in many other regions of the world, the subducting plate is segmented under South America, and each segment, after separating from its neighbor, descends with a different dip angle (Barazangi and Isacks, 1976; Stauder, 1973, 1975). The approximate location of the segments in the descending Nazca plate and their dip angles are shown in Figure 17 (modified after Swanson) where the segments are separated by dashed lines. The segment boundary in southern Peru indicated by question marks was recently found to be a warp rather than a tear by Hasegawa and Sacks (1981). The tectonics of Venezuela are dominated by the relative eastward motion of the Caribbean plate relative to the South American plate along the Bonoco fault zone (Dewey, 1972).

A study of the crustal structure in the Andes by James (1971) showed crustal thicknesses of up to 70 km under the western high plateau (Antiplano) of the Andes, thinning out towards the coast and the interior of the continent. Figure 18 shows a contour map of the Moho depth by James.

A cross section of the crust under the Andes is shown in Figure 19 (after James, 1971). Note the great change in crustal thickness from the coast to the central Andes. Such variations in the thickness of the crust, the primary waveguide for crustal phases such as L_g , is likely to have a profound influence on the propagation of such phases.

Studies of the anelastic attenuation in the mantle under South America using surface reflections of short-period body waves from deep earthquakes reveal three zones of extremely low Q in the mantle under the Andes. Figure 20 shows these zones as areas covered by black squares, while the stippled regions indicate the areas of high Q in the mantle. The blank areas correspond to regions where no surface reflections were available to delineate the Q variations.

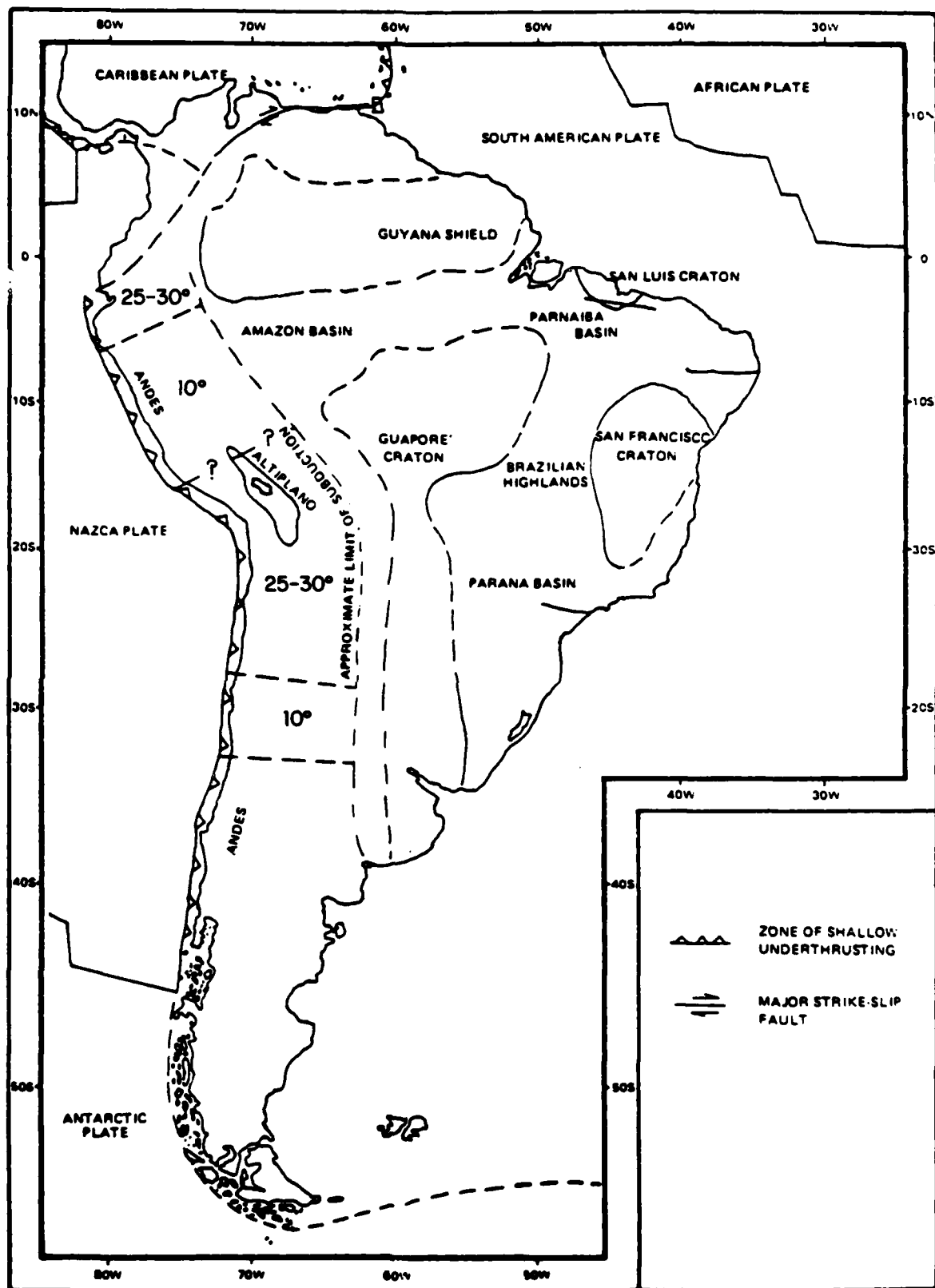


Figure 17. Tectonic features of South America (modified after Swanson, 1978).

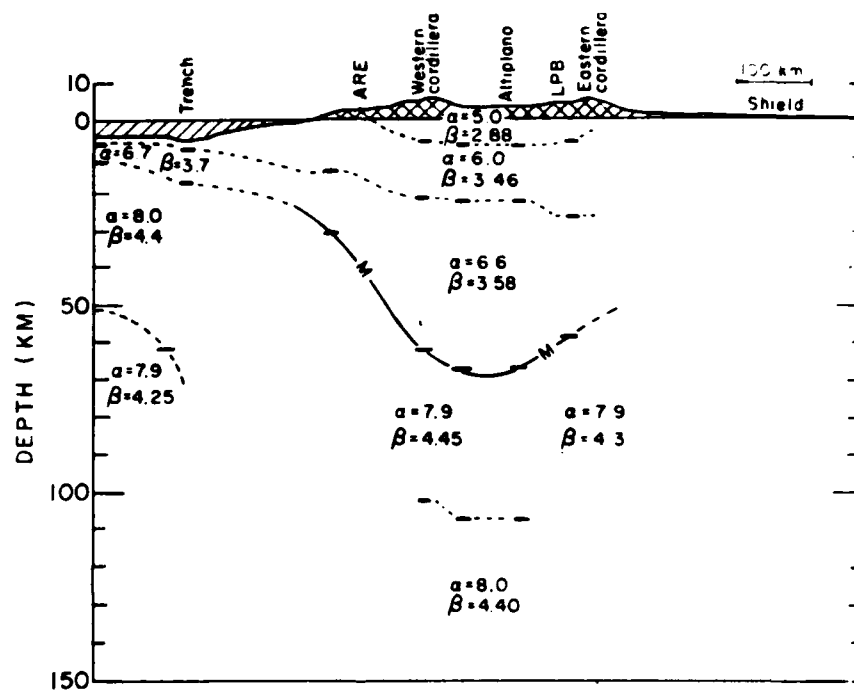


Figure 19. Cross section of the Andes and the coastal region (after James, 1971).

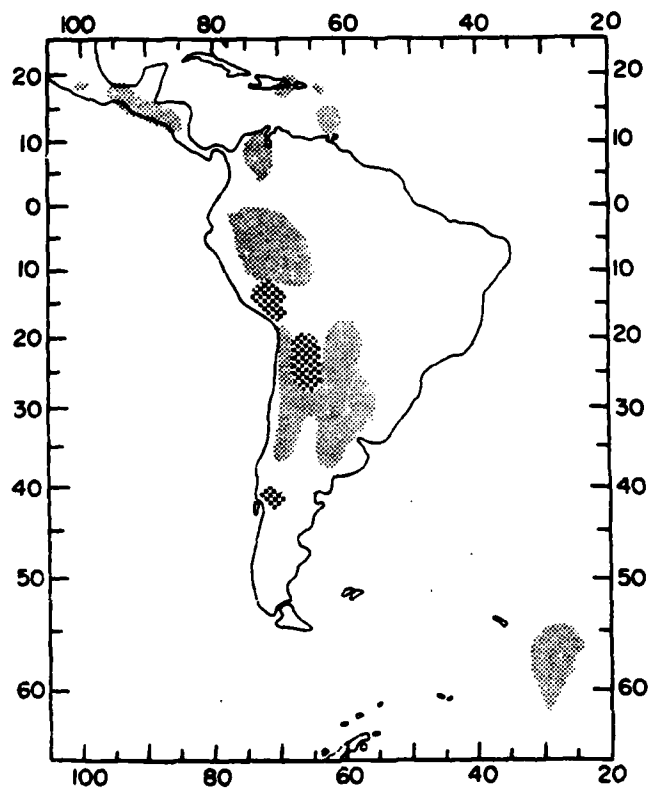


Figure 20. Regions of high (squares) and low (stippled) attenuation in the upper mantle under South America (after Barazangi et al., 1975).

Propagation of some regional phases, P_n and S_n in particular, involves the upper mantle "lid" zone. Consequently, variations of Q in the uppermost part of the mantle must affect these phases. This appears to be the case and will be shown later in this report.

With the exception of some parts of Venezuela, the eastern part of the continent can be considered a shield. Most of Brazil is located on a shield and exhibits all the typical shield characteristics. The shield areas are similar in all respects to other shield regions of the world and can be expected to behave similarly with respect to regional phase propagation.

Efficiency of Propagation and Amplitude-Distance Relationships

In an extensive study, Chinn, Isacks and Barazangi (1980) outlined regional patterns of efficient and inefficient propagation for S_n in South America. They also conducted a limited study of L_g in the same region. In their study, many quite unusual features of regional seismograms were noted which have not been observed previously in other areas of the world. Such features are 1) early and late arriving L_g phases, 2) highly scattered seismic waves with gradual buildup and decay of amplitudes without any clearly defined phases, or 3) wavetrains with such buildup and decay, not corresponding to any regional phase in rough group arrival time.

In Figure 21, we reproduce sketches of regional phase envelope shapes by Chinn et al for typical seismograms observed in South America. These envelopes show that many ideas and concepts derived from regional propagation in other areas of the world do not apply in South America. For example, the arrival of an "indeterminant wave" preceding the time of S_n has not been observed elsewhere. The same is true for the indeterminant waves having P and L_g arrival times. In Figure 22 we reproduce the symbols Chinn et al used for designating the various types of seismograms. These symbols are used in plots of propagation patterns, some of which we show in Figures 23, 24, and 25.

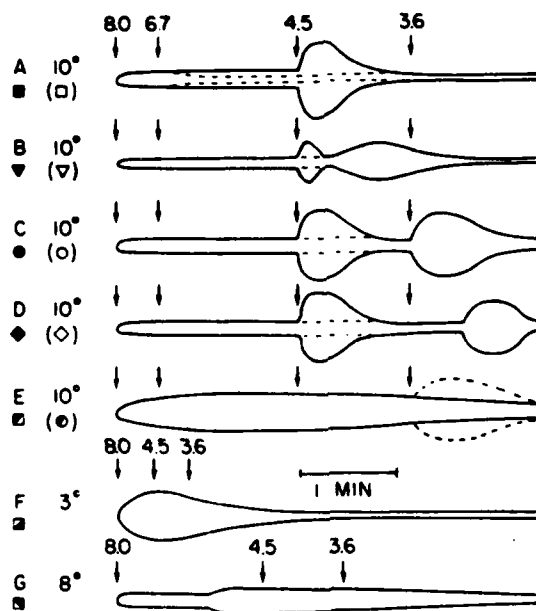


Figure 21. Sketches of regional seismogram envelope types in South America (after Chinn et al., 1980). Arrival velocities of some typical regional phases are marked on the figure.

Table 2. Categories of high-frequency shear arrivals.

Number	Symbol	Description
1	■	S_n only
2	□	no high-frequency shear arrivals
3	▼	S_n and "early L_g "
4	▽	"early L_g " only
5	●	S_n and L_g
6	○	L_g only
7	◆	S_n and "late L_g "
8	◇	"late L_g " only
9	◼	"indeterminant" waves consisting of a high-frequency energy build up beginning before the normal S_n arrival time and continuing through it
10	⊙	"indeterminant" waves but with a distinct L_g arrival
11	◻	"highly scattered" P waves with no strong S arrival produced by shallow sub-Andean sources located near ARE and recorded only at this station
12	◼	special kind of "indeterminant" waves observed only at ARE from intermediate-depth sources north of the station

Figure 22. Symbols used by Chinn et al (1980) for denoting various seismogram types from Figure 21 (after Chinn et al., 1980).

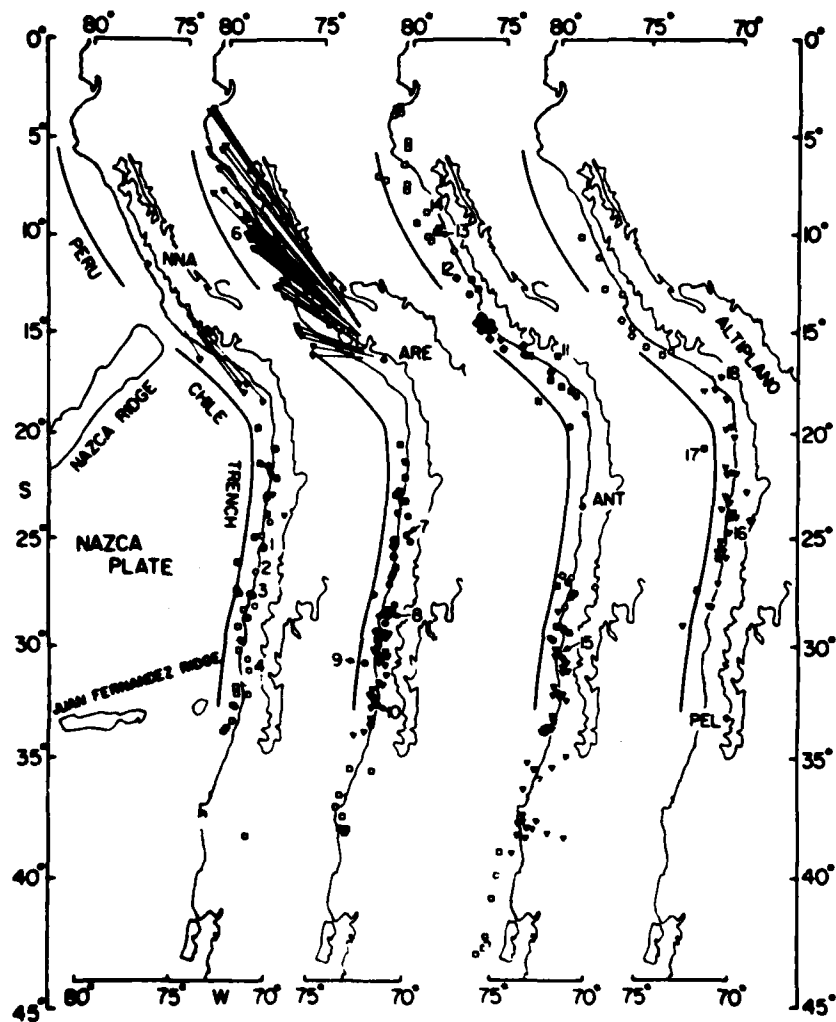


Figure 23. Propagation and the occurrence of various seismogram types along the western coast of South America. Symbols used are explained in Figure 22 (after Chinn et al., 1980).

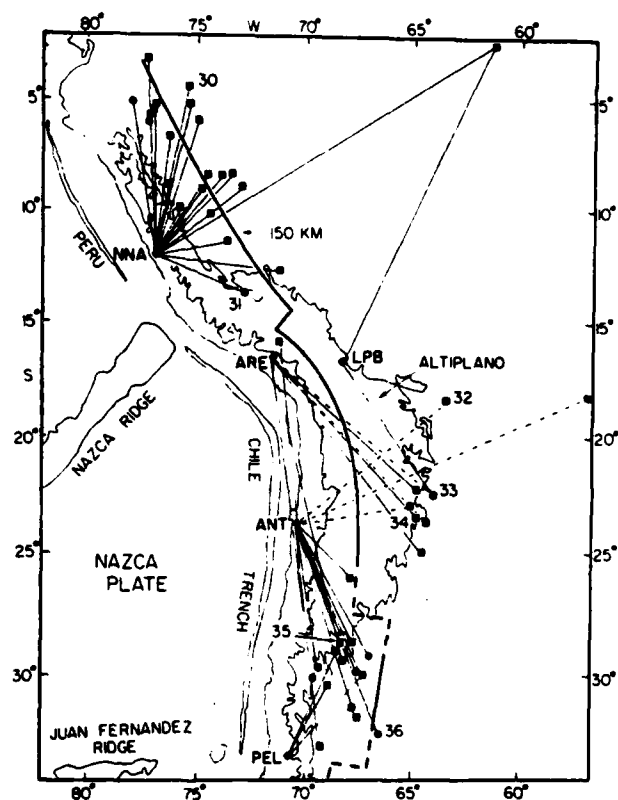
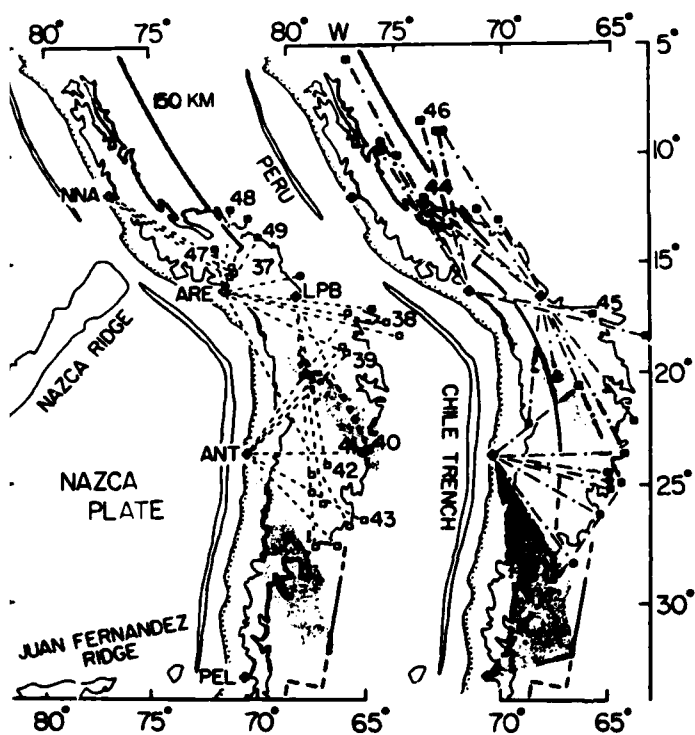


Figure 14. Propagation and seismogram types for shallow events along various Andean paths (symbols are from Figure 22, after Chinn et al., 1980). These paths were associated with S_n phases.



for which no S_n was observed. Symbols are explained in
 : 22 (after Chinn et al., 1980).

In Figure 23 the propagation patterns along the western coast of South America are depicted in terms of the wave types observable at the stations NNA, ARE, ANT and PEL. In looking at these figures one must keep in mind that the absence of L_g over paths crossing the Peru-Chile trench is to be expected and is not anomalous. At the stations north of the major bend in the coastline of South America, only early L_g is observed from nearby coast and S_n from the southern more distant coastal regions. There are some paths where L_g and S_n are both observed at ARE along the coast from the south. For ANT and PEL, the most common arrivals are early L_g and S_n , apparently indicating that in the coastal region of Chile, L_g does not propagate at all or only propagates a short distance after conversion from S_n .

Figure 24 shows another propagation map by Chinn et al (1980), indicating a region of relatively inefficient propagation for S_n between ARE, ANT and LPB. In the rest of the area, S_n is observed with short periods (2 Hz average frequency), indicating very effective propagation for S_n .

In Figure 25, we show another map by the same authors, giving paths over which scattered, "indeterminant", or no shear phases were observed from shallow events at ANT, ARE and LPB, along with the regions of effective propagation of S_n . There appears to be no relationship among the propagation paths of the various types of scattered, indeterminate and S_n phases. These observations indicate that regional phases in South America are poorly understood and that some extremely complex models involving mode theory and scattering will be necessary to properly describe them.

In contrast to the studies done before, we concentrated on the study of shallow events and also included more of the southern part of the continent than the study of Chinn et al (1980).

Outlining amplitude-distance curves for a region makes little sense unless the efficiency of propagation is investigated first. Clearly, if the observability of a phase is in question, it is not possible to reliably determine event magnitudes from it. We have constructed efficiency maps for S_n and L_g using data from WWSSN

stations and from the site in La Paz, Bolivia that was occupied first by an LRSM station and later by an SRO station. Table II lists the events analyzed by Swanson et al., (1979). Table III and IV list events we analyzed at WWNSS stations and the LRSM station at La Paz, Bolivia, respectively.

The efficiency map for S_n propagation is shown in Figure 26. It was constructed by using the efficiency criteria of Molnar and Oliver (1969). The map showing the four degrees of efficiency with various types of lines presents a confusing picture. As with the results of Chinn et al, there are efficient paths across the Brazilian shield from the west coast of South America, and S_n is also often observed from the southeasterly direction at ANT and ARE. At LPB, S_n is frequently seen from the south and across the shield. In other areas, the efficient and inefficient paths mingle, although part of Venezuela also appears to be efficient in transmitting S_n . Only one weak S_n was observed along the Andes south of PEL in this study.

The efficiency map for L_g , shown in Figure 27, is based on two criteria. For inefficient paths, no L_g could be seen; for the remaining two categories we subdivided the $m_b - \log_{10} (L_g \text{ amplitude})$ plane into two regions and the points falling above the dividing line represent paths for which L_g is large relative to the body wave magnitude were designated "very efficient", while those falling below were classified as "semi-efficient". The resulting efficiency map is considerably less complex than that for S_n . Most "efficient" paths are associated with the interior of the shield regions of the continent, while most "inefficient" paths are crossing the Andes mountains. No L_g was seen crossing lengthwise along the Andes south of PEL. North of NNA and LPB, there is a mixture of efficient and inefficient paths, indicating the unreliable detection of this phase for most of South America outside the shield area. Chinn et al (1980) have found that when L_g was seen propagating through the Andes it was always observed along paths running along the trend of the mountain range. We cannot confirm this based on our limited data. Nevertheless, it appears in any case, that one cannot count on the L_g phase for detecting or discrimination in the Andes region.

TABLE II

ISC Hypocenters for Analyzed South American Earthquakes
(after Swanson et al., 1979).

Shallow

Event Code	Date YrMoDa	Origin Time Hr:Min:Sec	Lat deg	Lon deg	Depth km	Mag ISC
NV 2	731117	06 50 24.7	10.757N	63.097W	0	3.99
NV 4	750305	13 47 58.3	9.130N	69.870W	25	5.50
NV 5	750415	09 47 44.8	9.420N	61.470W	52	5.30
NV 6	751025	15 23 23.5	7.790N	72.100W	36	4.26
NA 3	720419	10 57 33.0	0.523S	77.484W	38	4.40
NA 6	730209	09 53 16.5	4.804N	76.107W	52	5.00
NA 7	730223	23 10 52.6	2.256S	78.382W	41	4.50
NA12	731103	01 46 07.1	7.210N	74.426W	16	4.90
NA14	740310	16 17 10.2	0.389N	80.012W	53	5.20
NA17	740602	23 03 44.4	5.514N	76.827W	37	5.20
NA18	740609	14 16 02.4	5.769S	80.994W	36	5.60
NA19	740707	01 53 05.5	5.050N	74.114W	57	4.00
NA21	741214	13 26 02.2	6.295N	73.202W	57	4.60
NC 1	690724	02 59 20.9	11.840S	75.100W	1	5.90
NC 4	720311	00 38 33.1	9.413S	75.559W	43	4.90
NC 5	720320	07 33 48.7	6.792S	76.761W	52	6.10
NC 7	720717	10 03 28.7	14.871S	76.717W	0	3.80
NC14	740321	19 28 23.9	4.595S	73.512W	47	4.80
NC16	741007	14 21 29.3	12.241S	77.584W	9	6.20
NC18	750605	20 18 02.7	6.170S	75.160W	38	5.00
NC19	760515	23 28 17.3	11.540S	74.410W	43	5.30
NC20	760613	22 02 46.7	15.280S	75.400W	24	5.50
CA 3	711004	10 53 37.3	23.957S	70.008W	59	4.80
CA 5	711207	23 25 40.0	22.787S	70.382W	20	4.20
CA13	731019	10 11 15.1	19.466S	69.881W	56	5.40
CA15	731104	14 38 53.2	25.923S	67.764W	39	5.20
CA16	731109	11 19 32.0	24.577S	64.587W	12	5.60
CA18	740425	08 56 42.8	17.195S	70.683W	29	5.20
CA20	740706	07 04 25.1	22.128S	64.294W	15	4.30
CA27	741031	08 58 20.9	15.438S	71.050W	50	5.00
CA31	760222	08 09 22.7	18.330S	65.350W	41	5.20
CA32	760504	02 07 11.3	27.340S	65.790W	58	4.70
SC 1	640803	04 16 47.0	33.500S	68.500W	50	4.00
SC 2	710709	03 03 16.9	32.510S	71.206W	40	6.50
SC 5	720515	10 09 37.7	29.622S	69.435W	17	5.40
SC 6	720926	21 05 43.3	30.906S	68.209W	7	5.80
SC14	750506	18 10 02.0	32.930S	69.020W	14	5.00
SA 2	720121	21 56 42.1	35.039S	70.246W	11	5.00
SA 3	730731	05 41 03.7	37.661S	73.304W	28	5.10
SA 6	740715	09 30 19.1	39.627S	71.223W	55	4.80
SA 7	750510	14 27 44.0	38.030S	72.780W	30	6.20
SA 8	750618	04 16 18.0	36.400S	65.700W	0	4.90
SA 9	750915	07 37 46.0	42.260S	73.400W	21	4.90
SS 1	720209	20 44 36.5	51.779S	74.099W	33	5.70
SS 2	730413	22 36 39.5	52.486S	72.048W	11	5.00

TABLE II (cont.)

ISC Hypocenters for Analyzed South American Earthquakes
(after Swanson et al., 1979).

<u>Event Code</u>	<u>Date YrMoDa</u>	<u>Origin Time Hr:Min:Sec</u>	<u>Lat deg</u>	<u>Lon deg</u>	<u>Depth km</u>	<u>Mag ISC</u>
ES 1	640213	11 21 44.3	18.050S	56.750W	16	5.50
ES 2	650815	19 36 57.0	2.710S	60.240W	42	5.00
ES 3	680223	14 23 02.0	6.300S	38.230W	33	4.40
ES 6	710325	21 46 51.0	5.715N	60.638W	0	3.90
ES11	740224	03 19 40.0	20.079S	48.523W	0	4.30
ES13	740930	05 55 37.8	2.551N	71.264W	25	4.70
ES15	760222	03 24 46.0	0.310N	59.080W	10	4.80
ES16	761008	20 01 15.4	1.575S	60.523W	0	4.18

TABLE III

Additional South American Earthquakes for Which WWSSN Data Was Analyzed.

<u>Date</u>	<u>Origin Time</u>	<u>Lat</u>	<u>Lon</u>	<u>Depth</u>	<u>Mag</u>
740630	06 49 23.3	38.1S	70.4W	185	4.7
730413	22 36 39.3	52.5S	72.0W	11	5.1
740816	07 47 49.3	33.4S	68.2W	20	4.8
741006	14 40 52.5	30.8S	65.0W	15	4.8
730403	15 39 12.9	32.4S	72.1W	32	4.7
730404	08 18 27.1	30.3S	68.1W	50	3.8
730405	05 28 04.4	39.6S	74.6W	44	5.0

TABLE IV

(U) Additional South American Earthquakes for Which Data at LRSM Station
LZ-BV Was Analyzed.

<u>Date</u>	<u>Origin Time</u>	<u>Lat</u>	<u>Lon</u>	<u>Depth</u>	<u>Mag</u>
640527	20 48 44.9	22.3S	66.3W	94	3.9
640607	20 10 15.9	30.4S	67.6W	29	5.2
641023	10 07 35.7	30.8S	64.4W	79	4.0
640627	17 19 52.9	27.8S	65.6W	100	4.5
641110	04 16 47.5	24.4S	65.7W	76	4.4
641217	14 58 26.3	21.5S	66.9W	190	4.3
641214	00 05 39.8	2.3S	61.2W	36	4.8
630325	08 57 11.7	31.6S	69.5W	123	4.2
640424	08 19 41.5	28.0S	69.0W	30	4.2
640601	21 25 41.9	28.2S	65.9W	41	4.4
631029	06 04 52.7	27.8S	66.9W	106	3.7
631101	04 29 43.0	29.5S	64.2W	33	4.0
641112	14 26 18.5	33.1S	68.6W	19	4.3
631212	17 59 23.3	32.4S	69.0W	51	4.4
631222	03 56 15.9	32.3S	69.2W	33	4.3
640109	11 47 45.0	31.1S	64.4W	119	4.3
640113	04 00 48.0	28.9S	66.2W	33	4.8
640301	09 00 02.3	21.2S	65.7W	90	4.2
640324	11 57 09.2	24.7S	65.0W	95	4.4
640213	11 21 46.7	118.1S	56.8W	33	5.3
630815	19 14 27.4	38.2S	69.0W	65	4.1
631203	04 35 53.8	38.2S	69.0W	65	4.1
631219	01 47 33.8	38.2S	69.0W	65	4.1
640524	03 06 08.5	39.4S	70.7W	33	4.0
640364	12 29 20.8	10.5N	70.9W	33	4.1
640619	03 56 18.5	2.5N	58.9W	45	4.5

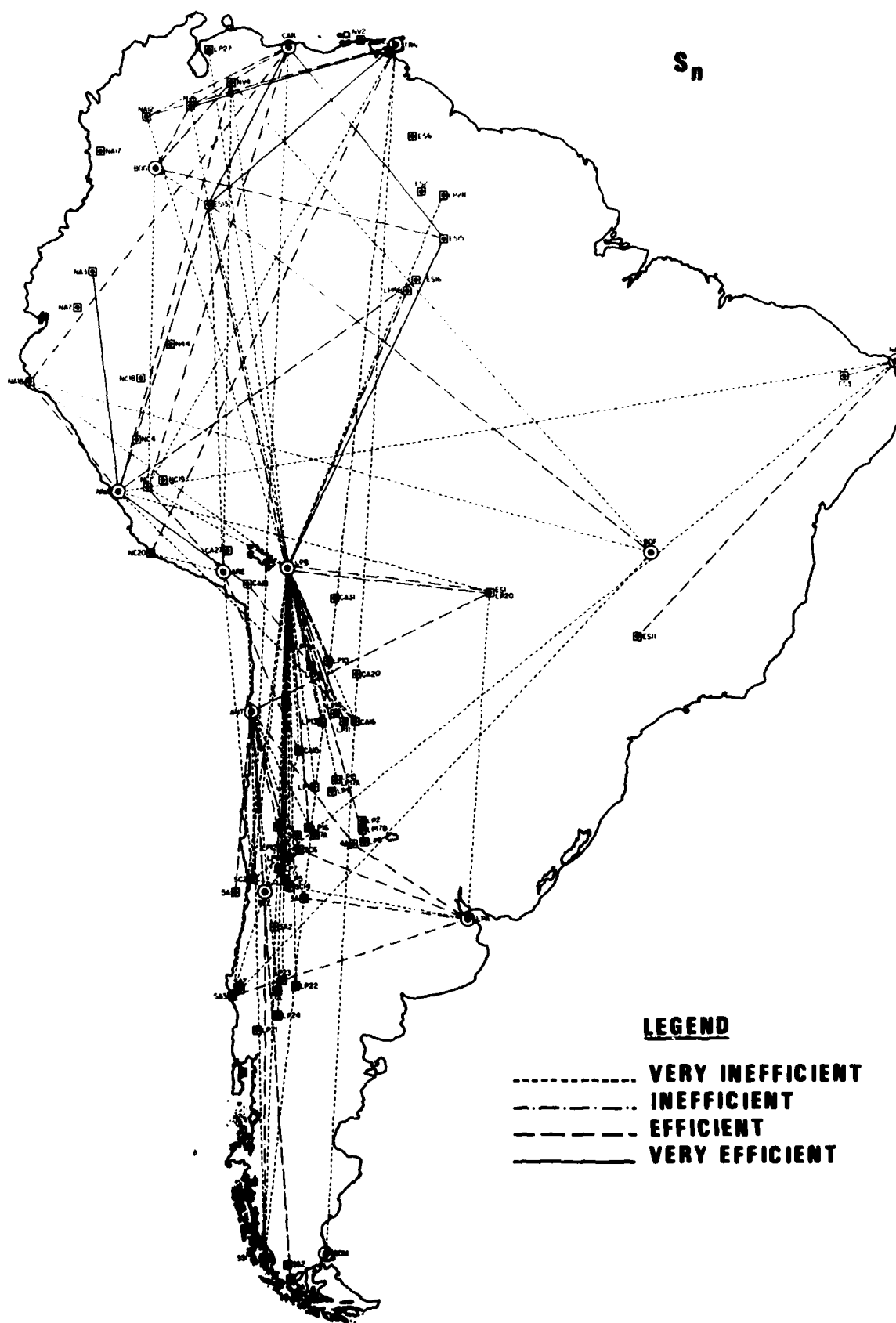


Figure 26. Efficiency map for S_n propagation from shallow events in South America. The efficiency criteria of Molnar and Oliver (1969) were used in constructing this map.

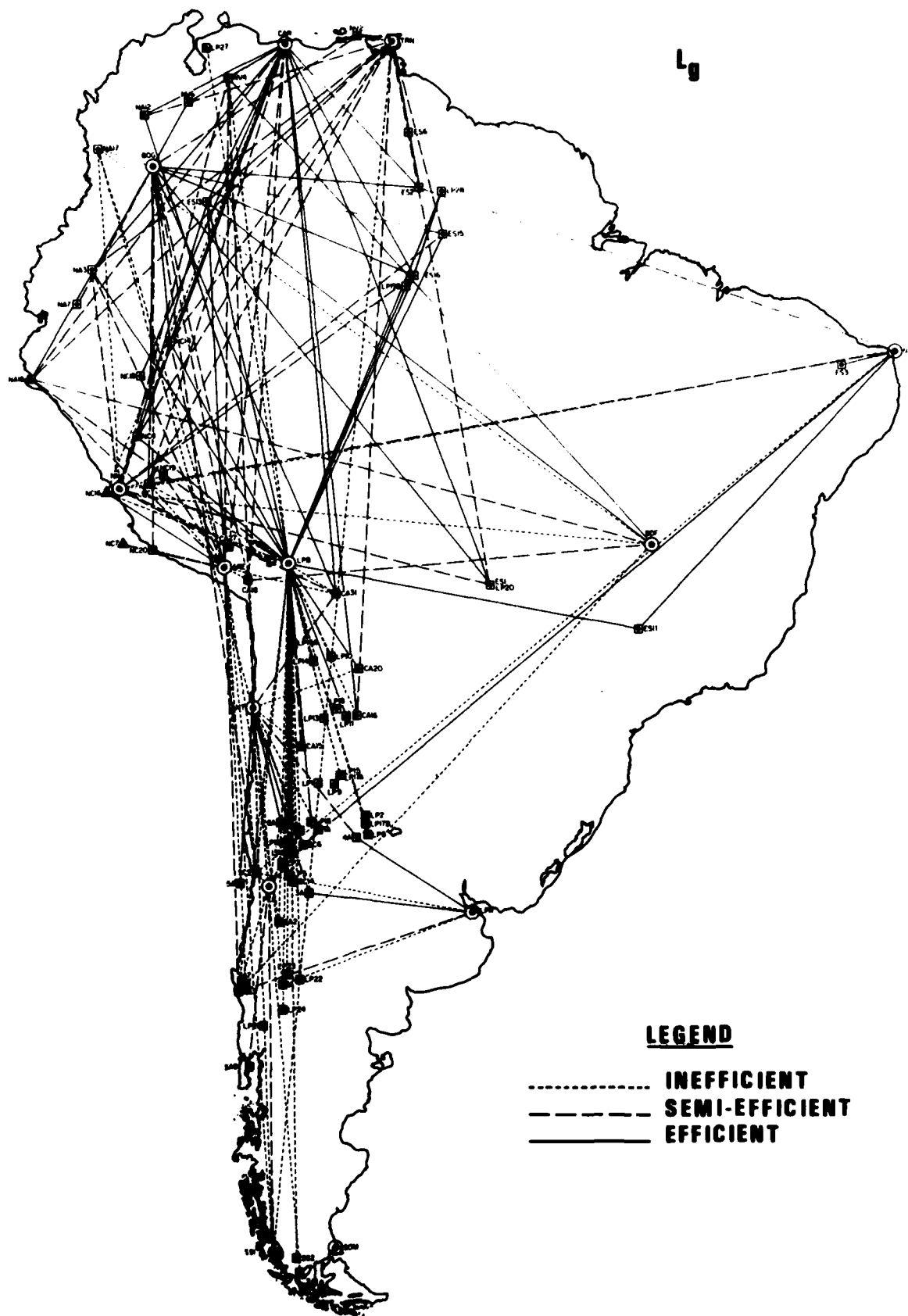


Figure 27. Efficiency of L_g phase propagation from shallow events. Criteria for classification are explained in the text.

Swanson (1979) has also constructed efficiency maps for South America, but our map differs from his in several respects. We have excluded all events with depths greater than 50 km, while his limit was 70 km, thus including subcrustal sources. Our data set was also larger, including many new events.

Having outlined the efficiency of propagation for L_g and S_n , we shall now look at the amplitude-distance behavior of various regional phases for paths where they could be observed. To distinguish between various types of propagation paths, we have used crosses for paths across the shield, circles and triangles for paths along and across the Andes mountain chain, and diamonds for paths that run through the continental shelf. The amplitude-distance curves normalized to a magnitude 5 event for the phases P_n , P_g , S_n and the vertical and horizontal components of L_g are shown in Figures 28 to 31. A common feature of these plots is that the scatter is considerably greater than that for the southern Africa data, even if one considers the shield-type paths only. This may be due to two factors: either the areas designated as shields are more heterogeneous, or the m_b available for this part of the world are less reliable. The magnitudes used for making the plots were taken from the NEIS event list and if too many of the South American stations were selected, using the regional phases to determine m_b , then some of the unreliability of propagation may have reduced the stability of m_b . Most of the events in our study were above a body wave magnitude of 4, and about half were close to an m_b of 5. It seems, therefore, that for at least half of the events, there were enough teleseismic stations to reliably determine the magnitude. The points along the various types of paths also intermingle, showing that all the regional phases, when observable along path types other than shield, may be as large as those observed along the shield paths.

Figures 32 to 35 show the dominant periods of the various regional phases in South America. Note that the scatter of the total data set is larger along all types of paths. For South America, we used events in the m_b range 4.5-5.5, which partially explains why the periods are somewhat longer than those presented for southern Africa, even for shield paths. Nevertheless, the scatter is also larger for the subpopulation of the shield type paths, indicating less homogeneity than in

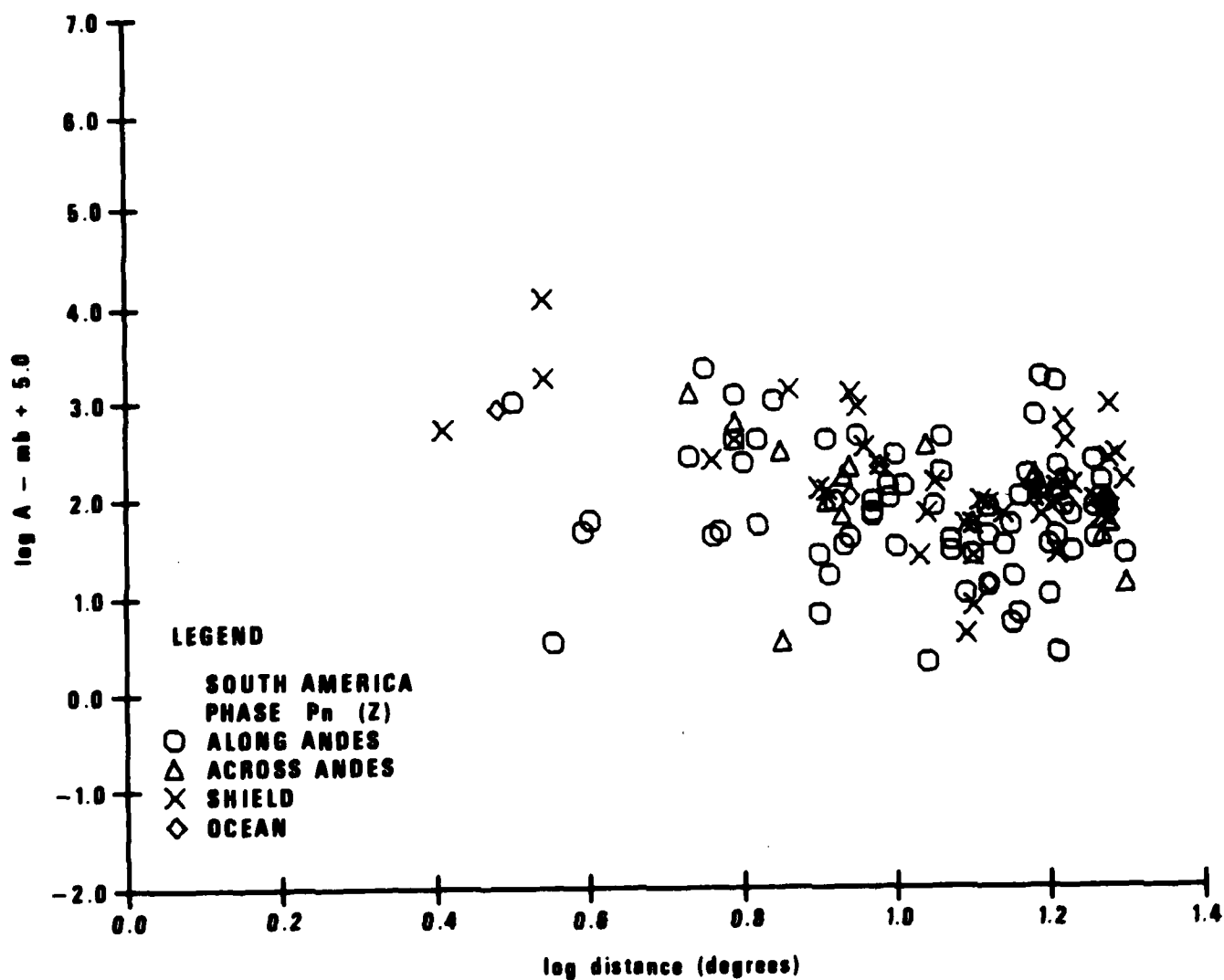


Figure 28. Trace amplitudes of P_n in South America, plotted against epicentral distance. The trace amplitudes were normalized to that of an earthquake with $m_b = 5$. The various types of propagation paths are denoted by symbols shown in the legend.

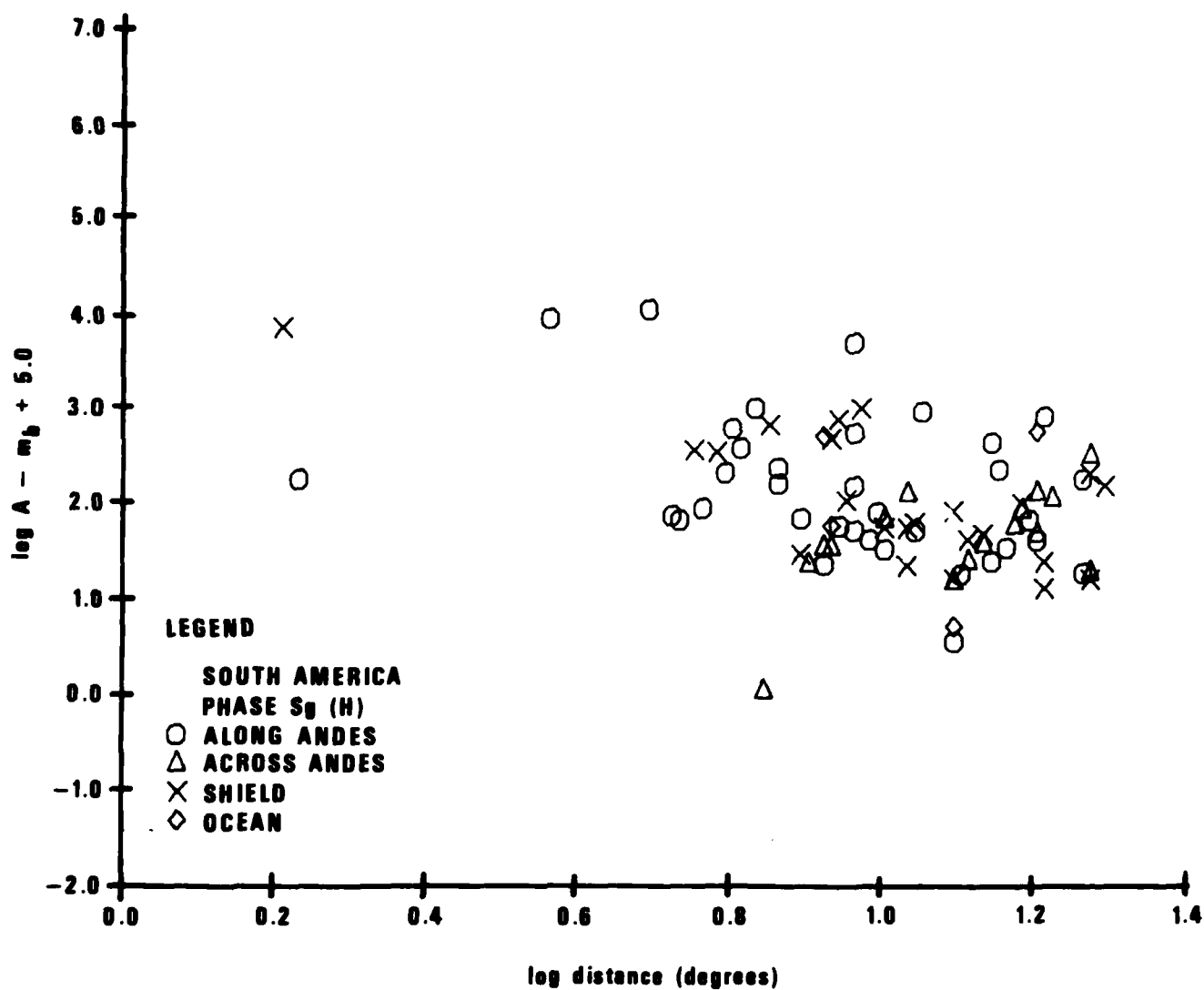


Figure 29. Trace amplitudes of S_0 in South America, plotted against epicentral distance. The trace amplitudes were normalized to that of an earthquake with $m_b = 5$. The various types of propagation paths are denoted by symbols shown in the legend.

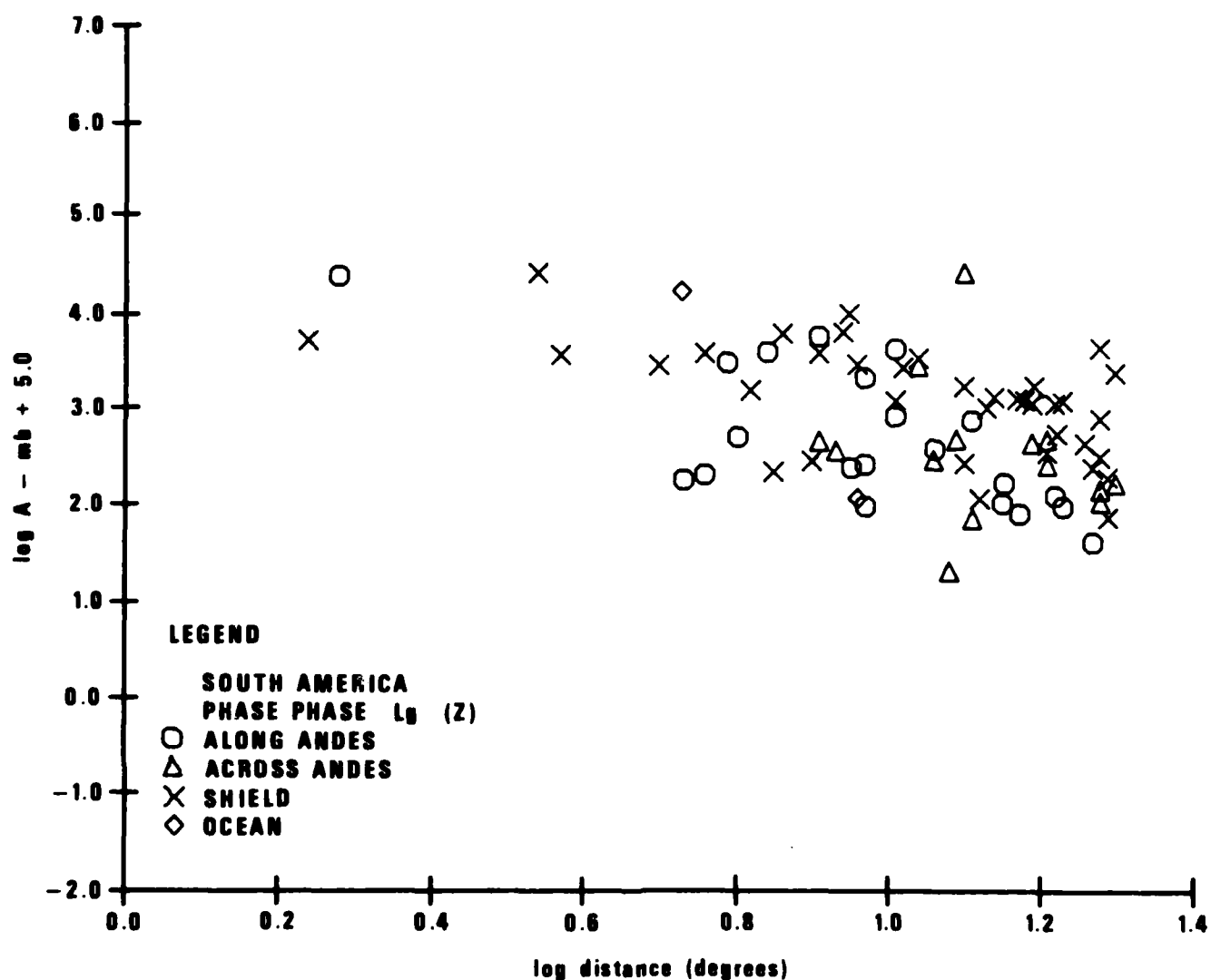


Figure 30. Trace amplitudes of L_g (vertical component) in South America, plotted against epicentral distance. The trace amplitudes were normalized to that of an earthquake with $m_b = 5$. The various types of propagation paths are denoted by symbols shown in the legend.

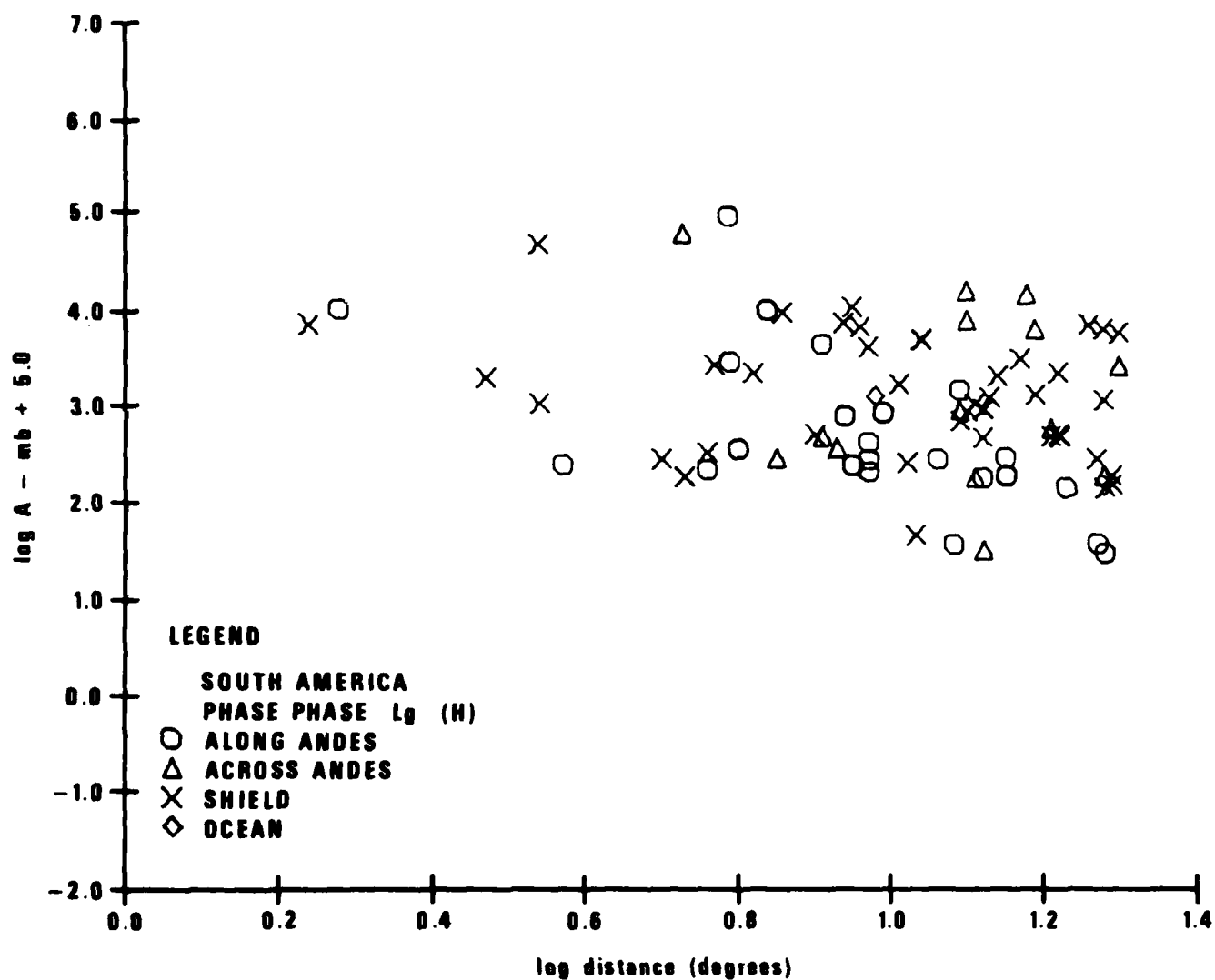
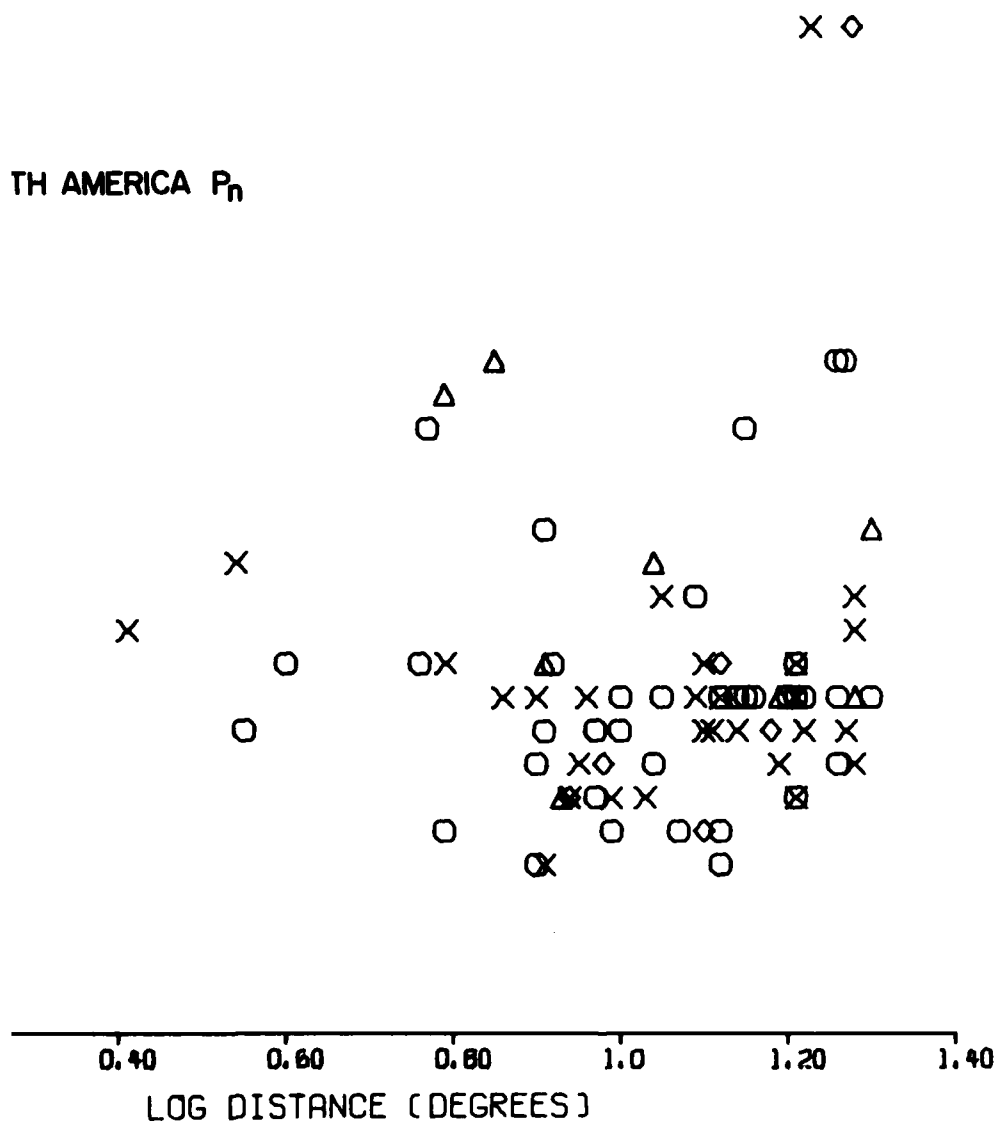


Figure 31. Trace amplitudes of L (horizontal component) in South America, plotted against epicentral distance. The trace amplitudes were normalized to that of an earthquake with $m_b = 5$. The various types of propagation paths are denoted by symbols shown in the legend.

TH AMERICA P_n



int periods of P_n in South America, plotted against
 utral distance for shallow earthquakes in the m_b range of
 .5. The various types of propagation paths are designated
 symbols shown in the legend.

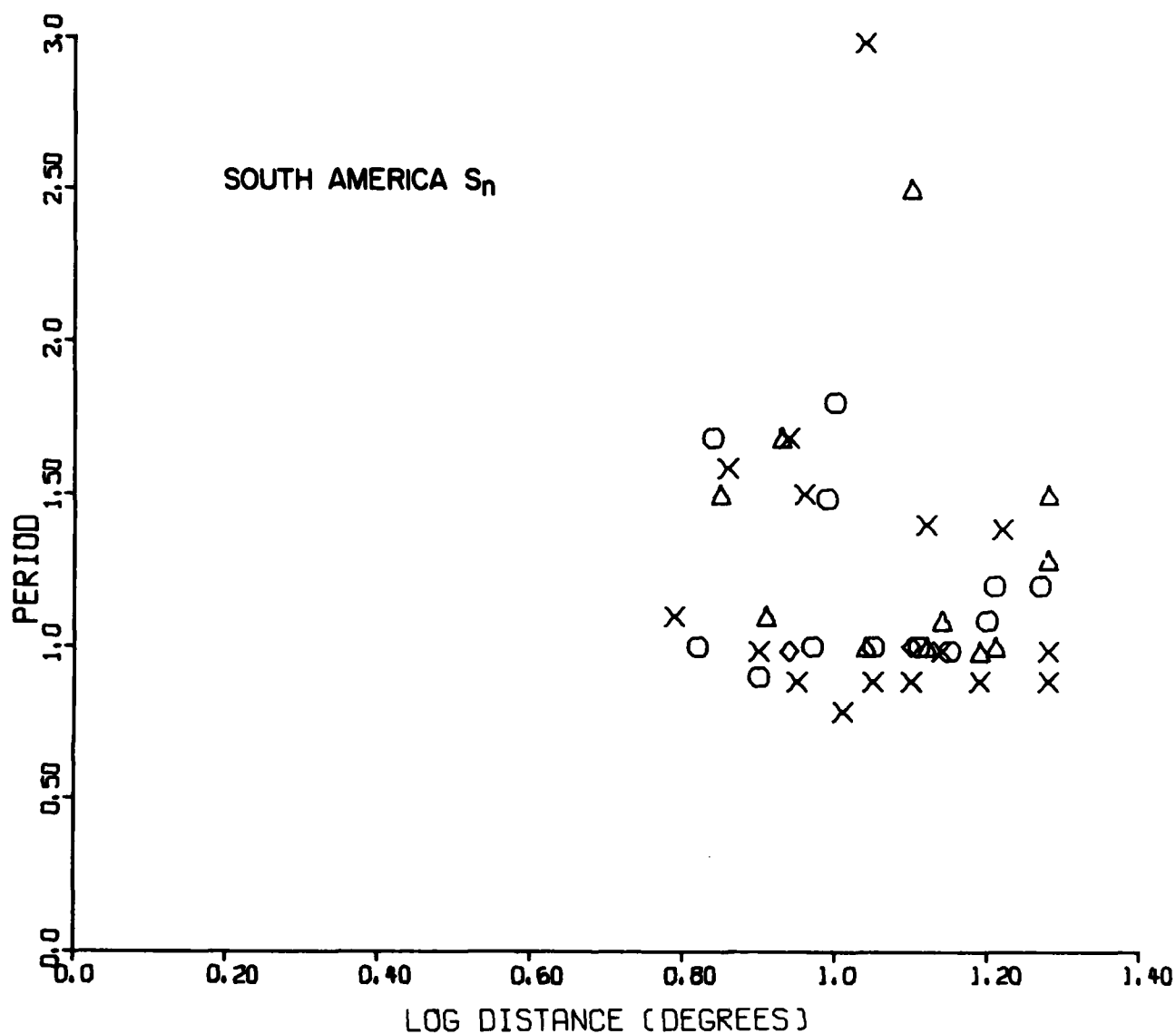


Figure 33. Dominant periods of S_n in South America, plotted against epicentral distance for shallow earthquakes in the m_b range 4.5-5.5. The various types of propagation paths are designated with symbols shown in the legend.

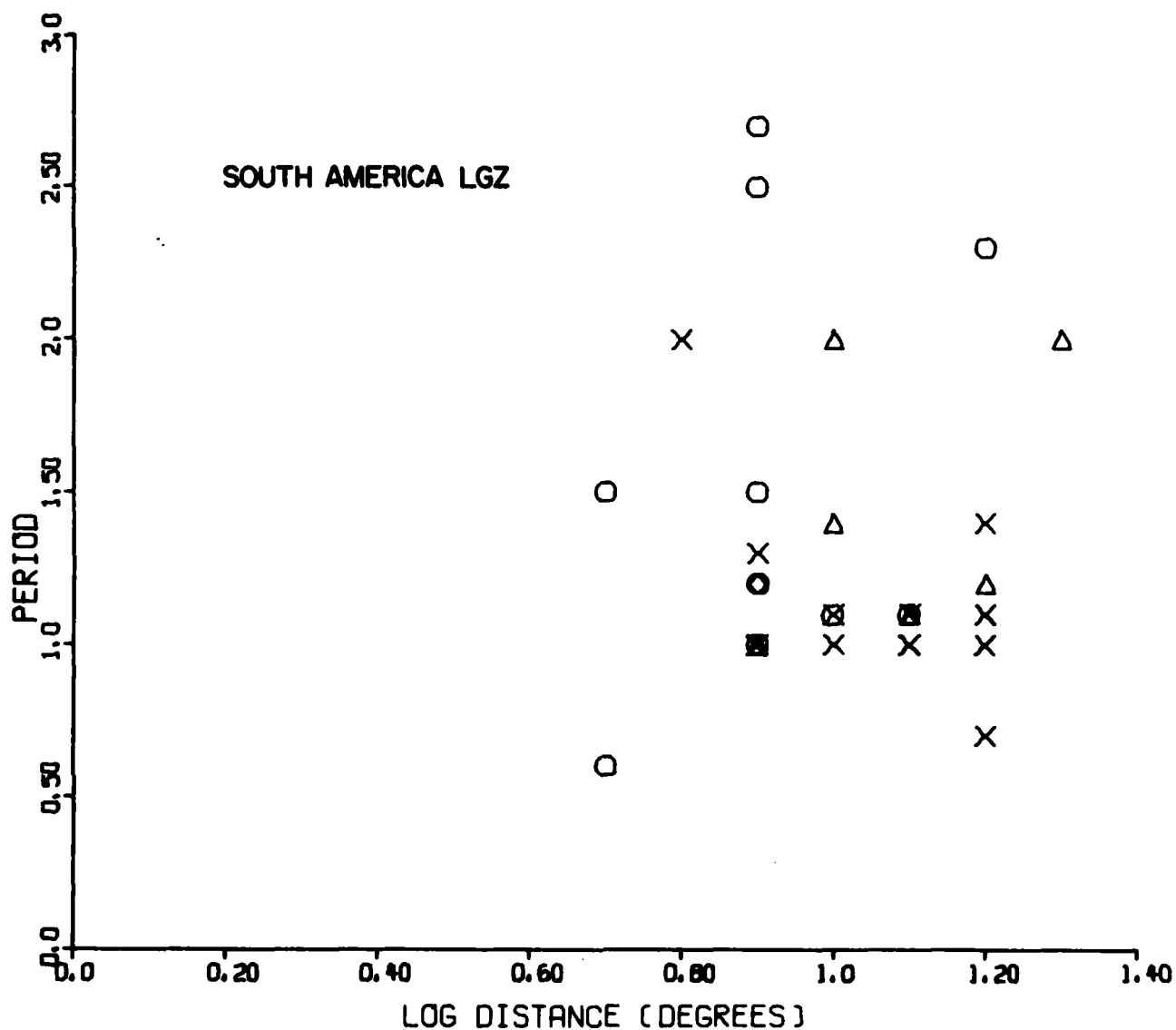


Figure 34. Dominant periods of L_v (vertical component) in South America, plotted against epicentral distance for shallow earthquakes in the m_b range 4.5-5.5. The various types of propagation paths are designated with symbols shown in the legend.

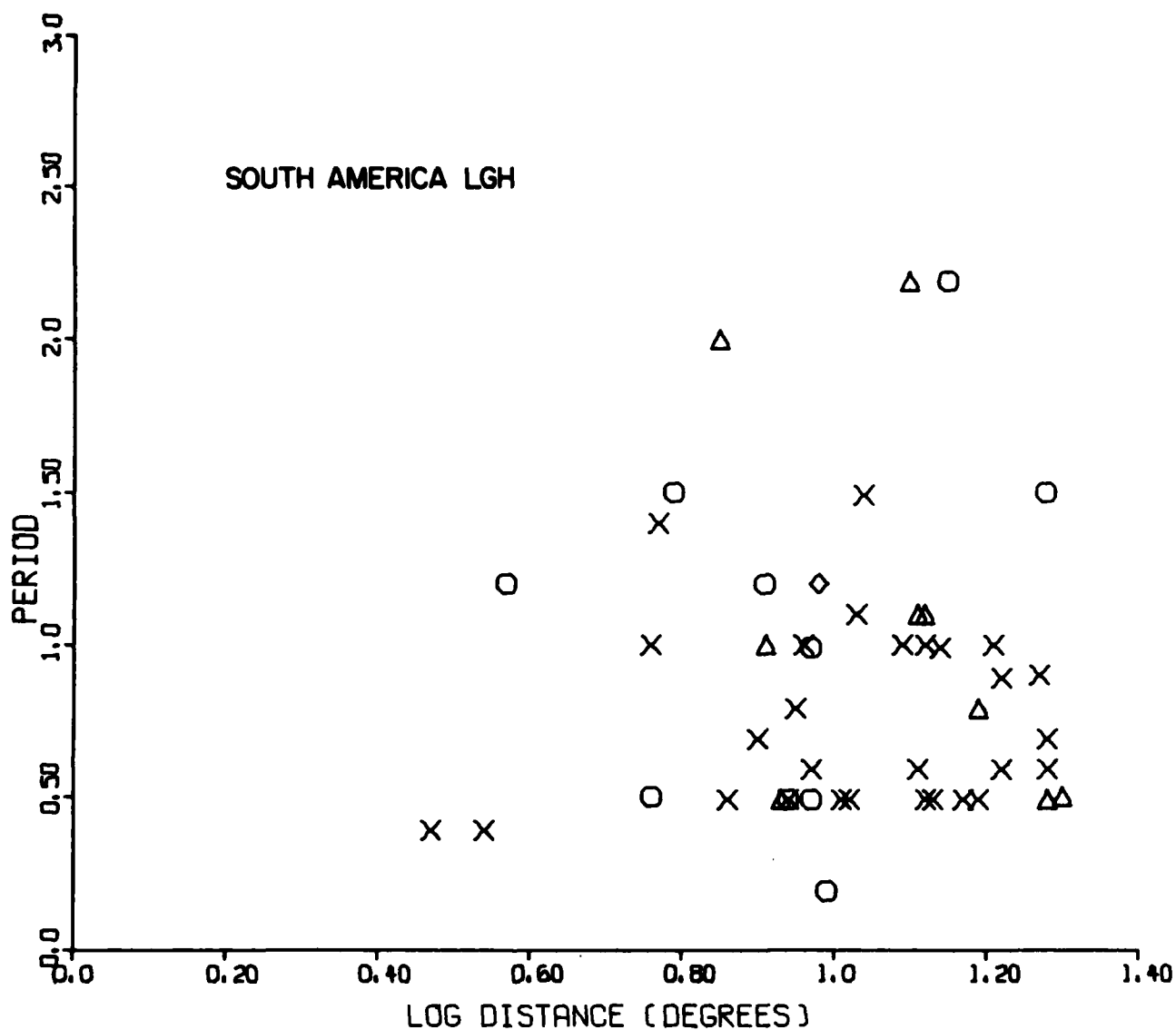


Figure 35. Dominant periods of L_g (horizontal component) in South America, plotted against epicentral distance for shallow earthquakes in the m_b range 4.5-5.5. The various types of propagation paths are designated with symbols shown in the legend.

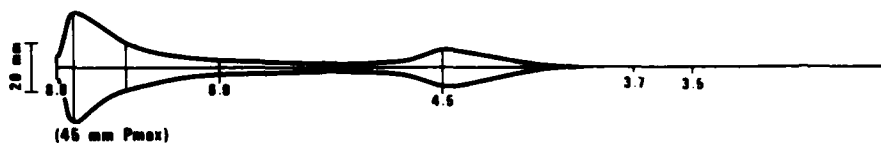
southern Africa. Due to the high degree of scatter, no clear dependence of period on distance is discernible on any of these paths. The plots do show, however, that the dominant periods of waves crossing the Andes mountains tend to be longer than those crossing the shield. In comparing the South American wave periods with those in southern Africa, one must remember that shield paths in South America often originate at earthquakes located in the mountains, while the sources of seismic waves in southern Africa are in the shield. Thus the greater scatter is not surprising for the South American data, assuming that even shield paths cross some of the attenuating mountain regions. The low relative amplitudes and longer periods of regional phases crossing the Andes mountain range is in agreement with the hypothesis that the tectonic, mountainous areas of South America are characterized by lower Q in the crust and upper mantle than the shield areas.

Seismograms with Unusual Characteristics

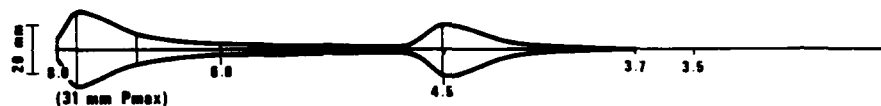
As we have mentioned earlier, regional phases recorded in South America along paths traversing the Andes display some very unusual characteristics (Chinn et al., 1980). Due to the diversity of propagation, the amplitude ratios of these regional phases are quite variable as opposed to those propagating in shields where there appears to be considerably more consistency. To illustrate the diversity in the relative balance of these regional phase amplitudes, we have, in Figure 36, assembled sketches of envelope shapes for some events in the manner of Chinn et al (1980). All possible regional phases, P_n , P_g , S_n and L_g are present only on a few seismograms. For the most part, one or several of these phases is missing, and the relative ratios of remaining phases varies. It is likely that some of the variability can be explained with mode theory, if the focal depth and the source depth and the source mechanisms of the events were adequately known, but much of the variability must be due to the changing effectiveness of

09 JAN 64 CORDOBA PROVINCE, ARGENTINA
11:47:45.0 $m_b = 4.3$ $h = 119$ km $\Delta = 15.2^\circ$

LZ-BV
SPZ - 164.0 K

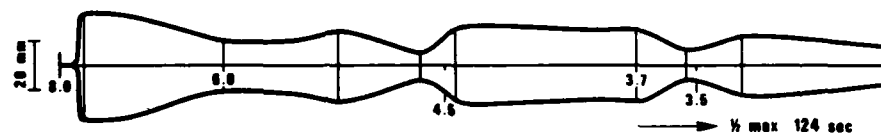


LZ-BV
SPT - 238.0 K

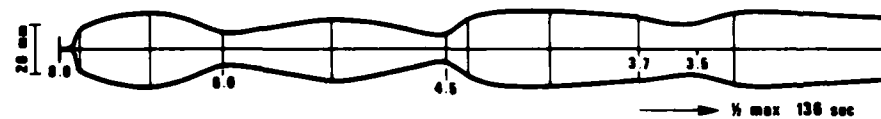


24 MAR 64 SANTA PROVINCE, ARGENTINA
11:57:08.2 $m_b = 4.4$ $h = 95$ km $\Delta = 9.0^\circ$

LZ-BV
SPZ - 215.0 K



LZ-BV
SPT - 277.0 K



25 MAR 64 SAN JUAN PROVINCE, ARGENTINA
08:57:21.7 $m_b = 4.2$ $h = 123$ km $\Delta = 15.3^\circ$

LZ-BV
SPZ - 216.0 K



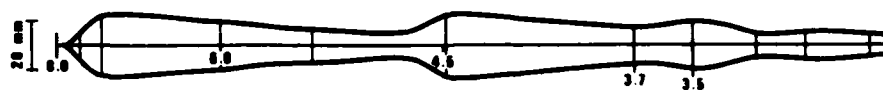
LZ-BV
SPT - 258.0 K



Figure 36. Sketches of regional seismogram envelope shapes for various paths.

27 MAY 64 JUV JUV PROVINCE, ARGENTINA
20:48:44.0 $m_b = 3.9$ $h = 94$ km $\Delta = 6.4^\circ$

LZ-BV
SPZ - 260.0 K



LZ-BV
SPT - 232.0 K



01 JUN 64 SANTIAGO DEL ESTERO
21:25:41.0 $m_b = 4.4$ $h = 41$ km $\Delta = 12.1^\circ$

LZ-BV
SPZ - 260.0 K

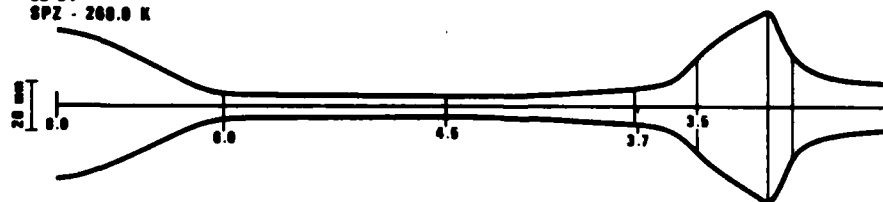


LZ-BV
SPT - 373.0 K



10 JUN 64 BR. GUIANA
03:56:10.5 $m_b = 4.5$ $h = 4.5$ km $\Delta = 10.6^\circ$

LZ-BV
SPZ - 200.0 K



LZ-BV
SPR - 204.0 K

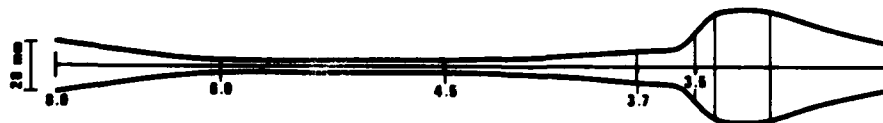


Figure 36 (cont.). Sketches of regional seismogram envelope shapes for various paths.

transmission of these regional phases. Some low L_g amplitudes are no doubt due to the larger source depth of some of the events.

In order to investigate the time-frequency structure of some of the regional seismograms, we band-pass filtered some recordings at La Paz, Bolivia. The 15 February 1979 event, Figure 37, begins gradually with a low amplitude P_n , and the amplitude of the wavetrain slowly increases through the expected arrival times of P_g , S_g-L_g (see unfiltered trace on top). Band-pass filter analysis reveals more structure in the signal. The bulk of the high frequency energy arrives with the P_n and S_n velocities although the arrival of S_n is not very clear on the unfiltered traces. There is a hint of a P_g wavetrain similar to those seen in the western United States on the band-pass filtered records in the 0.5-2 Hz band, and an S_g arrival may also be present.

Another event recorded on 23 January 1977, Figure 38, has a similar gradual buildup in amplitude, but the frequency-time structure is quite different: the amplitudes appear to change similarly in all bands. This is more in agreement with the interpretation of this wavetrain in terms of strong scattering given by Chinn et al (1980).

The 12 February 1979 event, Figure 39, shows a similar buildup of amplitudes following the P_n arrival, but it also shows hints of S_n on the high S_g arrival time at high frequencies, followed by the beginning of a presumably normal L_g wavetrain on the low frequency traces.

The above examples illustrate that the crude time domain analysis of unprocessed original traces employed in most of this report and in most of the literature, although it is a necessary first step, barely scratches the surface in promoting the understanding of the complex structure of regional seismograms. There is no adequate theoretical framework at present to interpret all the features of regional phases, although elements of it consisting of modal, ray and scattering theory exist.

SEIS/140
2000
15 FEB 79

O.T. = 13:43:00.0
BOLIVIA
 $\Delta = 5.8^\circ$

DEPTH = 30km
BACK AZIMUTH = 307°
 $m_b = 0.0$ (not determined)

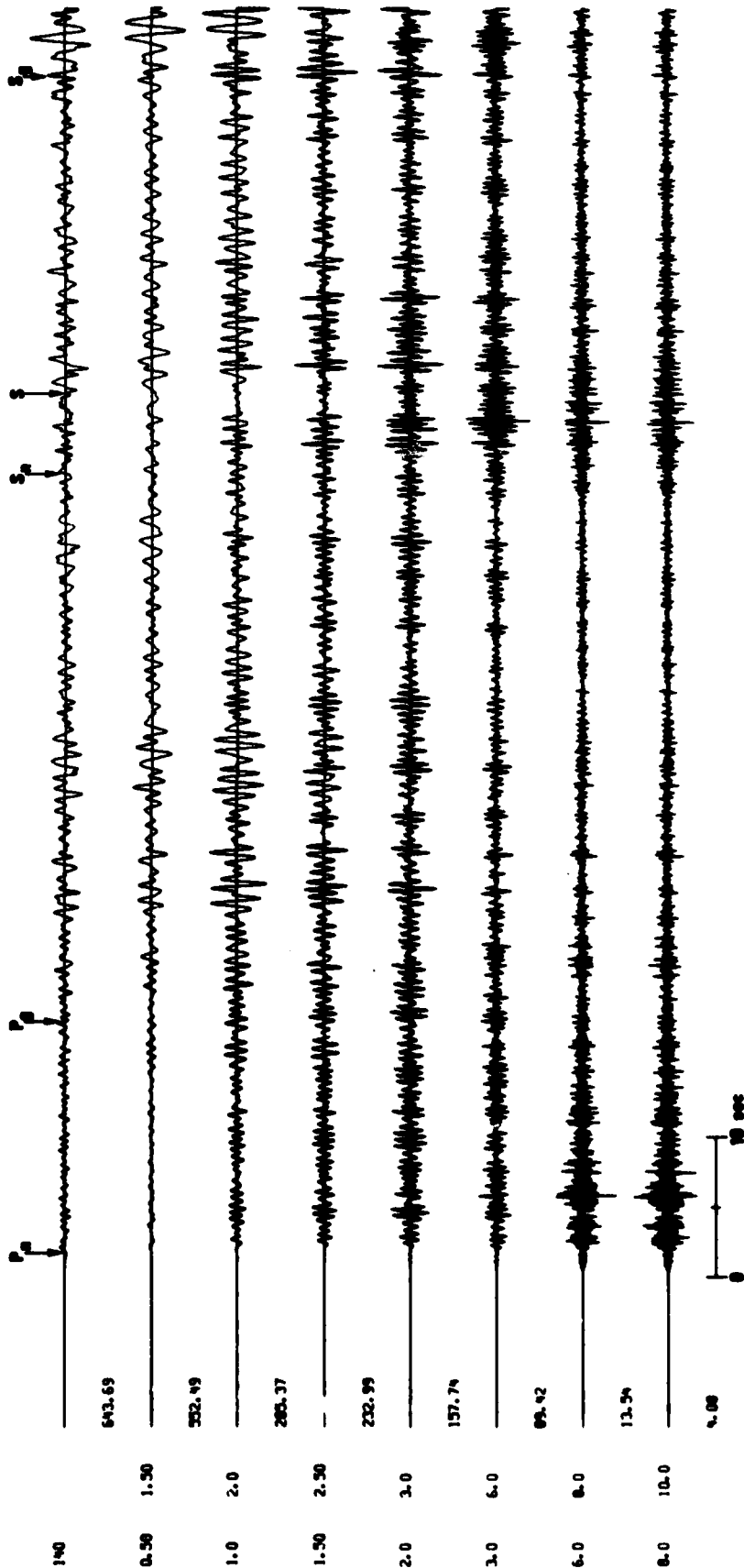


Figure 37. Band pass filtered vertical traces for the 15 February 1979 event observed in La Paz, Bolivia.

SEIS#20
2000
23 JAN 77

O.T. = 00:11:21.4
PERU
 $\Delta = 7.5^\circ$

DEPTH = 15km
BACK AZIMUTH = 307°
 $m_b = 4.88$

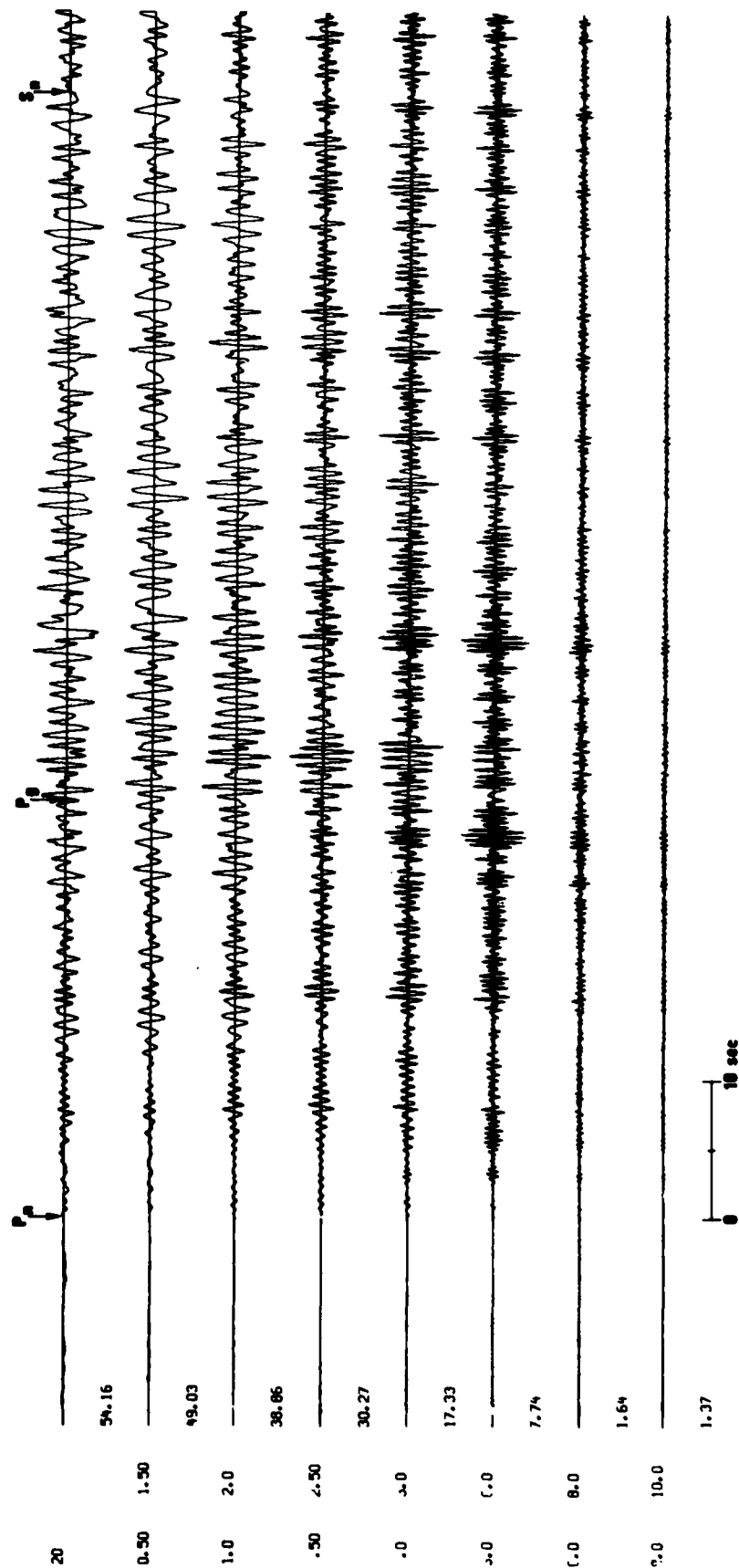


Figure 38. Band pass filtered vertical traces for the 23 January 1977 event observed in La Paz, Bolivia.

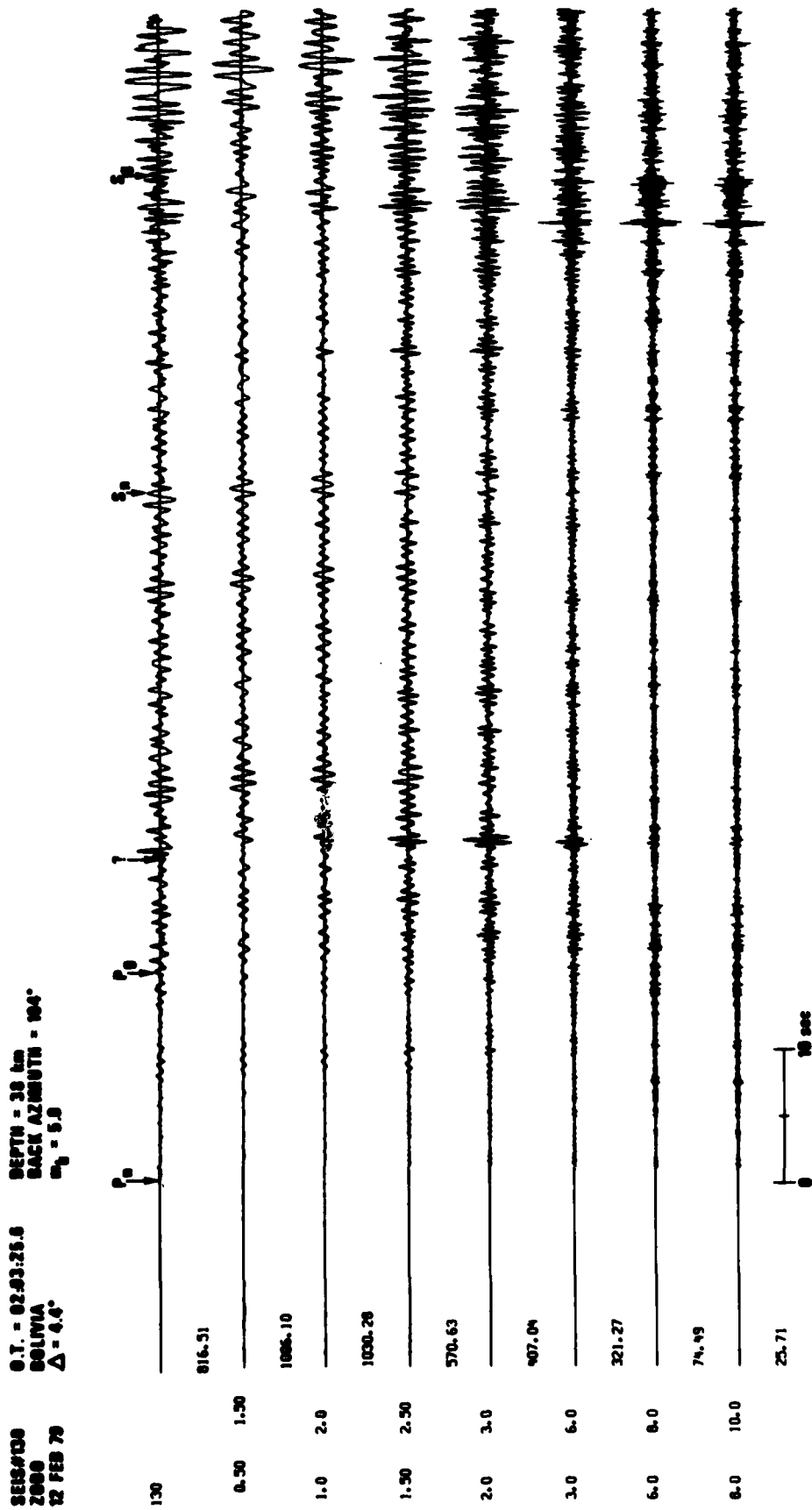


Figure 39. Band pass filtered vertical traces for the 12 February 1979 event.

PAKISTAN-INDIA REGION

Structural Setting

The area we examined includes Pakistan with the adjoining border regions of India, Afghanistan, Tibet, and Iran.

The tectonics and seismicity of the area are dominated by the collision of the Indian and Eurasian plates. The Himalayan, Hazara, and Salt ranges formed at the northern boundary of the Indian plate are characterized by folding and thrusting associated with the northward motion of the plate. Along the western edge of the Indian plate, in the Salaiman and Kirthar ranges, there is a left lateral component added to the folding and thrusting associated with the convergence.

Beyond the immediate regions of the colliding plate boundaries, the interior of the Eurasian plate is characterized by a complex deformation pattern that can be modelled by an indentation model of Taponnier and Molnar (1976,1977) and Molnar and Taponnier (1975). Great blocks of the Eurasian land mass separated by numerous strike-slip faults move laterally out of the way of the advancing Indian plate. As shown in Figure 40, such faults are the Chaman fault in Pakistan and Afghanistan, the Herat fault in Afghanistan and the Karokoram fault. Faults of similar nature in Tibet are the Altyn-Dagh and Kunlun faults.

The Pamir and Hindu Kush ranges are also part of the same complex deformation system. Most of the focal mechanisms in the Pamir area consist of thrust mechanisms associated with the Pamir thrust fault, but some events also show some left lateral motion in accordance with the indentation mechanism proposed by Taponnier and Molnar (1976). The Hindu Kush is a site of subduction with associated deep seismicity. The southern boundary of Pakistan and southeastern Iran is a plate boundary between the Eurasian and Arabian plates with active subduction of the oceanic portion of the Arabian plate under Eurasia. Further south, the Arabian plate contacts the Indian plate along the Murray-Ridge-Owen fracture zone boundary, with right lateral motion along the boundary.

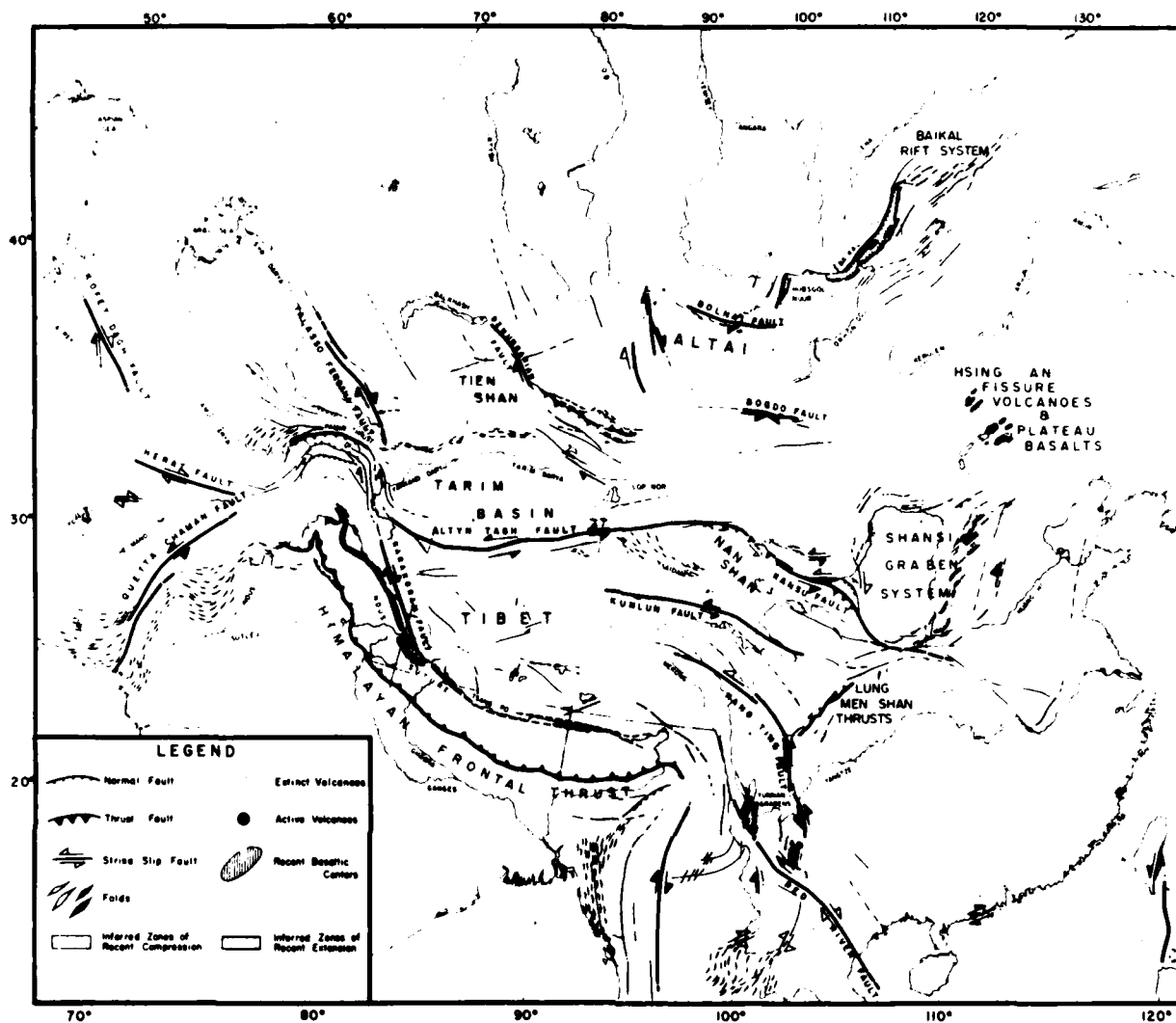


Figure 40. Simplified tectonic map of the region studied (after Tapponier and Molnar, 1979).

The area is highly seismic, and aside from the clear zone of seismicity along the northern boundary of the Indian plate, the seismicity is diffuse and spread over wide areas. The shield areas of India and eastern Pakistan are relatively aseismic. This can be seen in Figure 41, a seismicity map of the area. As mentioned before, the Hindu Kush region is the site of some intermediate to deep focus earthquakes while the rest of the region is characterized by shallow seismicity.

The above description shows that the area is extremely complex in structure and tectonic motion.

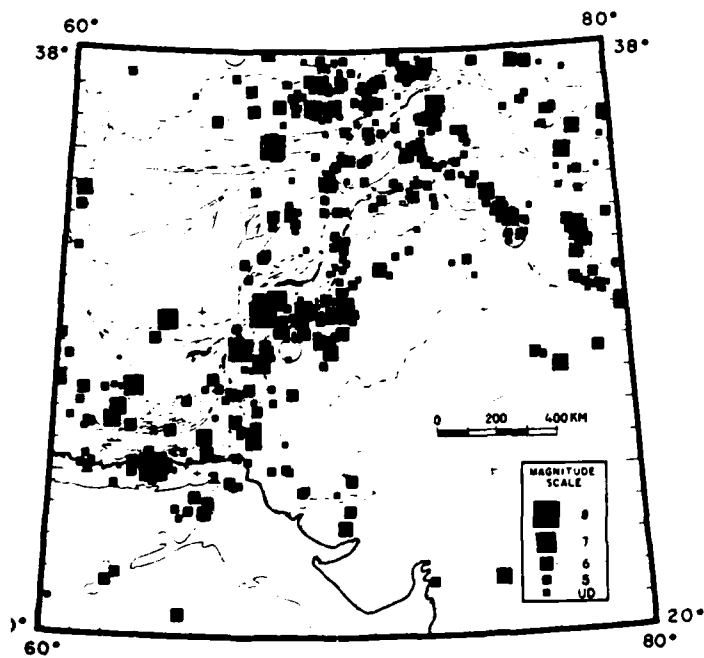
Efficiency of Propagation and Amplitude-Distance Relationships

Figure 43 shows the set of events used to obtain regional phase data for the Pakistan-India region. The events are listed in Table V. Also shown are the WWSSN receiving stations in the region. Efficiency maps for S_n and L_g were constructed from this data using criteria identical to those used for the South American data.

The efficiency map for S_n shown in Figure 44 indicates efficient propagation through the shield region and inefficient propagation through the eastern part of the Tibetan Plateau, while mixed efficient and inefficient paths dominate the rest of the area.

In their worldwide study of short-period S_n propagation, Molnar and Oliver presented some data for southern Asia including the India-Pakistan area. In Figure 42 we reproduce their map showing paths of efficient (solid lines) and inefficient (dashed lines) S_n propagation. The map shows efficient propagation in the Indian shield and inefficient propagation throughout most of Iran and Tibet. Their coverage is not very detailed and allows a number of interpretations as to the detailed location of blockage in S_n .

The efficiency map for L_g , Figure 45, shows a similar picture with respect to regional variations. There are only efficient paths through the shield, and there is an absence of L_g for paths crossing the eastern part of the Tibetan Plateau. The rest of the area is mixed with respect to efficiency, although there are quite a few paths along



Seismicity map of the Pakistan-India region (after Quittmayer and Jacob, 1979).

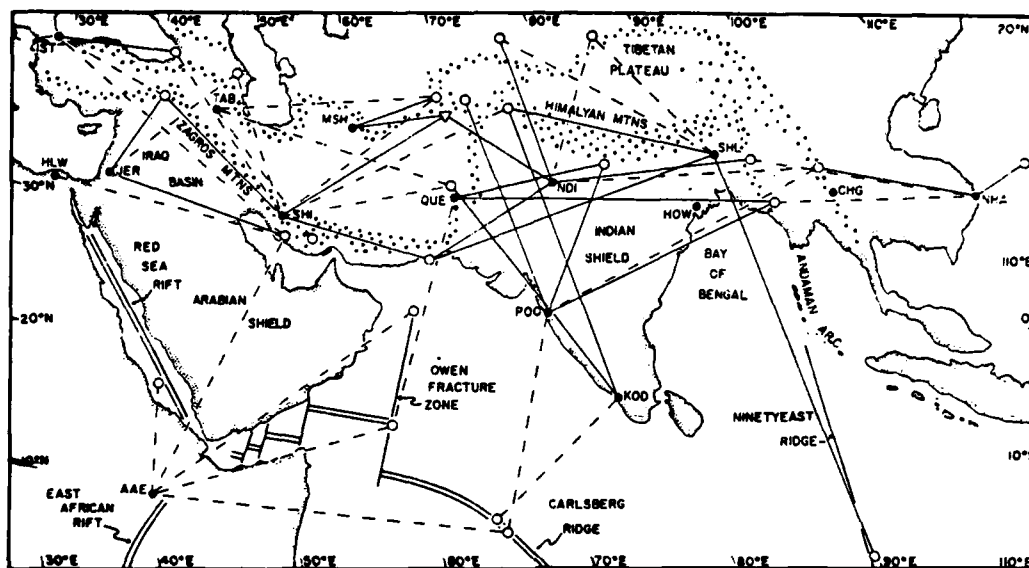


Figure 42. Efficiency of S_n propagation (after Molnar and Oliver, 1969).

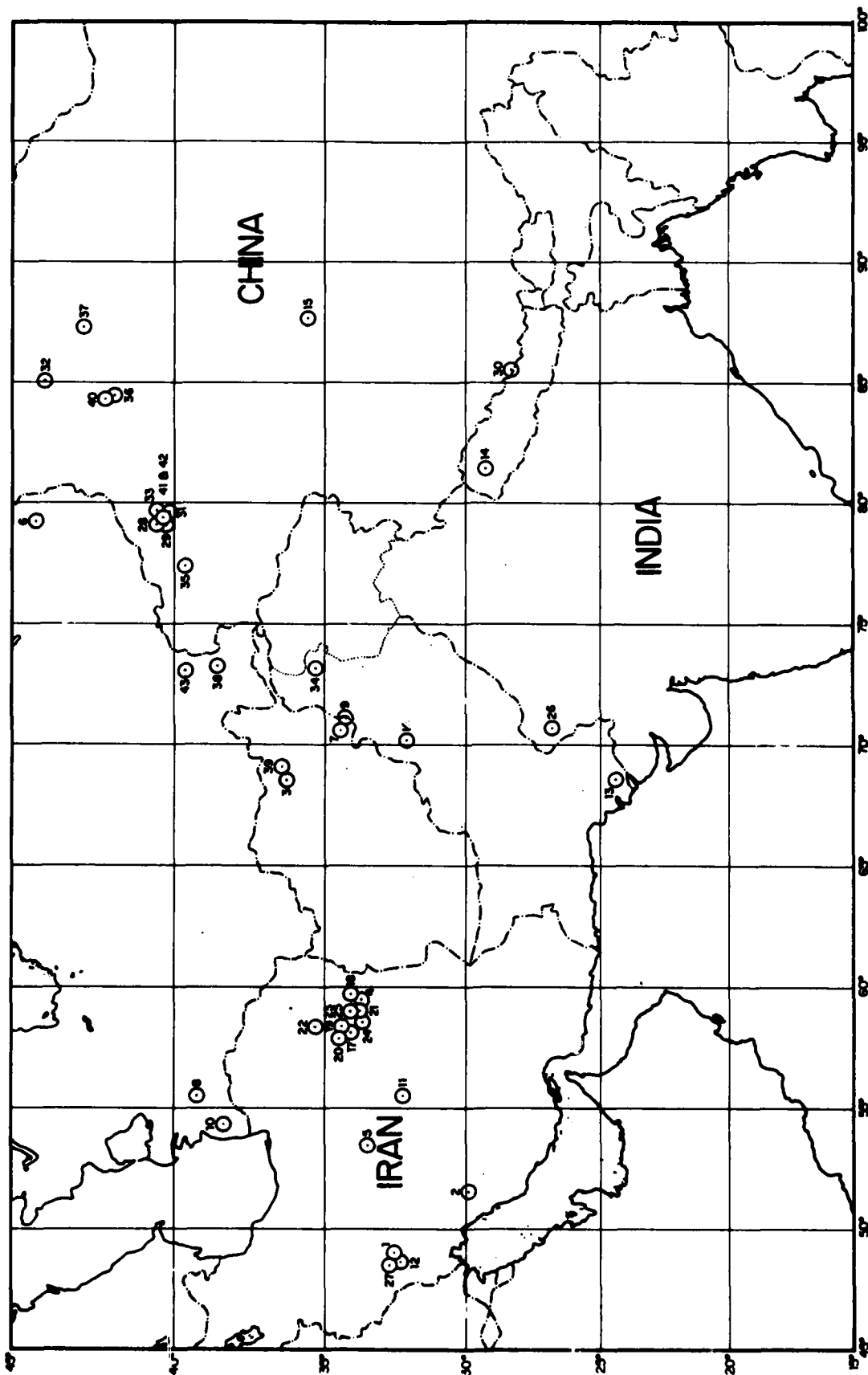


Figure 43. Map of events and WSSN stations used in this study.

TABLE V

NEIS Hypocenters for Earthquakes in the Pakistan/India Region.

<u>Date</u>	<u>Origin Time</u>	<u>Lat</u>	<u>Lon</u>	<u>Depth</u>	<u>Mag</u>
641110	15 47 49.3	32.6N	49.10E	28	5.3
680701	23 42 21.0	29.9N	51.55E	33	4.7
680715	01 25 36.0	36.2N	68.42E	35	4.1
680911	19 17 12.9	33.88N	59.41E	33	5.2
740510	13 47 02.7	35.5N	53.50E	-	4.4
680701	19 14 52.4	44.18N	79.29E	9	4.5
680704	09 23 12.0	34.65N	70.73E	33	-
680714	23 34 38.1	39.10N	55.71E	46	-
680628	19 39 50.2	34.59N	70.83E	28	4.5
691124	15 44 18.0	38.50N	54.44E	-	5.0
650604	18 40 58.0	32.40N	55.50E	18	4.8
660731	12 31 26.7	32.40N	48.80E	11	4.4
660527	22 14 13.7	24.40N	68.70E	5	5.1
670311	18 45 44.5	29.32N	81.41E	33	4.8
670707	23 49 23.5	35.50N	87.80E	33	-
680726	20 48 03.2	32.07N	70.07E	35	4.8
680901	07 27 30.2	34.03N	58.22E	15	5.9
680901	11 04 02.1	34.02N	59.04E	33	4.8
680901	19 16 37.3	34.23N	58.25E	23	5.0
680901	21 16 44.7	34.40N	58.03E	44	4.8
680903	09 53 47.0	33.84N	59.22E	16	5.0
680904	05 54 08.3	35.11N	58.54E	33	4.7
680904	08 08 44.3	33.92N	59.23E	24	5.0
680904	11 19 35.6	33.80N	59.08E	25	5.1
680904	23 24 47.2	33.99N	58.23E	15	5.4
740518	02 34 55.3	26.95N	71.70E	-	5.0
680715	08 33 37.5	32.54N	48.741E	33	4.6
710323	09 52 12.3	41.5N	79.26E	33	5.7
710331	20 47 17.4	41.4N	79.25E	33	6.0
710606	10 34 49.0	28.1N	85.63E	33	4.9
710617	15 20 12.0	41.32N	79.39E	33	4.9
711101	05 29 57.2	44.0N	85.0E	33	5.0
711212	13 41 39.8	41.4N	79.24E	33	4.7
711227	20 59 34.1	35.1N	73.12E	10	5.4
711230	23 35 27.6	39.7N	77.45E	33	4.9
720102	10 27 34.9	41.80N	84.47E	33	-
720324	08 11 52.8	42.90N	87.43E	33	5.0
711124	08 23 24.6	38.40N	73.35E	33	5.1
720624	21 17 58.3	36.40N	69.40E	33	4.6
720420	00 35 56.7	42.0N	84.58E	33	5.1
710323	09 52 12.3	41.5N	79.26E	33	5.7
710303	20 47 17.4	41.4N	79.25E	33	6.0
711212	22 27 41.1	39.5N	73.22E	33	4.8

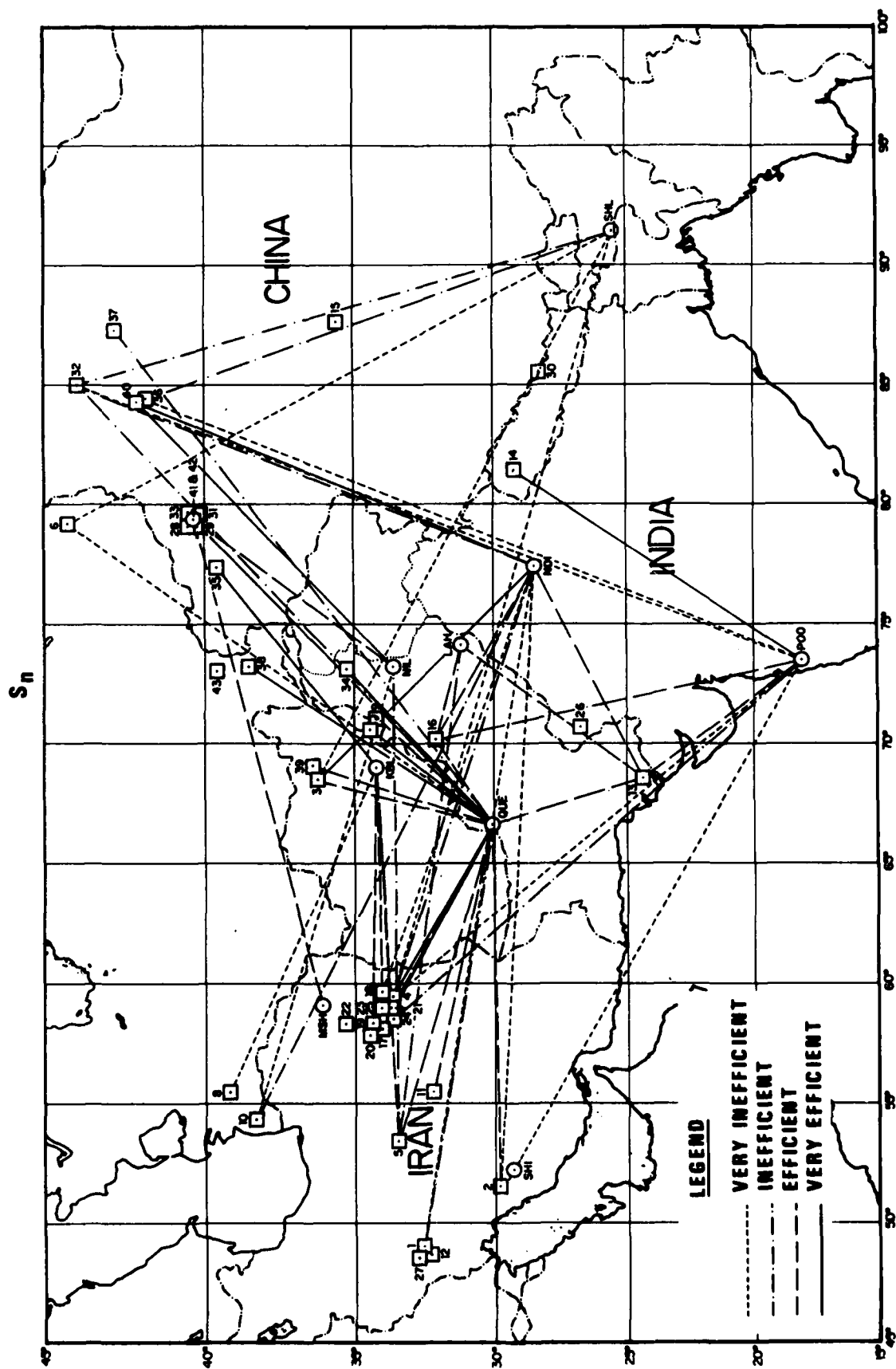


Figure 44. Efficiency map of S_n determined in this study.

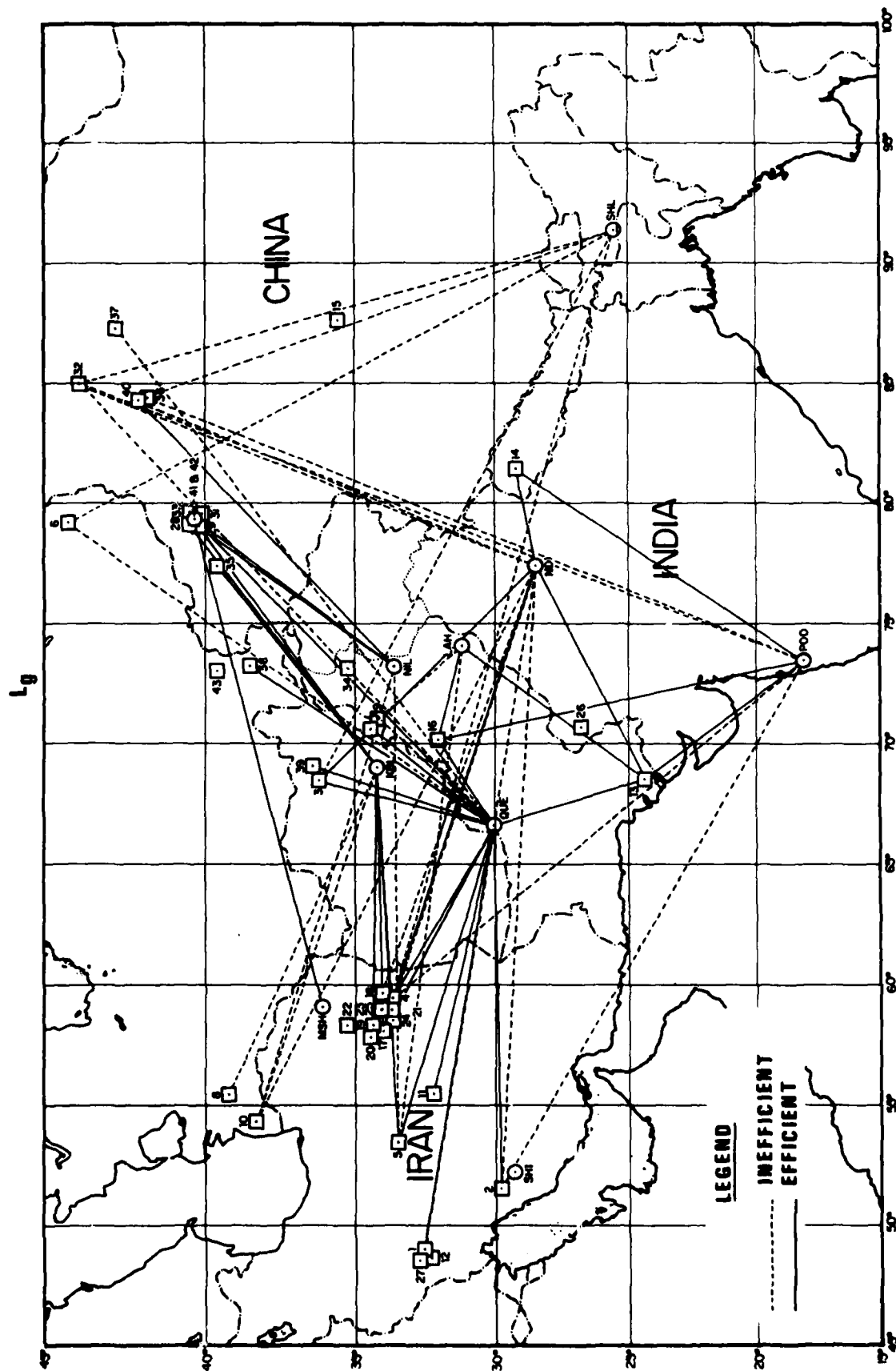


Figure 45. Efficiency of propagation for L_g .

which L_g propagates very efficiently. These findings are similar to those of Ruzaikin et al (1977).

The variability of the efficiency of propagation exhibited by the S_n and L_g phases is very unfavorable to the reliable detection, magnitude estimation and discrimination of events in tectonically complex areas such as the mountainous regions of the western part of the Pakistan area or the Andes mountains of South America. In such areas one cannot depend on the detectability of these regional phases. The solution to this problem may be found in mapping in fine detail the geological features that block the various phases, but the feasibility of this is doubtful. The features causing the blockage may be too small, and some energy may in some cases go around them by diffraction or alternate non-minimum time paths. On the other hand, in shield areas it is probably feasible to determine formulas for yield estimation and discrimination.

The normalized logarithmic amplitude-distance plots for P_n , P_g , S_n and L_g phases in the Pakistan area are shown in Figures 46 to 50. Circles designate paths through shield areas, including paths that start from the mountains but propagate predominantly through the shield, and squares designate those that have a significant portion of the path through the mountainous regions outside the shield.

The plot of P_n data, Figure 46, shows a fairly tight grouping of the points through the shield paths, a feature not dissimilar to that for southern Africa. The P_n from the mountain type paths scatter more and are somewhat below those from the shield. This may indicate some attenuation of P_n in mountainous areas, a finding that is not unexpected.

The plot for P_g , Figure 47, has only paths for mountainous regions. This agrees with Nuttli's (1979) observation that P_g is present in tectonic areas of southern Asia with appreciable amplitudes. P_g is not a prominent phase in shields and stable platforms, the EUS

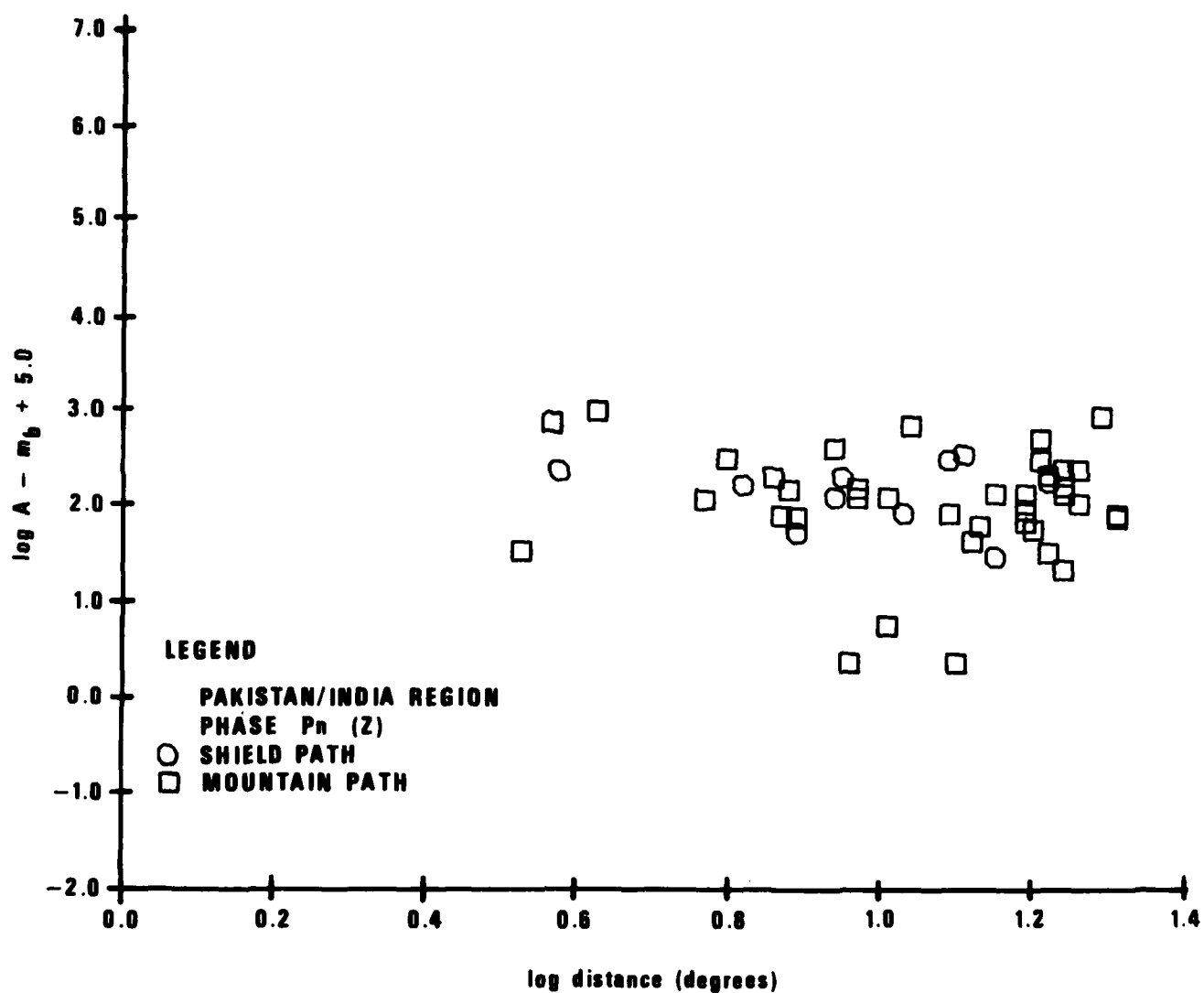


Figure 46. Trace amplitudes of P_n in the Pakistan-India region plotted against epicentral distance. The trace amplitudes were normalized to that of an earthquake with m_b = 5. Various symbols explained in the legend denote various types of propagation paths.

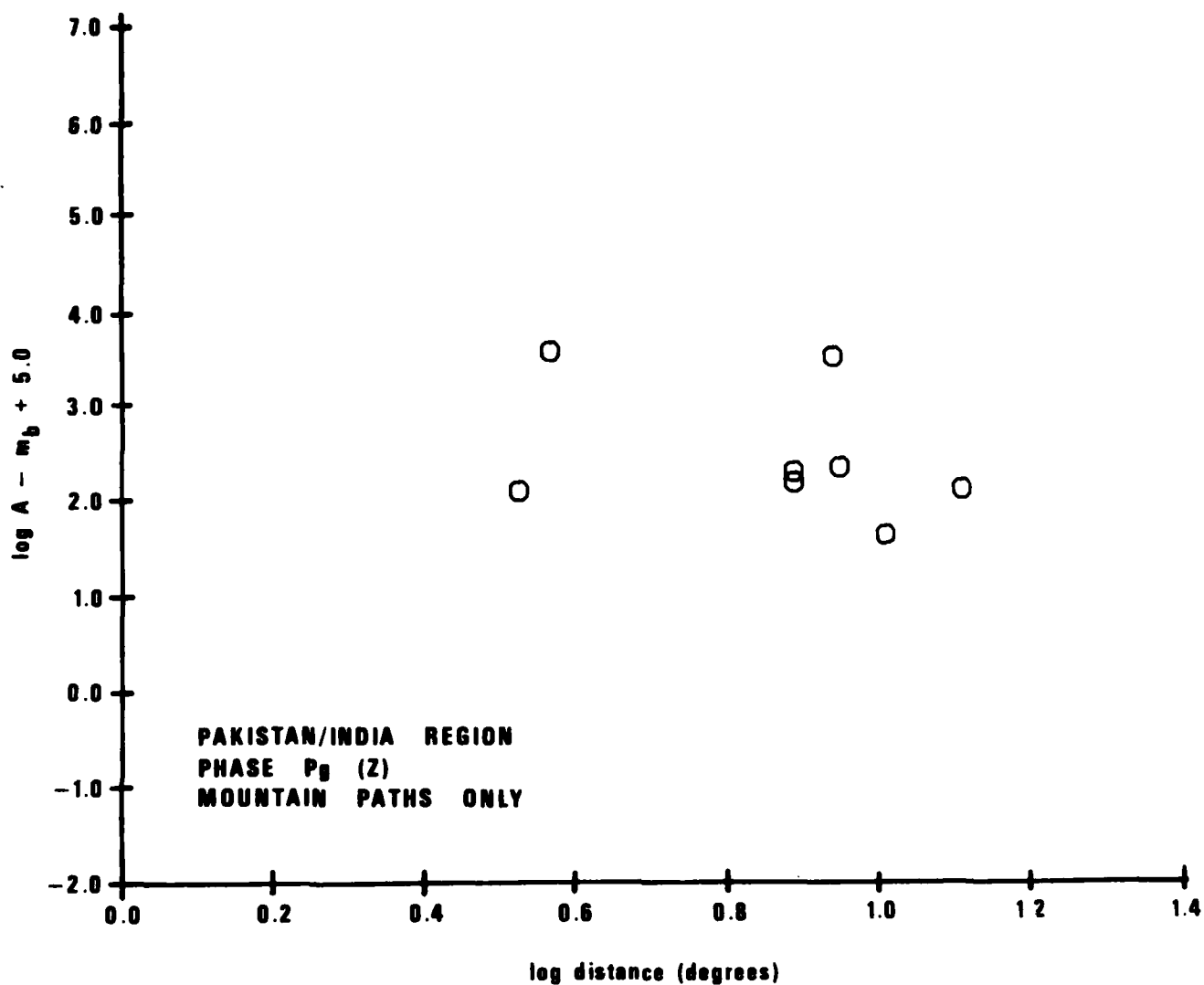


Figure 47. Trace amplitudes of P_g in the Pakistan-India region plotted against epicentral distance. The trace amplitudes were normalized to that of an earthquake with $m_b = 5$. Various symbols explained in the legend denote various types of propagation paths.

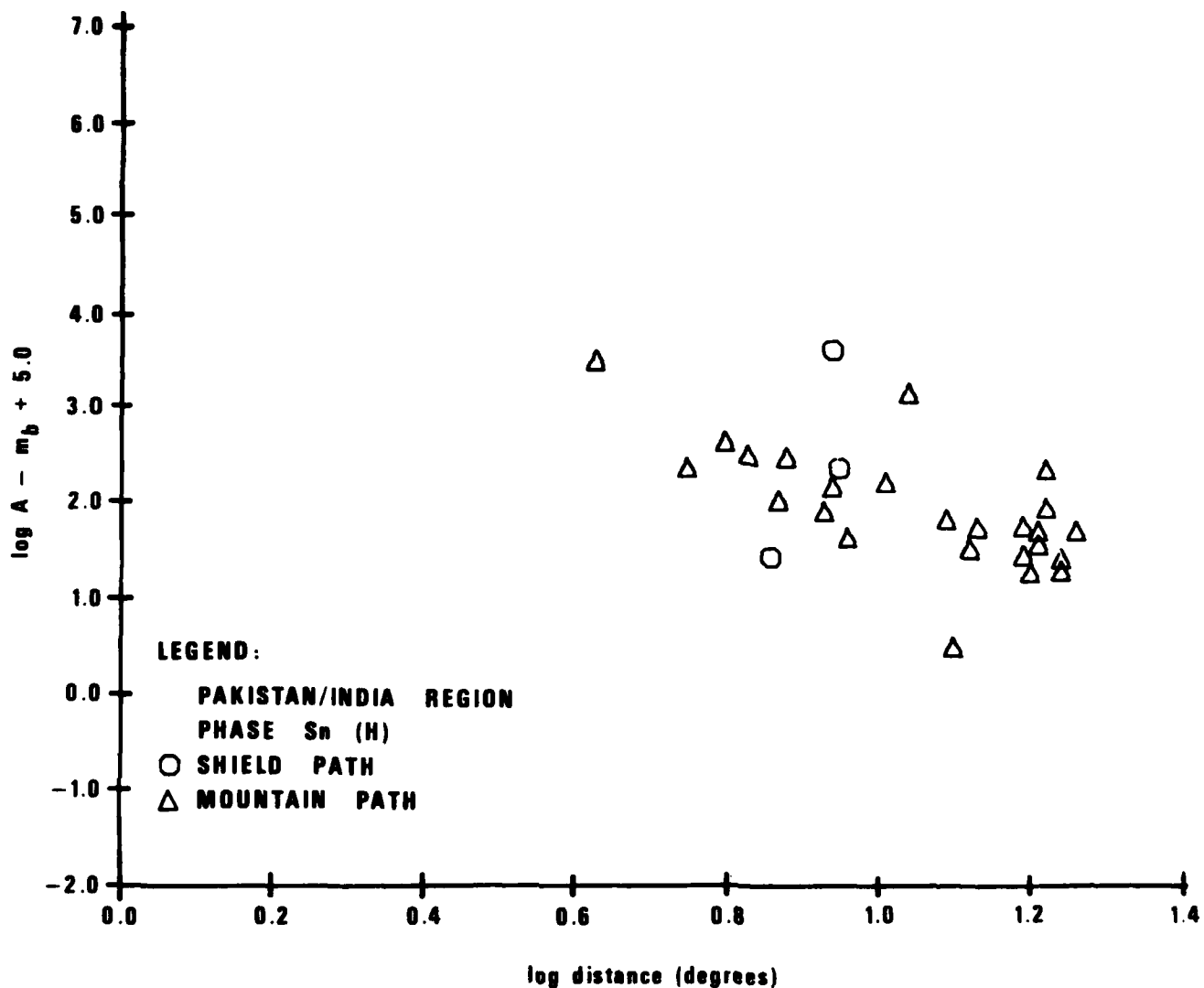


Figure 48. Trace amplitudes of S_n in the Pakistan-India region plotted against epicentral distance. The trace amplitudes were normalized to that of an earthquake with $m_b = 5$. Various symbols explained in the legend denote various types of propagation paths.

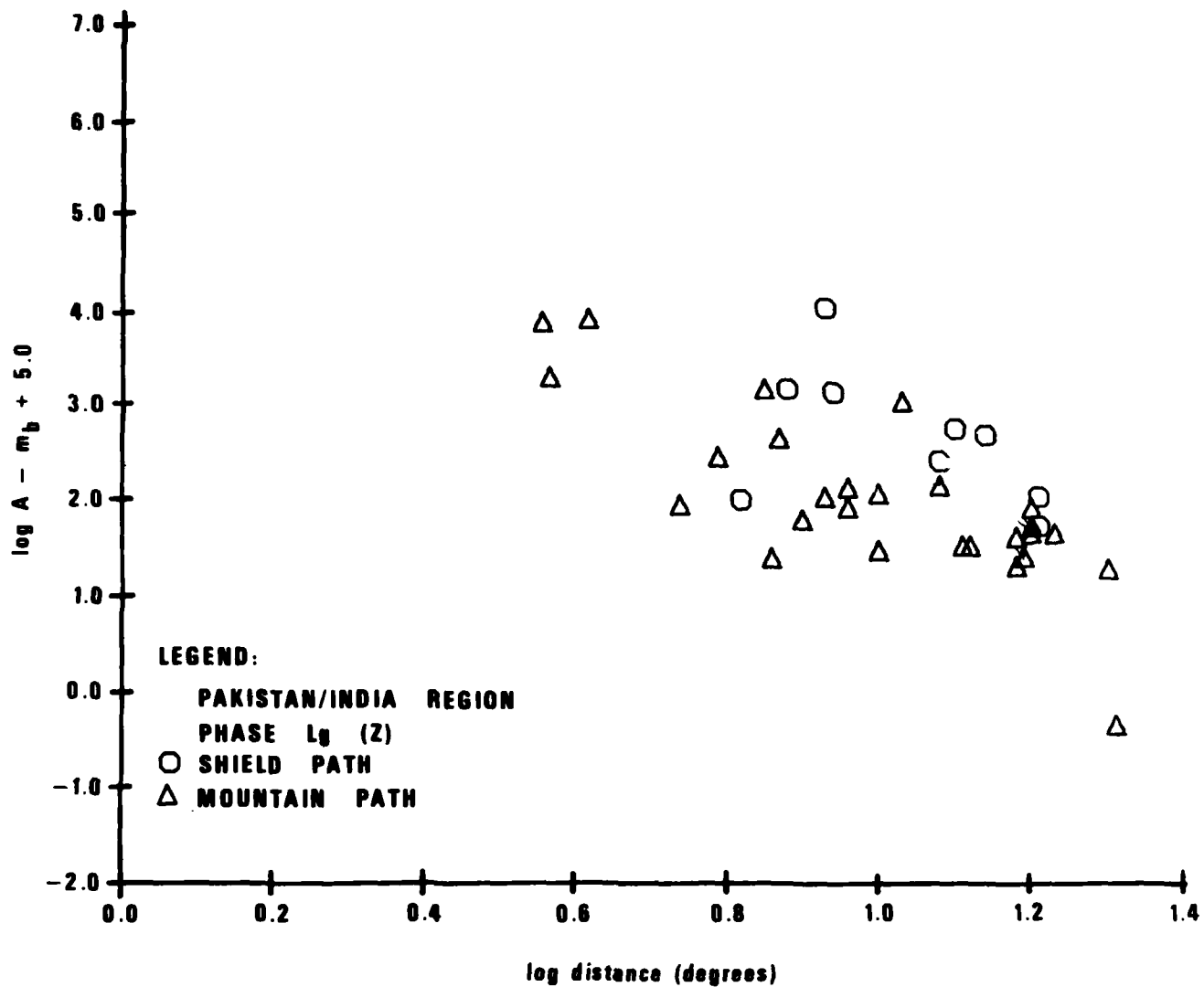


Figure 49. Trace amplitudes of L_g (vertical component) in the Pakistan-India region plotted against epicentral distance. The trace amplitudes were normalized to that of an earthquake with $m_b = 5$. Various symbols explained in the legend denote various types of propagation paths.

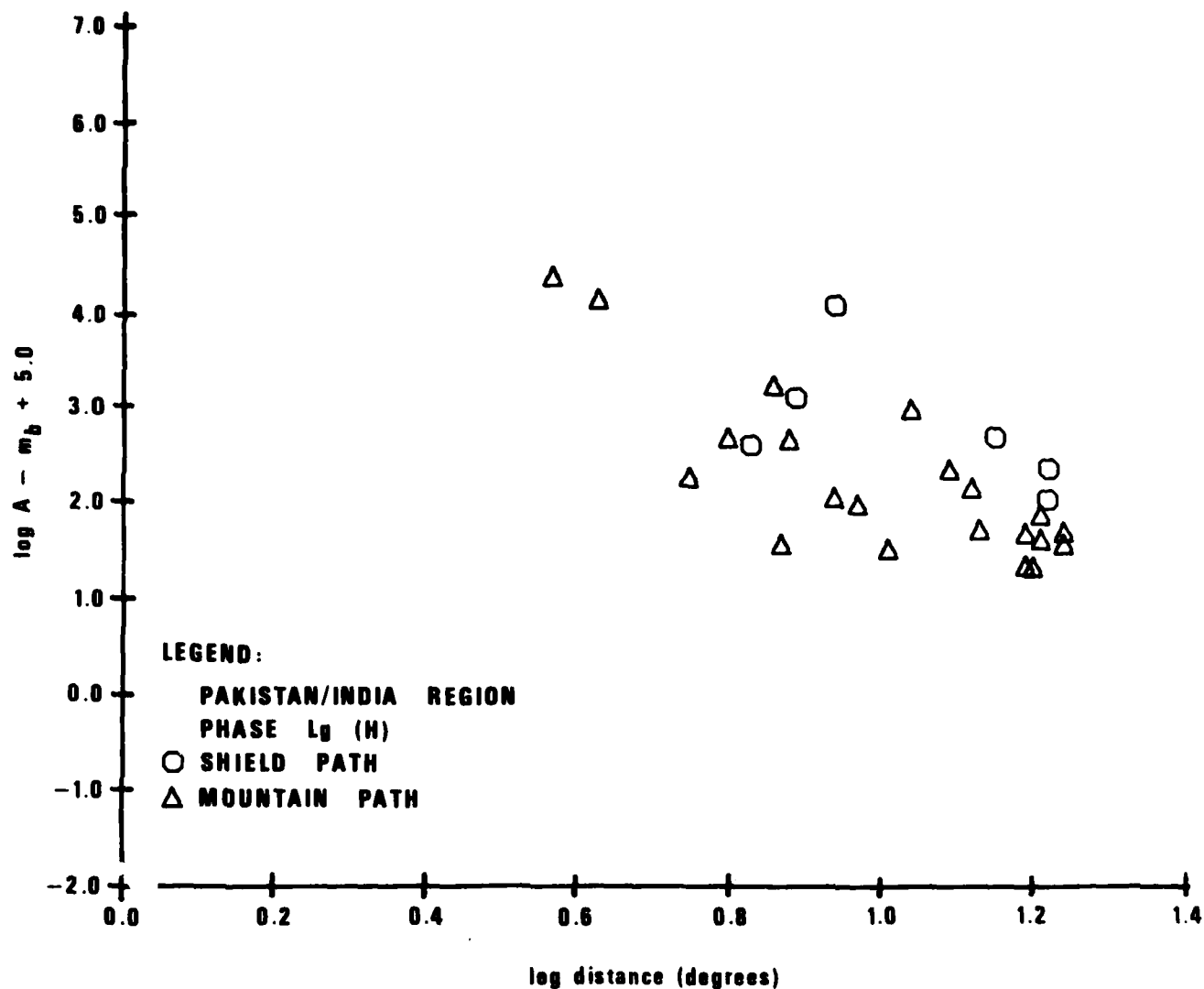


Figure 50. Trace amplitudes of L_g (horizontal component) in the Pakistan-India region plotted against epicentral distance. The trace amplitudes were normalized to that of an earthquake with $m_b = 5$. Various symbols explained in the legend denote various types of propagation paths.

being a prominent example. The S_n data in Figure 48 are sparse and do not group tightly.

The plots for the vertical and horizontal components of L_g in Figures 49 and 50 respectively show a tendency for the mountain paths to have lower amplitudes. This indicates higher attenuation for L_g across the mountainous areas. The plots of dominant periods of various regional phases are shown in Figures 51 to 55. The range of event body wave magnitudes for this data set is 4.5-5.5. The plot for P_n , Figure 51, shows no recognizable trend in dominant periods versus distance along shield paths. Along "mountain" paths, however, there is a slight trend toward longer periods as the epicentral distance increases. The plot for P_g , Figure 52, is unfortunately too scattered to draw any conclusions. The same can be said about the plot for S_n , Figure 53, although there appears to be an increasing trend there. For P_g we have only mountain paths. For the vertical and horizontal components of L_g , Figures 54 and 55, no trend can be discerned for the shield paths because of the scarcity of the data, but there is a strong increase in the dominant periods of L_g with distance for mountain paths.

Considering both amplitudes and dominant periods for the Pakistan-India area, these data are consistent with the hypothesis that whereas shield areas have small attenuation for regional phases, the "mountain" areas are characterized by a faster decrease of regional phase amplitudes with distance that is also accompanied by a marked increase of dominant periods of most phases. These facts are consistent with the assumption of lower Q in the crust and upper mantle of the mountain regions in the area.

THE SOUTHWESTERN UNITED STATES

Structural Setting

The part of the U.S. we studied is commonly subdivided into five major geological provinces, which are outlined in Figure 56. The

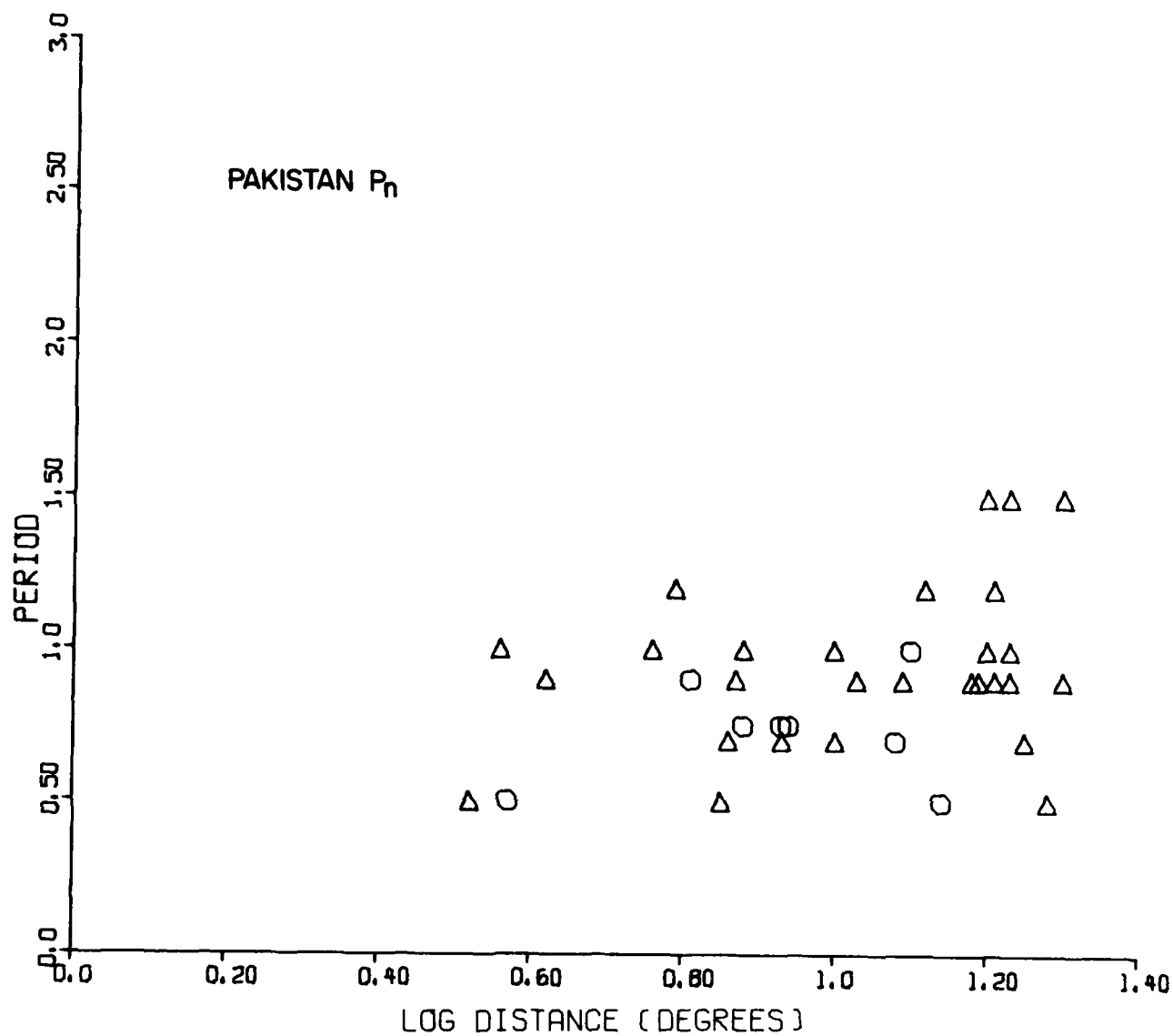
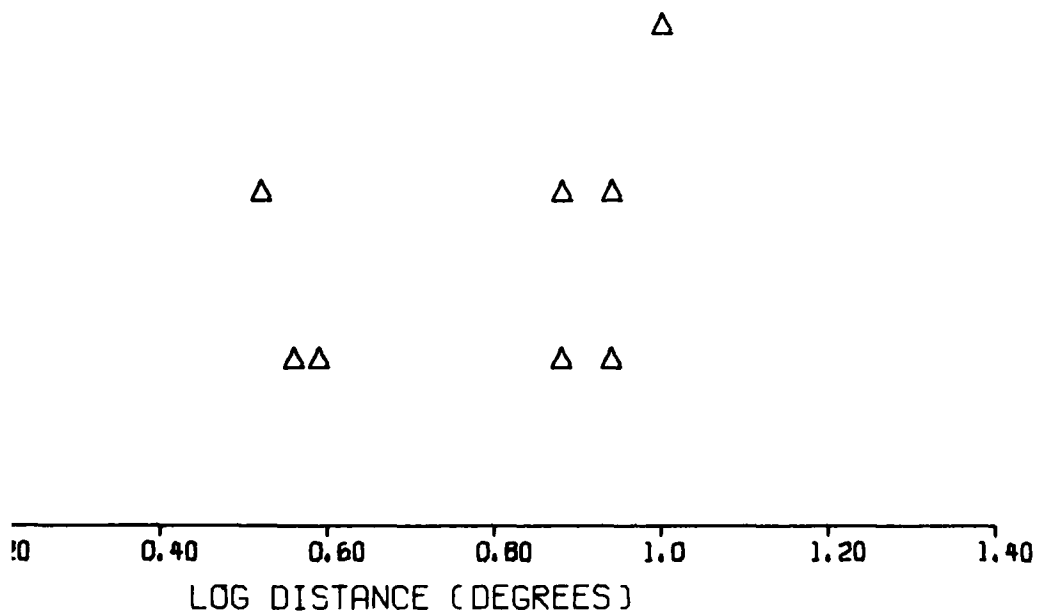


Figure 51. Dominant periods of P_n waves from shallow earthquakes in the m_b range 4.5-5.5, plotted against epicentral distance.

PAKISTAN P_g



inant periods of P_g waves from shallow earthquakes in the m_b range 4.5-5.5, plotted against epicentral distance.

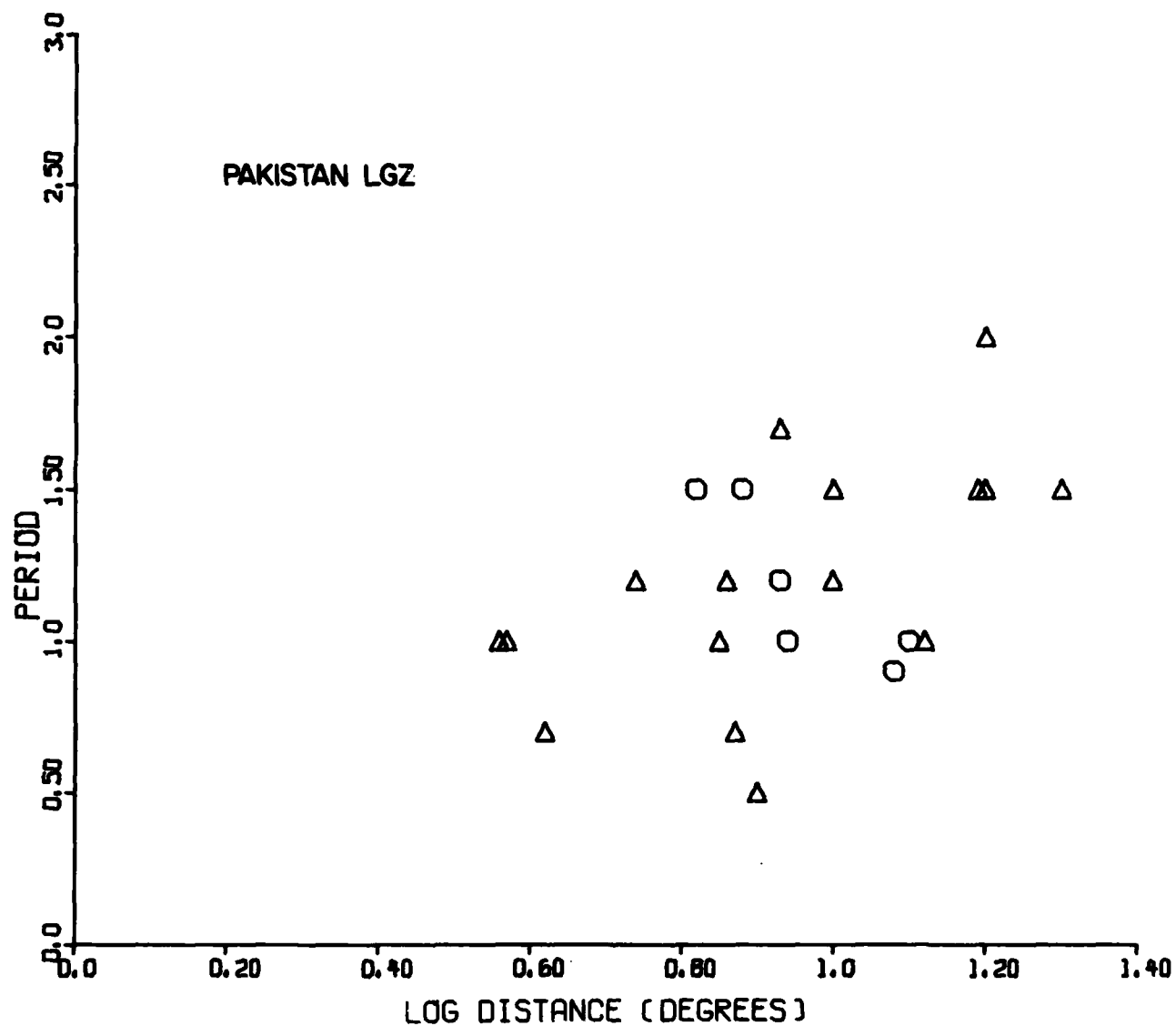


Figure 54. Dominant periods of L_v (vertical component) waves from shallow earthquakes in the m_b range 4.5-5.5, plotted against epicentral distance.

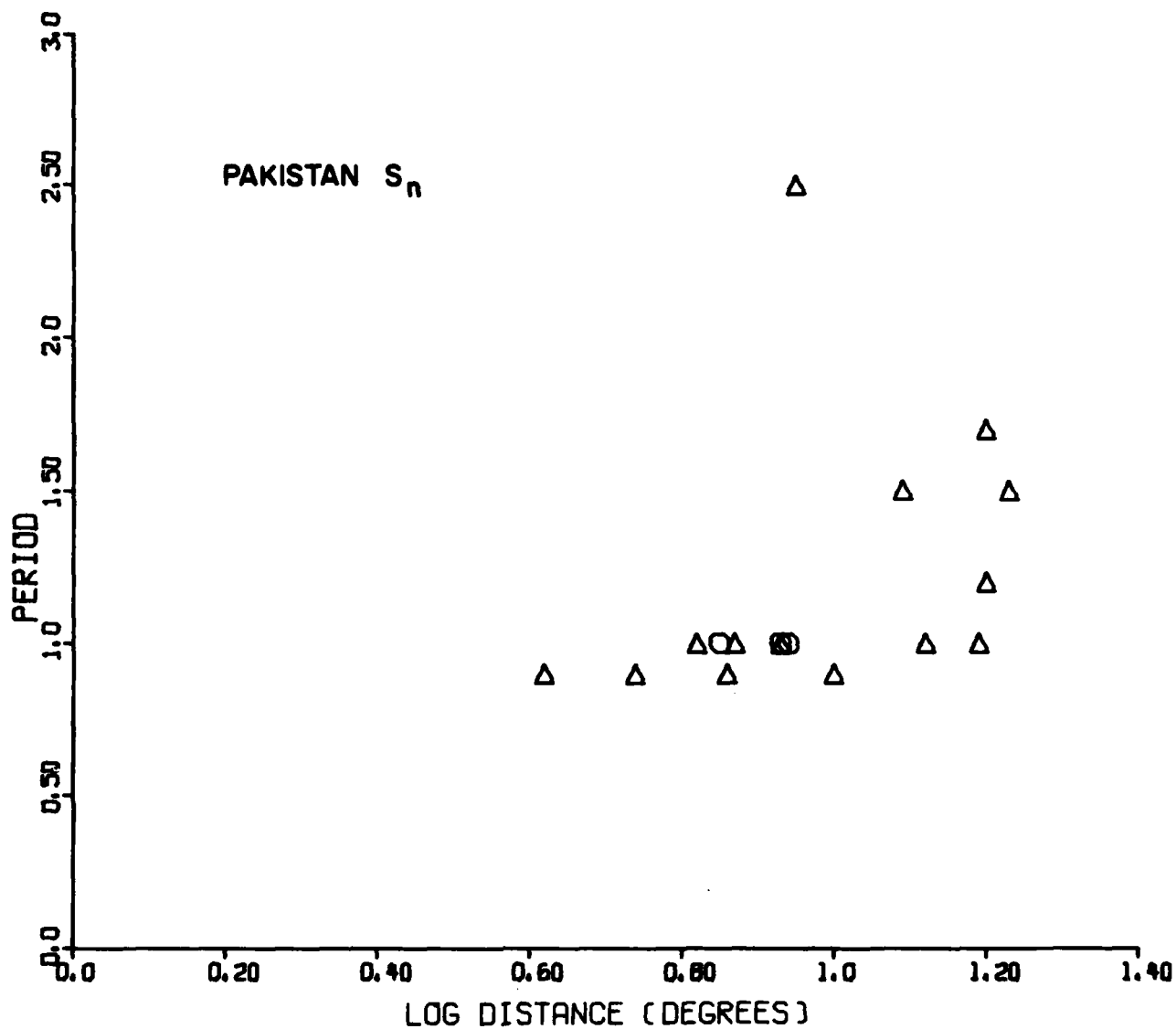


Figure 53. Dominant periods of S_n waves from shallow earthquakes in the m_b range 4.5-5.5, plotted against epicentral distance.

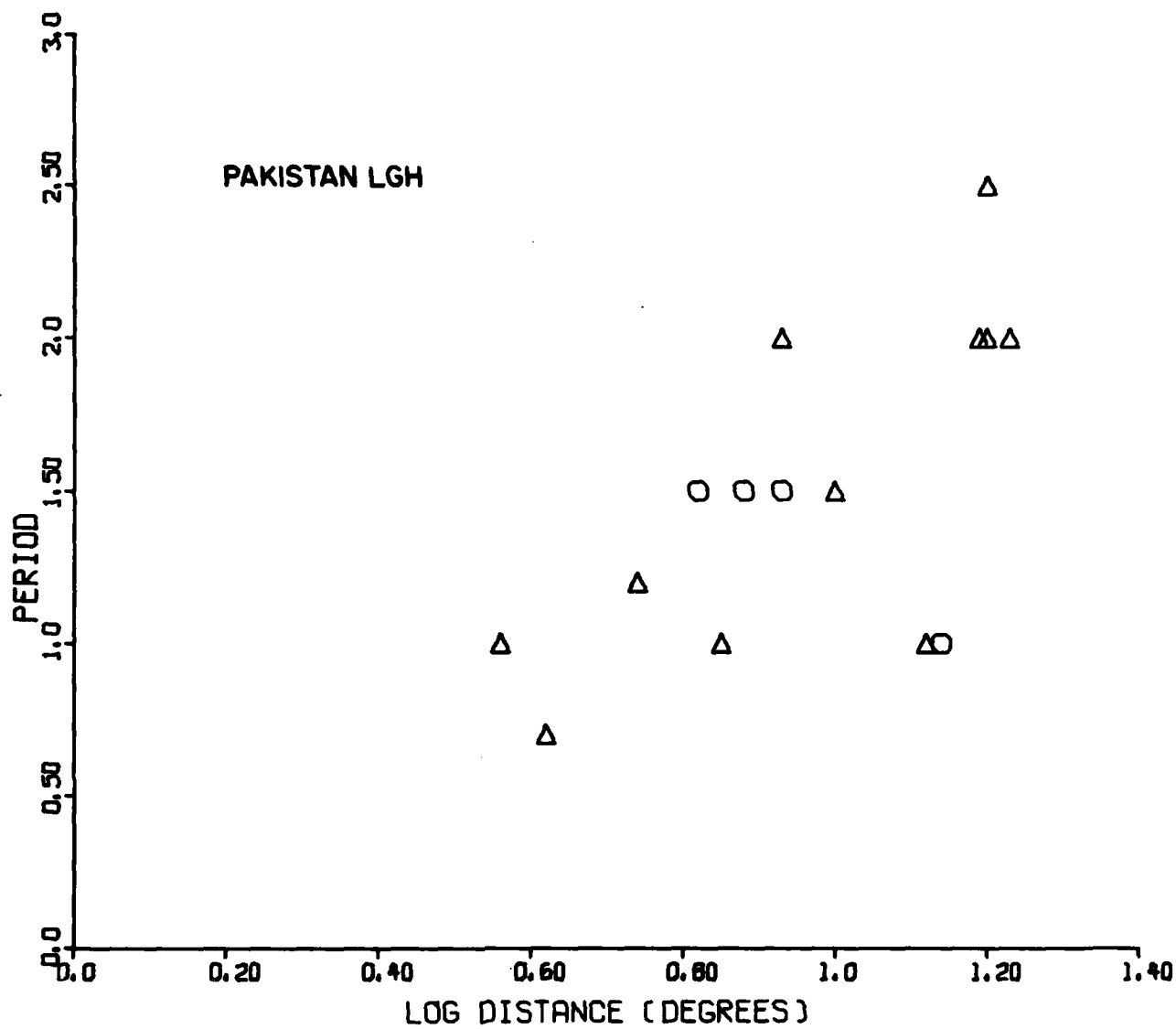


Figure 55. Dominant periods of L (horizontal component) wave from shallow earthquakes in the m_b range 4.5.-5.5, plotted against epicentral distance.

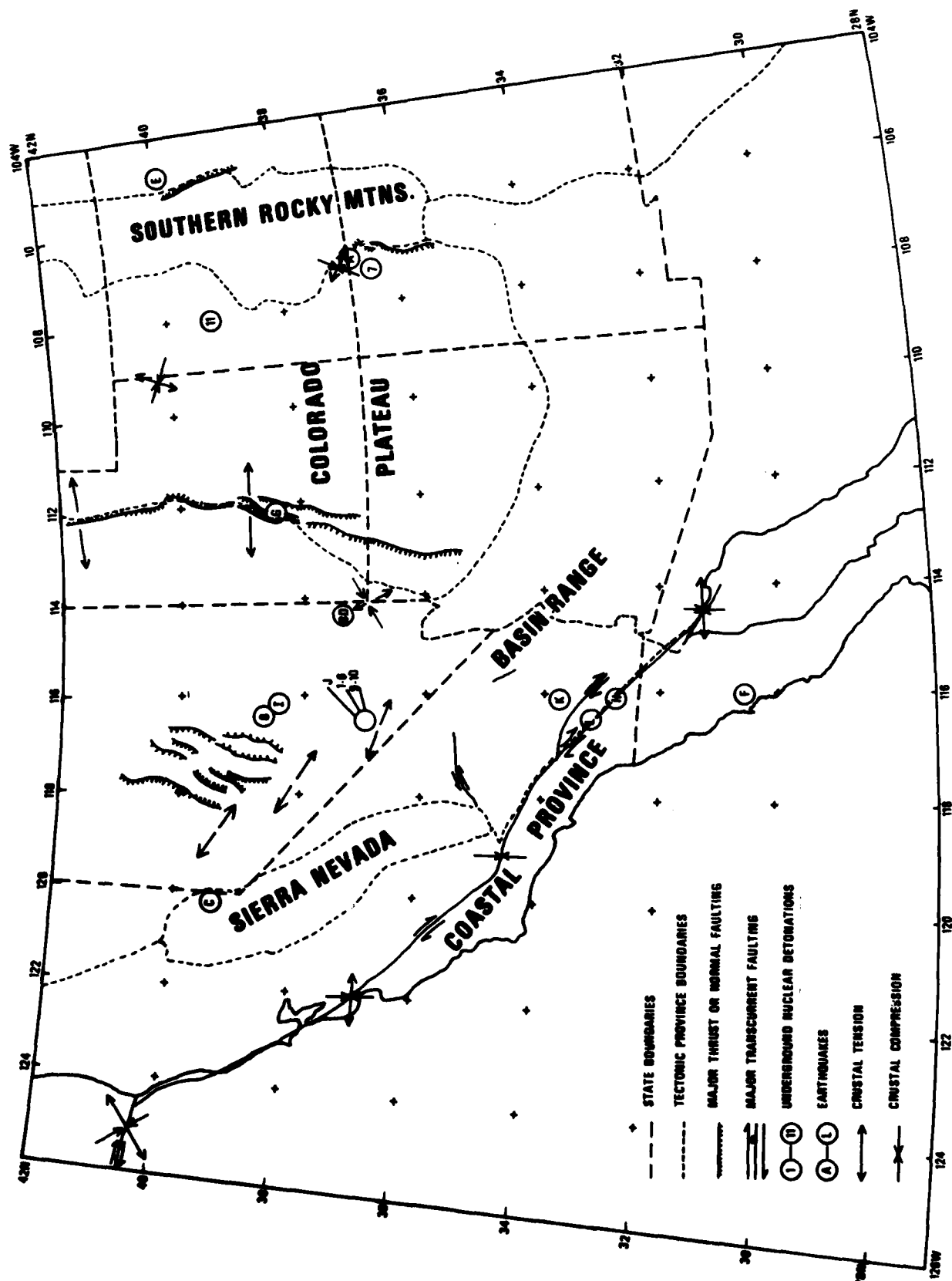


Figure 56. Major tectonic provinces in the western United States.

five provinces are the Sierra Nevada, the Basin and Range, the coastal province, the Colorado Plateau and the southern Rocky Mountains. Each of these provinces has a complex tectonic history and present tectonic activity. The most important factor determining the present day tectonic activity is the relative motion of the Pacific and North American plates. Practically all of the area is underlain by a low velocity-low Q upper mantle (Solomon and Toksoz, 1970; Archambeau et al., 1969; Der et al., 1981). The crust, which is primarily responsible for the propagation characteristics of the region, is laterally quite variable. The individual provinces can be characterized as follows:

Sierra Nevada

The Sierra Nevada orogeny is a large uplifted granitic body with a typical mountain "root". The crustal thickness under the region is at least 40 km in contrast to the surrounding areas.

Basin and Range

The Basin and Range is one of the most anomalous continental areas in the world with respect to its geophysical characteristics. The crust is unusually thin, less than 30 km. It is underlain by a low velocity upper mantle; the velocities of observed P_n are low relative to the rest of the United States (Herrin and Taggart, 1960). According to Archambeau et al, the upper mantle "lid" zone may be missing under most of the province. The low velocity upper mantle is also characterized by high attenuation of the body waves traveling through it, as evidenced by numerous studies (Archambeau et al., 1969; Solomon and Toksoz, 1970; Der et al., 1981). According to most evidence, the upper mantle is partially molten under the region, resulting in high conductivity, high heat flow, lowered body wave velocities, and high attenuation (Yasar and Nuttli, 1974; Der, 1976; Gough, 1973; Sass et al., 1971; Roy et al., 1968; Reitzel et al, 1970; Hales and Roberts, 1970). Besides the anomalously low velocities of P_n and S_n phases in the region, their attenuation with distance is also greater than in other areas of the United States (Alsup, 1970; Molnar and Oliver, 1969). Moreover, the attenuation of L_g and modal phases of similar

nature in the crust (P and P_g) is also greater than in the eastern, tectonically more static part of the continent. The tectonics of the Basin and Range is primarily extensional, with block faulting and rugged topography (Mitchell, 1975).

The Colorado Plateau

The Wasatch Front marks the eastern boundary of the Basin and Range province, where the crustal thickness increases rapidly to 40-45 km (Keller et al., 1975; Prodehl, 1970). This change in crustal thickness, however, does not correspond to drastic changes in upper mantle properties. On the contrary, the upper mantle under the Colorado Plateau still attenuates high frequency body waves passing through it. On the other hand, the upper mantle "lid" zone is present (Archambeau et al., 1969), and the P_n velocities are not anomalous in the area (Herrin and Taggart, 1962).

The Southern Rocky Mountains

This province is characterized by a fairly thick crust on the order of 50 km. The upper mantle has an extremely high conductivity (Gough, 1973) and high heat flow. Although present studies do not define the upper mantle LVZ well, it is probably present. In addition, a lid zone above the LVZ may also exist, such that the propagation of P_n and S_n may still be possible.

Efficiency of Propagation and Amplitude-Distance Relationships

For the most part, observations of S_n are absent throughout the WUS (Molnar and Oliver, 1969). This is shown in Figure 57. The absence of S_n can be explained by some combination of two factors: upper mantle attenuation and the discontinuity of the waveguide, most likely the upper mantle lid zone beneath the crust. Nevertheless, there were a few paths for which S_n was observed. Curiously, S_n was visible for two paths from NTS to KNUT and FSAZ, as seen in Figure 58 which shows the efficiency of propagation for explosion generated S_n . For earthquakes, a similar map, Figure 59, shows a few paths along which S_n was observed. The available data can be interpreted as an

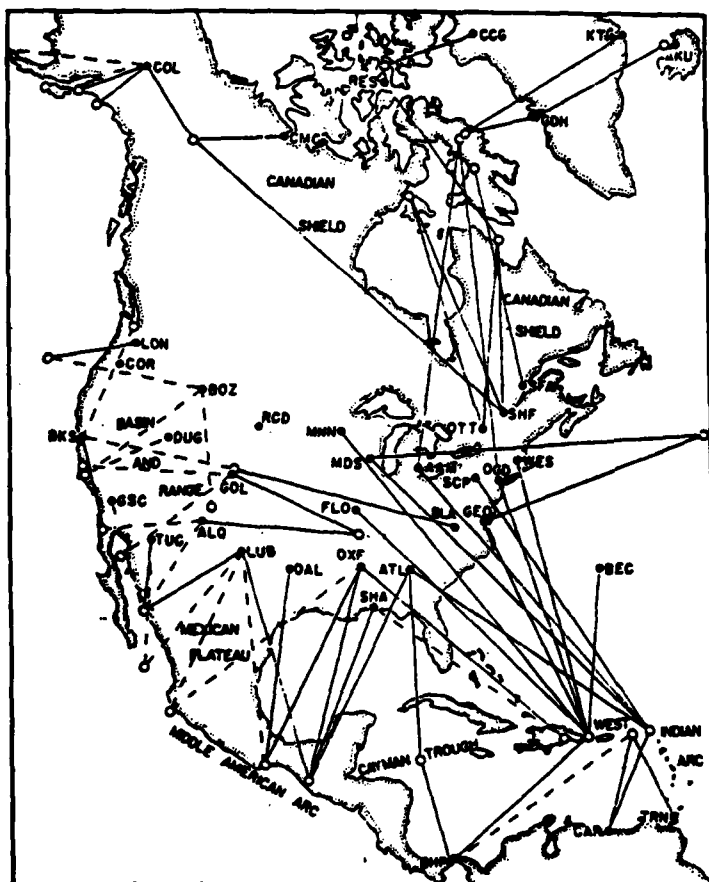


Figure 57. Efficiency of S_n propagation in North America (after Molnar and Oliver, 1969).

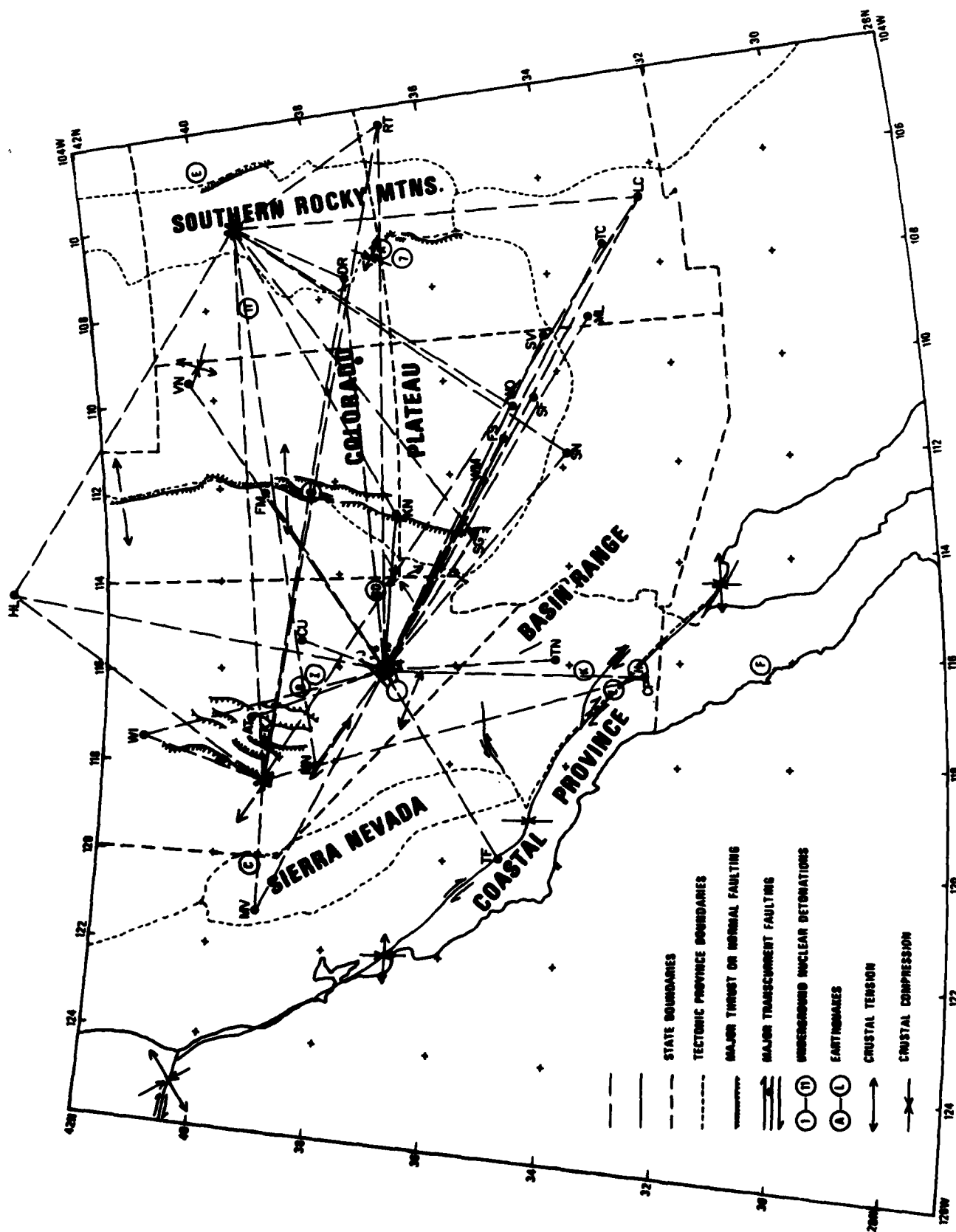


Figure 58. Efficiency of S_n propagation from explosions.

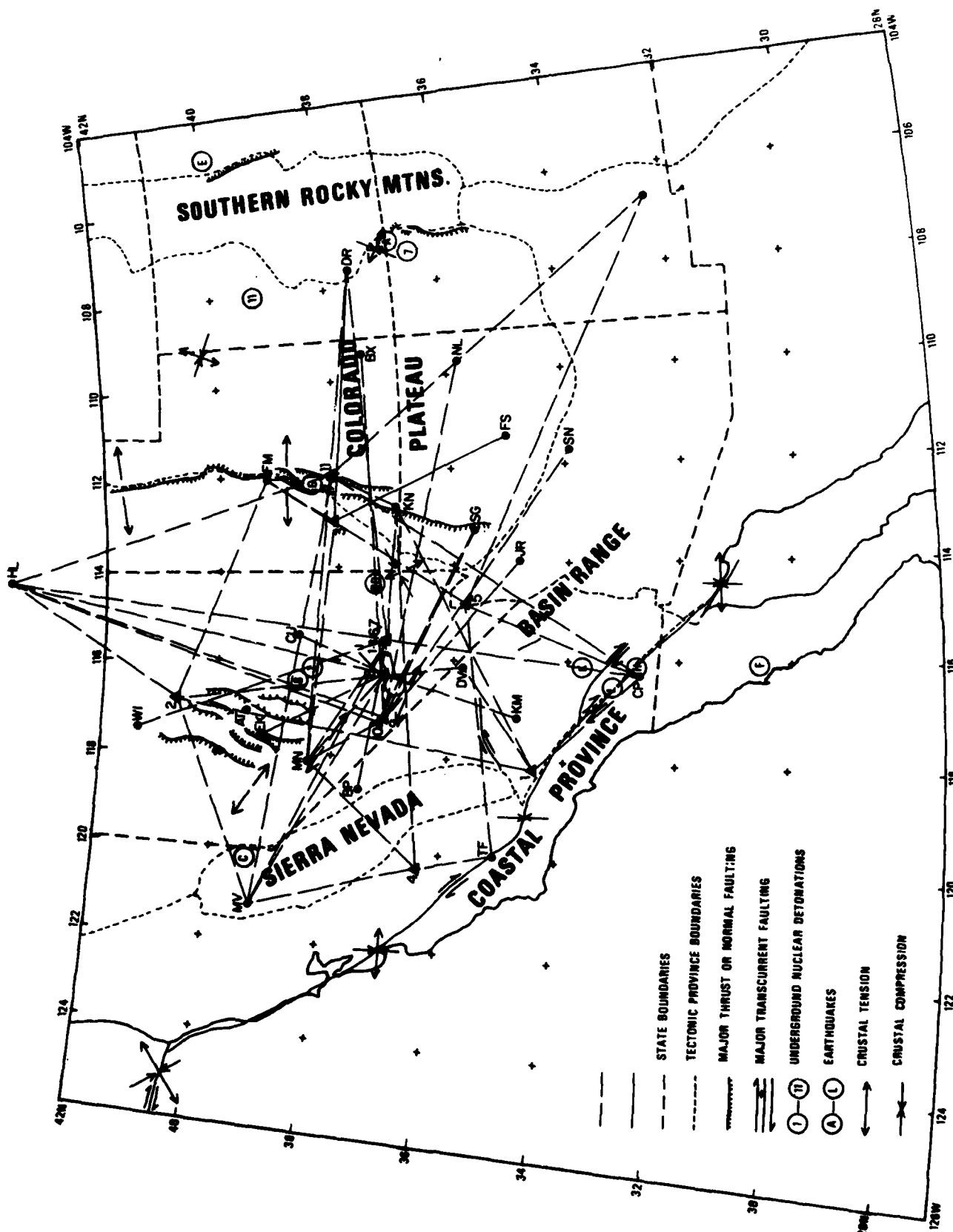


Figure 59. Efficiency of S_n propagation from earthquakes.

indication of a lid zone under the Colorado Plateau province, a fact that was also demonstrated by Archambeau et al (1969).

The normalized amplitude-distance curves for the regional phases P_n , P_g , S_n and L_g are shown in Figures 60 to 64, where earthquakes and nuclear explosions are depicted by different symbols. These figures illustrate that the amplitude-distance curves in the southwestern United States are different from those in the other regions discussed in this report. The phases P_g and L_g start out at higher amplitudes but decrease quite rapidly with distance. The falloff rates of both types of phases appear to be -3 . P_n amplitudes seem to be quite scattered.

In addition, there appears to be a shift between the earthquake and explosion populations for all phases; it is especially great for P_n . This shift could be caused by the fact that we used m_b values from NEIS lists for earthquakes, while most explosion m_b 's were taken from Geotech studies that used Evernden's (1967) formulas for computing m_b . The NEIS may have used some regional readings that tend to overestimate m_b when using the Gutenberg "B" factors, according to the standard practice of NEIS. This can at least partially explain the shift in the populations in the direction indicated by the figures. Unfortunately, there is no way to correct exactly for this shift, since we do not know which stations were used by NEIS in deriving their m_b values. Furthermore, it was not possible to obtain the m_b values for explosions from the same type of event list because NEIS did not list the body wave magnitudes for most of the explosions in this report. Since the rest of this report also uses the NEIS body wave magnitudes, the vertical position of the NEIS (earthquake) points is comparable to those presented for the rest of this report, although we have to live with the uncertainties in NEIS procedures for estimating m_b . The dominant periods of the various regional phases in the southwestern United States are plotted against epicentral distance in Figures 65 to 72. In these plots we have separated explosion data from earthquake data. Due to the wide range of event magnitudes, restricting the range of amplitudes in the manner of the previous sections would reduce the data volume to very low levels. Consequently, we have plotted all the data, using different symbols for various ranges of event magnitude.

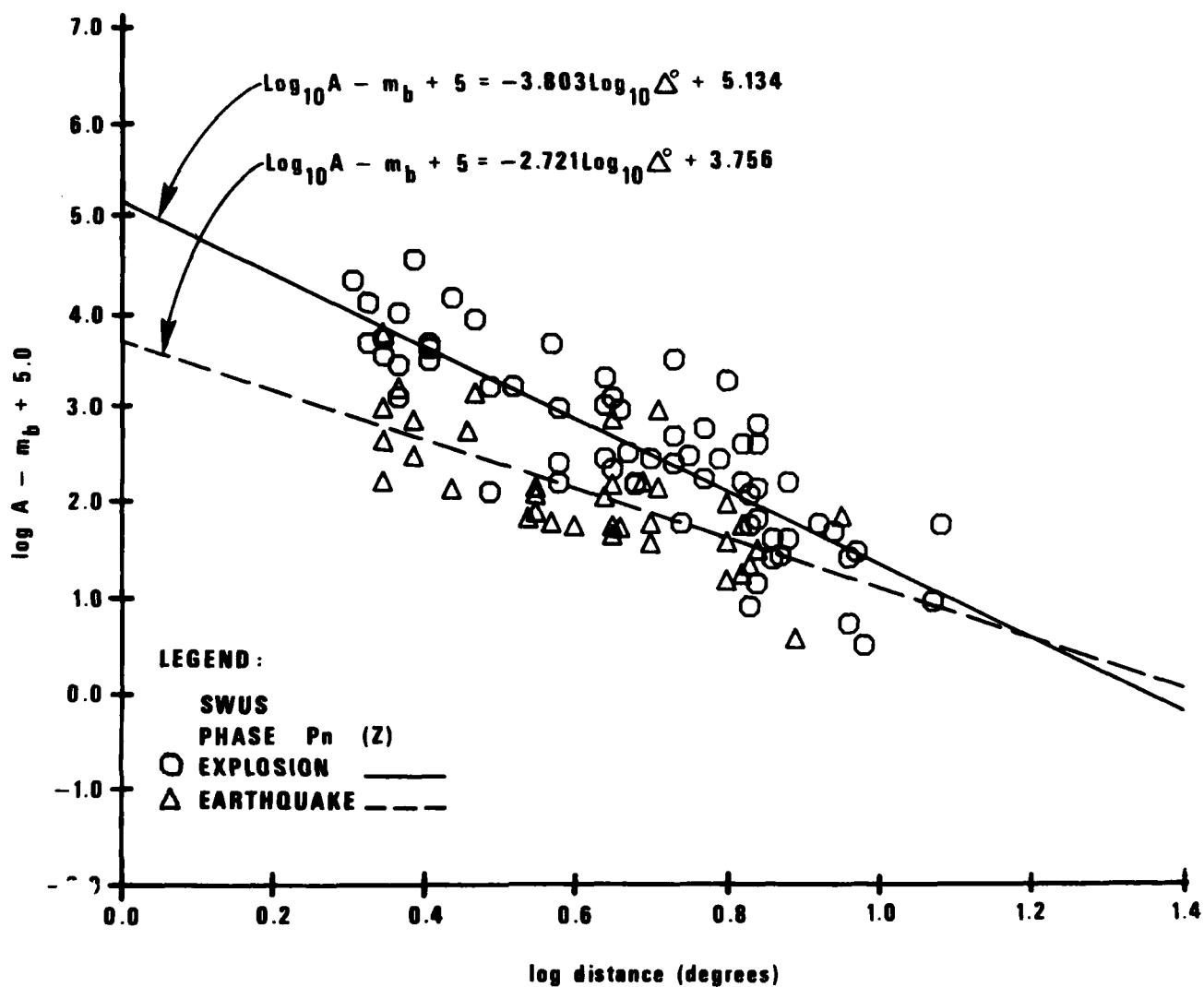


Figure 60. Trace amplitudes of P_n in the southwestern United States plotted against epicentral distance. Nuclear explosion data are denoted by circles and earthquake data by triangles.

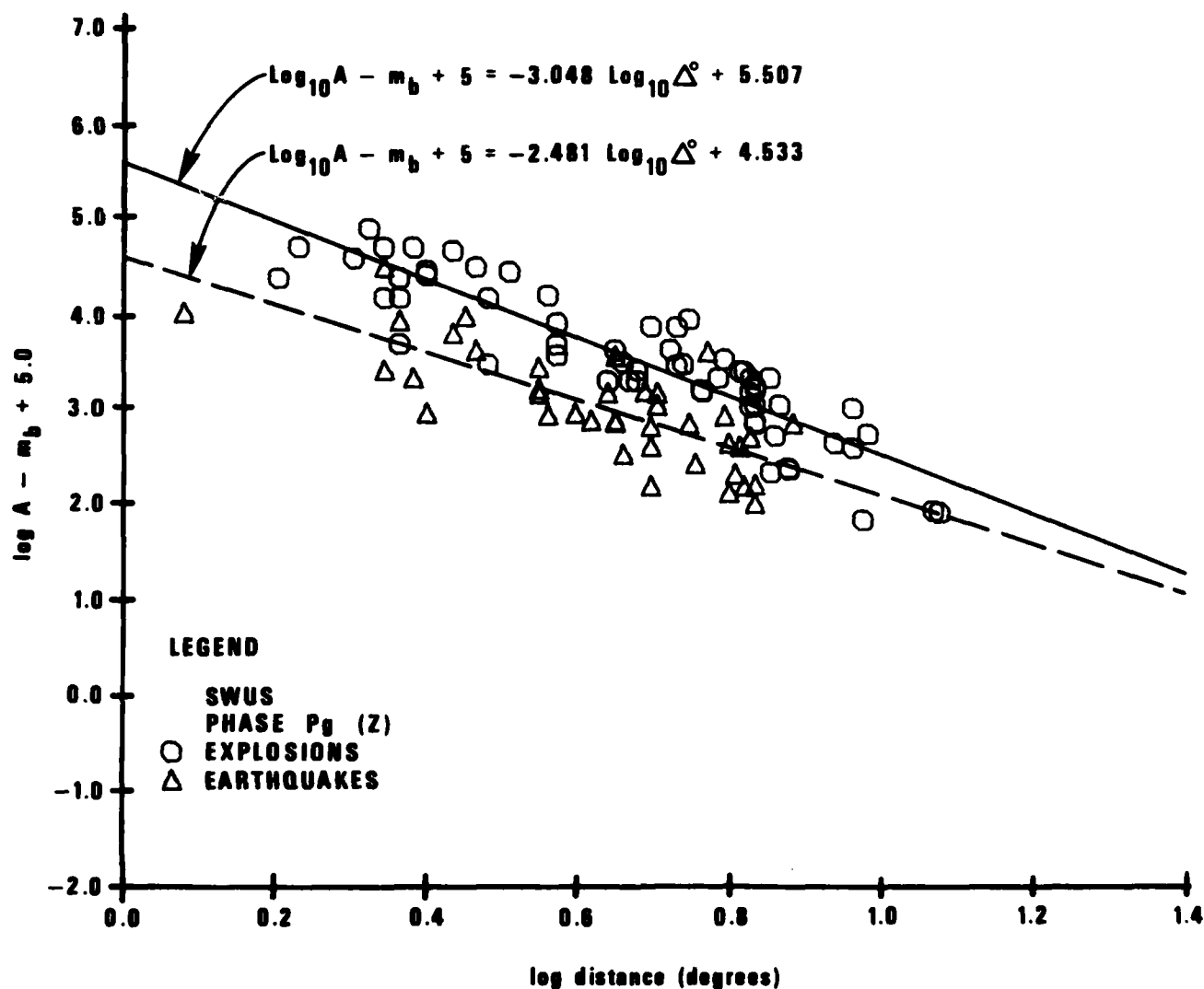


Figure 61. Trace amplitudes of P_g in the southwestern United States plotted against epicentral distance. Nuclear explosion data are denoted by circles and earthquake data by triangles.

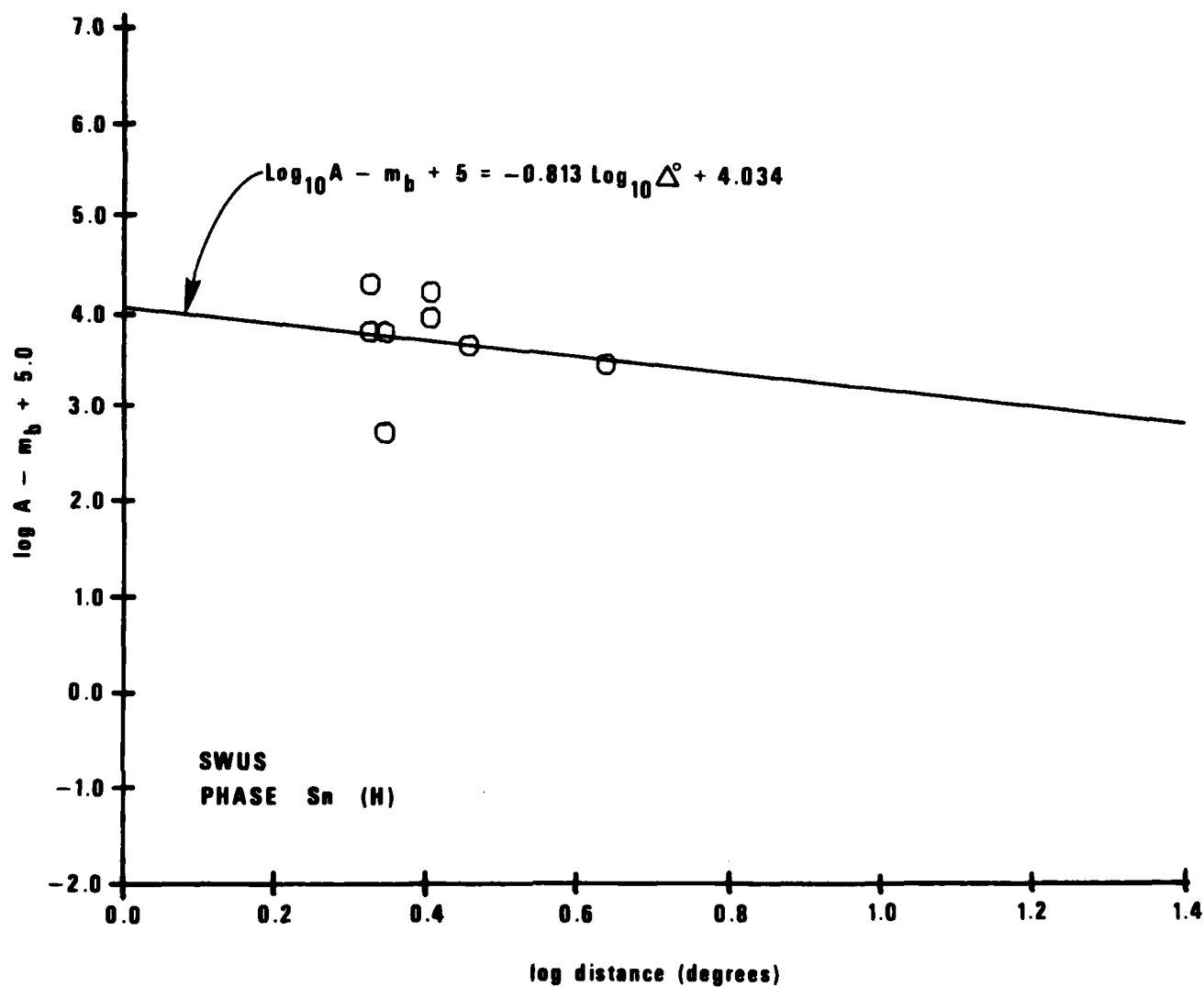


Figure 62. Trace amplitudes of S_n in the southwestern United States plotted against epicentral distance. Nuclear explosion data are denoted by circles and earthquake data by triangles.

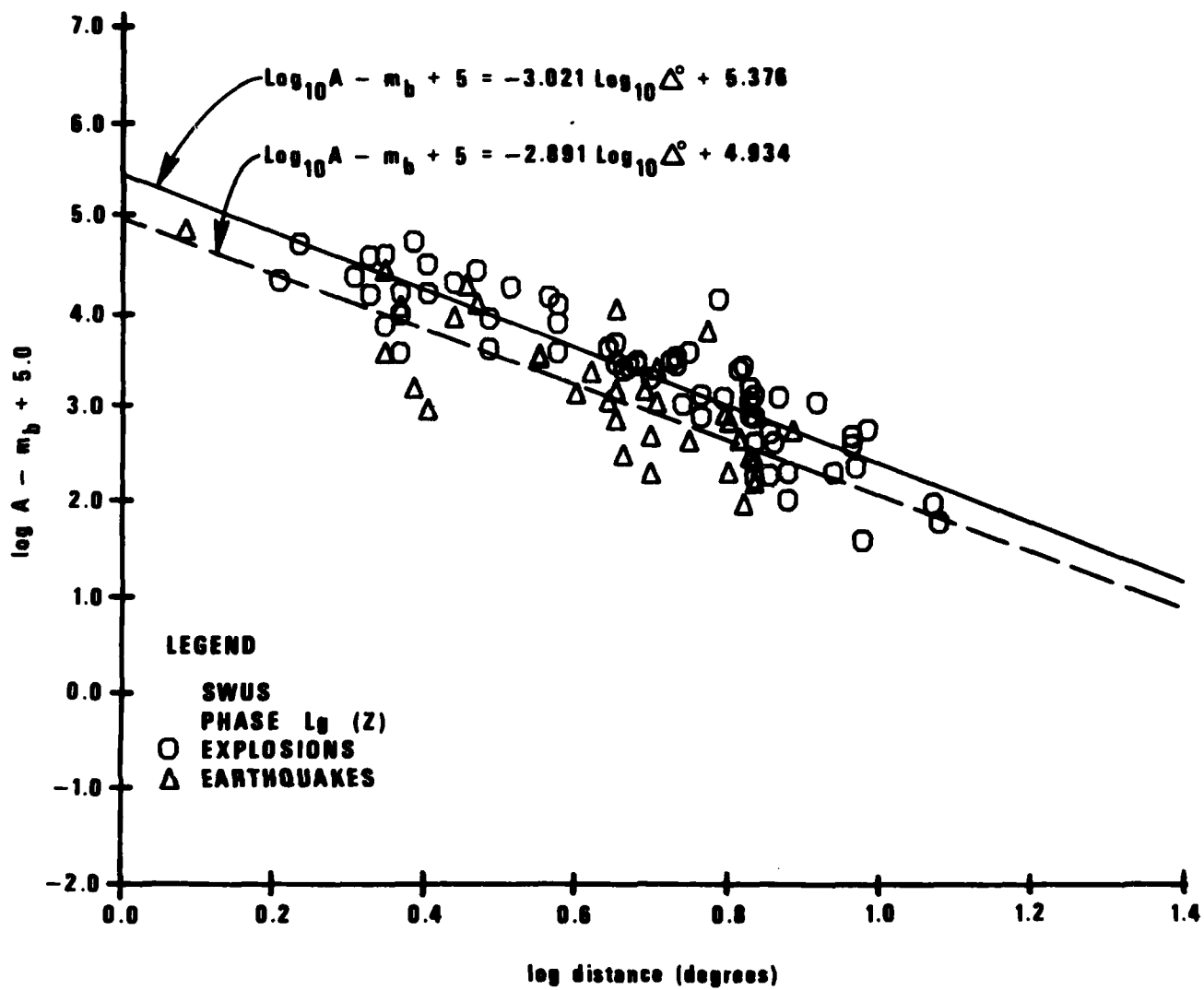


Figure 63. Trace amplitudes of L_g (vertical component) in the southwestern United States plotted against epicentral distance. Nuclear explosion data denoted by circles and earthquake data by triangles.

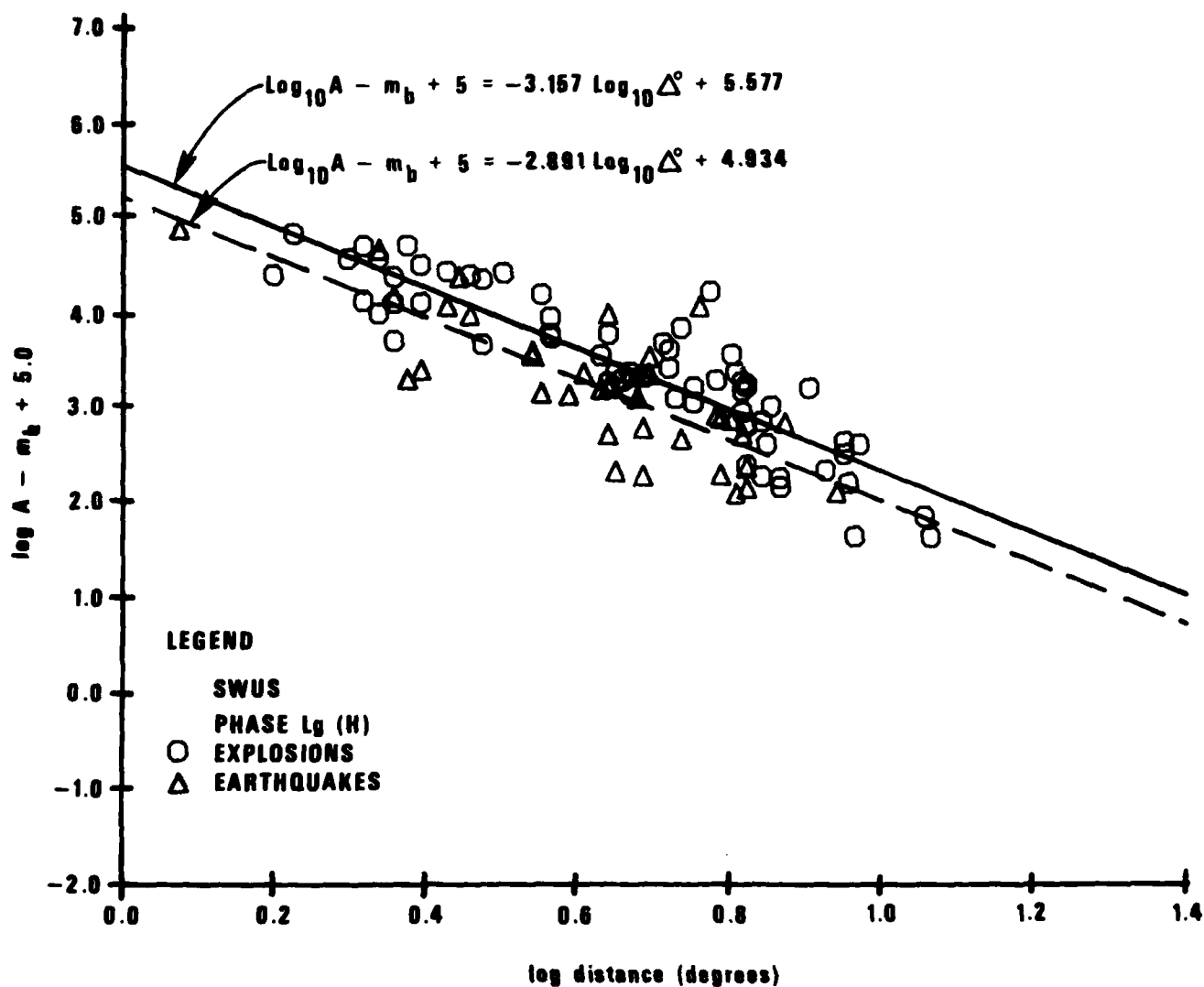


Figure 64. Trace amplitudes of L (horizontal component) in the southwestern United States plotted against epicentral distance. Nuclear explosion data denoted by circles and earthquake data by triangles.

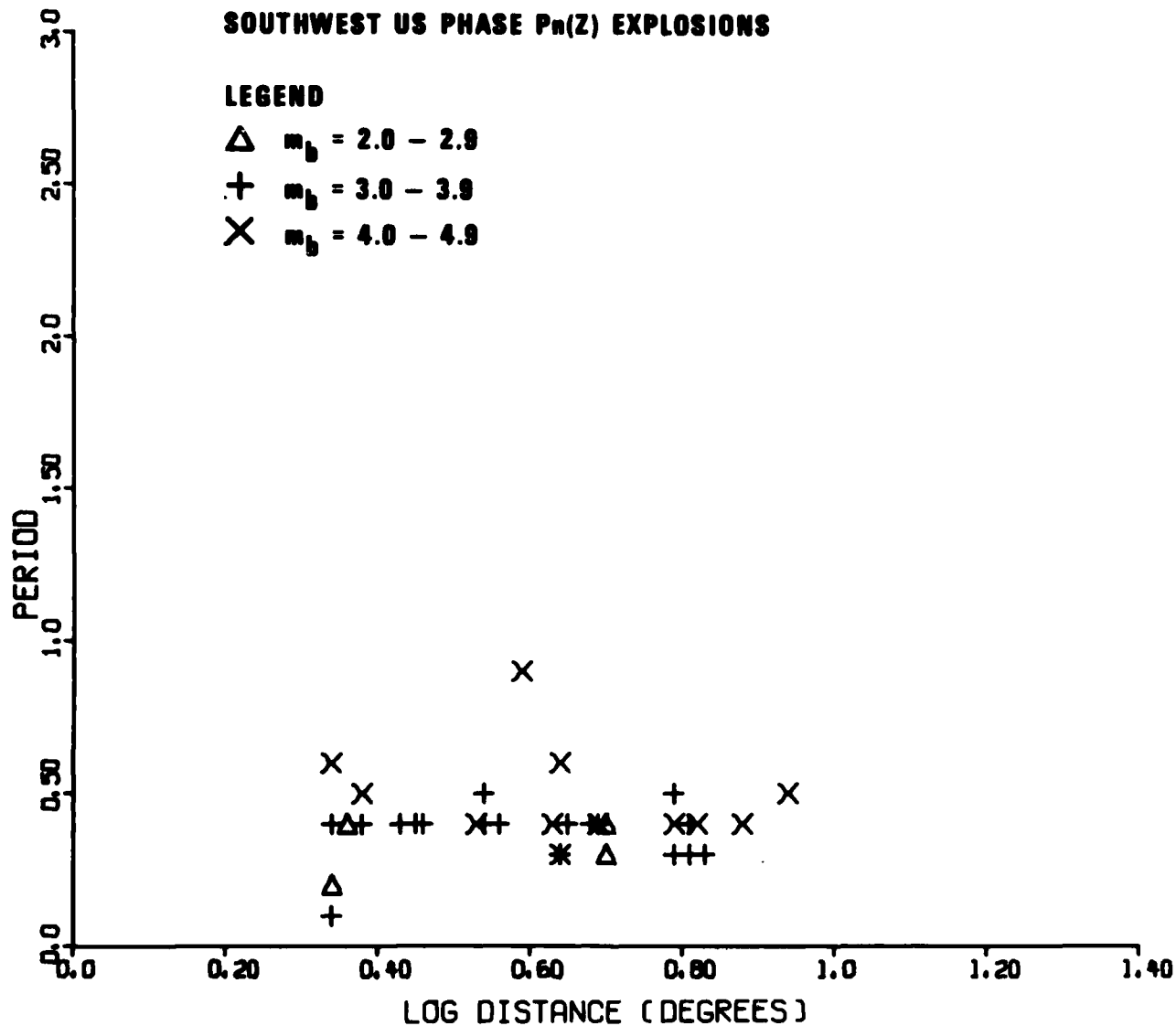


Figure 65. Dominant period of P_n for earthquakes in the southwestern United States plotted against epicentral distance. The symbols denote various ranges of event magnitude.

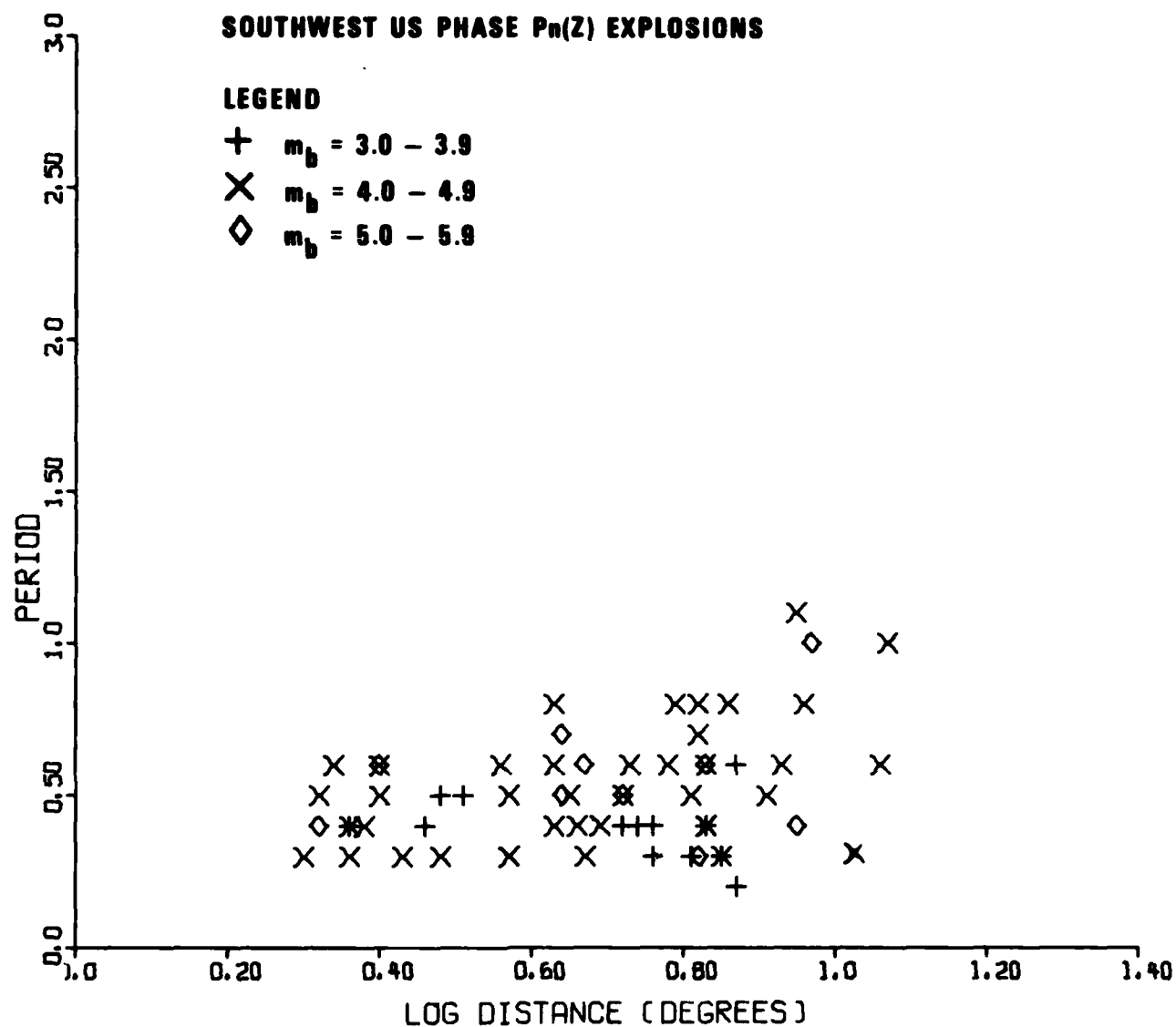


Figure 66. Dominant period of Pn for explosions in the southwestern United States plotted against epicentral distance. The symbols denote various ranges of event magnitude.

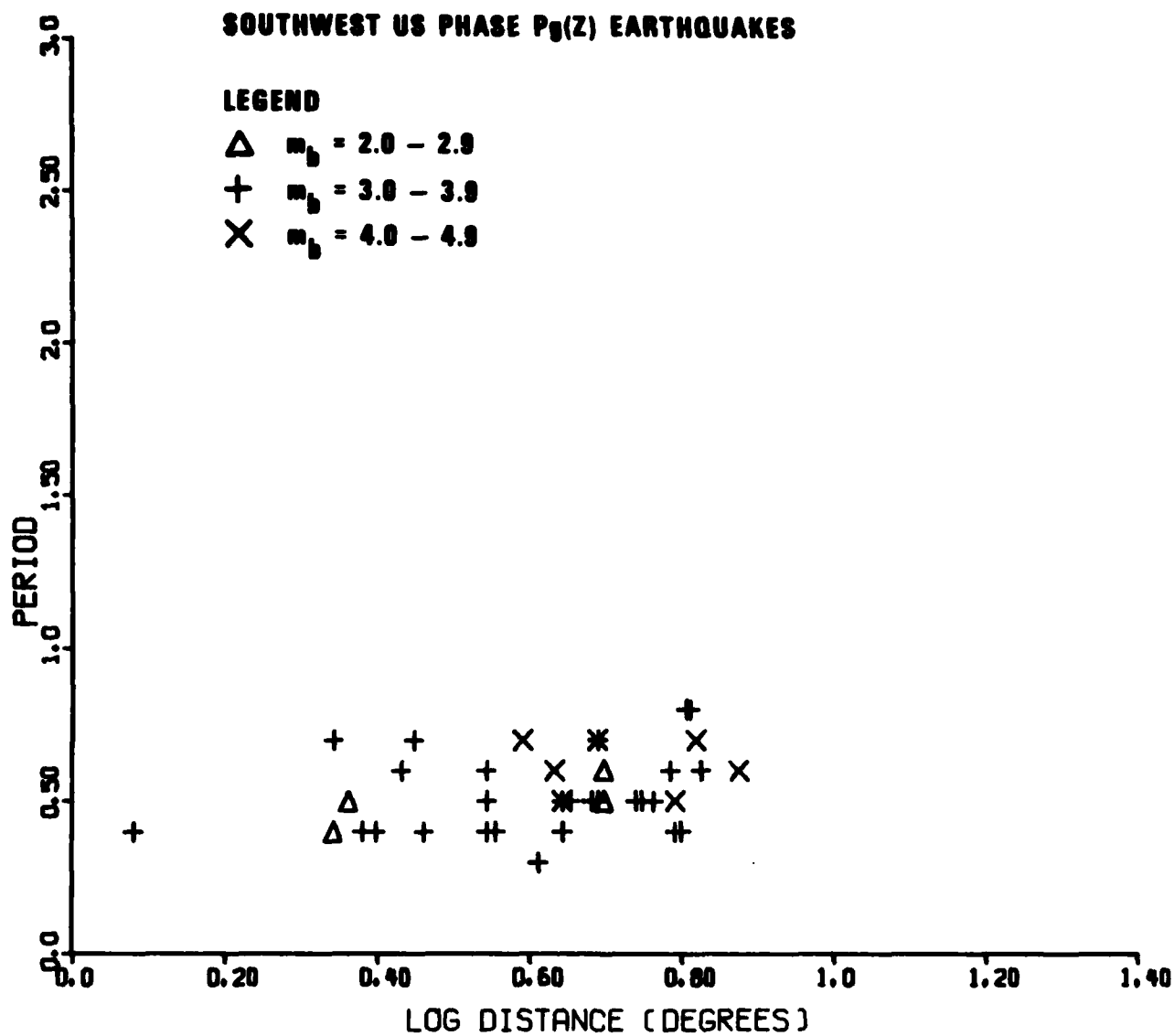


Figure 67. Dominant period of P for explosions in the southwestern United States plotted against epicentral distance. The symbols denote various ranges of event magnitude.

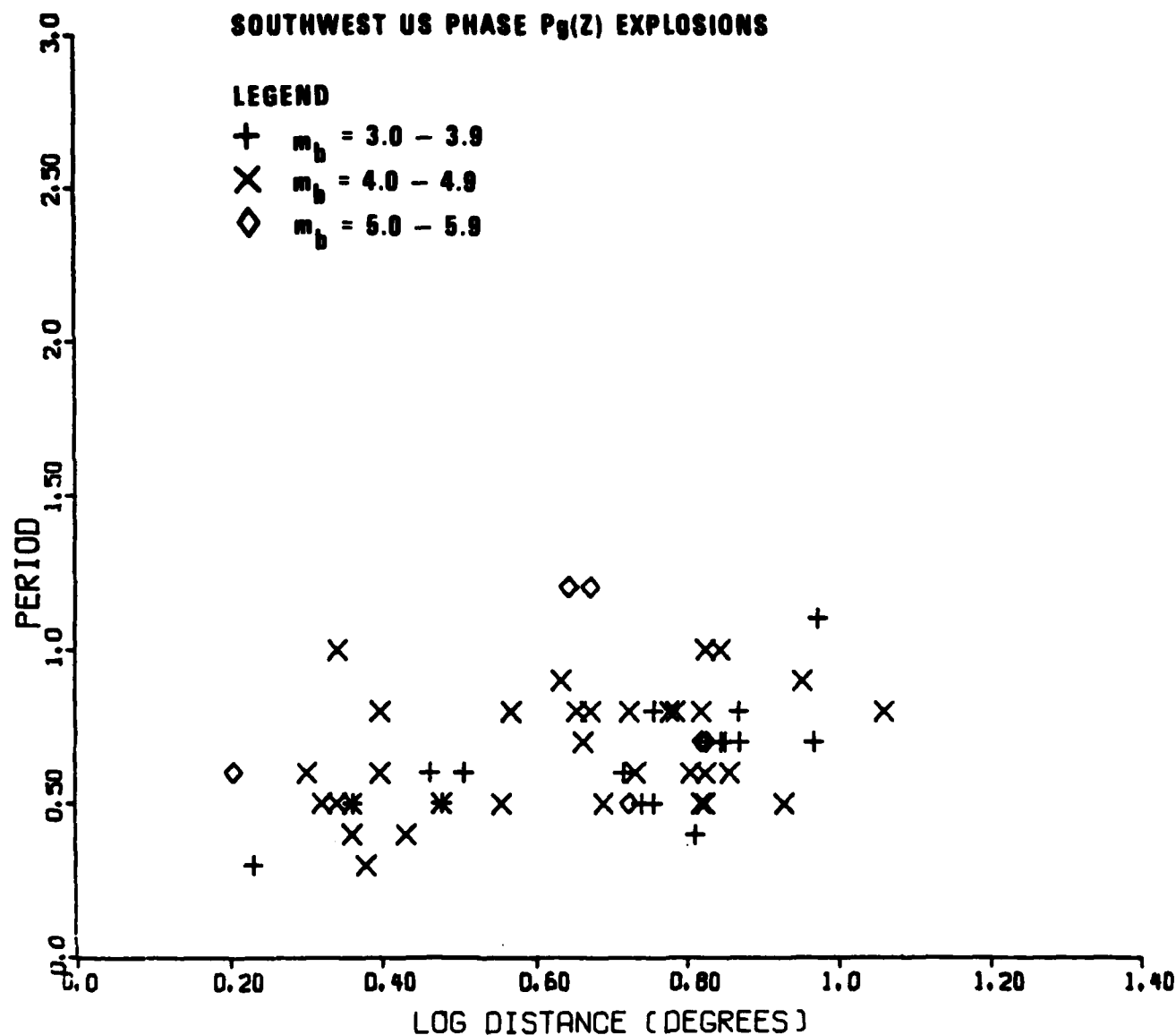


Figure 68. Dominant period of Pg for earthquakes in the southwestern United States plotted against epicentral distance. The symbols denote various ranges of event magnitude.

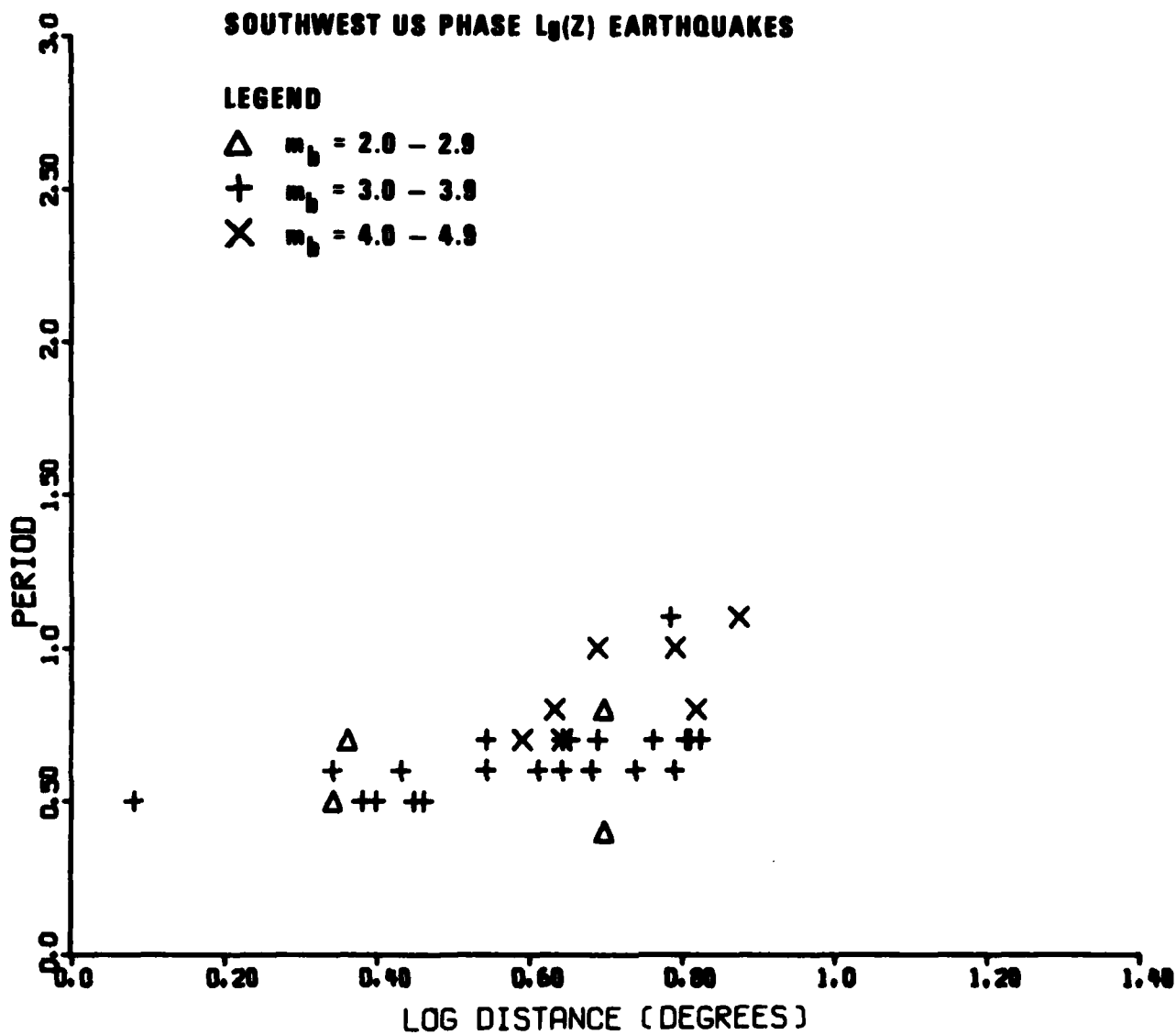


Figure 69. Dominant period of L_g (vertical component) for earthquakes in the southwestern United States plotted against epicentral distance. The symbols denote various ranges of event magnitude.

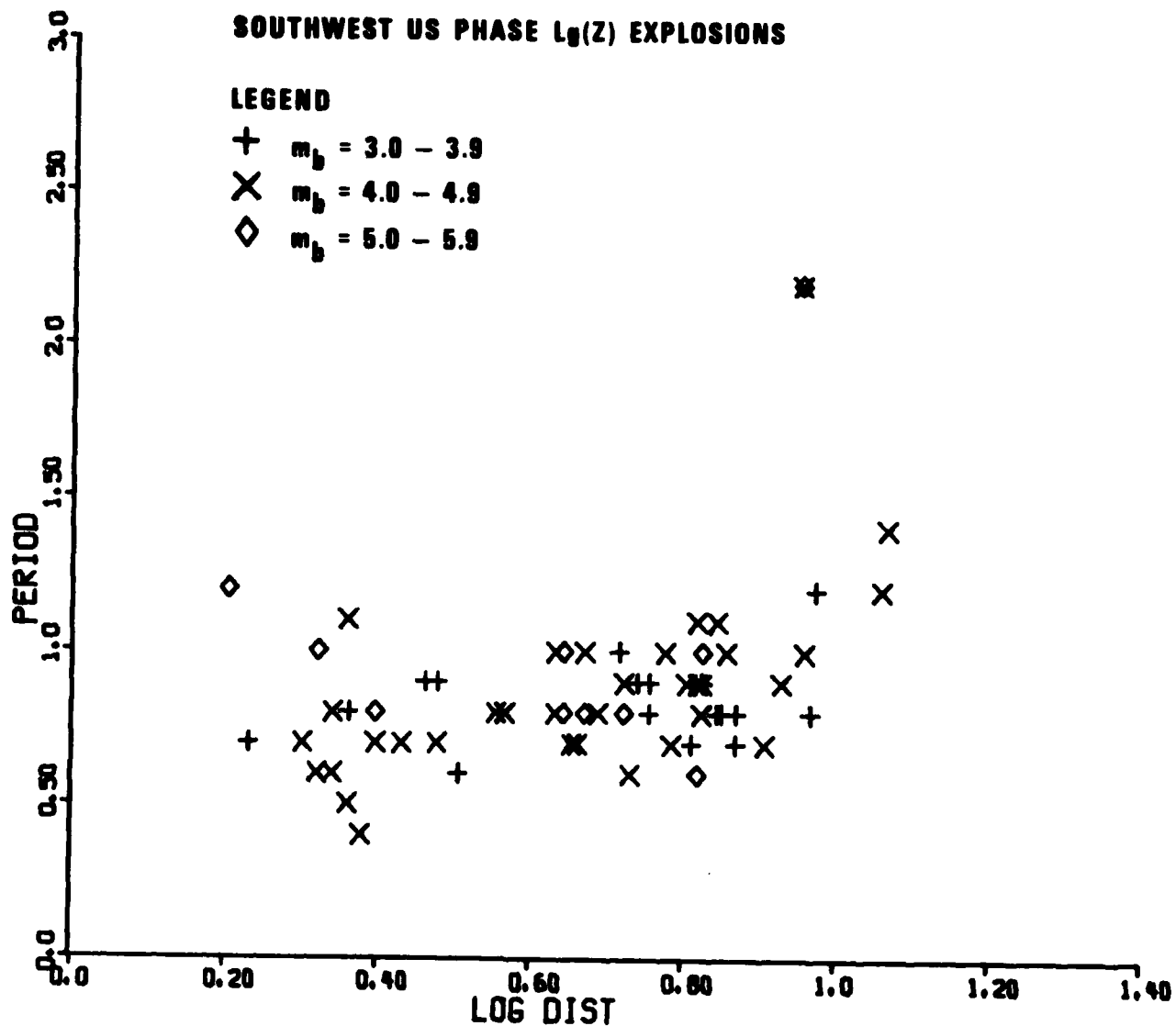


Figure 70. Dominant period of L_g (vertical component) for earthquakes in the southwestern United States plotted against epicentral distance. The symbols denote various ranges of event magnitude.

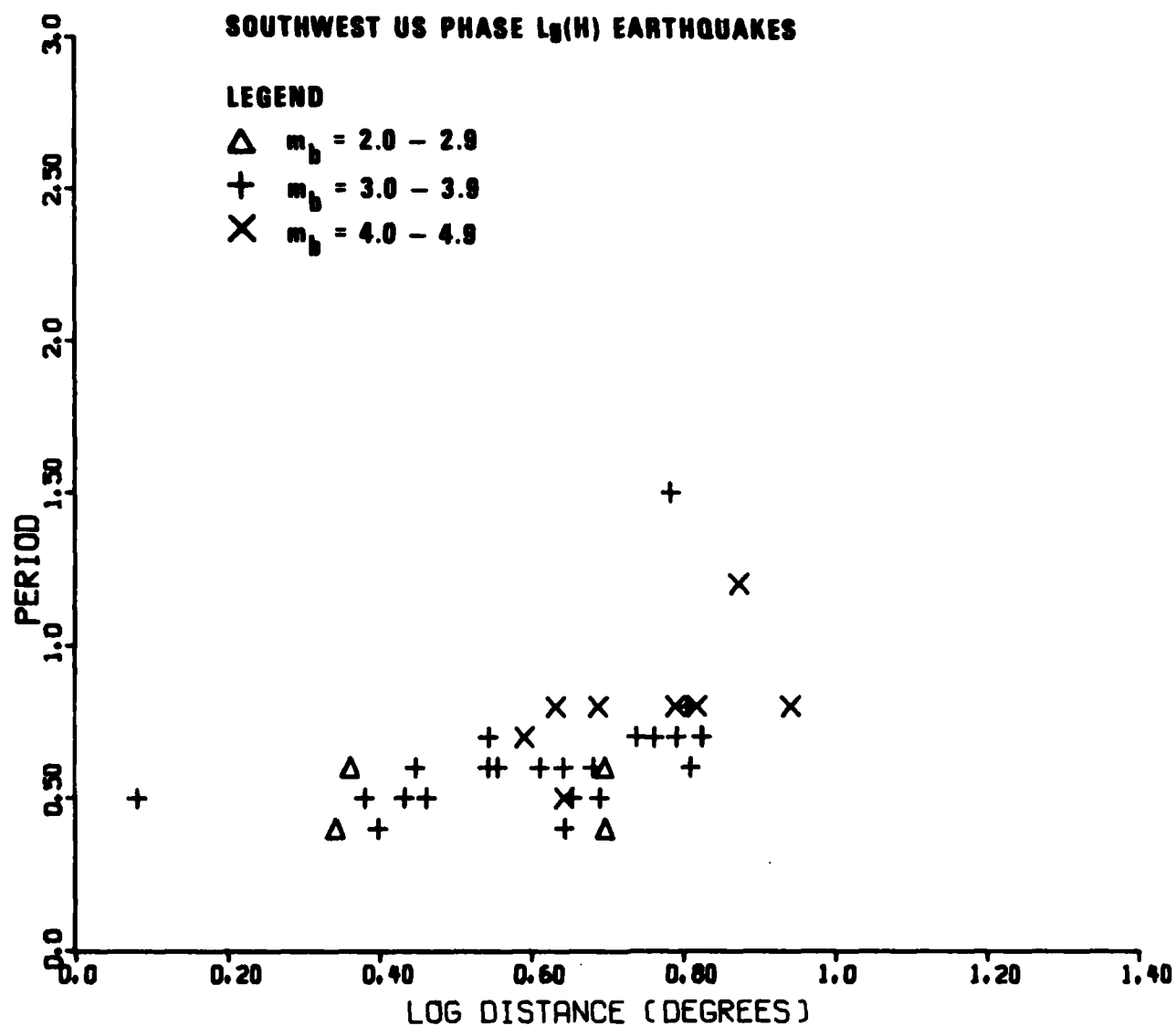


Figure 71. Dominant period of L_g (horizontal component) for earthquakes in the southwestern United States plotted against epicentral distance. The symbols denote various ranges of event magnitude.

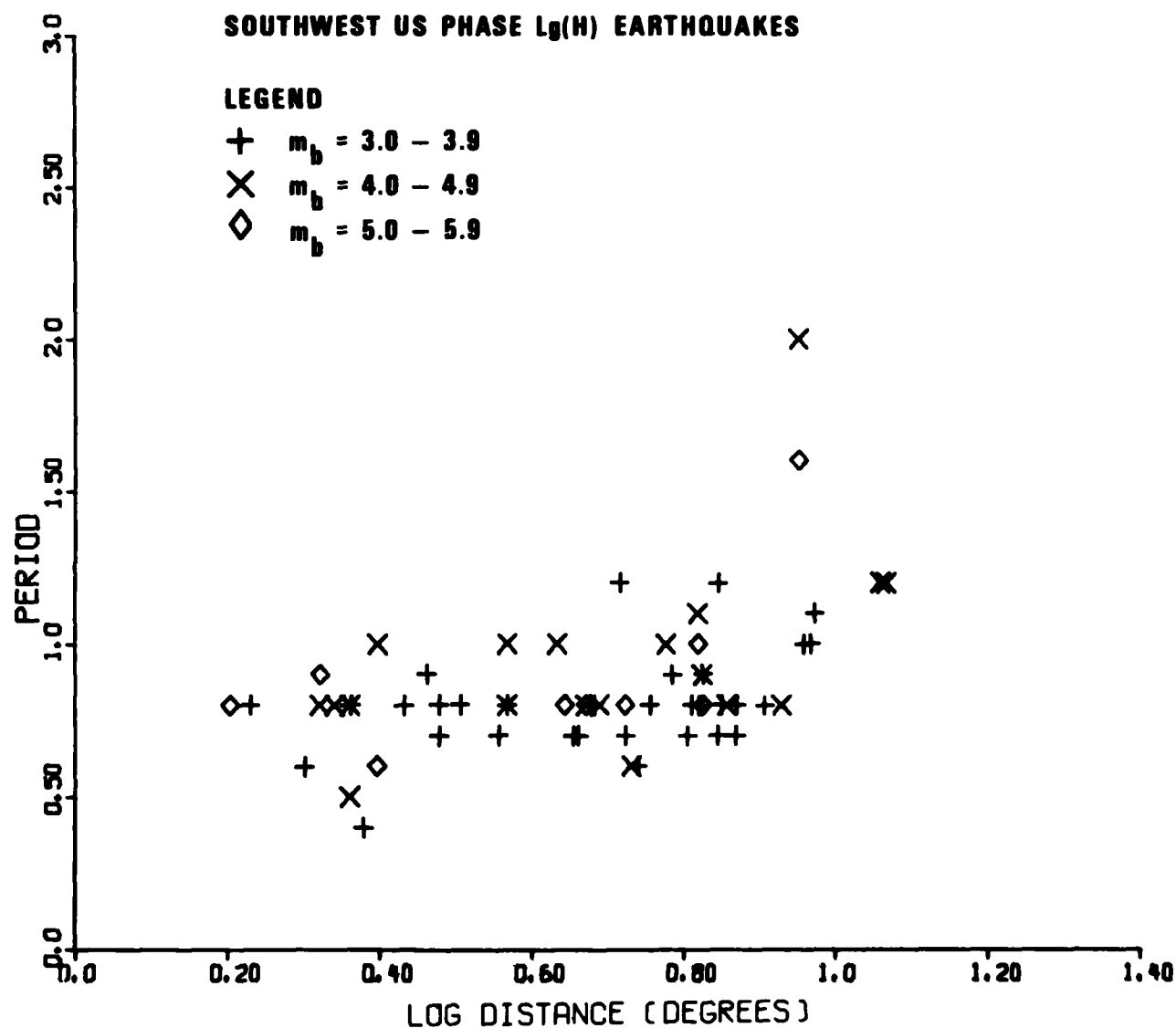


Figure 72. Dominant period of L_g (horizontal component) for explosions in the southwestern United States plotted against epicentral distance. The symbols denote various ranges of event magnitude.

Since the explosion data set contains events with higher average body wave magnitude, the dominant periods of regional phases from explosions also resulted in the reduction of the distance range over which earthquake data could be measured and detected. This was unavoidable, given the patterns of seismicity in the region.

Considered together, the plots of P_n periods against distance for earthquakes and explosions seem to indicate a trend towards increasing periods with increasing distance. This is shown in Figures 65 and 66. The trend is not clear for the earthquake data, but the distance range is also small. The same remarks apply to the periods of P_g , Figures 67 and 68, where the trend is visible in the explosion data but not in the earthquake data. These increasing trends for P_n and P_g , although weak, appear to be larger than those for corresponding phases in southern Africa, possibly indicating higher attenuation in the southwestern United States compared to southern Africa.

The plots of dominant periods of the vertical and horizontal components of L_g , Figures 69 to 72, exhibit strong increasing trends with distance, which appear to be stronger compared to the southern African data.

In spite of the scatter and the limitations of the data set, it appears that the dominant periods of regional phases as functions of epicentral distance support the hypothesis that attenuation for all types of regional phases is greater in the southwestern United States than in shield regions. This is, of course, also supported by the amplitude data shown earlier.

Investigation of the Discrimination Capability of Various Combinations of Regional Phases in the Southwestern United States

The amplitude ratio of various regional phases have been studied by several investigators in order to evaluate their discrimination capability (Blandford, Hartenberger and Naylor, 1980; Pomeroy and Chen, 1980; Bennett and Murphy, 1980; Barker, 1981). Most investigators agree that the ratio of P_g to L_g amplitudes has a potential for discrimination of nuclear explosions and earthquakes, but they disagree on the degree of effectiveness of such a discriminant. Pomeroy and Chen (1980) feel that the discriminant has too much scatter to be effective. Although the earthquake and explosion populations of P_g and L_g amplitude ratios are clearly different, the explosions have relatively small L_g amplitudes. On the other hand, Blandford, Hartenberger and Naylor (1980) found an almost perfect separation of the P_g and L_g amplitude ratios for earthquakes and explosions at TFO.

In order to further investigate the question, we have compiled regional phase amplitudes for a set of events in the SWUS including both types of sources. The events are listed in Table VI, and their locations are plotted in Figure 73. The amplitude ratios of the various regional phase combinations are shown in Figures 74 to 83, plotted against distance and event magnitude. Of all the amplitude ratios, the ratio of L_g to P_g appears to have the greatest potential for discrimination, regardless of whether the vertical or horizontal component of L_g is used. This is essentially the same discriminant as the L_g/P_{\max} ratio proposed by Blandford as a discriminant, because P_{\max} is identical to P_g maximum in the western United States. Although there appears to be clear difference in the populations of this ratio for earthquakes and explosions, there is also a considerable mixing of the data points when plotted against either epicentral distance or body wave magnitude. This is shown in Figures 74 to 77. Unfortunately, there is also some separation of the populations of the two types of events with respect to body wave magnitude, but there is a slight separation of the two populations even at similar magnitudes. This seems to confirm Pomeroy and Chen's (1980) statement that the L_g to P_g

TABLE VI

NEIS Hypocenters for Earthquakes and Explosions in the Southwest U.S.

<u>Date</u>	<u>Origin Time</u>	<u>Geo.</u>	<u>Lat</u>	<u>Lon</u>	<u>Depth (ft)</u> <u>W.T. Depth (ft)</u>	<u>m_b</u>
EX HARDHAT						
15 Feb 62	18 00 00.1	NTS	37.2N	116.1W	943 614	4.34 5.9(kt)
AARDVARK						
12 May 62	19 00 00.1	NTS	37.1N	116.0W	1424 1670	4.73 36.0(kt)
BILBY						
13 Sep 63	17 00 00.1	NTS	37.1N	116.0W	1600 2344	5.45 235.0(kt)
SHOAL						
26 Oct 63	17 00 00.1	CENT NV	39.2N	118.4W	1205 ?	4.76 12.0(kt)
CLIMAX MOLY						
23 May 64	21 44 59.0	S. CO	39.4N	106.2W		3.82 3.8
PALANQUIN						
14 Apr 65	13 14 00.1	NTS	37.3N	116.5W	280 2194	3.76 4.3(kt)

TABLE VI (cont.)

NEIS Hypocenters for Earthquakes and Explosions in the Southwest U.S.

<u>Date</u>	<u>Origin Time</u>	<u>Geo.</u>	<u>Lat</u>	<u>Lon</u>	<u>Depth (ft) W. T. Depth (ft)</u>	<u>m_b</u>	<u>m</u>
EQ							
17 Feb 62	01 07 25.1	S. CA	34.5N	118.2W	1.5 km	2.8	0.0
20 Mar 62	11 23 26.0	N. NV	41.7N	116.9W	0.0 km	0.0	3.0
03 Jun 62	19 19 02.0	SW UT	38.0N	113.0W	33.0 km	0.0	0.0
05 Jun 62	22 29 45.0	CENT UT	38.0N	112.1W	33.0 km	0.0	0.0
15 Dec 62	00 40 18.7	W. CA	36.4N	120.4W	3.8 km	0.0	3.1
25 Mar 63	09 28 41.4	W. AZ	35.8N	114.8	0.0	4.9	0.0
18 Jul 63	04 01 16.3	S. NV	37.2N	115.6W	25.0 km	3.9	0.0
20 Jul 63	19 13 05.9	S. NV	37.1N	115.6W	25.0 km	4.1	0.0
06 Feb 64	16 17 52.0	S. NV	37.2N	116.3W	30.0 km	0.0	0.0
25 May 65	00 48 13.3	CA-NV BORD.	37.1N	117.2W	33.0 km	3.8	0.0
28 May 65	08 18 51.1	CA-NV BORD.	37.2N	117.3W	15.0 km	3.8	0.0

(Explosion m_b's from SDL Report #245, Teledyne Geotech; SHOAL
from R. R. Blandford study in progress)

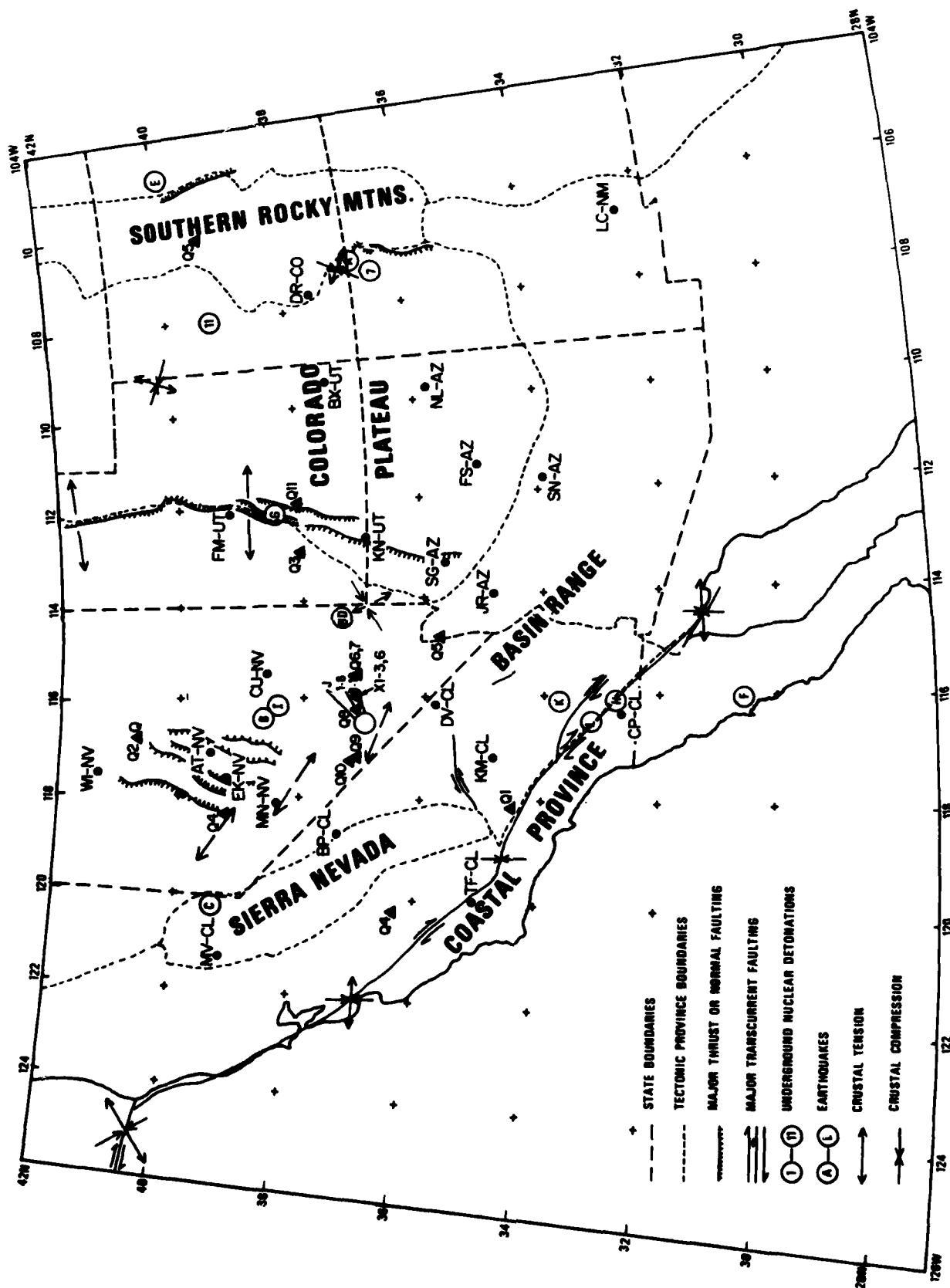


Figure 73. Map of events analyzed and stations utilized for the south-western United States.

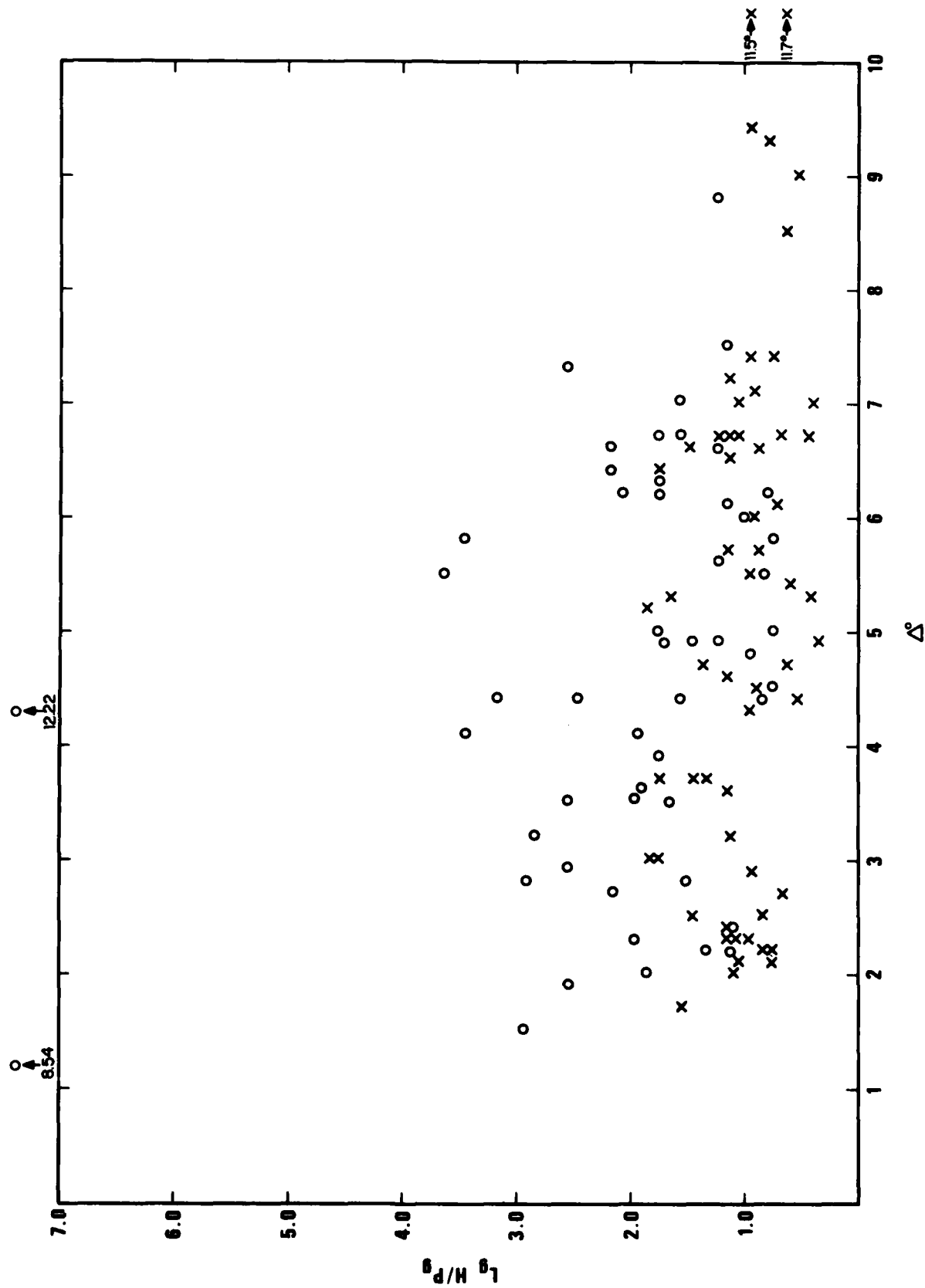


Figure 74. Trace amplitude ratios of L_g (horizontal component) to P_g plotted against epicentral distance. Explosion and earthquake data are designated with circles and triangles respectively.

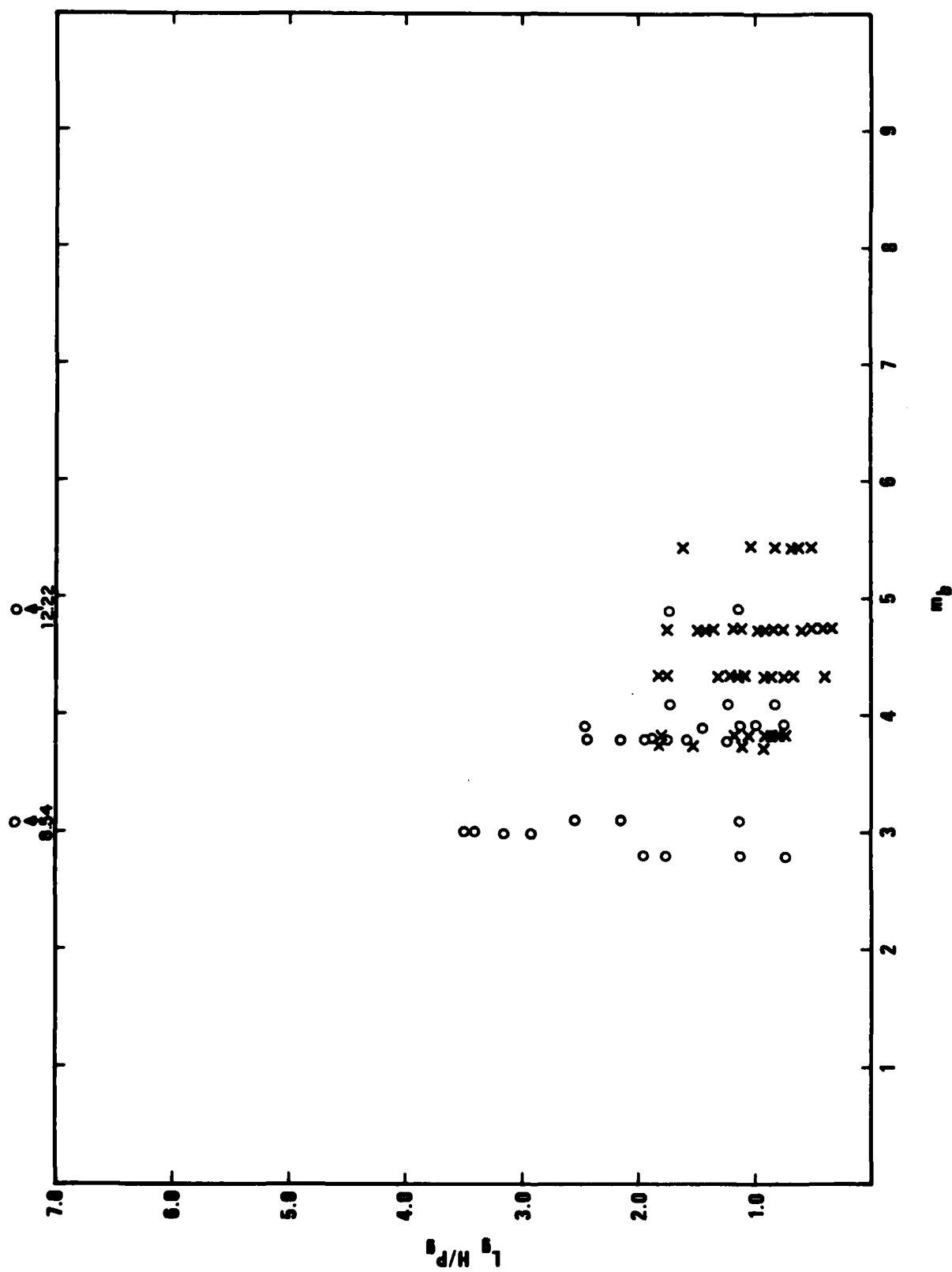


Figure 75. Trace amplitude ratios of L_g (horizontal component) to P_g plotted against event magnitude. Explosion and earthquake data are designated with circles and triangles respectively.

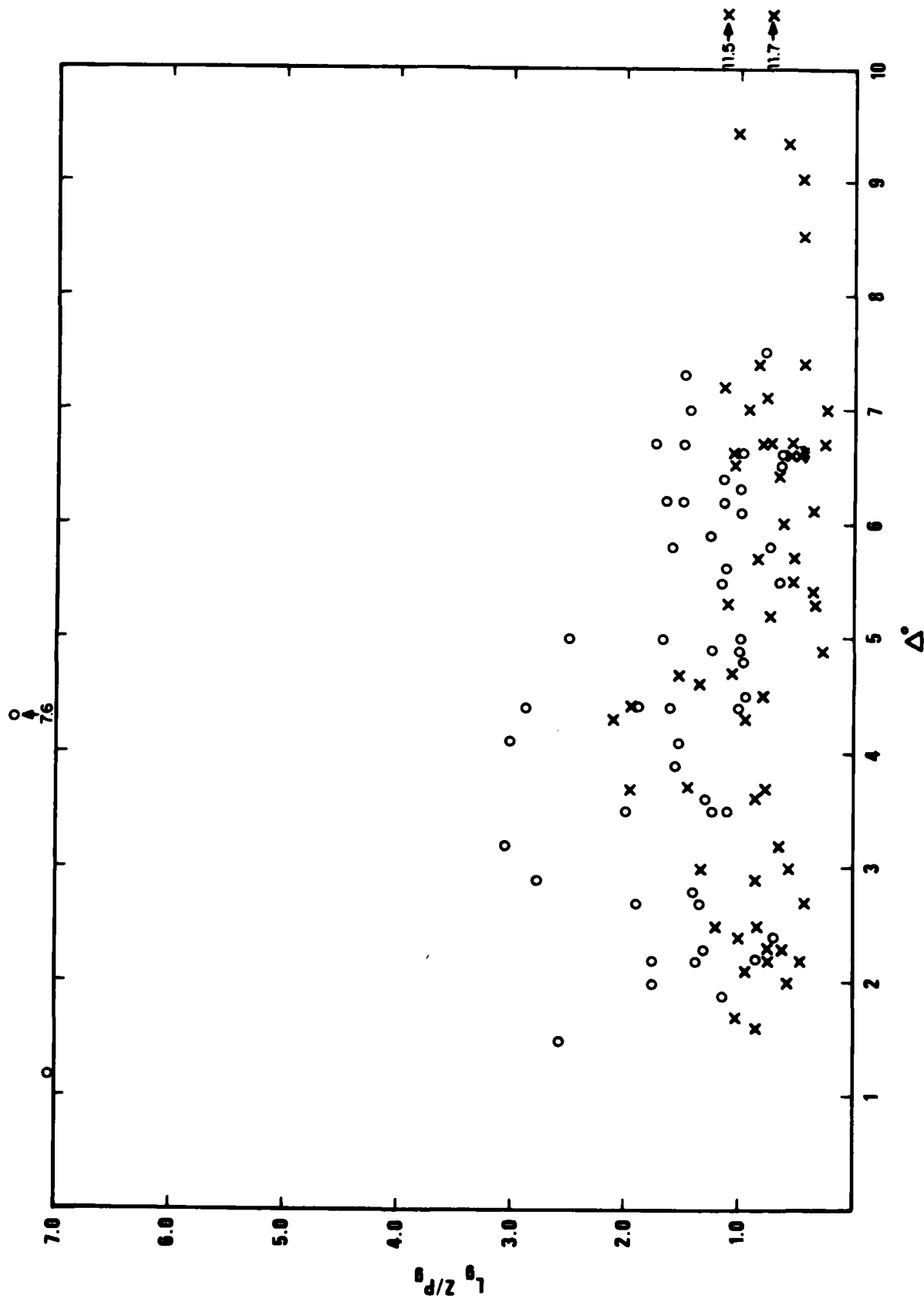


Figure 76. Trace amplitude ratios of L_g (vertical component) to P_g plotted against epicentral distance. Explosion and earthquake data are designated with circles and triangles respectively.

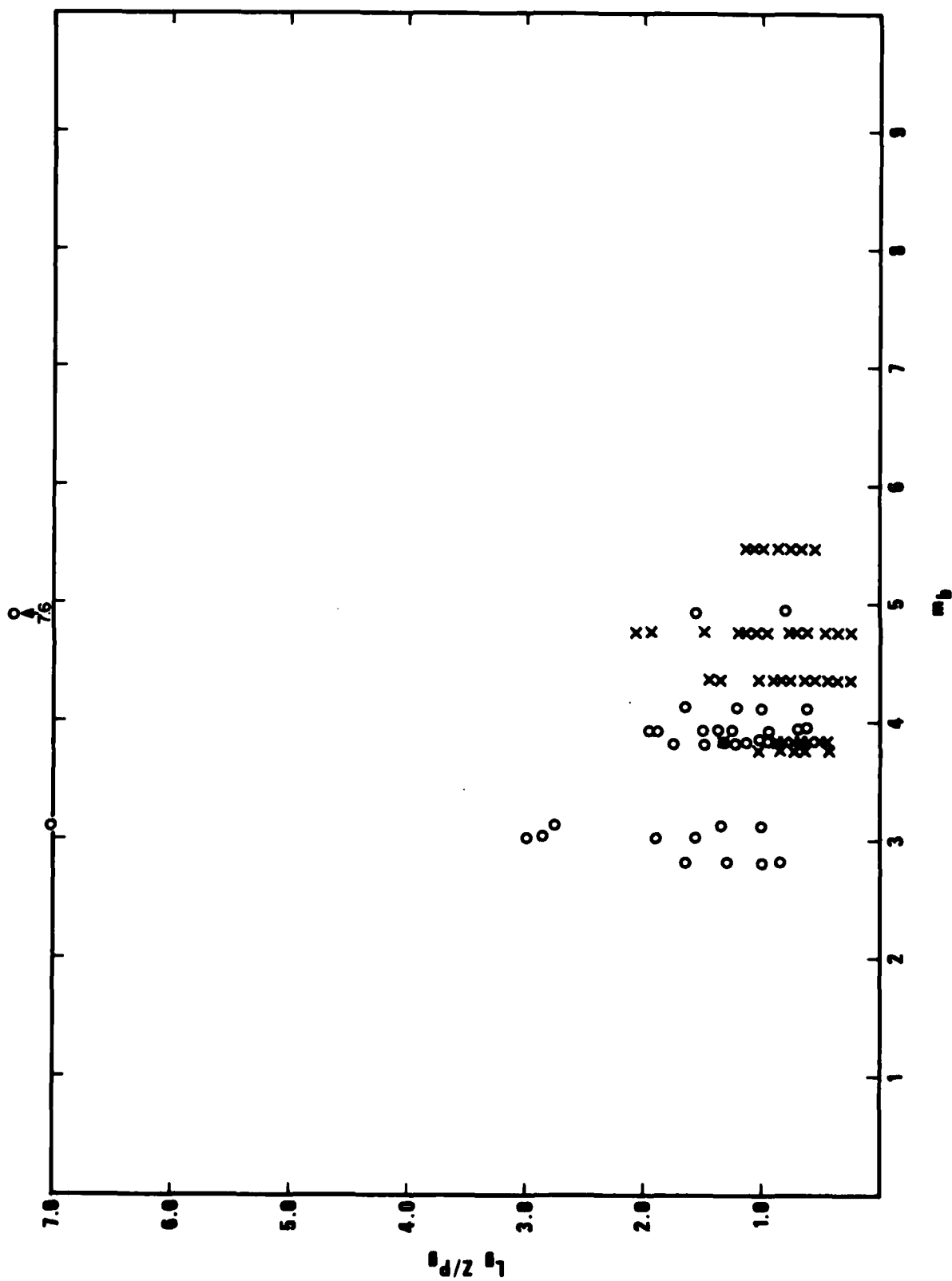


Figure 77. Trace amplitude ratios of L_g (vertical component) to P_g plotted against event magnitude. Explosion and earthquake data are designated with circles and triangles respectively.

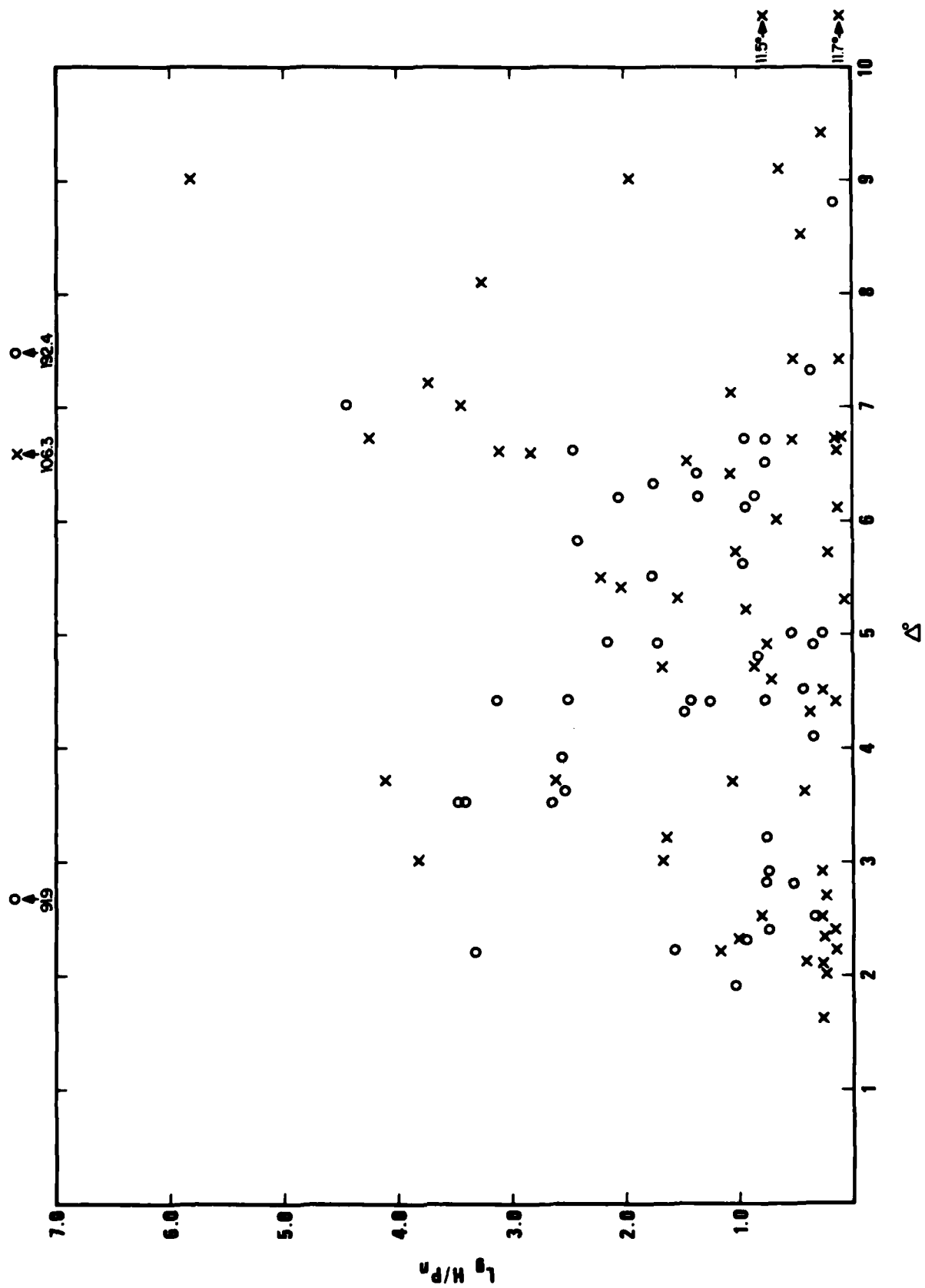


Figure 78. Trace amplitude ratios of L (horizontal component) to P (vertical component) plotted against epicentral distance. Explosion and earthquake data are designated with circles and triangles respectively.

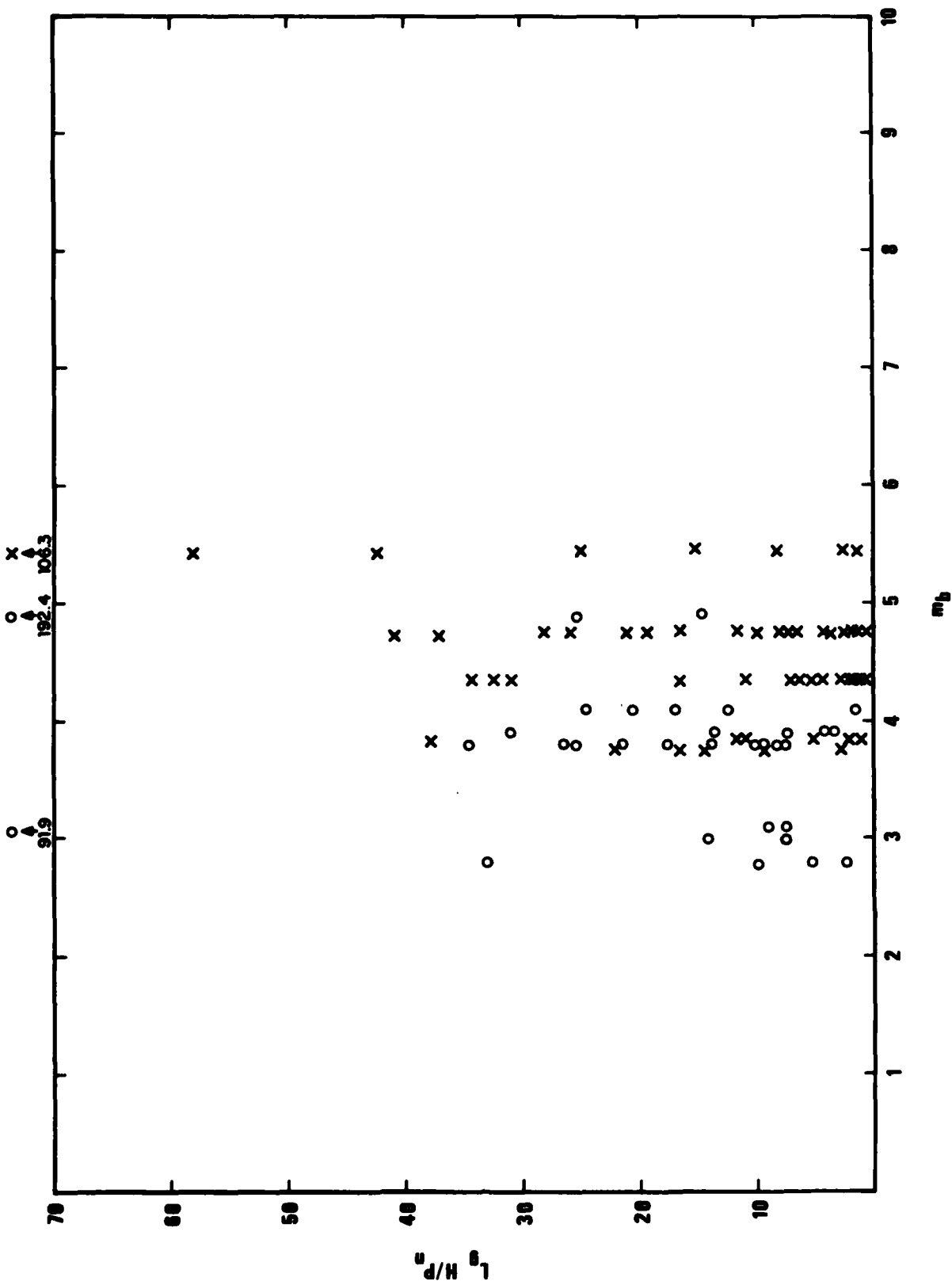


Figure 79. Trace amplitude ratios of L_g (horizontal component) to P plotted against event magnitude. Explosion and earthquake data are designated with circles and triangles respectively.

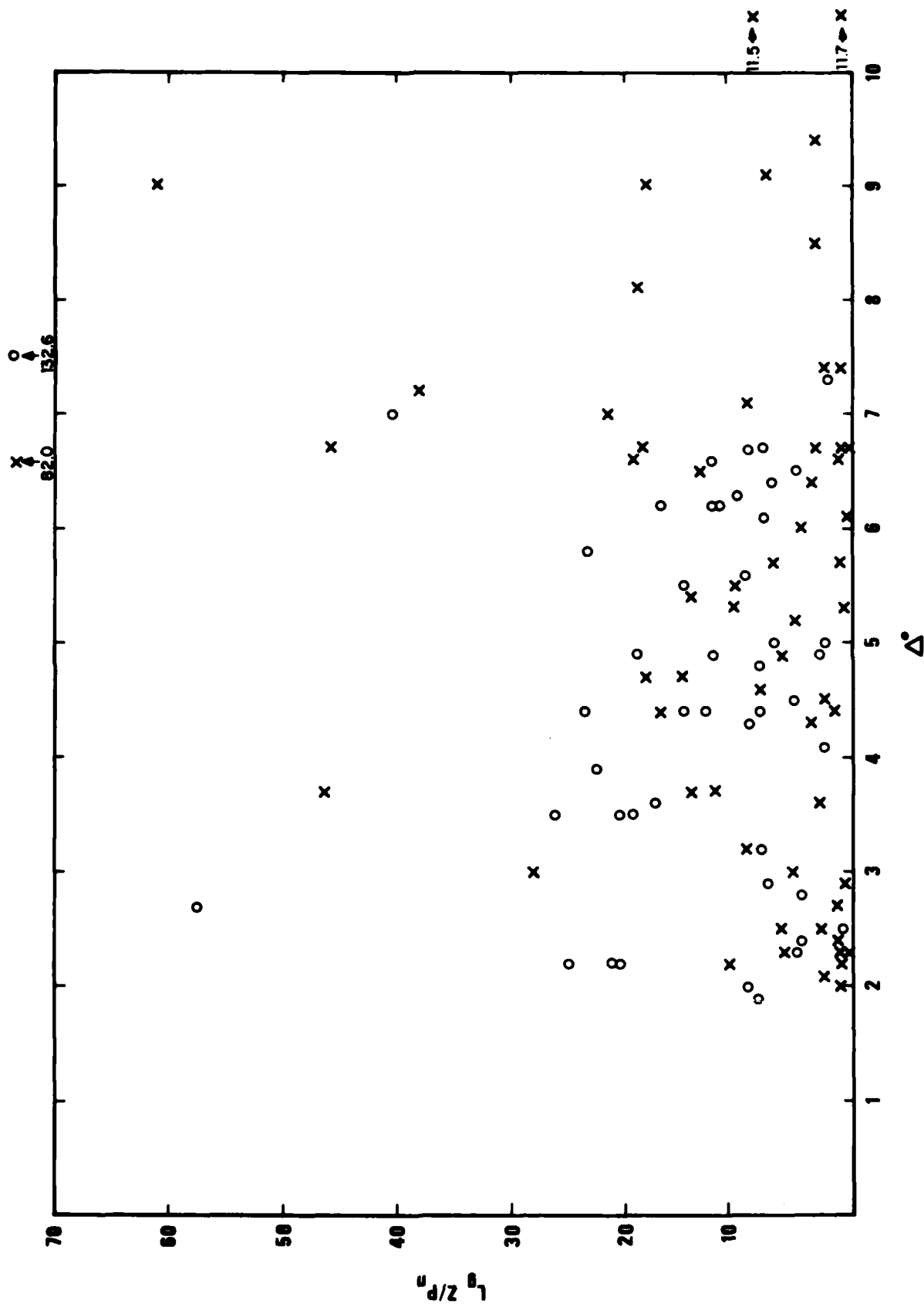


Figure 80. Trace amplitude ratios of L_g (vertical component) to P_n plotted against epicentral distance. Explosion and earthquake data are designated with circles and triangles respectively.

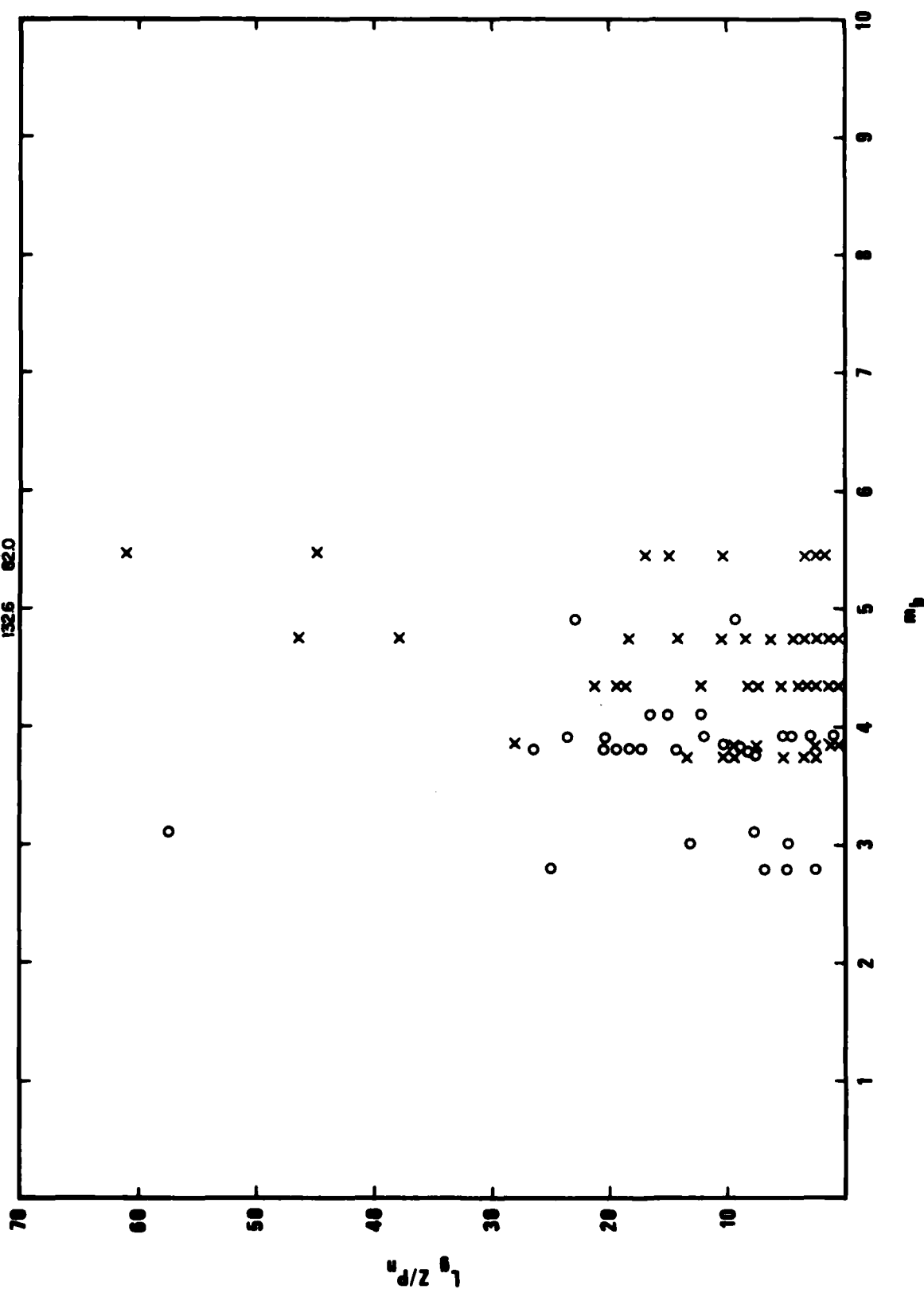


Figure 81. Trace amplitude ratios of L_g (vertical component) to P_n plotted against event magnitude. Explosion and earthquake data are designated with circles and triangles respectively.

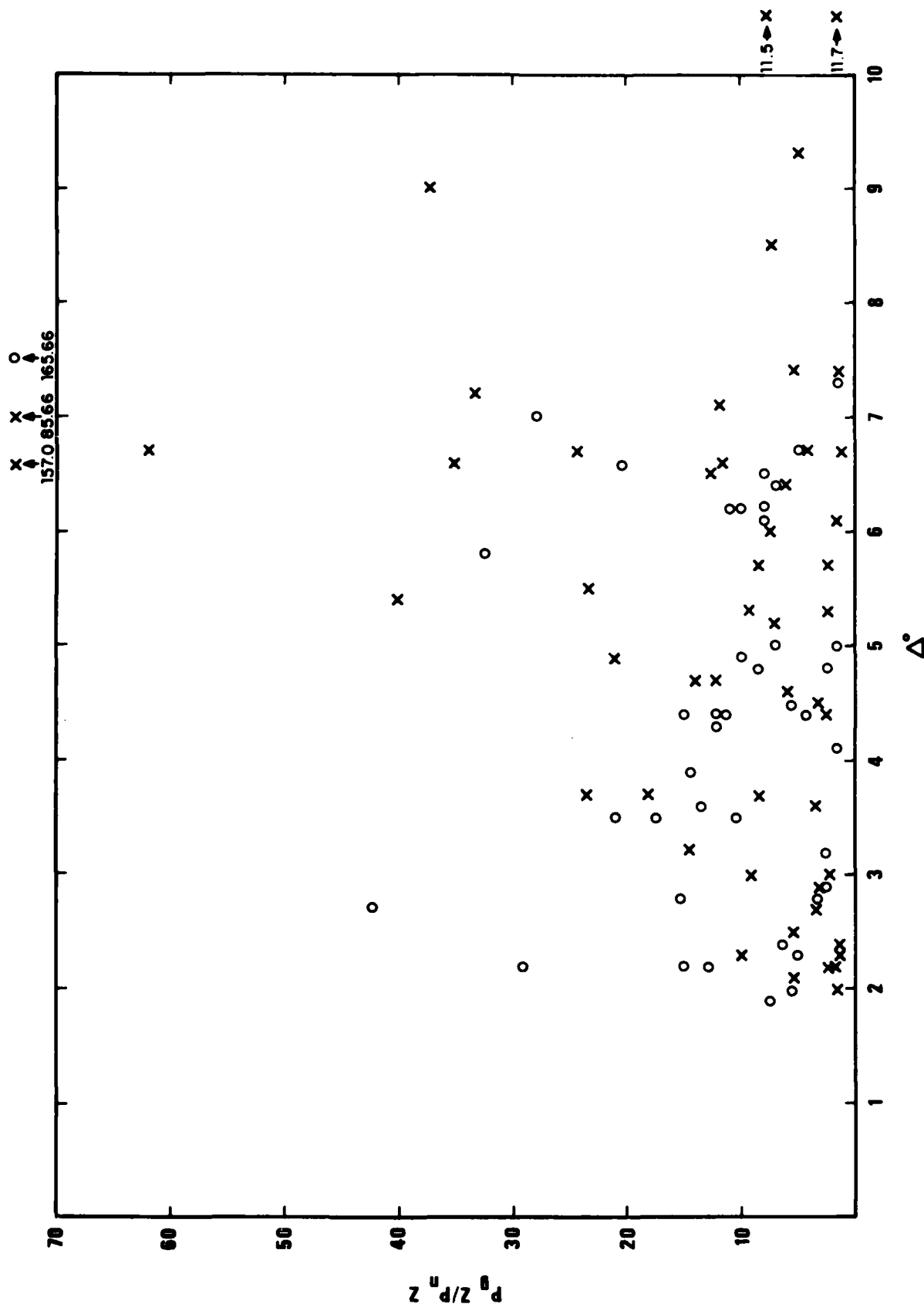


Figure 82. Trace amplitude ratios of P_n to P_n/Z plotted against epicentral distance. Explosion and earthquake data are designated with circles and triangles respectively.

amplitude ratio is only a moderately effective discriminant, not comparable in effectiveness to $M_s - m_b$.

The amplitude ratios involving P_n are shown in Figures 78 to 83. These confirm the findings of many investigators that P_n amplitudes in the western United States are quite unstable and cannot be used for discrimination (Evernden, 1967; Barker, 1981). The scatter in these plots is great, and there appears to be no clear separation between the explosion and earthquake data points.

The above data indicate that P_g to L_g amplitude ratios or m_b versus L_g amplitude may be useful discriminants in the SWUS. The weaker L_g amplitude for explosions may be partially a depth effect (Noponen, 1980; Bennett and Murphy, 1980).

KAMCHATKA-KURILES REGION

Structural Setting

Kamchatka-Kuriles is a typical island arc region with a deeply penetrating subduction zone under it. The whole region is highly active seismically, as Figure 84 shows. Most of the seismicity is confined to the region south of the junction of the Kamchatka-Kurile arc and the Aleutian arc. The depths of the earthquakes increase with the distance behind the arc. The focal mechanisms of the events in the trench are tensional in nature, to the bending of the lithosphere before subduction. The contact between the plates is characterized by thrust type focal mechanisms and moderate depths of the events. Deeper events behind the arc are either compressional or of indeterminate type. It also appears that the subducting plate is broken up into segments in the process of subduction, and the relative motion between these segments results in transverse slip type events at various depths. Figure 85 (after Veith, 1974) shows the types of focal mechanisms determined for a large number of events in the area along with the depth contours of the seismically active zone coinciding with the position of the subducting Pacific plate.

In detecting and identifying events at regional or teleseismic distances from this area, a thorough knowledge of the factors affecting the propagation of seismic waves is necessary in all the structural parts of the geology. For regional propagation, the structure of the crust is the prime controlling factor. Variations in thickness of both the crust and the overlying sediments are quite important. The nature of regional phases observable in areas outside the Kurile-Kamchatka arc must be quite different from those observed on large land masses, since the phases must propagate through ocean basins, trenches and other quite complicated regions. At teleseismic distances the body waves propagate through slabs, low Q zones in the upper mantle beneath

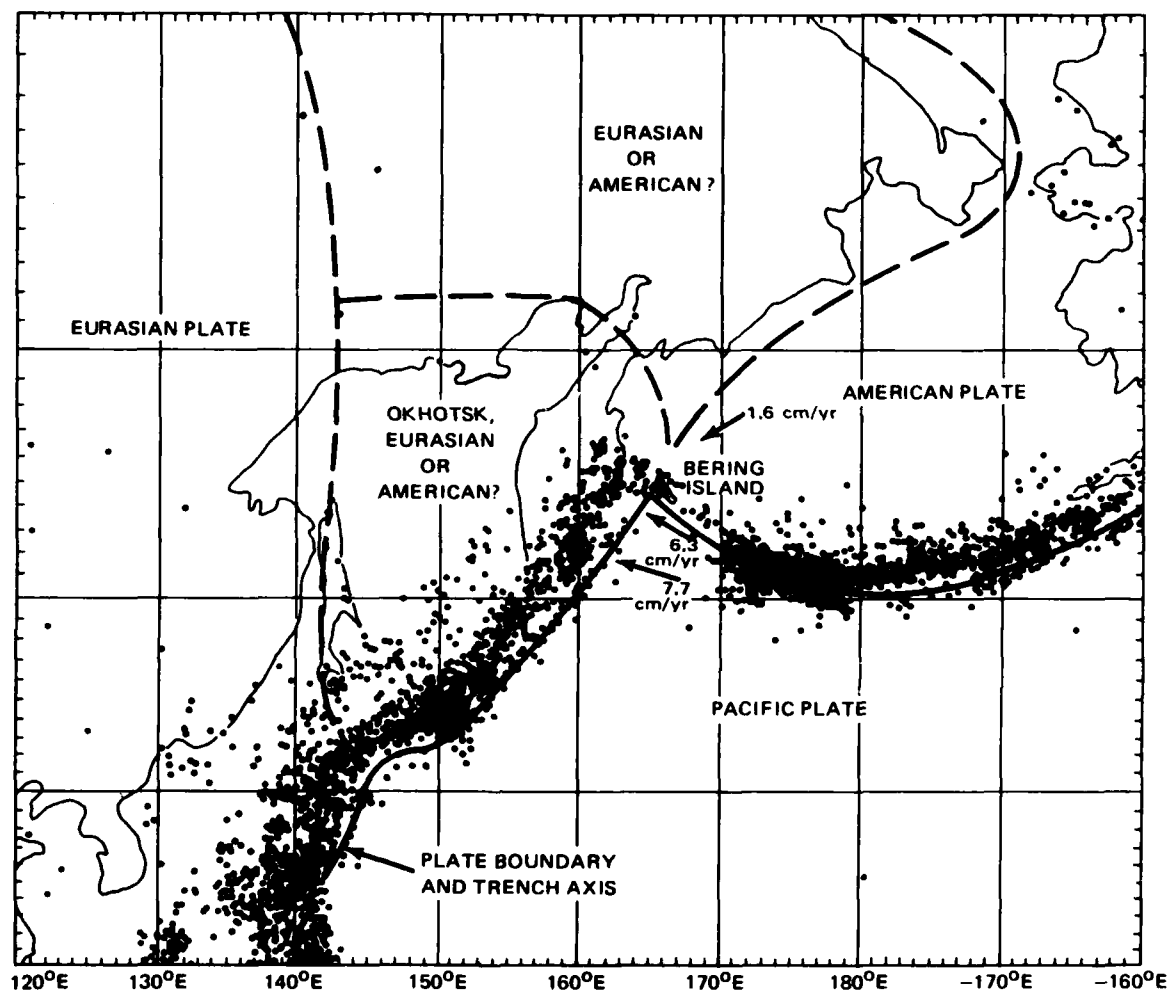


Figure 84. Seismicity map of the Kamchatka-Kuriles area.

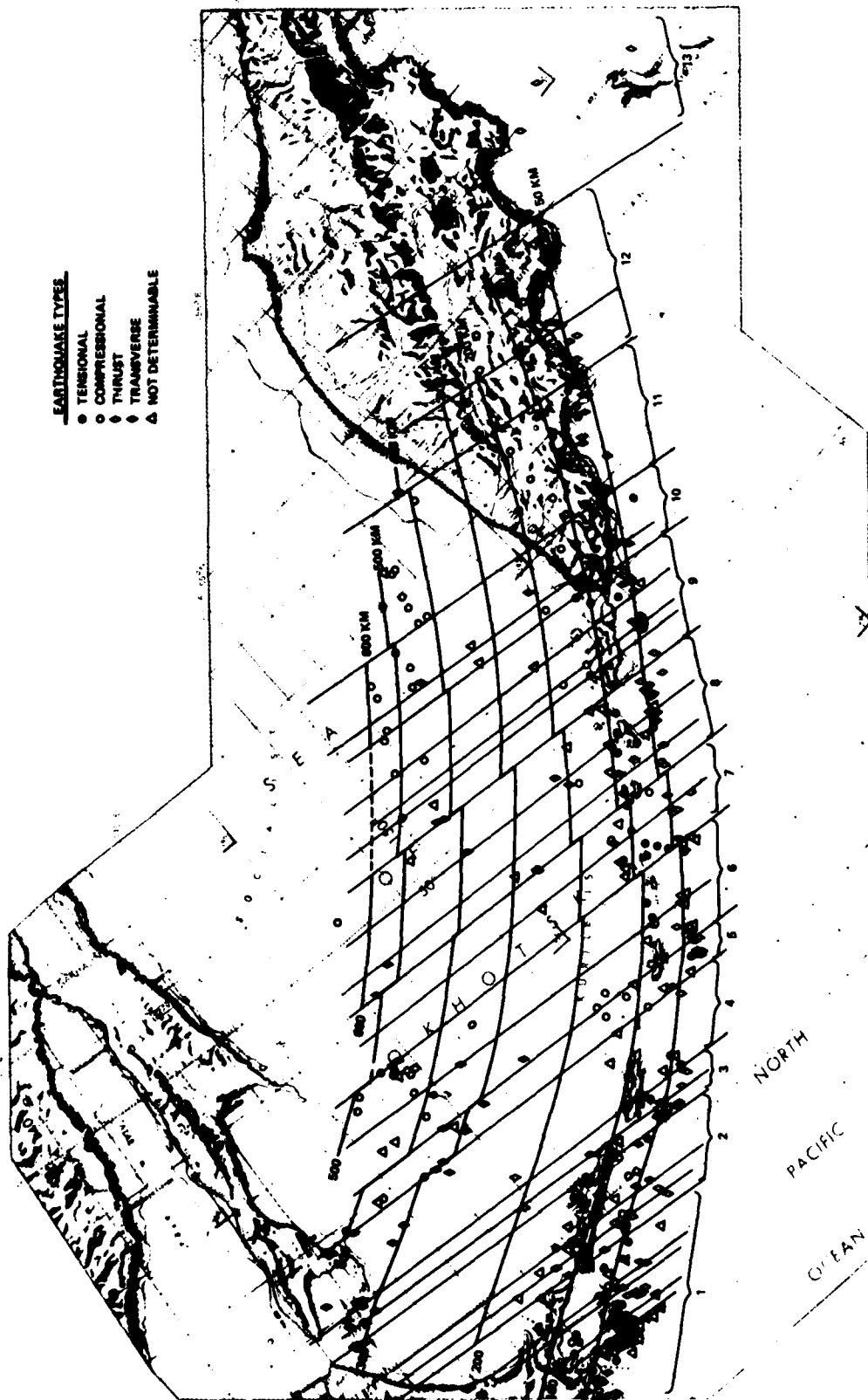


Figure 85. Focal mechanism types and depth contours of the seismic zone (after Veith, 1974).

marginal basins and, on the Pacific side, relatively old ocean type asthenosphere. We cannot expect to see continental type crustal phases such as L_g , but we may see high frequency oceanic type P_n and S_n unless some near-source structural feature prevents their propagation into the oceanic crust.

In addition to the western Pacific, the Kamchatka-Kuriles arc is surrounded by the Okhotsk Sea and the Bering Sea basins. Each of these has some quite characteristic features in crustal and upper mantle properties. The Bering Sea basin is bounded by the Aleutian arc in the south and the Alaskan and Siberian land masses. As shown in Figure 86, the Bering Sea has two shallow rises--the Boers ridge in the east and the Shirsov ridge in the West. The Shirsov ridge subdivides the Bering Sea basin into the Aleutian and the Kamchatka basins. All of the features are covered by sediments of appreciable thickness, but the Komandorsky basin has thinner sediments than the Aleutian basin. The heat flow is anomalously high under the Kamchatka basin, which may signify high attenuation in the mantle under this region. The crustal thickness is also thinnest in this area.

The Okhotsk Sea is also a marginal basin behind the subduction zone. The southern part of the basin adjoining Hokkaido is deeper and is also distinguished by the name of Kurile Basin. There are a few rises on the sea floor further north. The crustal thickness varies considerably over the region. As shown in Figure 87, it is less than 10 km in the Kurile basin but may be as high as 25 km under some portions of the Okhotsk Sea. The heat flow is considerably higher in the Okhotsk region than in the adjoining parts of the Pacific plate, indicating a high temperature upper mantle. An anomalous feature of the upper mantle in the Okhotsk area is the extremely high attenuation of body waves as evidenced by the reduction in the high frequency content of pP waves relative to direct P from deep events reflected under the Sea of Okhotsk. According to Toksoz and Bird (1977), the Sea of Okhotsk is a marginal basin in the "mature" stage where subduction has been active long enough to develop a high attenuation zone in the upper mantle. This is in contrast to the Aleutian basin, which is still in the "undeveloped" stage and does not have anomalously high

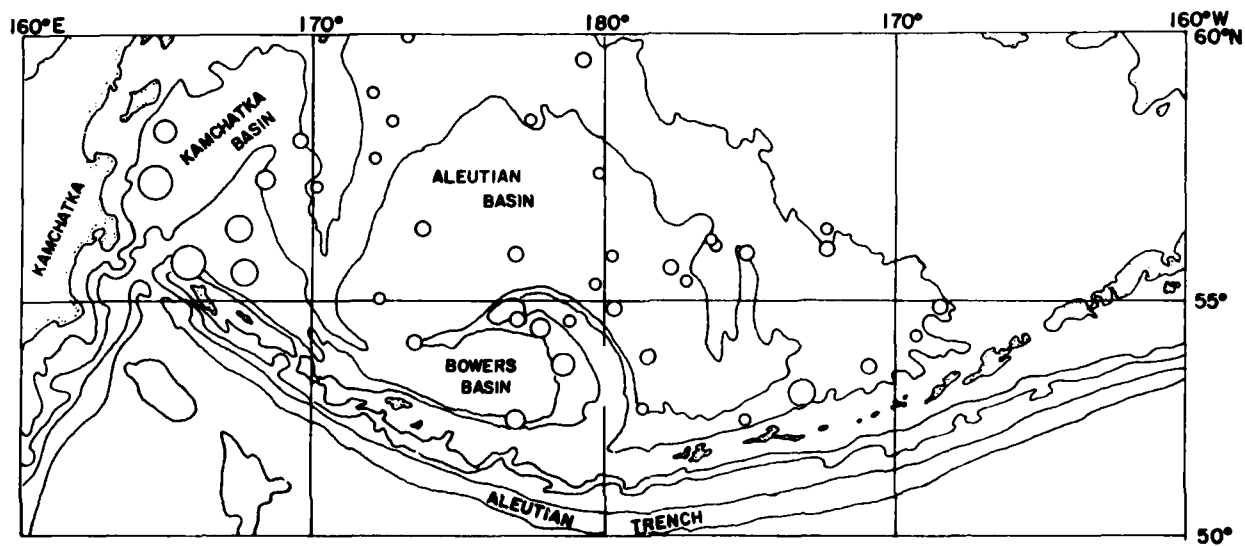


Figure 86. Major features of the Bering Sea region with the stations used in this study.

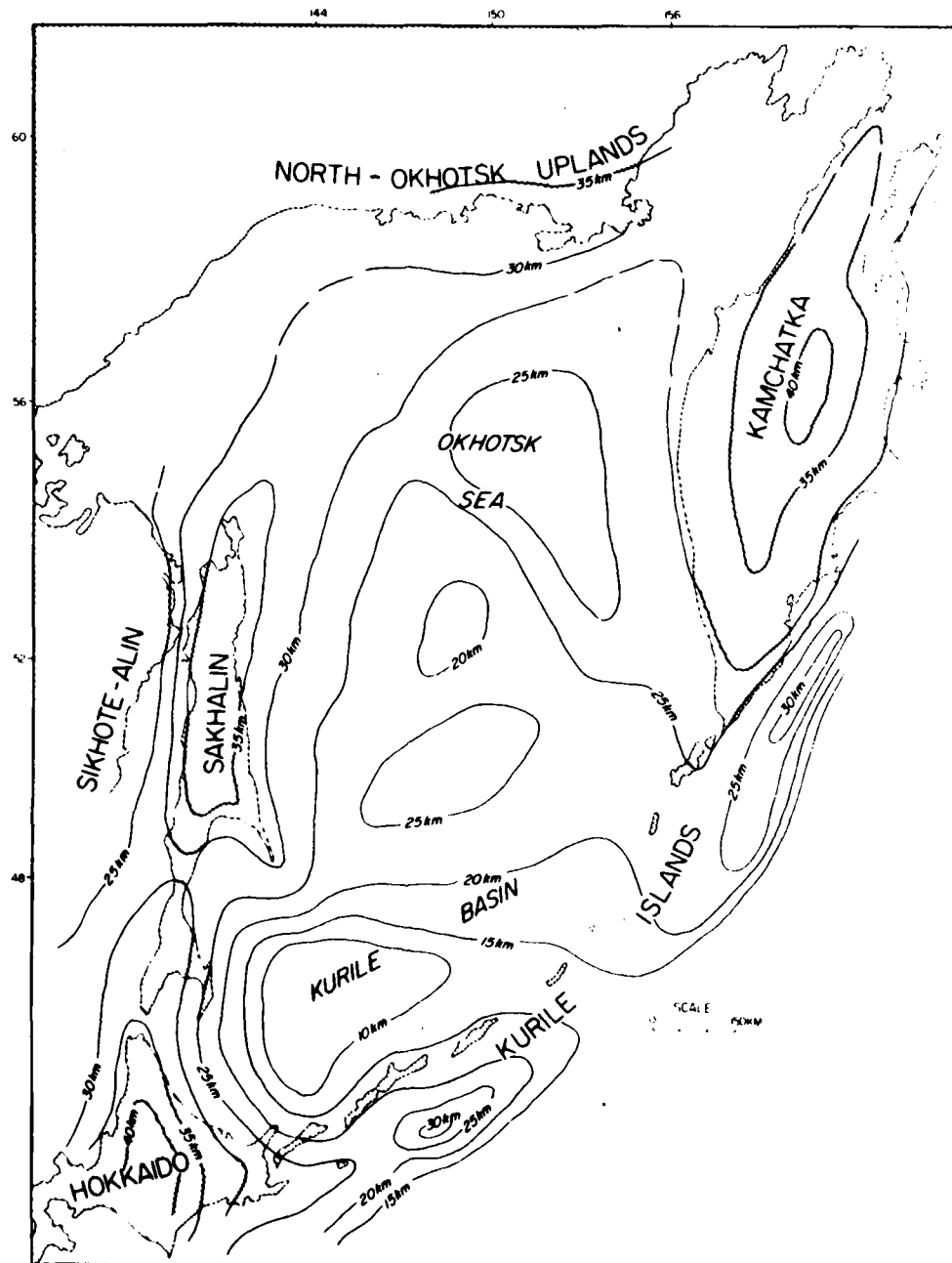


Figure 87. Major features of the Okhotsk Sea region. Crustal thickness map superposed.

attenuation in the mantle compared to the Sea of Okhotsk, Lau or other basins where the pP phases attenuate drastically (Barazangi, Pennington and Isacks, 1975).

Efficiency of Propagation and Amplitude-Distance Relationships

The Kamchatka-Kuriles area is the only region in our study that does not involve propagation over continental paths. Instead, the paths cross the complex areas described earlier in this report. The epicentral distances to the nearest stations are not truly regional but teleseismic. Consequently, the types of phases seen are typically oceanic rather than continental. Of course no L_g or P_g can be seen; only P_n and S_n are observable. Figure 88 shows a set of typical seismograms recorded at A from shallow events along the Kamchatka-Kuriles arc. The event parameters are listed in Table VII, and their locations are plotted on the map in Figure 89. Figure 88 shows P_n phases followed by a typical high frequency oceanic S_n . The travel times of these phases follow the graphs for velocities of 8.0 km/sec and 4.7 km/sec fairly well, Figure 90, and the deviations from these lines may be due only to event mislocation. The normalized amplitude-distance curves for S_n and P_n are shown in Figures 91 and 92. P_n appears to be smaller at A than at MAT and ADIS. S_n could be observed only at MAT and A, while at ADIS and other LRSM stations, no S_n could be observed. The reason for this is not known. The LRSM stations are further east than A, and there may be some feature along the Aleutians that causes blockage of S_n .

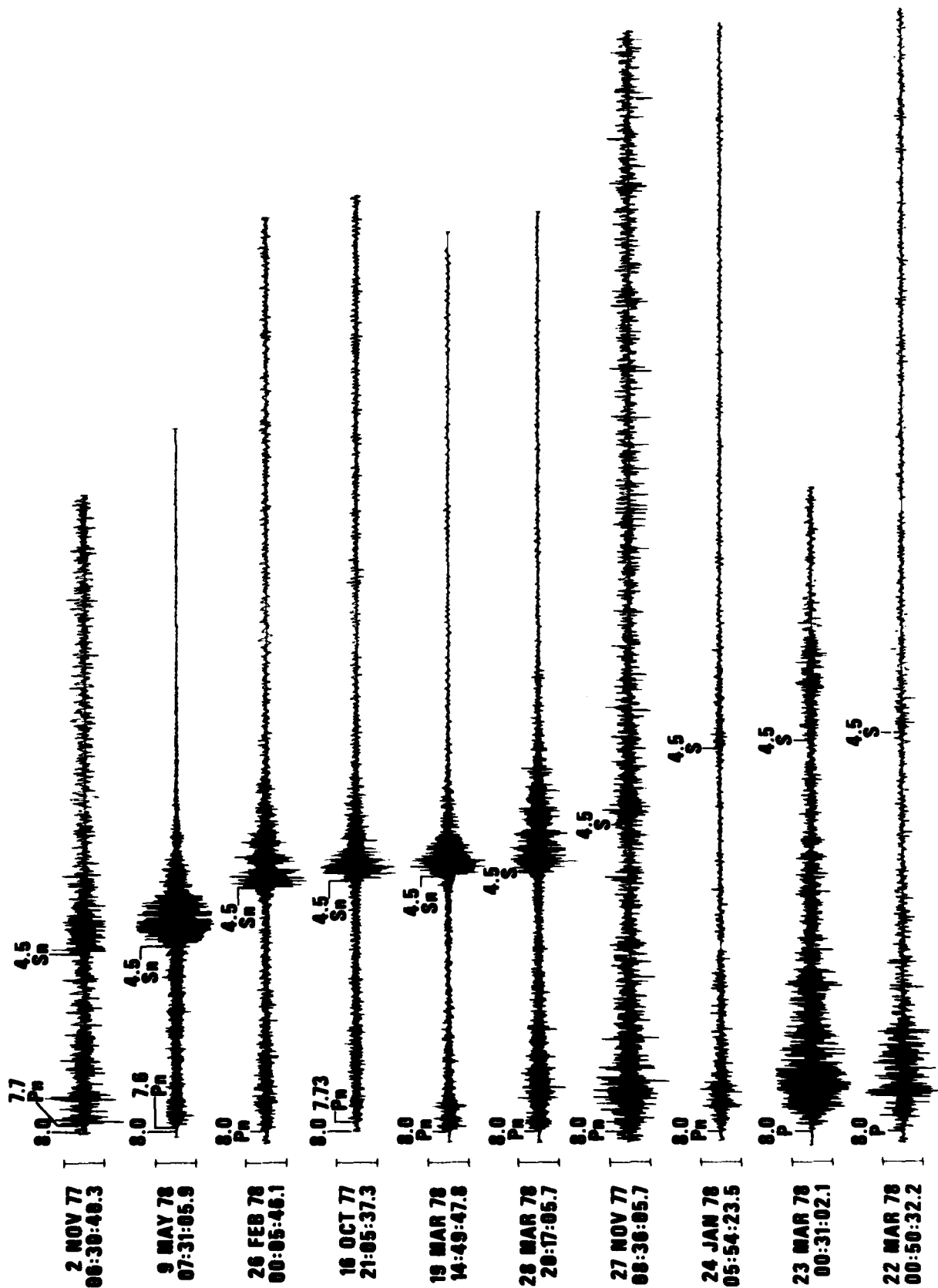


Figure 88. Seismograms from shallow events in the Kamchatka-Kuriles area as recorded at ATAK at various epicentral distances.

TABLE VII

NEIS Hypocenters for Earthquakes in the Kamchatka/Kuriles Region.

ADIS

<u>Date</u>	<u>Origin Time</u>	<u>Lat</u>	<u>Lon</u>	<u>Depth</u>	<u>m_b</u>
24 Jul 64	13 25 18.3	47.0N	153.9E	33	5.9
13 Oct 64	02 20 49.3	44.4N	151.6E	33	5.2
05 Dec 64	22 31 44.3	54.0N	161.5E	38	5.2
29 Jan 65	09 35 25.7	54.8N	161.7E	33	5.8
20 Apr 65	06 50 17.6	54.6N	161.4E	33	5.3
11 Jun 65	03 41 02.3	44.5N	149.0E	33	5.7
12 Jun 65	05 40 55.9	44.1N	149.3E	24	5.8
22 Dec 65	07 27 18.4	52.6N	160.2E	11	5.4
10 Aug 67	11 21 22.3	45.4N	150.3E	37	5.7
30 Aug 67	13 33 26.4	45.4N	151.5E	33	5.5
24 Jul 64	08 12 40.0	47.2N	153.8E	33	5.9
24 Jul 64	17 02 49.2	47.1N	153.6E	33	5.8
28 Mar 65	13 22 57.6	55.1N	162.1E	33	5.9
23 Oct 64	21 06 24.2	44.0N	147.5E	45	5.9
11 Jun 65	03 33 45.8	44.7N	148.9E	50	6.0

TABLE VII (cont.)

NEIS Hypocenters for Earthquakes in the Kamchatka/Kuriles Region.

MAT

<u>Date</u>	<u>Origin Time</u>	<u>Lat</u>	<u>Lon</u>	<u>Depth</u>	<u>m_b</u>
09 Jul 70	11 24 39.5	43.9N	148.5E	41	5.4
02 Aug 70	01 36 10.6	46.7N	152.5E	60	5.0
07 Aug 70	01 43 19.0	43.8N	148.3E	33	5.0
25 Aug 70	03 43 01.6	45.5N	150.0E	50	4.8
08 Jan 71	14 45 29.5	47.4N	154.4E	32	5.6
16 Oct 77	21 05 37.3	49.4N	155.4E	41	4.9
02 Nov 77	06 30 40.3	51.9N	160.1E	33	4.9
27 Nov 77	08 36 05.7	46.4N	153.3E	33	5.5
24 Jan 78	05 54 23.5	44.7N	149.7E	56	5.7
26 Feb 78	00 05 46.1	49.3N	155.6E	44	5.3
19 Mar 78	14 49 47.8	48.8N	155.2E	61	5.2
22 Mar 78	00 05 32.2	44.0N	149.0E	33	6.3
23 Mar 78	00 31 02.1	44.3N	149.1E	46	6.1
28 Mar 78	20 17 05.7	48.8N	154.9E	53	5.7
09 May 78	07 31 05.9	52.5N	158.1E	109	5.1

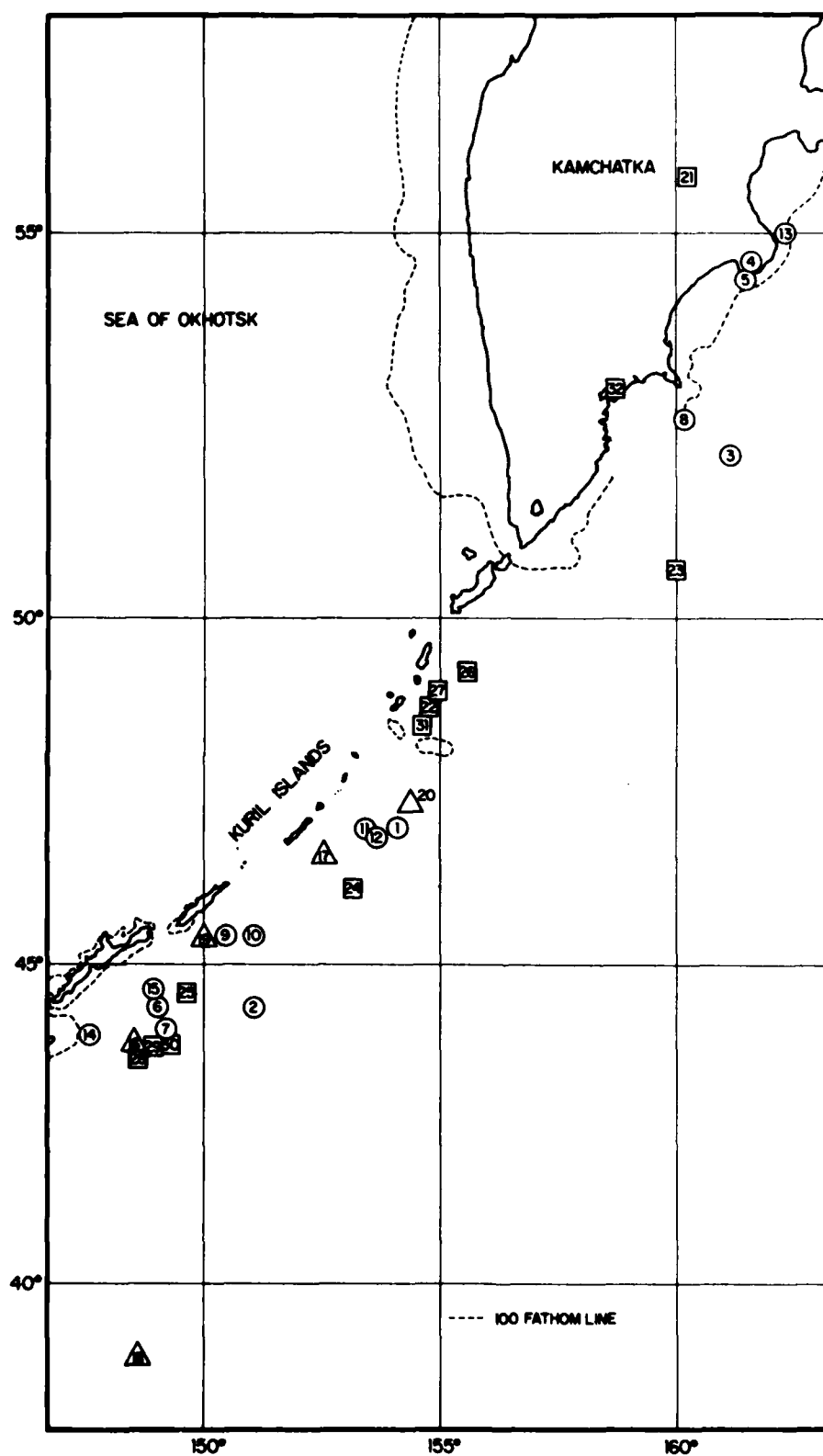


Figure 89. Location of the events used for the study of the Kamchatka-Kuriles area.

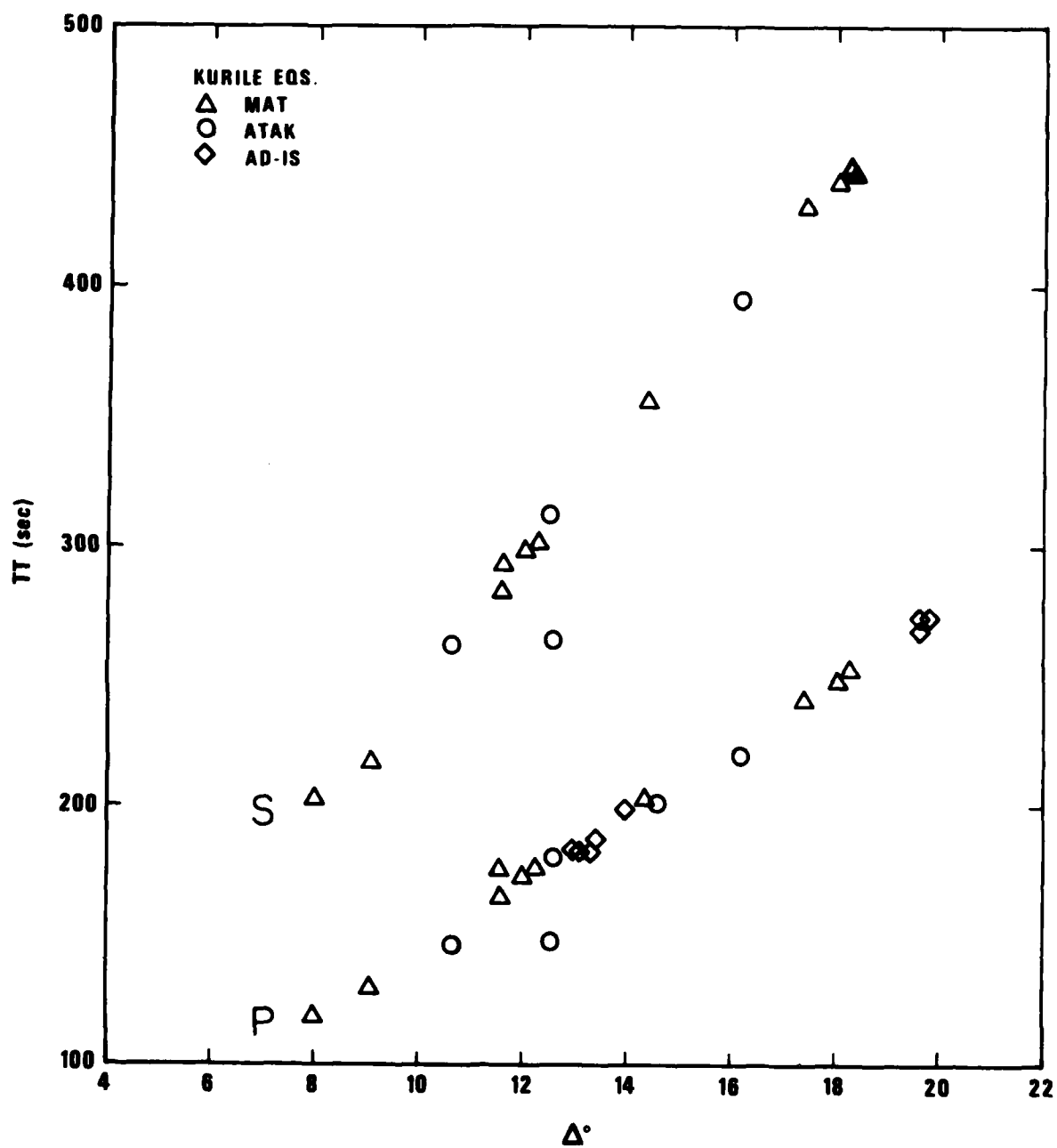


Figure 90. Travel time curves for the oceanic P_n and S_n .

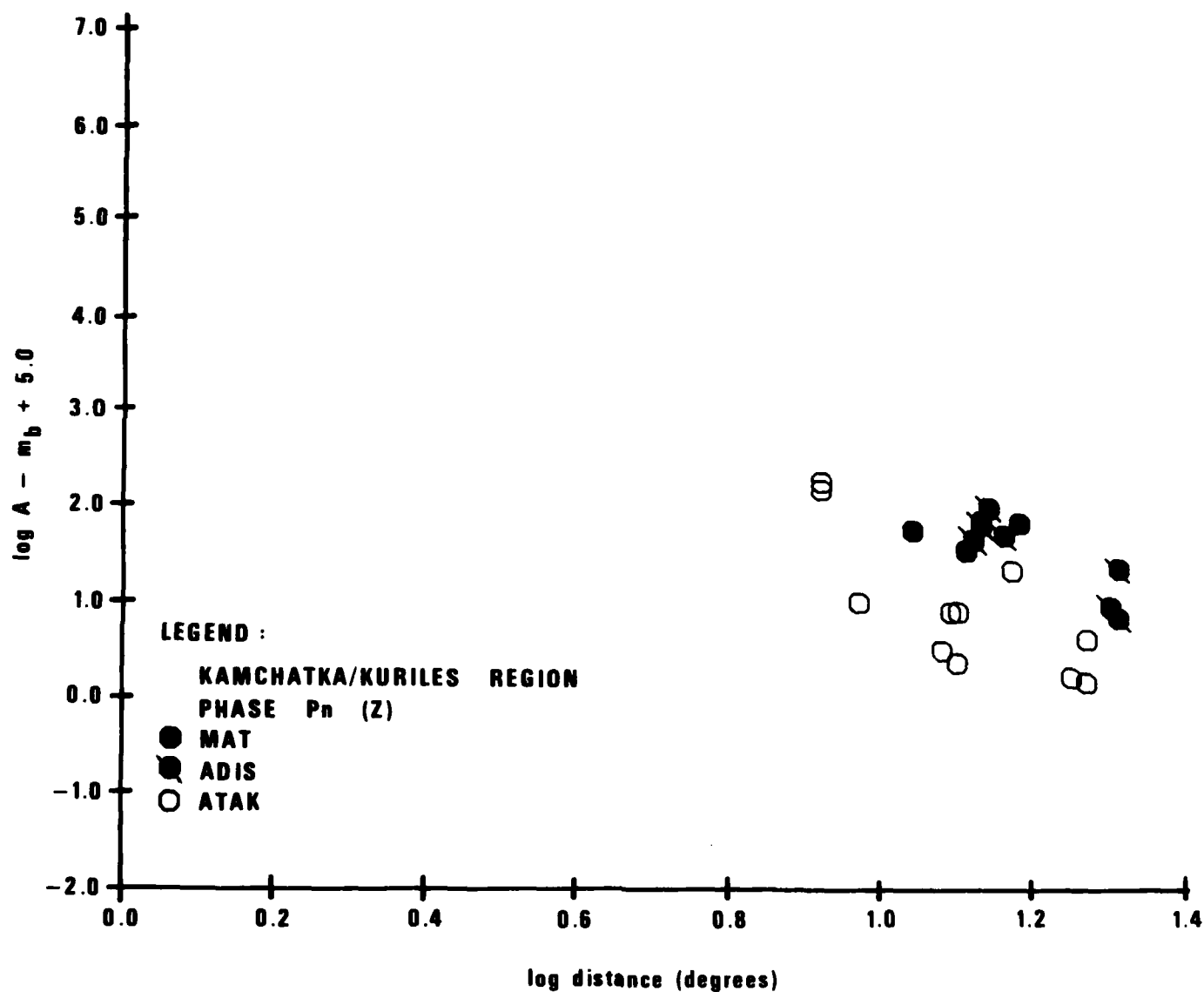


Figure 91. Trace amplitudes of P_n plotted against epicentral distance. The data points for the various stations are denoted by different symbols.

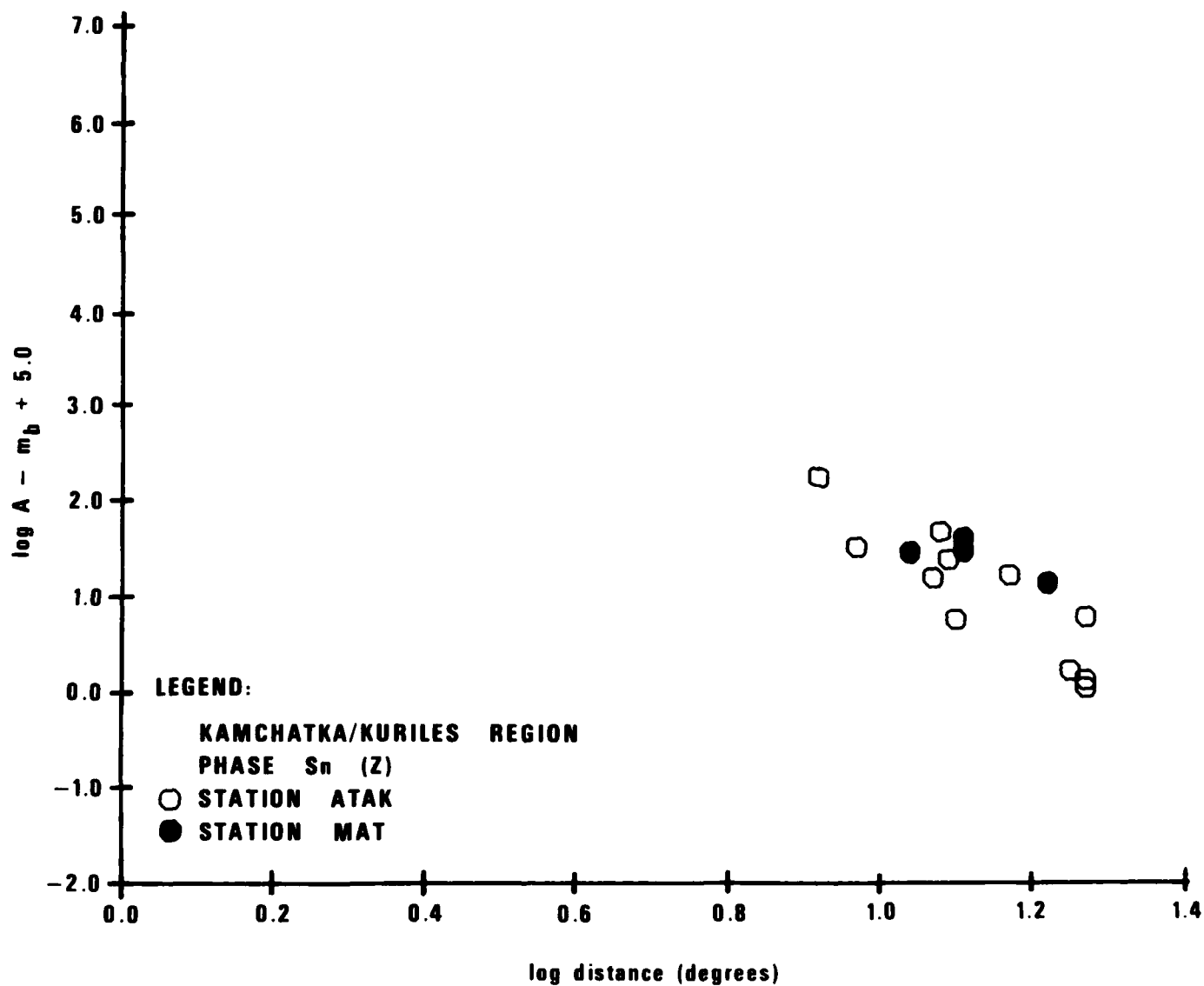


Figure 92. Trace amplitudes of S_n plotted against epicentral distance. The data points for the various stations are denoted by different symbols.

COMPARISON OF THE AMPLITUDE-DISTANCE RELATIONSHIPS IN THE VARIOUS REGIONS STUDIED

During the past 20 years, many formulations of amplitude-distance relationships for regional phases have been published for various regions of the Earth. The forms of the proposed relationships and the quantities measured vary. Some workers use wave amplitudes corrected in a manner similar to that employed in computing the body wave magnitude m_b . Others use trace amplitudes more in agreement with new proposed measures of magnitude such as the "a", "b" and "c" phases for measuring the energy in P arrivals. Some amplitude-distance relationships involve linear formulas in terms of logarithms of the amplitudes (or A/T) and the epicentral distance, while others use formulas derived from the assumed decrease of Airy phases with distance (Nuttli, 1973). The latter is used especially for L_g . Thus, there is an abundance of often incompatible formulations of amplitude-distance relationships, even within the same region. Moreover, the scatter in the data does not always allow one to say with certainty which of the formulations is more appropriate.

In this section, we shall attempt to compare our amplitude-distance relationships in a consistent manner from region to region. The reader can verify these comparisons by overlaying the various plots shown in previous section of this report. For the purpose of facilitating this, we have plotted all of the data to the same scale. We shall use the southern African data as our base of reference because southern Africa appears to have the simplest crustal structure from the point of view of lateral heterogeneity. It also exhibits the least scatter in the amplitude-distance plots for all regional phases. In addition, the greatest amount of data having the best coverage with respect to distance comes from southern Africa, making this data set very suitable for comparison with other areas.

From a geophysical point of view, southern Africa is a typical shield; therefore, all comparisons with other regions will reflect differences with respect to a shield.

Consider first the scatter plots of amplitude versus distance for P_n . Comparing the South American data with southern Africa, no clear difference can be seen for the shield type paths. Similarly, there appears to be no difference for shield paths in Pakistan. It appears that the level of excitation and the decay of amplitudes with distance is the same for shields in all of the regions studied. One could make a case for a slightly faster falloff rate for the SWUS. The shield curve would also fit the Kamchatka-Kuriles data with the exception of station A which has lower amplitudes. We therefore conclude that the same formula can be made to measure event magnitude from P_n in all shield paths and also along some oceanic paths. This is not true, however, for non-shield paths. Mountain paths in South America and Pakistan would attenuate P_n at a higher rate, and paths in the SWUS would require a quite different formula for estimating event magnitude from P_n (Evernden, 1967). It must be noted that P_n has the most scatter in amplitude even along shield type paths, indicating that it is less stable than other regional phases.

Inspecting the plots for P_g , it appears that P_g was observed along certain paths in South America. Unfortunately, our data is not sufficient to discern any differences with respect to amplitude-distance curves between southern Africa and South America. The same can be said about Pakistan, although the observed P_g , mostly along shield paths, overlays the curve for Africa. The P_g for the SWUS is unique. It has an extremely high amplitude and decays rapidly with distance. Nuttli (1978) notes similar P_g phases in southern Asia. It is possible that the stations used in this study were too far from the sources to observe P_g of this type along mountainous paths from Iran or Tibet.

For S_n the South American data fall roughly where the southern African points are, although a somewhat higher falloff rate in South America may be present. The Pakistan results are not significantly different from the southern African data, but the data are sparse. The few S_n observations in the SWUS also overlay the southern African points. The Kamchatka-Kuriles data for oceanic S_n fall off more

rapidly with distance and indicate lower S_n amplitudes over oceanic paths than over shield type paths.

The vertical and horizontal components of L_g exhibit amplitude-distance relationships for shield type paths in South America and Pakistan that appear to be identical to those in southern Africa. However, the scatter is greater than in Africa. Mountain paths in general show reduced amplitudes for L_g . In the SWUS, the amplitude of L_g near the source is about the same as in shields, but it decays faster with distance. Naturally no L_g was seen in the Kamchatka-Kuriles region.

Having made the comparisons outlined above, we can now state approximate formulas for estimating magnitudes of events in the various regions studied. These formulas are directly comparable and use the same measured quantities.

Based on the amplitude-distance plots for regional phases in southern Africa, the following magnitude formulas can be given for shield areas (including those in South America and Pakistan-India as well).

For the phase P_n

$$m_b = \log_{10} A_{m\mu} + 1.275 \log_{10} \Delta^\circ + 1.745$$

For P_g

$$m_b = \log_{10} A_{m\mu} + 1.839 \log \Delta^\circ + 0.908$$

For S_n

$$m_b = \log_{10} A_{m\mu} + 1.890 \log \Delta^\circ + .788$$

For the transverse component of L_g

$$m_b = \log_{10} A_{mu} + 1.858 \log_{10} \Delta^\circ + .091$$

And for the vertical component of L_g

$$m_b = \log_{10} A_{mu} + 1.912 \log_{10} \Delta^\circ + 0.157$$

The formula for P_n can be used for magnitude estimation in the Kamchatka-Kurile region as well. We do not have sufficient data to

specify reliable magnitude formulas for mountainous paths in either the South American or Pakistan-India regions, provided such formulas can be defined at all. Although Nuttli (1979) gave such results, the available evidence indicates that the results obtained for individual events would be quite unreliable due to the laterally varying nature of the propagation efficiency in these areas. The application of the formulas for the shield regions given above to the mountainous paths would tend to underestimate the event magnitudes because of the higher attenuation along those paths.

Clearly, we need different magnitude formulas for the southwestern United States. For explosions, we can deduce the following formulas from the amplitude-distance plots given in this report.

For P_n

$$m_b = \log_{10} A_{m\mu} + 3.803 \log_{10} \Delta^\circ - .134$$

For P_g

$$m_b = \log_{10} A_{m\mu} + 3.048 \log_{10} \Delta^\circ - .507$$

For the transverse component of L_g

$$m_b = \log_{10} A_{m\mu} + 3.157 \log_{10} \Delta^\circ - .577$$

And for the vertical component of L_g

$$m_b = \log_{10} A_{m\mu} + 3.021 \log_{10} \Delta^\circ - .376$$

These formulas reflect the high attenuation of regional phases with distance in the southwestern United States (Δ^{-3}) as compared to that in shield areas. Due to the problems associated with the NEIS magnitudes for the earthquakes in our data set, we are, at this state, not able to give magnitude formulas for earthquakes.

STUDIES OF CRUSTAL Q USING CODAS OF REGIONAL EVENTS

Attenuation in the crust as well as in other parts of the Earth is the prime factor determining the detectability of seismic waves, since relatively small changes in Q or t^* make a great difference in the detectability of signals. This is because amplitudes depend exponentially on these quantities. Besides the detectability of signals, any source diagnostic that depends on the frequency content of signals is likewise influenced by Q , and its application may be seriously hampered by low Q . For example, decoupled explosions may generate proportionately more high frequency seismic energy than tamped ones and may be diagnosed by this property (Rodean, 1979; Terhune et al., 1979; Murphy, 1980). Since regional phases primarily propagate in the crust and the uppermost part of the mantle, the value of Q in the lithosphere will determine the frequency content and detectability of these phases.

A new and practical method for the determination of crustal Q_β was devised by Aki (1969) and Aki and Chouet (1975) using the characteristics of codas from local earthquakes. Since the late coda of an event consists of scattered waves arriving from increasing distance with increasing time, the frequency content of the coda will change in a manner that is determined by the Q of the crust and its frequency dependence. Various versions of the method have been developed. One approach employs band pass filtering of the coda and independently determines the Q for each frequency from the rate of decay of band (Aki and Chouet, 1975; Tsujiura, 1978; Der, O'Donnell and Klouda, 1981). Another version uses the change with time of the dominant period of the coda to determine Q , assuming no dependence of Q on frequency. This version involves comparisons with master curves derived from the instrument response and various constant Q values assuming a flat source spectrum (Aki, 1969; Herrmann, 1980). This assumption restricts the analysis to frequencies below the corner frequency.

In our past work and in the work presented in this report, we use the former approach, i.e., we band pass filter the data. This has the advantage that the frequency dependence of Q can be readily evaluated,

and it does not depend on the assumption that the source spectrum is flat for the frequencies used in the analysis (Herrmann, 1980). Thus the entire range of available signal frequencies can be utilized in the analysis, instead of only frequencies below the corner frequency of the event.

In addition to frequency dependence of Q , the problem may be complicated by possible mode conversions, variable Q 's and group velocities for the converted modes. We believe, however, that for the later coda of L_g , the mode conversions to lower order modes, that are preferably excited, will have decayed due to lower Q for such modes. Thus the original assumption used by Aki (1969) and Herrmann (1980, that the modal composition of the scattered and primary waves is the same, is probably valid. In our analyses, we assume that the modal compositions, Q values and group velocities of the scattered and primary waves are identical. The computer algorithms used to compute theoretical coda envelopes as functions of frequency have been described in a previous report (Der, O'Donnell and Klouda, 1981). The Q used in all discussions is an effective Q , consisting of both the anelastic attenuation and the losses due to scattering. Our use of the method by Aki (1969) does not imply acceptance (or non acceptance) of later developments by Aki (1980) claiming that practically all loss in the lithosphere is due to scattering.

The effective Q derived by this method is a measure of the total loss in the crust regardless of the causes, as long as the assumption of negligible mode conversion and the scattering interpretation of coda are valid. It will properly characterize the detectability and changes in the frequency content of regional seismic signals of prime interest for detection and discrimination.

The analysis of seismic codas in this report involved the following steps:

- 1) At each station, regional or local events having the best available S/N in the coda were selected. (The main part of L_g often clipped.) A starting time in the coda was selected well beyond

the arrival of fundamental modes of L_g that are often hidden in the coda.

2) The codas were filtered using a set of fixed band pass filters. The smoothed RMS coda levels were normalized and plotted as a function of time for the various band pass outputs. The program also determined the dominant frequencies of the outputs automatically. These may not coincide exactly with the centers of the band-pass filters because of the interactions of the coda spectrum with the filter responses. The noise preceding the first arrivals was also filtered using the same set of filters, and the RMS noise levels and twice these levels were indicated on the coda graphs to prevent the misinterpretation of noise as coda in the final determination of Q .

3) Using the actual dominant frequencies of the band-pass outputs, the group velocities of L_g observed for the main part of the wavetrain and the distance of the events, families of theoretical curves for the coda decay were computed using various Q values. These theoretical curves, plotted on the same scale, were used to determine Q by comparison with the actual coda RMS plots. Since the Q values were determined for a set of frequencies, the frequency dependence of Q was also plotted.

Figures 93a and b show typical plots of RMS coda levels in various bands along with the best fits to determine Q . The noise levels are indicated by bars at the end of the plots (RMS and 2XRMS). In fitting Q , we disregarded the portions of the coda which were below twice the RMS level of the background noise.

Figures 94 to 100 show Q^{-1} from codas at the NTS station OB2NV plotted against frequency. The events used for coda analysis are listed in Table VIII. All of the curves for OB2NV show a rapid decrease of Q^{-1} , i.e., increase of Q with frequency, but the details differ. The differences are due either to uncertainties in the method or to differences in the areas sampled by the various events. There appears to be no discernible pattern of change in the character of these coda Q estimates with epicentral distance up to nearly 1000 km.

08 JUN 77

$\Delta = 512.4$

E. AZ - MEXICO BORDER REGION

$m_b = 4.8$

O.T. = 13:09:07.4

ANMO

31.0°N, 109.2°W

h = 56

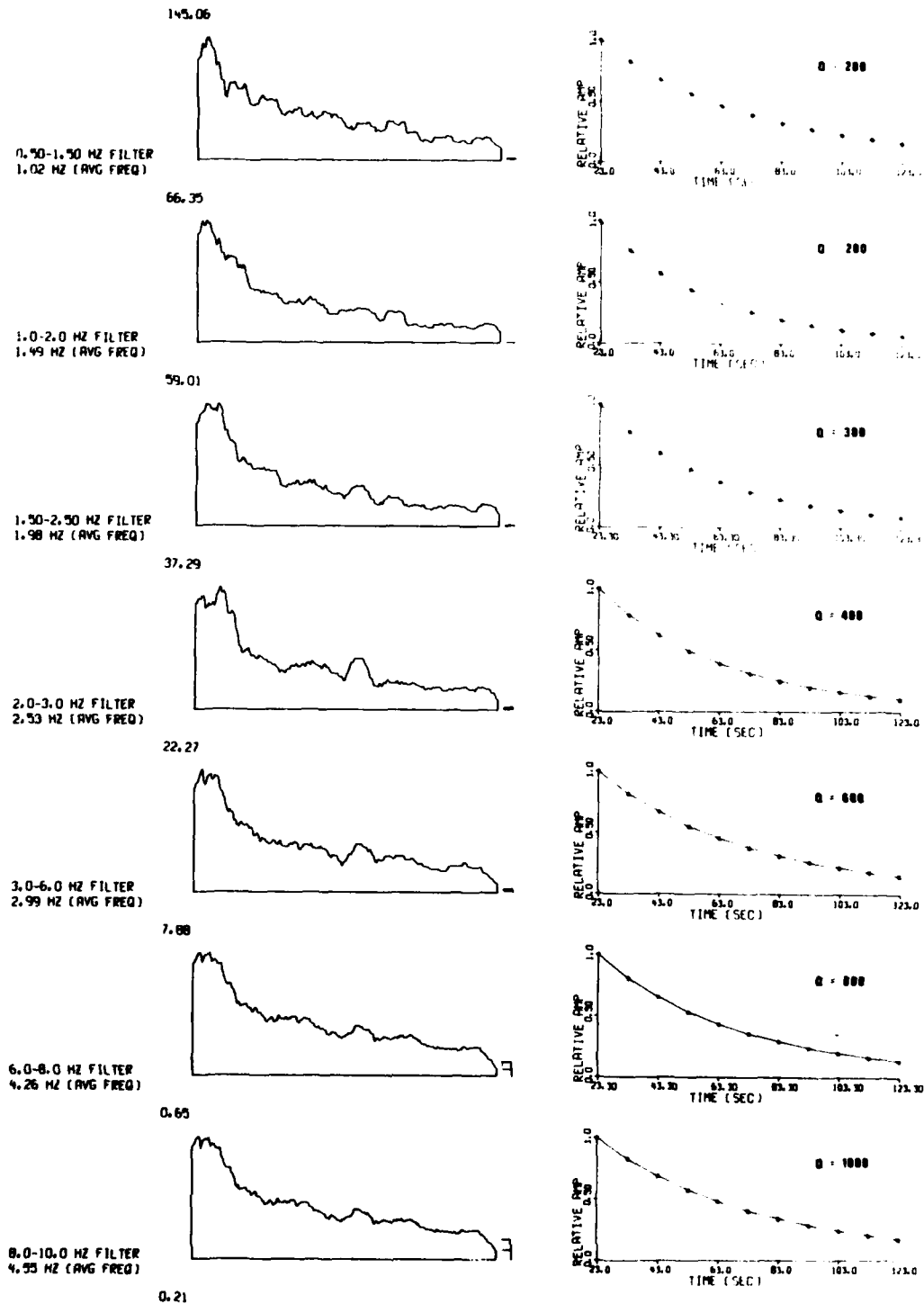


Figure 93. Illustration of the procedure for determining Q in the crust.

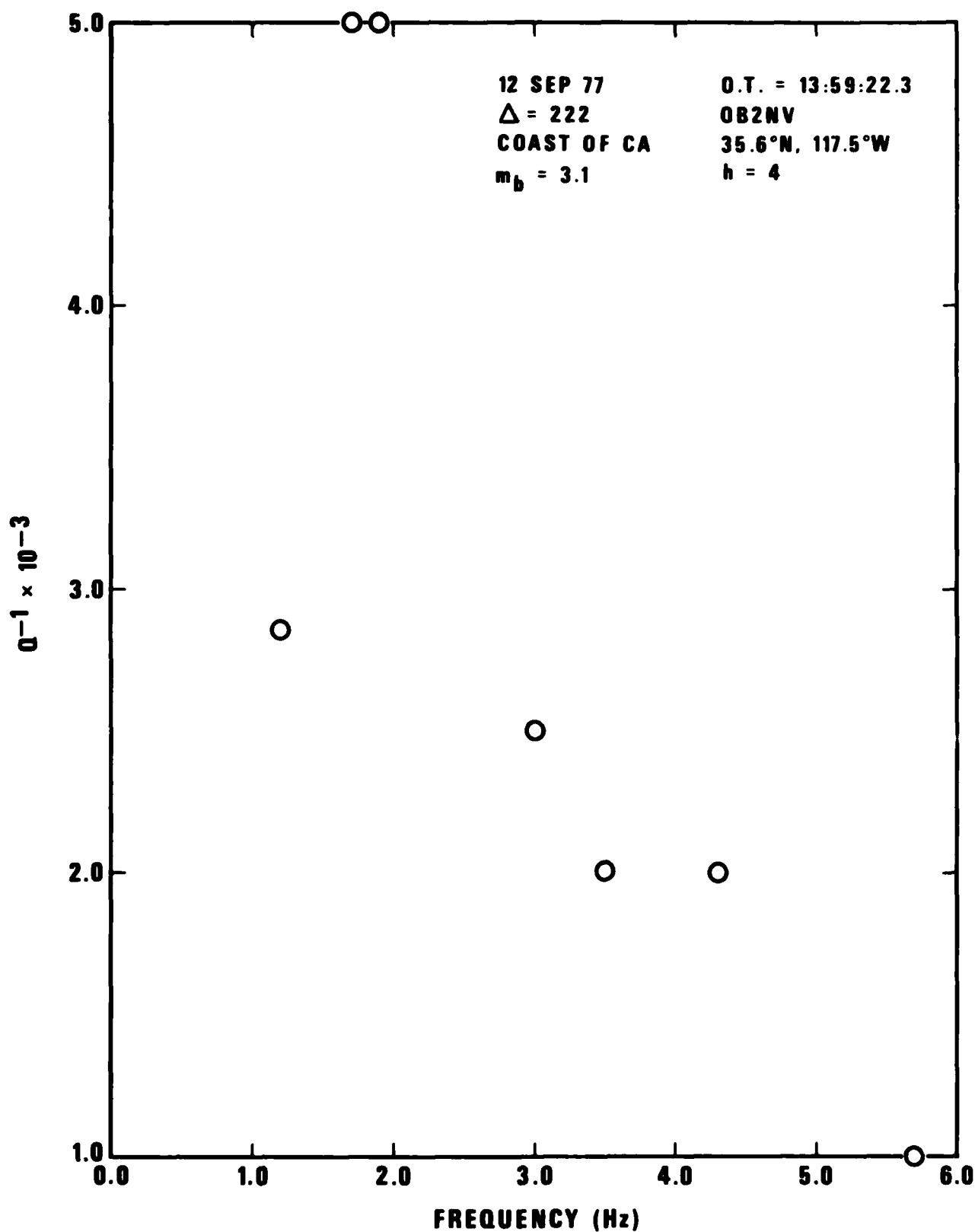


Figure 94. Q^{-1} as a function of frequency at OB2NV for the event of 12 Sep 77, O.T. = 13:59:22.3.

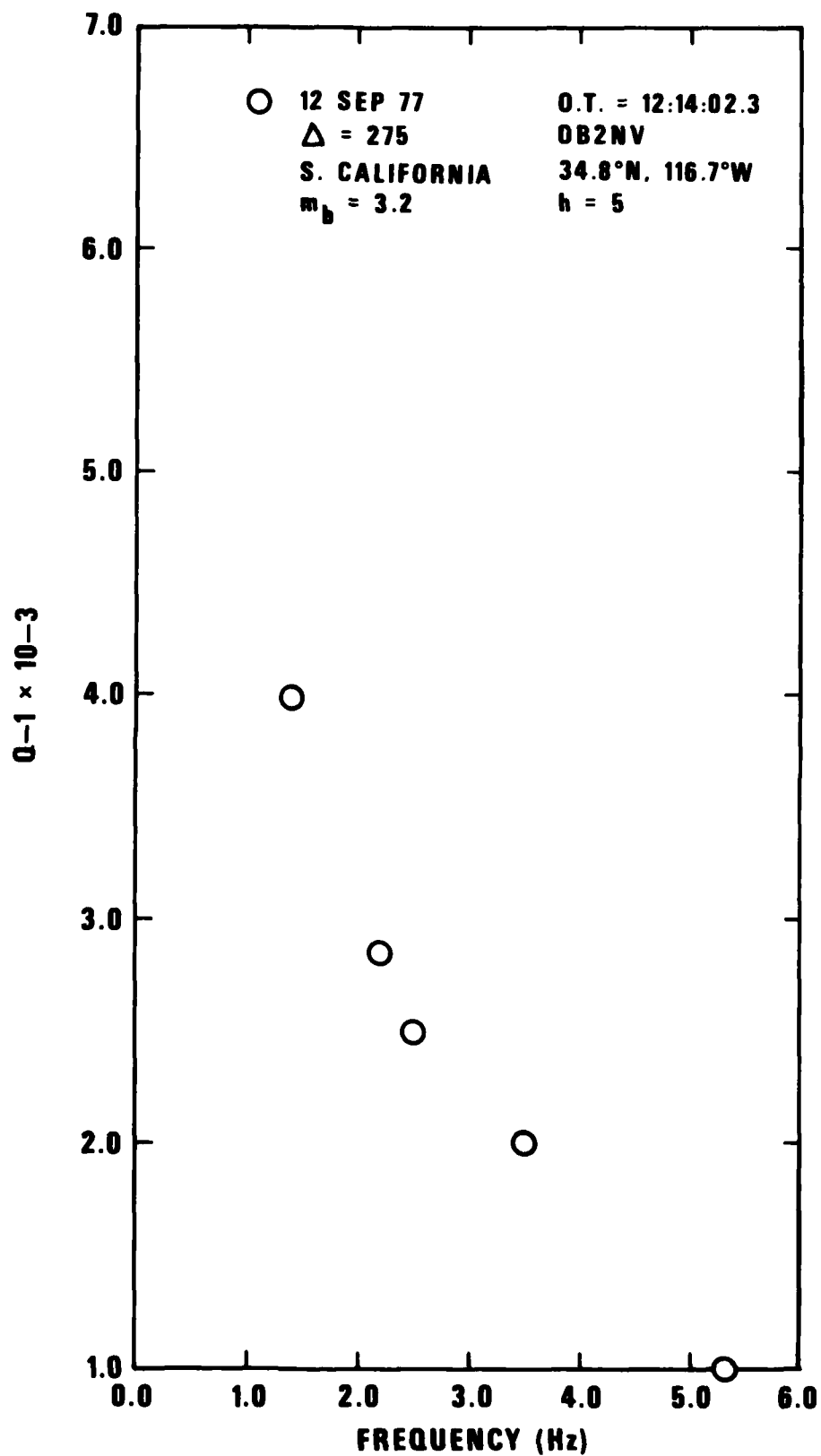


Figure 95. Q^{-1} as a function of frequency at OB2NV for the event of 12 Sep 77, O.T. = 12:14:02.3.

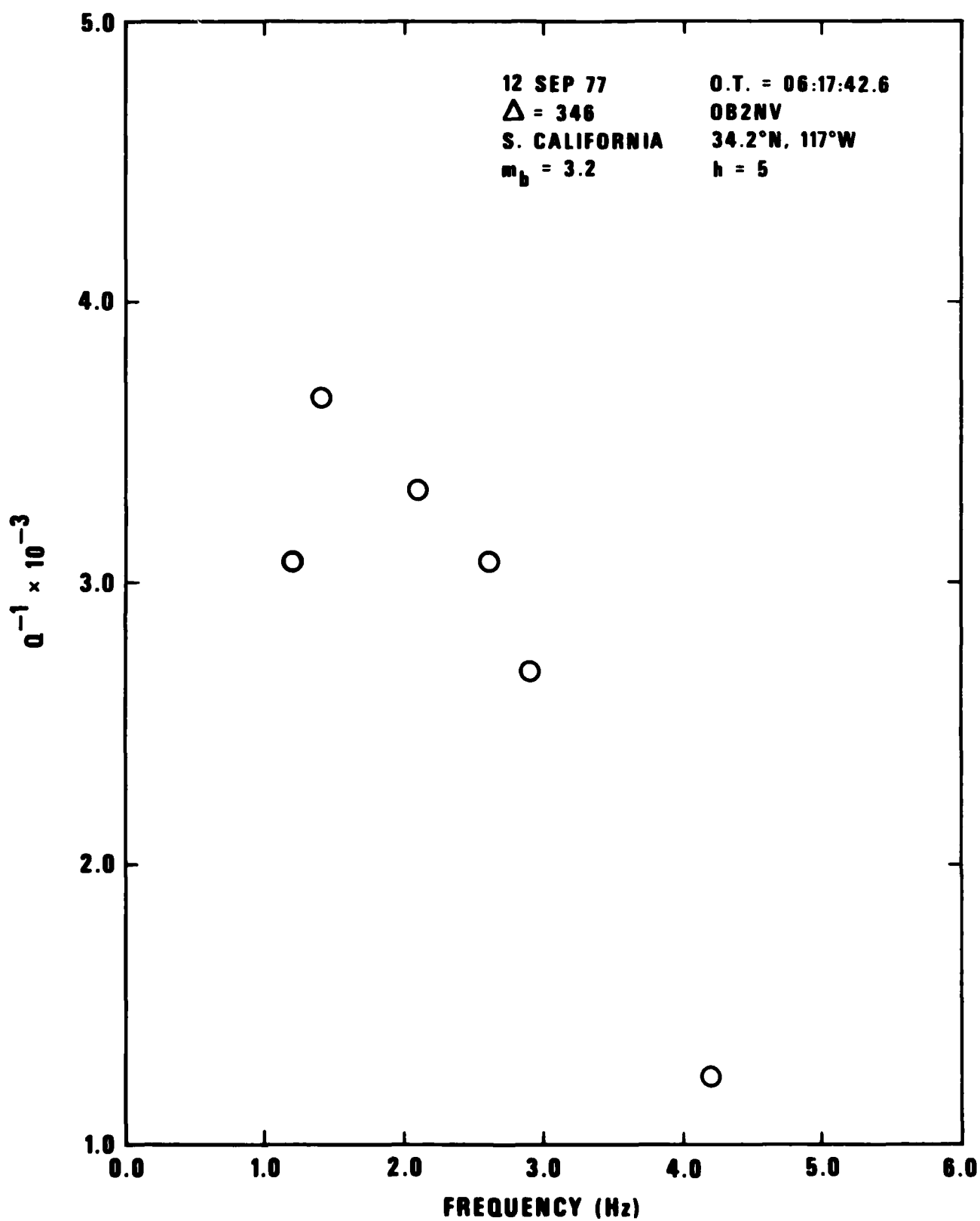


Figure 96. Q^{-1} as a function of frequency at OB2NV for the event of 12 Sep 77, O.T. = 06:17:42.6.

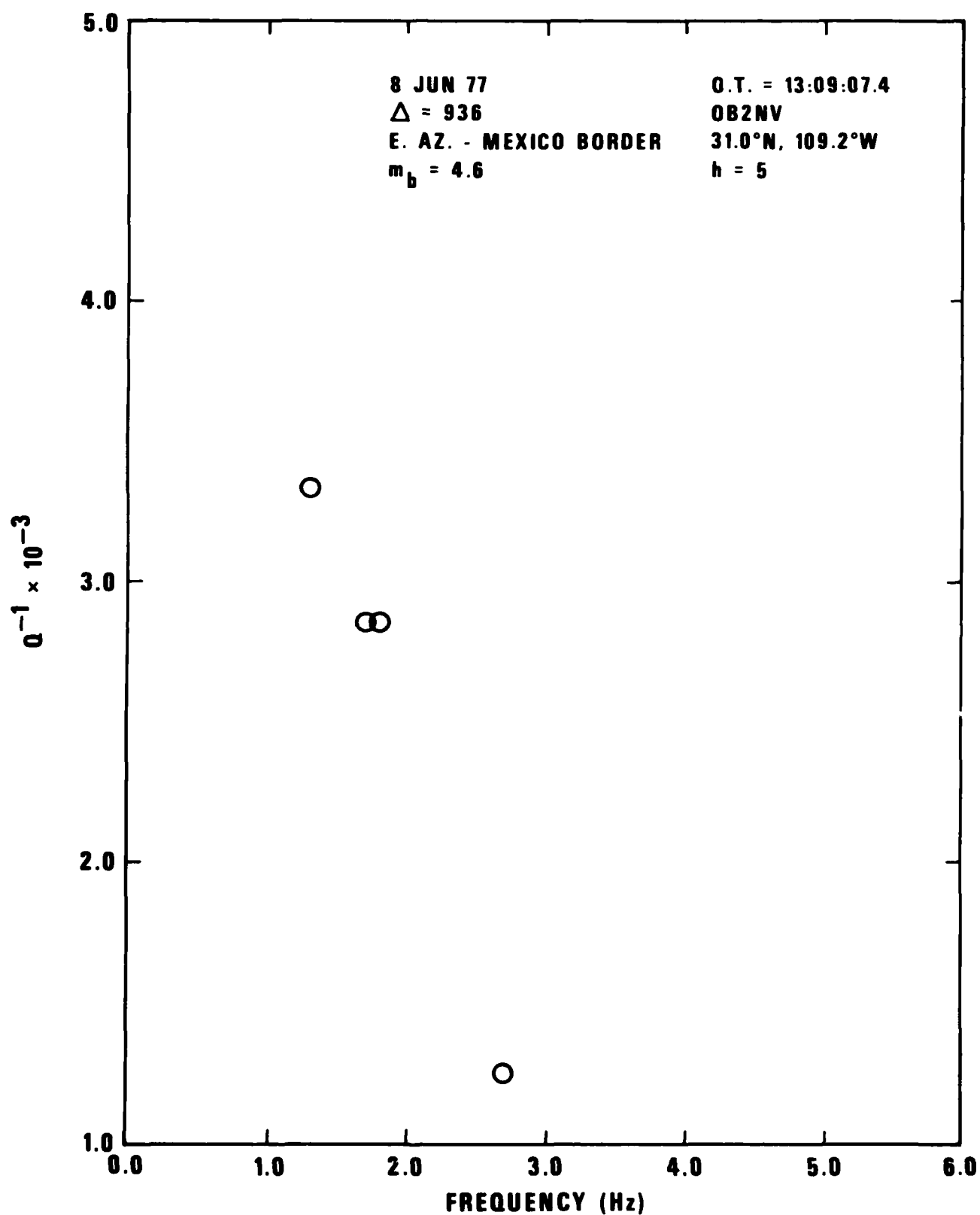


Figure 97. Q^{-1} as a function of frequency at OB2NV for the event of 08 Jun 77, O.T. = 13:09:07.4.

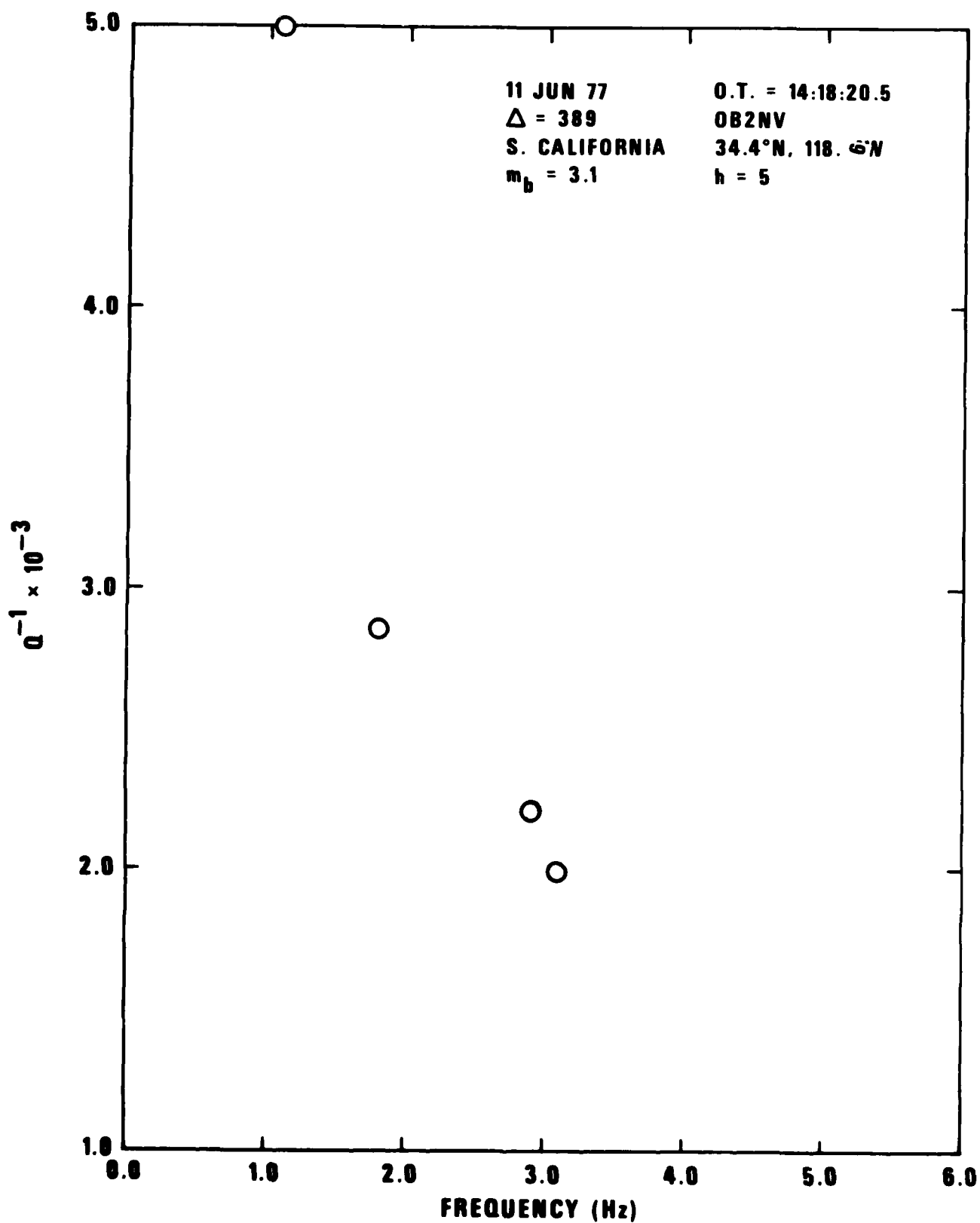


Figure 98. Q^{-1} as a function of frequency at OB2NV for the event of 11 Jun 77, O.T. = 14:18:20.5.

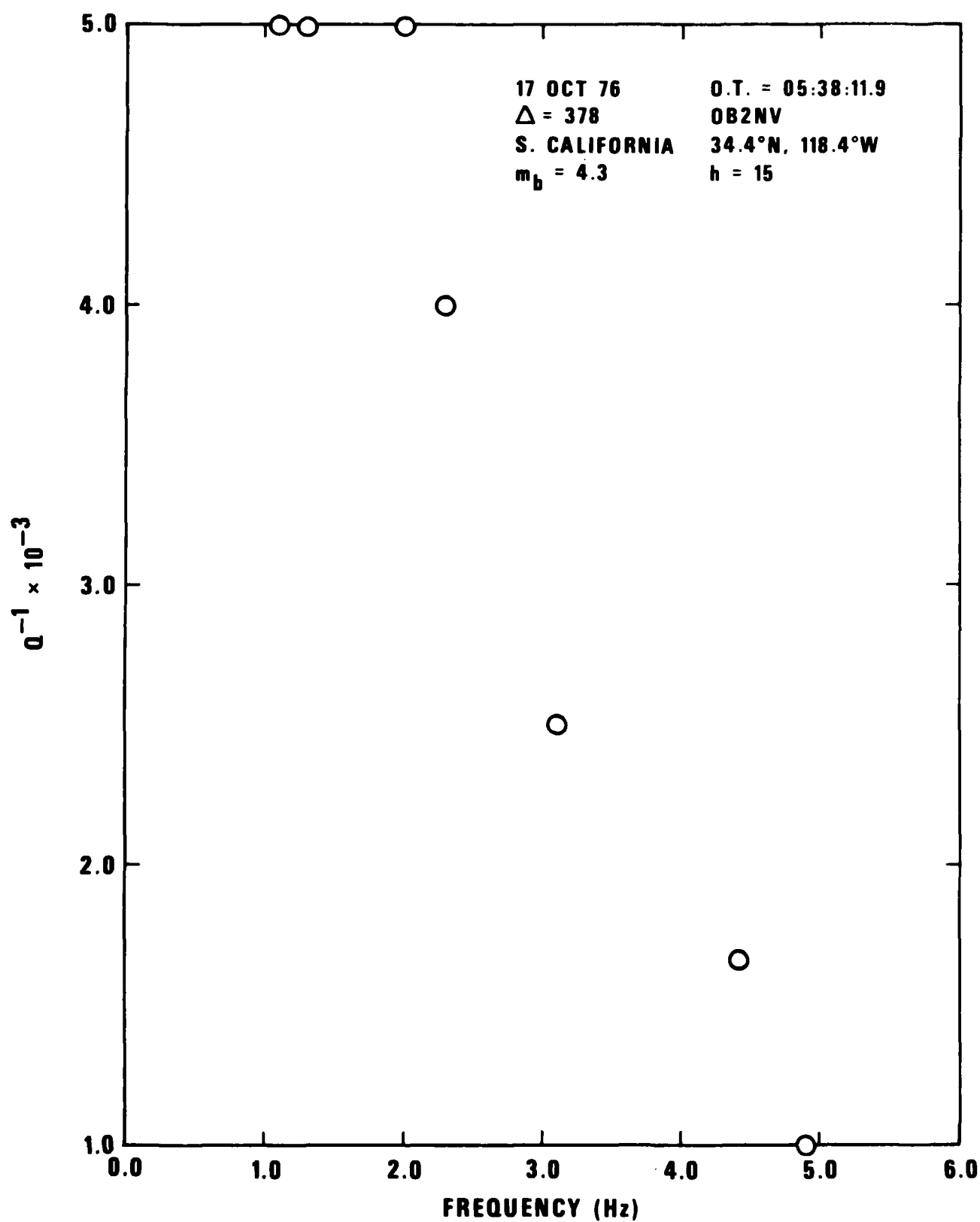


Figure 99. Q^{-1} as a function of frequency at OB2NV for the event of 17 Oct 76, O.T. = 05:38:11.9.

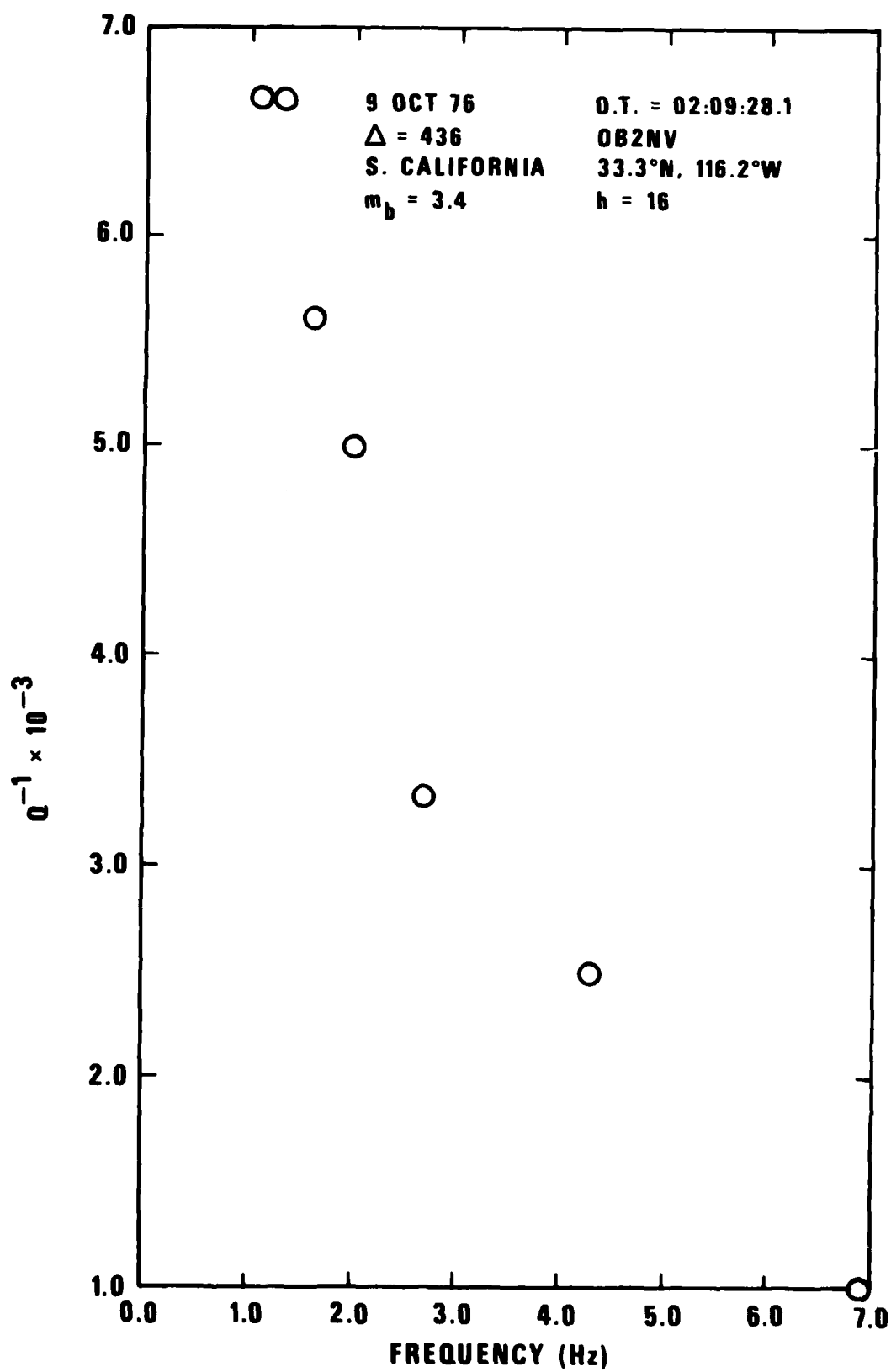


Figure 100. Q^{-1} as a function of frequency at OB2NV for the event of 09 Oct 76, O.T. = 02:09:28.1.

TABLE VIII

Events Used in Coda Analyses.

Date	Origin Time	Lat	Lon	m_b	Depth	Station	(km)
12/08/76	14 40 59.1	44.8N	110.7W	5.5	5	RKON	1446
09/30/77	10 19 21.0	40.5N	110.4W	5.0	56	RKON	1724
03/25/76	00 41 20.5	35.6N	90.5W	4.9	15	RKON	1712
09/03/76	04 18 16.2	44.0N	106.2W	4.8	106	RKON	1201
03/05/77	03 00 54.7	35.9N	108.3W	4.6	22	ANMO	200.2
10/11/77	07 56 06.5	40.5N	110.5	4.8	6	ANMO	711.7
04/08/76	15 21 37.9	34.4N	118.7	4.7	16	ANMO	1123
01/17/76	03 58 51.4	32.1N	115.4W	4.5	56	ANMO	889.6
02/09/76	03 07 22.0	34.6N	112.5W	4.6	106	ANMO	556.0
01/08/77	13 09 07.4	31.0N	109.2	4.6	56	ANMO	512.4
09/12/77	13 59 22.3	35.6N	117.5W	3.1	4	OB2NV	222
09/12/77	06 17 42.6	34.2N	117.0W	3.2	5	OB2NV	346
06/08/77	13 09 07.4	31.0N	109.2W	4.6	5	OB2NV	936
06/11/77	14 18 20.5	34.4N	118.6W	3.1	5	OB2NV	389
10/17/76	05 38 11.9	34.4N	118.4W	4.3	15	OB2NV	378
10/09/76	02 09 28.1	33.3N	116.2W	3.4	16	OB2NV	436
09/12/77	12 14 02.3	34.8N	116.7W	3.2	5	OB2NV	275
12/26/78	01 40 33.3	23.9S	65.4W	4.7	43	ZOBO	900.7
11/01/79	21 50 46.9	2.6N	22.1E	4.6	100	BCAO	444.8

This may indicate that first order scattering theory is applicable to these fairly large regional distances. We must note that these distances are considerably larger than the "mean free path" implied by the theory of Aki (1980) that attributes all or most of the losses to scattering and beyond which the first order scattering theory must break down.

In Figures 101 to 106 show similar results for the SRO station ANMO (Albuquerque, N.M.). All plots indicate a rapid increase of Q with frequency; however, the event at 222 km shows a less rapid change of Q than the others. At present, the available data do not allow us to determine the cause of this. The results at OB2NV and ANMO are similar to those presented by Aki (1980) using local events at much closer distances in the western United States. These also show a rapid change of Q with frequency. In most of our coda analyses in the western United States, the coda envelopes are essentially the same or change very little from one frequency band to the other.

Figure 107 shows a coda analysis result from the station ZOBO (La Paz, Bolivia) for an event in the Juyjuy province in Argentina. The Q estimate for this event is considerably higher than those found for OB2NV and ANMO, but it still exhibits a rapid change of Q with frequency. The overall estimate of Q in the short-period band is on the order of 1000 in contrast to values near 200 for OB2NV and ANMO in the same band (1-3 Hz).

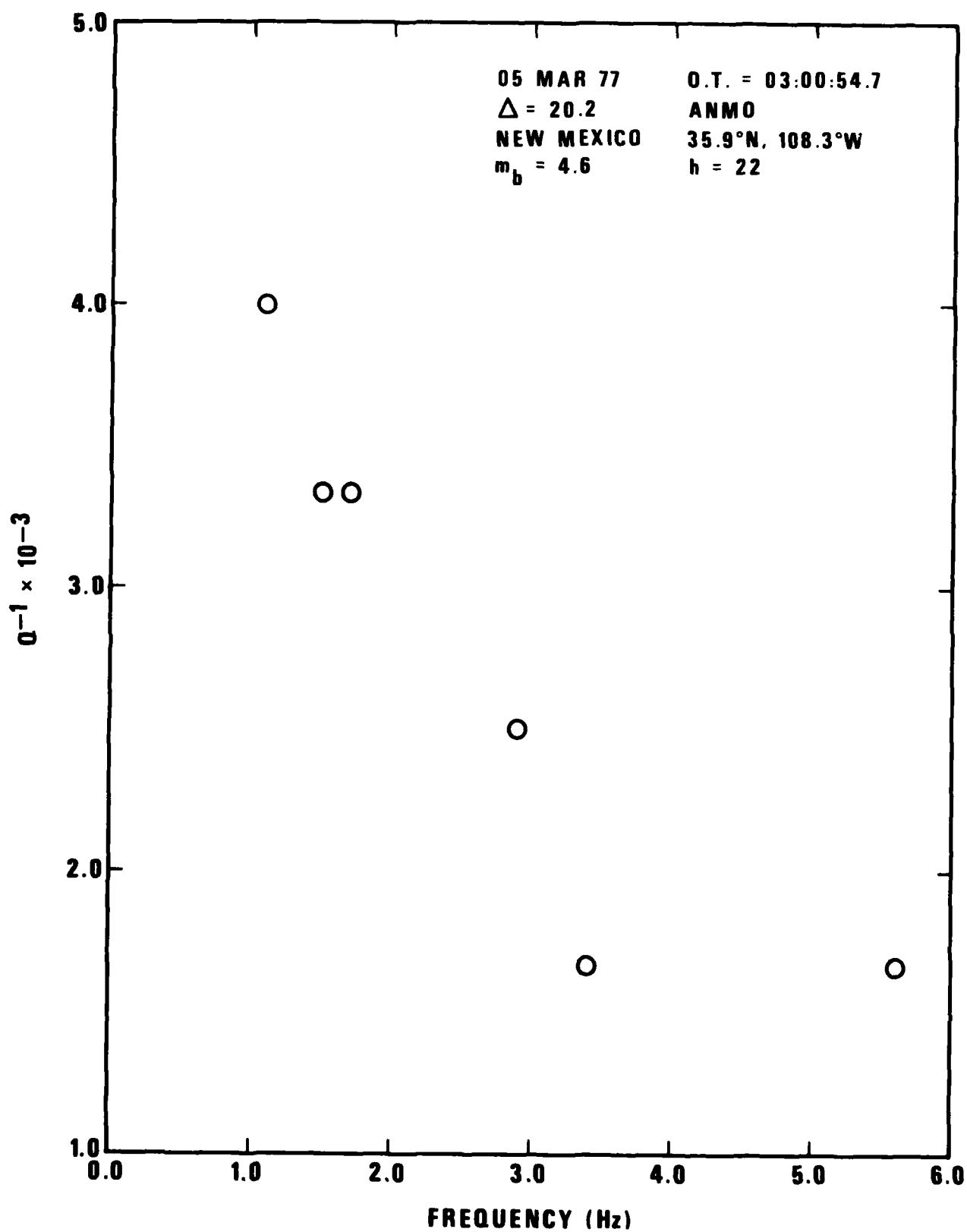


Figure 101. Q^{-1} as a function of frequency at ANMO for the event of 05 Mar 77, O.T. = 03:00:54.7.

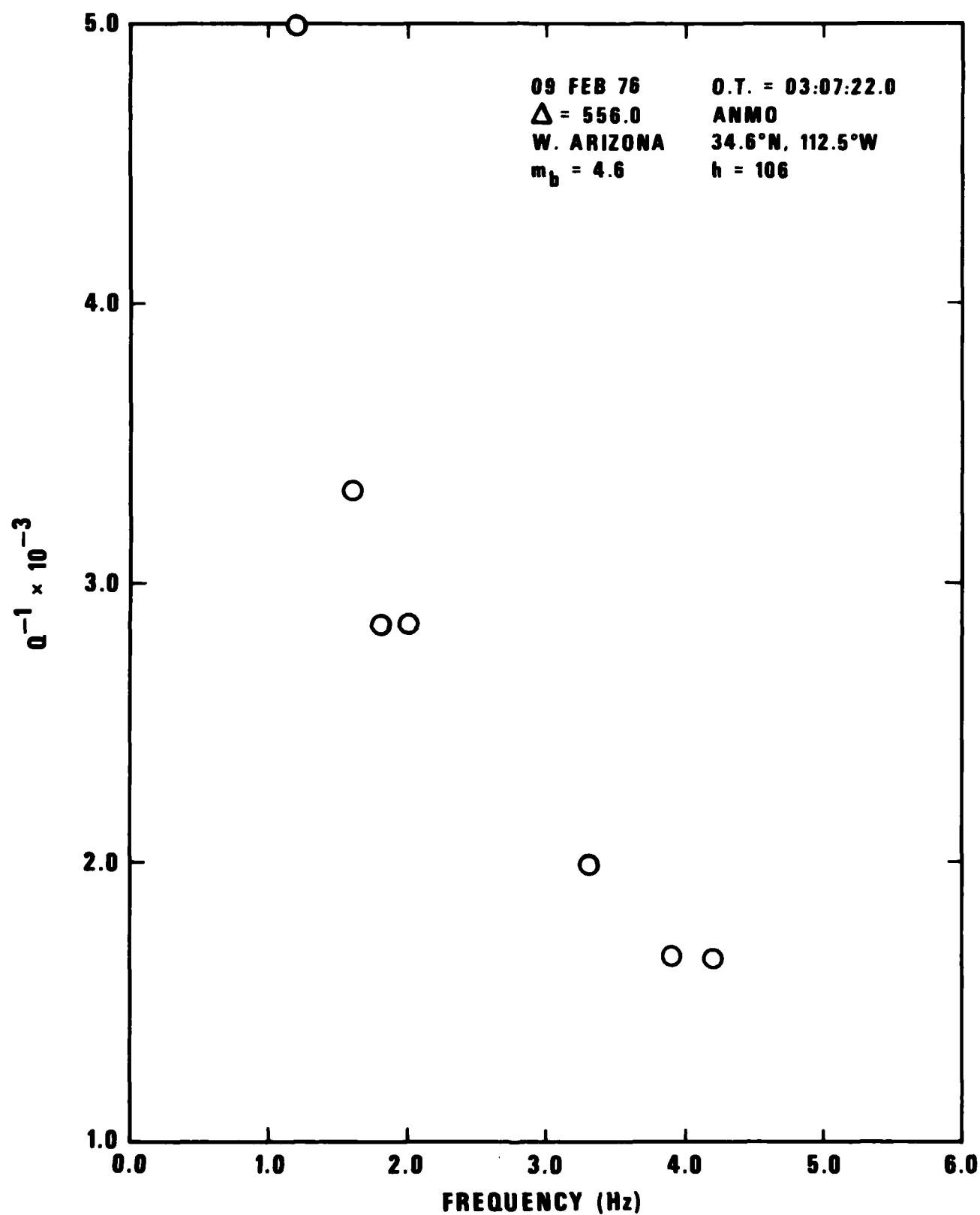


Figure 102. Q^{-1} as a function of frequency at ANMO for the event of 09 Feb 76, O.T. = 03:07:22.0.

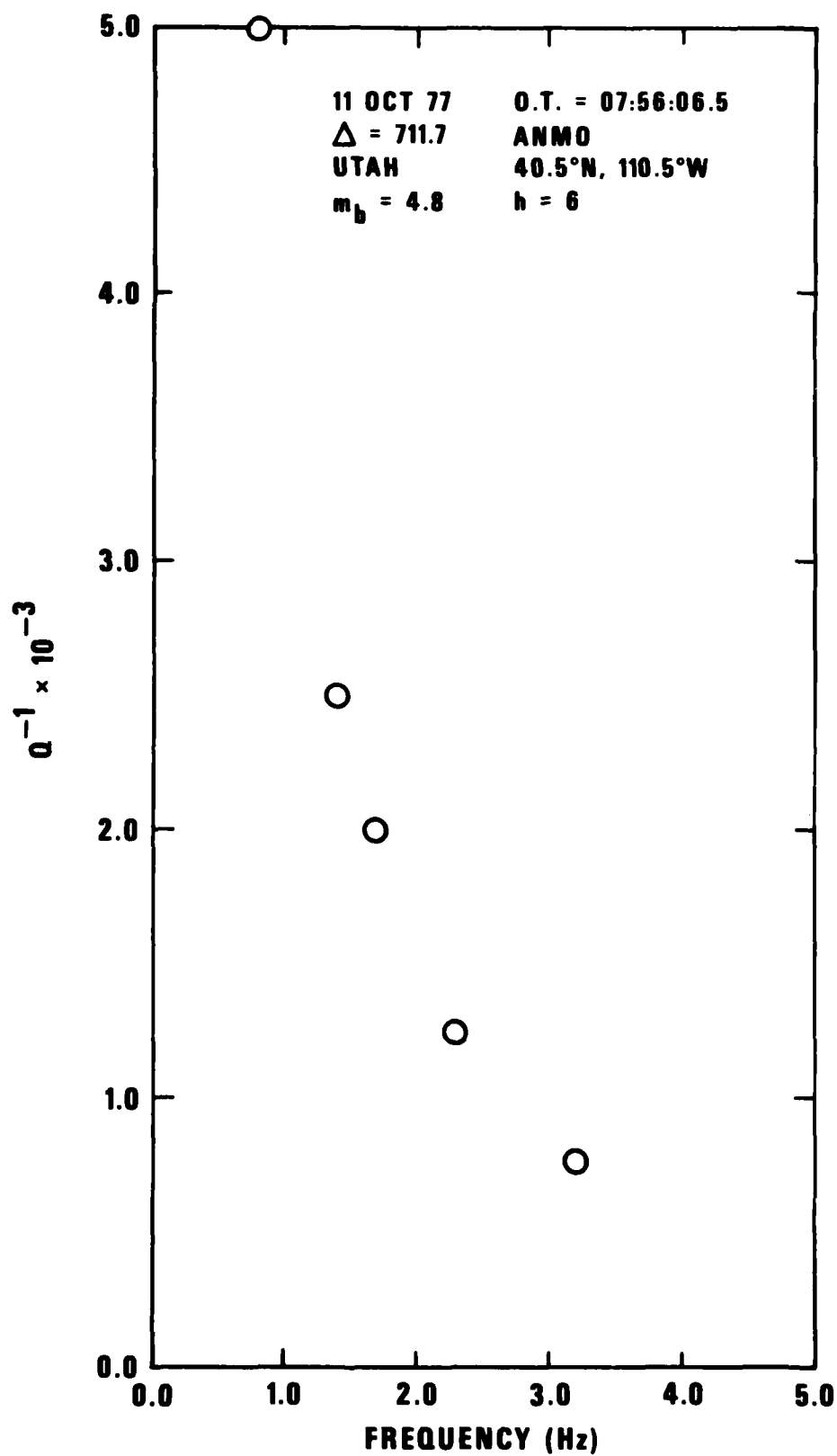


Figure 103. Q^{-1} as a function of frequency at ANMO for the event of 11 Oct 77, O.T. = 07:56:06.5.

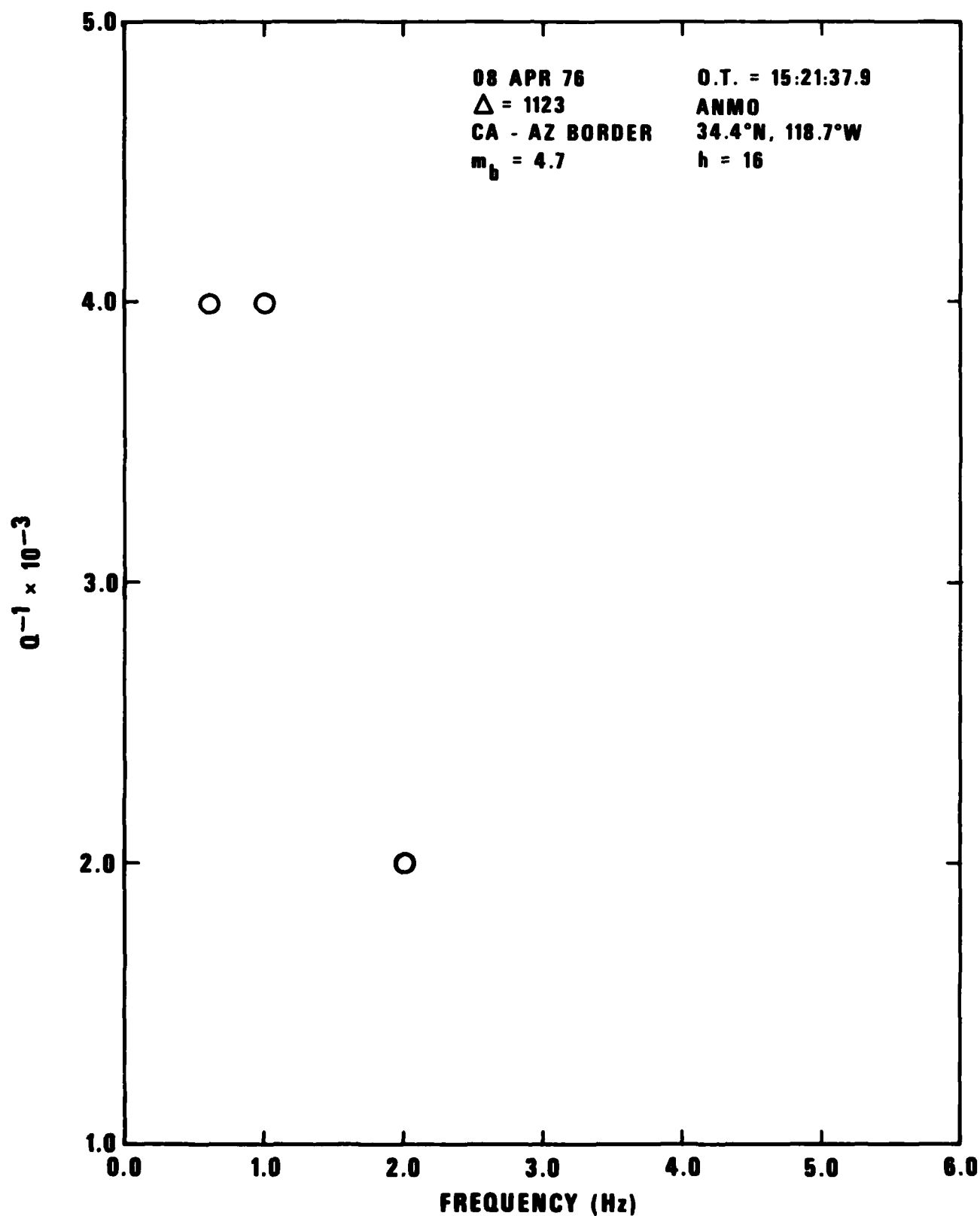


Figure 104. Q^{-1} as a function of frequency at ANMO for the event of 08 Apr 76, O.T. = 15:21:37.9.

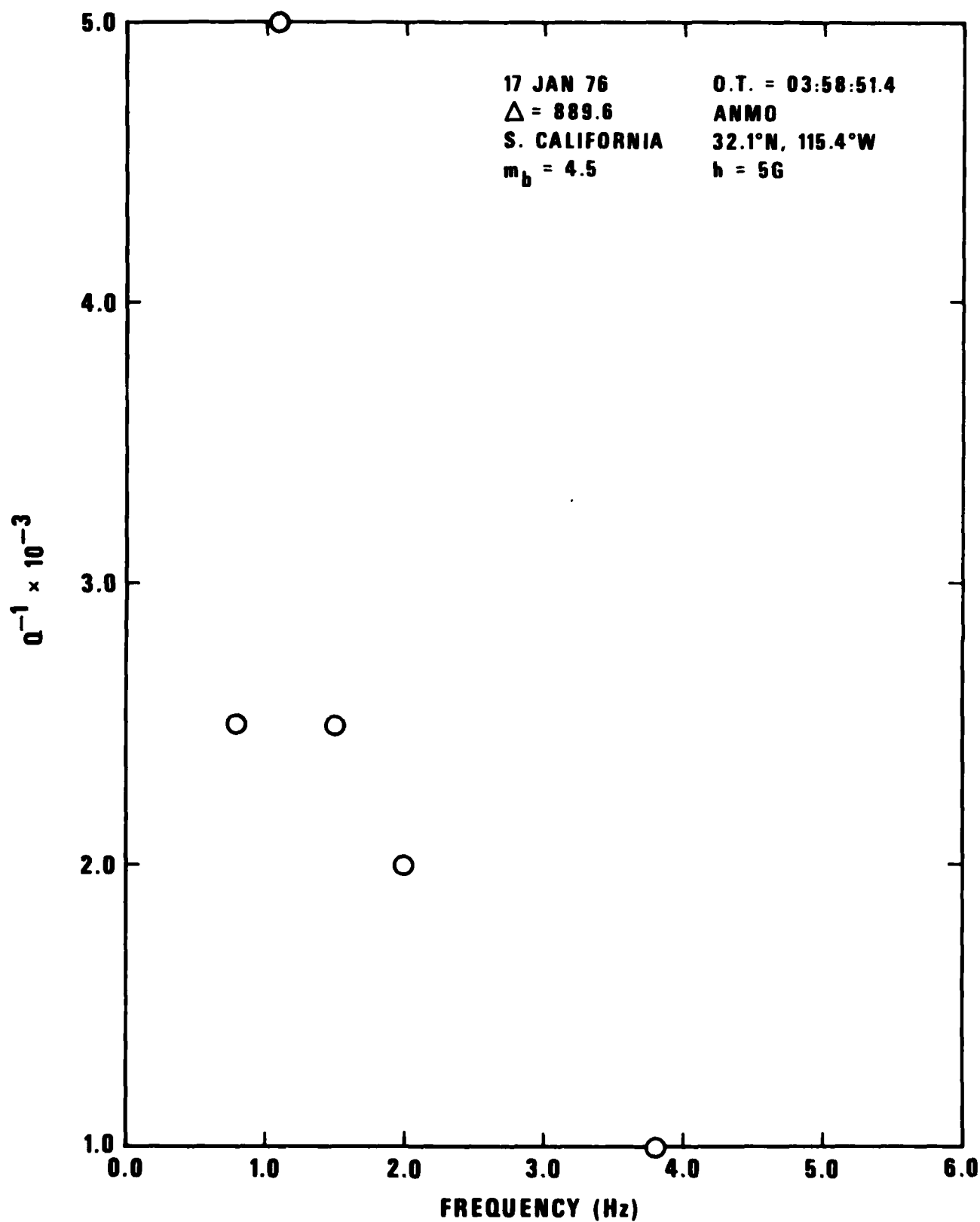


Figure 105. Q^{-1} as a function of frequency at ANMO for the event of 17 Jan 76, O.T. = 03:58:51.4.

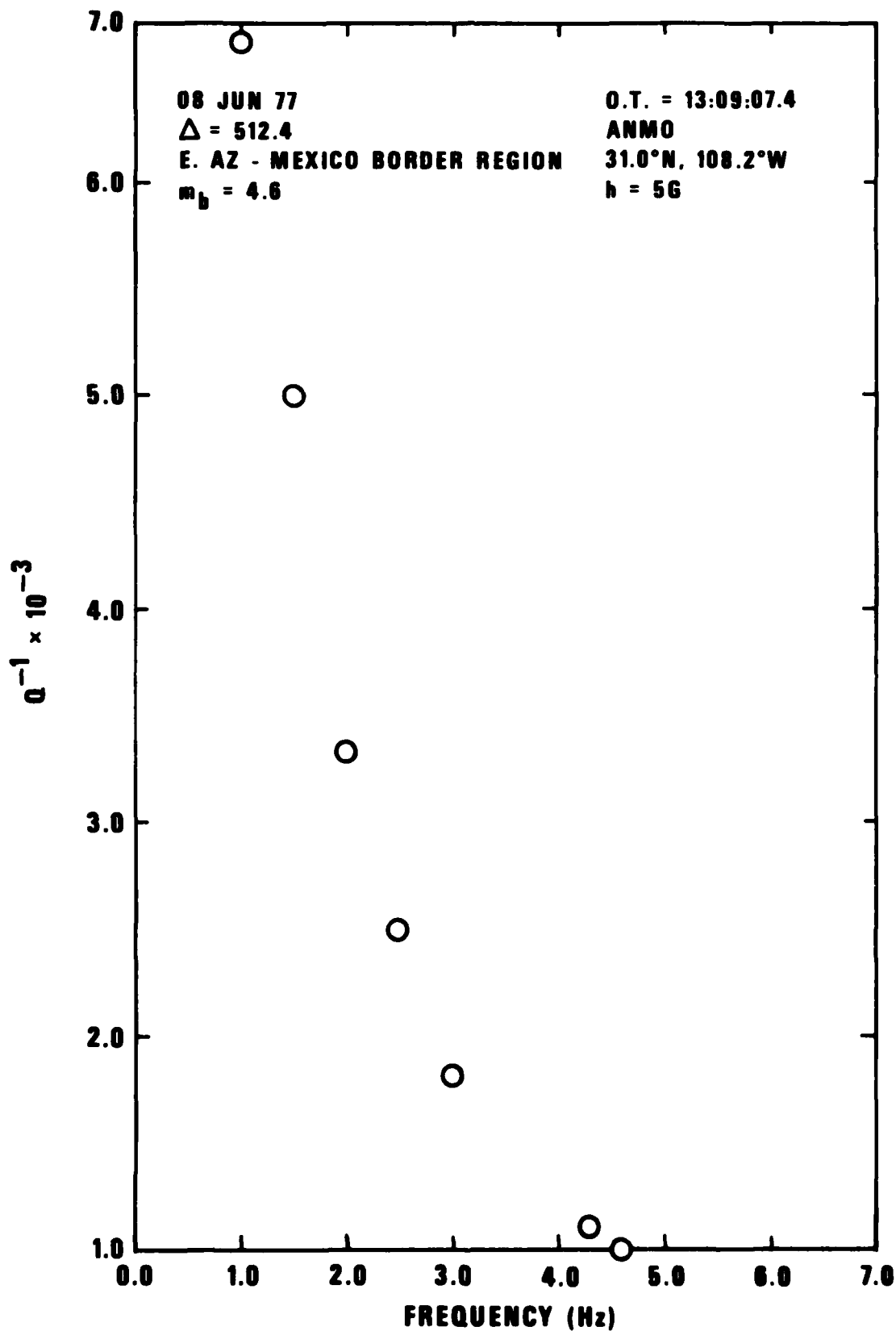


Figure 106. Q^{-1} as a function of frequency at ANMO for the event of 08 Jun 77, O.T. = 13:09:07.4.

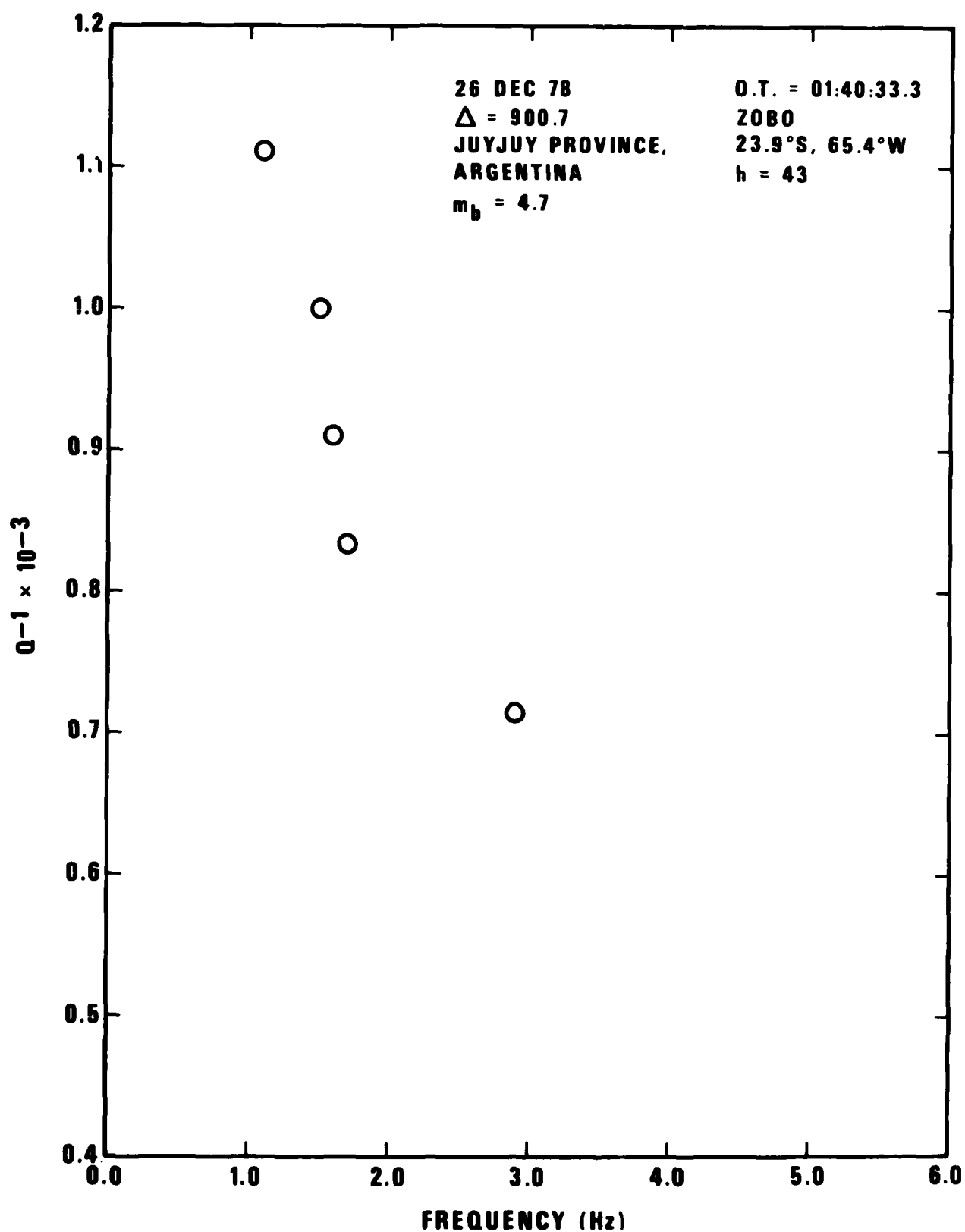


Figure 107. Q^{-1} as a function of frequency at ZOBO for event (26 Dec 78, O.T. = 01:40:33.3) in Argentina.

STATION NOISE LEVELS

Since noise levels are a limiting factor in detection and magnitude determination (Ringdal, 1976; Wirth, 1970), the statistics of seismic noise at stations to be used in monitoring are of great importance. Since many of the stations we used in our analyses may be used later in detecting and diagnosing an event, we have compiled noise data for each station. These data consist of noise amplitude measurements throughout the year and are displayed in the form of cumulative distribution plots in Figures 1 to 29 of Appendix A. The mean noise levels and the standard deviations of the samples are given in Table I of the same appendix. The regional phase amplitude-distance curves in shown in this report and the data in Table I can be used together to estimate yields of small events without a noise related bias (Ringdal, 1976). Alternatively, Wirth's (1970) program NETWORTH can be used, with some modifications, to estimate detection threshold for individual regional phases or entire regional events as well as discrimination thresholds for the areas studied.

SUMMARY AND CONCLUSIONS

The seismic wave propagation at regional distances has been studied in five areas of the world; southern Africa, South America, India-Pakistan, Southwestern United States and the Kamchatka-Kuriles.

The least scatter in the regional phase amplitudes and the best defined amplitude-distance relationships for such phases were observed in southern Africa. These facts seem to indicate a great degree of lateral homogeneity and simplicity in the structure of the crust in this region.

Seismic waves from rockbursts associated with mining can be distinguished from those originating from natural earthquakes by their low frequency character. The reason for this phenomenon is not understood.

Shield areas of southern Africa, South America and Pakistan-India are similar with respect to the excitation and propagation of regional phases. The amplitude-distance relationships for all regional phases are similar and the same magnitude-distance formulas can be used for estimating magnitudes.

Tectonic, mountainous areas, in general, show less efficient propagation of all regional phases; the wave amplitudes decrease faster with increasing distance, and the dominant periods of the phases also increase fast. The data used for this report is not sufficient to define reliable amplitude-distance relationships for these highly variable regions.

The propagation characteristics of regional phases are especially anomalous relative to shields in the Andes region of South America. In this region the efficiency of propagation is highly variable, even L_g may not be detectable along certain paths especially in the southern Andes of Chile and Argentina. Therefore regional phases cannot be relied on for detection and discrimination.

The regional seismograms crossing the Andes often exhibit unusual characteristics resembling lunar seismograms with gradual buildup and

decay in amplitudes of P, indicating extreme scattering of the seismic energy.

The southwestern United States seems to be different from the other regions studied with respect to the excitation and propagation of regional phases. P_g is a more prominent phase than elsewhere but it also decays faster with distance than in shield and many tectonic areas elsewhere. The P_g/L_g amplitude ratio appears to be not very effective discriminant between earthquakes and explosions in this area.

Propagation of seismic waves from the Kamchatka-Kuriles to the nearest stations in Japan and the Aleutians is characterized by oceanic type P_n and S_n phases with extremely high frequency content. The LRSM stations ADIS does not observe S_n .

Analyses of seismic codas at the stations OB2NV, ZOBO and ANMO show that Q increases fast with frequency in the crust in the tectonic areas of the southwestern United States and South America. The values of Q in these areas are around 200 at 1-2 Hz and increase to 1000 towards 6-7 Hz.

REFERENCES

- Aki, K. (1980). Scattering and attenuation of shear waves in the lithosphere, J. Geophys. Res., 85, 6496-6504.
- Aki, K. (1969). Analysis of the seismic coda of local earthquakes as scattered waves, J. Geophys. Res., 74, 615.
- Aki, K. and B. Chouet (1975). Origin of coda waves, source attenuation and scattering effects, J. Geophys. Res., 80, 3322.
- Alsup, S. A. (1972). Estimation of upper mantle Q beneath the United States from P_n amplitudes, Ph.D. Thesis, George Washington University, Washington, D.C.
- Archambeau, C. B., E. A. Flinn and D. G. Lambert (1969b). Detection analysis and interpretation of teleseismic signals, 1. Compressional waves from the SALMON event, J. Geophys. Res., 73, 3877-3883.
- Barazangi, M., Ni, J., Kadinski-Cade, K., Isacks, B. and J. Oliver (1981). Regional investigation of seismic wave propagation and velocities in the Middle East and in South Asia, DARPA-AFOSR Seismic Wave Propagation and Source Characterization Symposium, Las Vegas, Nevada, 18-20 May 1981, DARPA-NMR-81-03.
- Barazangi, M., B. L. Isacks (1976). Spatial distribution of earthquakes and subduction of the Nazca plate beneath South America, Geology, 4, 686-692.
- Barazangi, M., Pennington, W. and B. Isacks (1975). Global study of seismic wave attenuation in the upper mantle behind island arcs using pP waves, J. Geophys. Res., 80, 1079-1092.
- Barker, B. W. (1981). Regional phases from explosions and earthquakes in the southwest U.S. as recorded by station ANMO (prepared for oral presentation at the AFOSR Research Conference, May 1981, Las Vegas, Nevada, AFTAC, VELA Seismological Center, Alexandria, Virginia.
- Bennett, T. J. and J. R. Murphy (1980). A study of the relative excitation of regional phases for use in event discrimination, (paper presented at the Annual Meeting of the Eastern Section of the Seismological Society of America, October 1980).
- Blandford, R. R., Hartenberger, R. and R. Naylor (1981). Regional amplitudes distance relations, discrimination and detection, SDAC-TR-80-6, Teledyne Geotech, Alexandria, Virginia, VSC-TR-81-15, VELA Seismological Center, Alexandria, Virginia.
- Burk, C. A. and H. S. Gribidenko, Talwani, M. (Ed.), and Pitman, W. C. III (Ed.), (1977). The structure and age of acoustic basement in the Okhotsk Sea, Island Arcs, Deep Sea Trenches and Back-Arc Basins, 451-461.

REFERENCES (Continued)

- Chinn, D. S., Isacks, B. L. and M. Barazangi (1980). High frequency seismic wave propagation in western South America along the continental margin, in the Nazca plate across the Altiplano, Geophys. R. Astr. Soc., 60, 209-244.
- Cooper, A. K., Marlow, M. S. and D. W. Scholl (1977). The Bering Sea-a multifarious marginal Basin, in "Island Arcs, Deep Sea Trenches and Back-Arc Basins". M. Talwani and W. C. Pitman III, editors, American Geophysical Union, Maurice Ewing series.
- Der, Z. A., O'Donnell, A. and P. J. Klouda (1981). An investigation of attenuation, scattering and site effects on regional phases, SDAC-TR-81-14, Teledyne Geotech, Alexandria, Virginia.
- Der, Z. A. and T. W. McElfresh (1976a). Short-period P-wave attenuation along various paths in North America as determined from P-wave spectra of the SALMON nuclear explosion, Bull. Seism. Soc. Am., in press.
- Der, Z. A. and T. W. McElfresh (1976b). The effect of attenuation on the spectra of P-wave from nuclear explosions in North America, SDAC-TR-76-7, Teledyne Geotech, Alexandria, Virginia, ADA 030857.
- Dewey, J. W. (1972). Seismicity and tectonics of western Venezuela: Bull. Seism. Soc. Am., 62(6), 1711-1751.
- Evernden, J. F. (1967). Magnitude determination at regional and near-regional distances in the United States, Bull. Seism. Soc. Am., 57, 591-639.
- Fedotov, S. A. and S. A. Boldyrev (1969). Frequency dependence of the body-wave absorption in the crust and the upper mantle of the Kuril-Island chain, Isz. Acad. Nauk, USSR (Geophysics), English Transl., 553-562.
- Gough, D. I. (1973). The geophysical significance of geomagnetic variation anomalies, Phys. Earth Planet. Int., 7, 379-388.
- Gupta, I. N. and J. A. Burnetti (1981). An investigation of discriminants for events in western USSR based on regional phases recorded at station Kabul, Bull. Seism. Soc. Am., 71, 263-274.
- Gupta, I. N., Barker, B. W., Burnetti, J. A. and Z. A. Der (1980). A study of regional phases from earthquakes and explosions in western Russia, Bull. Seism. Soc. Am., 70, 851-872.
- Gupta, I. N. and J. A. Burnetti (1980). Amplitude-distance relationships for regional phases in shield regions, SDAC-TR-80-7, Teledyne Geotech, Alexandria, Virginia.

REFERENCES (Continued)

- Hales, A. L. and J. Roberts (1970). The travel times of S and SKS, Bull. Seism. Soc. Am., 60, 461-489.
- Hasegawa, A. and I. S. Sacks (1981). Subduction of the Nazca plate beneath Peru as determined from seismic observations, J. Geophys. Res., 86, 4971-4980.
- Herrin, E. and J. Taggart (1962). Regional variations in P velocity and their effect on the location of epicenters, Bull. Seism. Soc. Am., 52, 1037-1046.
- Herrmann, R. B. (1980). Q estimates using the coda of local earthquakes, Bull. Seism. Soc. Am., 70, 447-468.
- Isacks, B. L., Barazangi, M., Talwani, M. (Ed.) and Pitman, W. C. III (Ed), (1977). Geometry of Benioff zones; lateral segmentation and downwards bending of the subducted lithosphere, DARPA-AFOSR Seismic Wave Propagation and Source Characterization Symposium, Las Vegas, Nevada, 18-20 May 1981, DARPA-NMR-81-03.
- James, D. E. (1971). Andean crustal and upper mantle structure, J. Geophys. Res., 76, 3246-3271.
- Kadinski-Cade, K., Barazangi, M., Oliver, J. and B. Isacks (1981). Lateral variations of high-frequency seismic wave propagation at regional distances across the Turkish and Iranian plateaus, J. Geophys. Res., 86, 9377-9396.
- Keller, G. R., R. B. Smith, and L. W. Braile (1975). Crustal structure along the Great Basin - Colorado Plateau transition from seismic refraction studies, J. Geophys. Res., 80, 1093-1098.
- Mitchell, B. J. (1981). Regional variation and frequency dependence of Q in the crust on the United States, Bull. Seism. Soc. Am., 71, 1531-1538.
- Mitchell, B. J. (1980). Frequency dependence of shear wave internal friction in the continental crust of eastern North America, J. Geophys. Res., 85, 5212-5218.
- Mitchell, B. J. (1979). Higher mode attenuation in the Middle-East, Iran and Turkey, Semi-annual Technical Report #1, for the AFOSR, Saint Louis University, St. Louis, Mo.
- Molnar, P. and P. Taponnier (1975). Cenozoic tectonics of Asia; Effects of a continental collision, Science, 189, 419-426.
- Molnar, P. and J. Oliver (1969). Lateral variations of attenuation in the upper mantle and discontinuities in the lithosphere, J. Geophys. Res., 74, 2648-2682.

REFERENCES (Continued)

- Murphy, J. R. (1980). An evaluation of the factors influencing the seismic detection of decoupled explosions at regional distances, Systems, Science and Software, Inc. SSS-R-80-4579.
- Noponen, I. and J. Burnetti (1980). Studies of seismic wave characteristics at regional distances, Alaskan Regional Data Analysis, vol. II, AL-80-1, Teledyne Geotech, Alexandria, Virginia.
- Nuttli, O. (1981). On the attenuation of L waves in the western and central Asia, Bull. Seism. Soc. Am., 71, 249-261.
- Nuttli, O. W. (1980). The excitation and attenuation of seismic crustal phases in Iran, Bull. Seism. Soc. Am., 70, 469-486.
- Nuttli, O. W. (1979). Excitation and attenuation of short period phases in southern Asia, Semi-annual Technical Report # 1 for AFOSR, Saint Louis University, St. Louis, Mo.
- Nuttli, O. W. (1973a). Seismic wave attenuation and magnitude relations for eastern North America, J. Geophys. Res., 78, 876-885.
- Pomeroy, P. W. and T. C. Chen (1980). Regional seismic wave propagation (Final Report for the AFOSR), Rondout Associates, Inc., Stone Ridge, N.Y.
- Prodehl, C. (1970). Seismic refraction study of crustal structure in the Western United States, Geol. Soc. Am. Bull., 81, 2629-2646.
- Quittmeyer, R. . and K. H. Jacob (1979). Historical and modern seismicity of Pakistan, Afghanistan, northern India, and southeastern Iran, Bull. Seism. Soc. Am., 69, 773-823.
- Rautian, T. G. and V. Khalturin (1978). The use of coda for determination of the earthquake source spectra, Bull. Seism. Soc. Am., 68, 923-948.
- Reitzel, J. S., D. I. Gough, H. Porath, and C. W. Anderson III (1970). Geomagnetic deep sounding and upper mantle structure in the Western United States, Geophys. J., 19, 213-236.
- Ringdal, F. (1976). Maximum-likelihood estimation of seismic magnitude, Bull. Seism. Soc. Am., 66, 789-802.
- Rodean, H. C. (1979). Optimum frequencies for regional detection of cavity-decoupled explosions, Lawrence Livermore Laboratory, University of California, UCRL-52690.
- Roy, R. F., D. D. Blackwell and E. R. Decker (1972). Continental heat flow. The Nature of the Solid Earth (E. C. Robertson, Editor), McGraw-Hill International Series in the Earth and Planetary Sciences.

REFERENCES (Continued)

- Ruzaikin, A. I., L. Nersesov, V. I. Khalturin, and P. Molnar (1977). Propagation of L_g and lateral variations in crustal structure in Asia, J. Geophys. Res., 82, 307-316.
- Sass, J. H., A. H. Lachenbruch, R. J. Munroe, G. W. Greene, and T. H. Moses, Jr. (1971). Heat flow in the Western United States, J. Geophys. Res., 76, 6376-6413.
- Solomon, S. C. and M. N. Toksoz (1970). Lateral variations of attenuation of P and S-waves beneath the United States, Bull. Seism. Soc. Am., 60, 819-838.
- Stauder, W. (1975). Subduction of the Nazca plate under Peru as evidence by focal mechanisms and by seismicity, J. Geophys. Res., 80(8), 1053-1064.
- Stauder, W. (1973). Mechanism and spatial distribution of Chilean earthquakes with relation to subduction of the oceanic plate, J. Geophys. Res., 78(23), 5033-5061.
- Swanson, J. (1979). The seismic characteristics of South America and southern Africa, 79-15, Garland, Texas.
- Swanson, J. G. and Goforth, T. T. (1978). The seismic characteristics of southern Africa, TR-78-9, Garland, Texas, Teledyne Geotech, 71.
- Tapponnier, P. and P. Molnar (1977). Active faulting and tectonics in China, J. Geophys. Res., 82, 2905-2930.
- Tapponnier, P. and P. Molnar (1976). Slip-line theory and large scale continental tectonics, Nature, 264, 319-324.
- Terhune, R. W., C. M. Snell and H. C. Rodean (1979). Enhanced coupling and decoupling of underground nuclear explosions, Lawrence Livermore Laboratory, University of California, UCRL-52806.
- Tsujiura, M. (1978). Spectral analysis of coda waves from local earthquakes, Bull. Earthqu. Res. Inst., Tokyo, 53, 1-48.
- Toksoz, M. N. and P. Bird (1977). Formation and evaluation of marginal basins and continental plateaus, Island Arcs, Deep Sea Trenches and Back-Arc Basins, 1, 379-393.
- Veith, K. F. (1974). The relationship of island arc seismicity to plate tectonics, Ph.D. Thesis, Southern Methodist University, Dallas, Texas.

REFERENCES (Continued)

- Watanabe, T., Langseth, M. G. and R. N. Anderson (1977). Heat flow in back-arc basins of the western Pacific, Island Arcs, Deep Sea Trenches and Back-Arc Basins, 1, 137-161.
- Wirth, M. H. (1970). Estimation of network detection and location capability, Research Memorandum, Air Force Technical Applications Center, Washington, D.C., (revised by R. R. Blandford and H. Husted).
- Yasar, T. and O. W. Nuttli (1974). Structure of the shear-wave low-velocity channel in the Western United States, Geophys. J., 37, 353-364

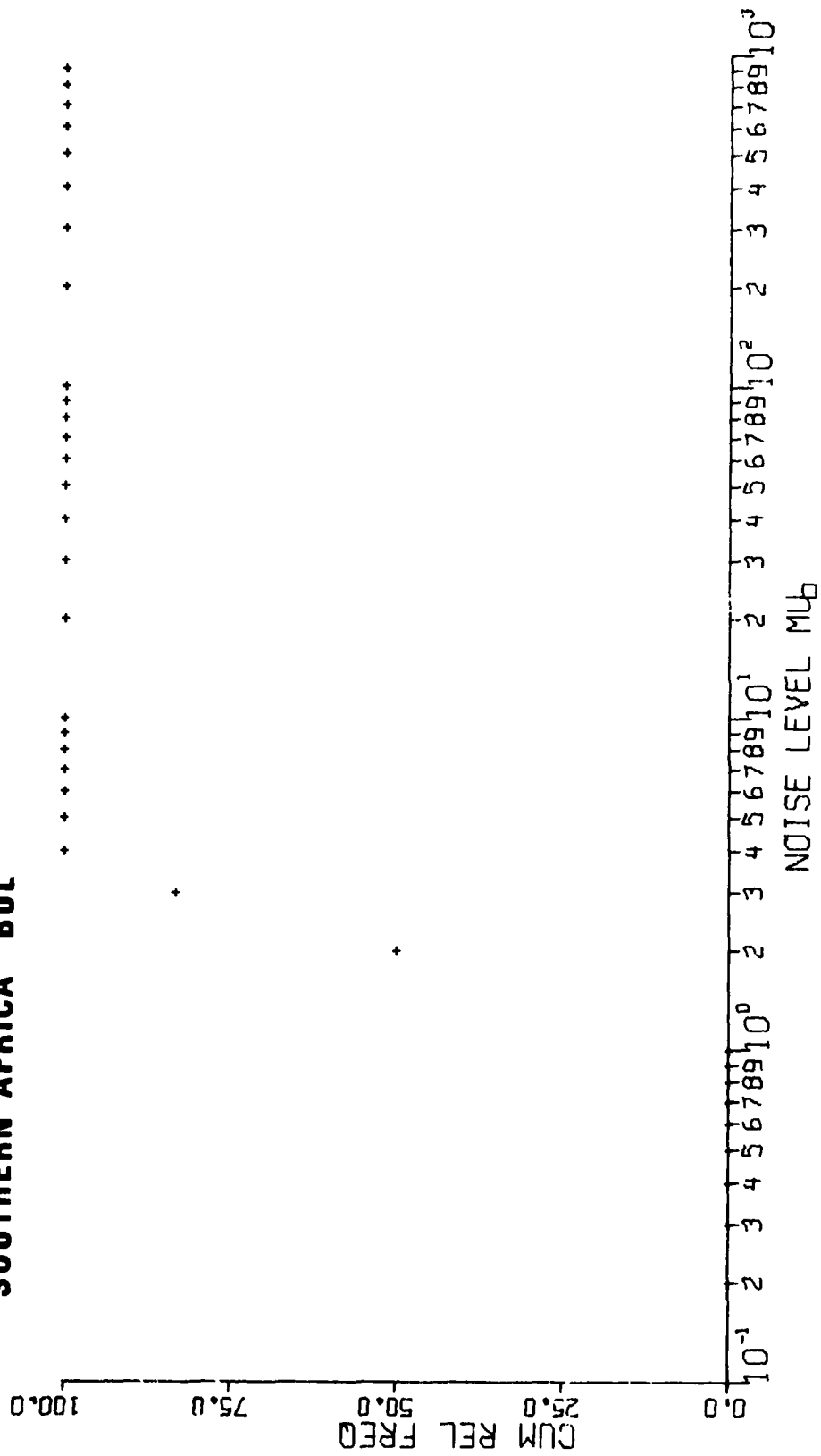
APPENDIX A

Cumulative Noise Probability in South America,
Southern Africa, the India/Pakistan Region, and
the Kumchatka/Kurile Region

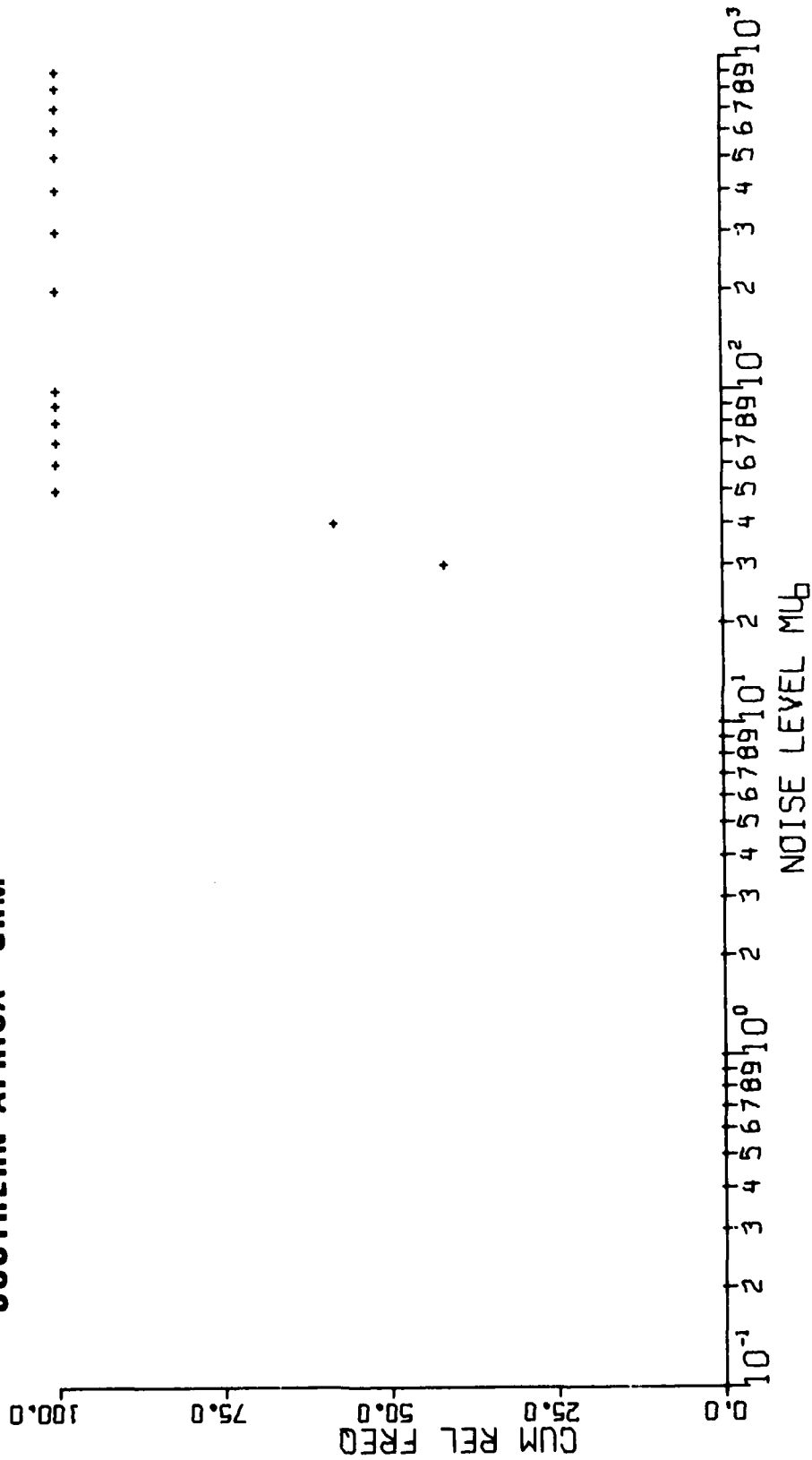
TABLE I
Mean Noise Levels of Stations Studied

Station	Mean Noise Level (m)	Standard Deviation
Alaska		
ADIS	54.729	19.064
Southern Africa		
PRE	15.000	4.000
WIN	13.333	2.944
BUL	1.792	0.457
SDB	1.375	0.287
GRM	30.000	6.325
NAI	10.417	2.218
India/Pakistan Region		
QUE	2.875	0.939
SHI	16.333	6.855
NIL	1.591	0.683
NDI	20.000	54.852
LAH	730.594	112.548
POO	25.833	8.814
SHL	3.625	1.945
CHG	3.542	0.830
MSH	163.468	138.144
KBL	4.375	1.698
South America		
ANT	25.000	3.464
ARE	18.000	4.761
BDF	638.636	630.509
BOG	48.333	17.027
CAR	33.167	8.773
LPA	264.785	72.777
LPB	15.250	7.845
NAT	38.833	7.725
NNA	23.333	5.164
PEL	25.833	5.973
SOM	187.515	77.105
TRN	60.833	40.644

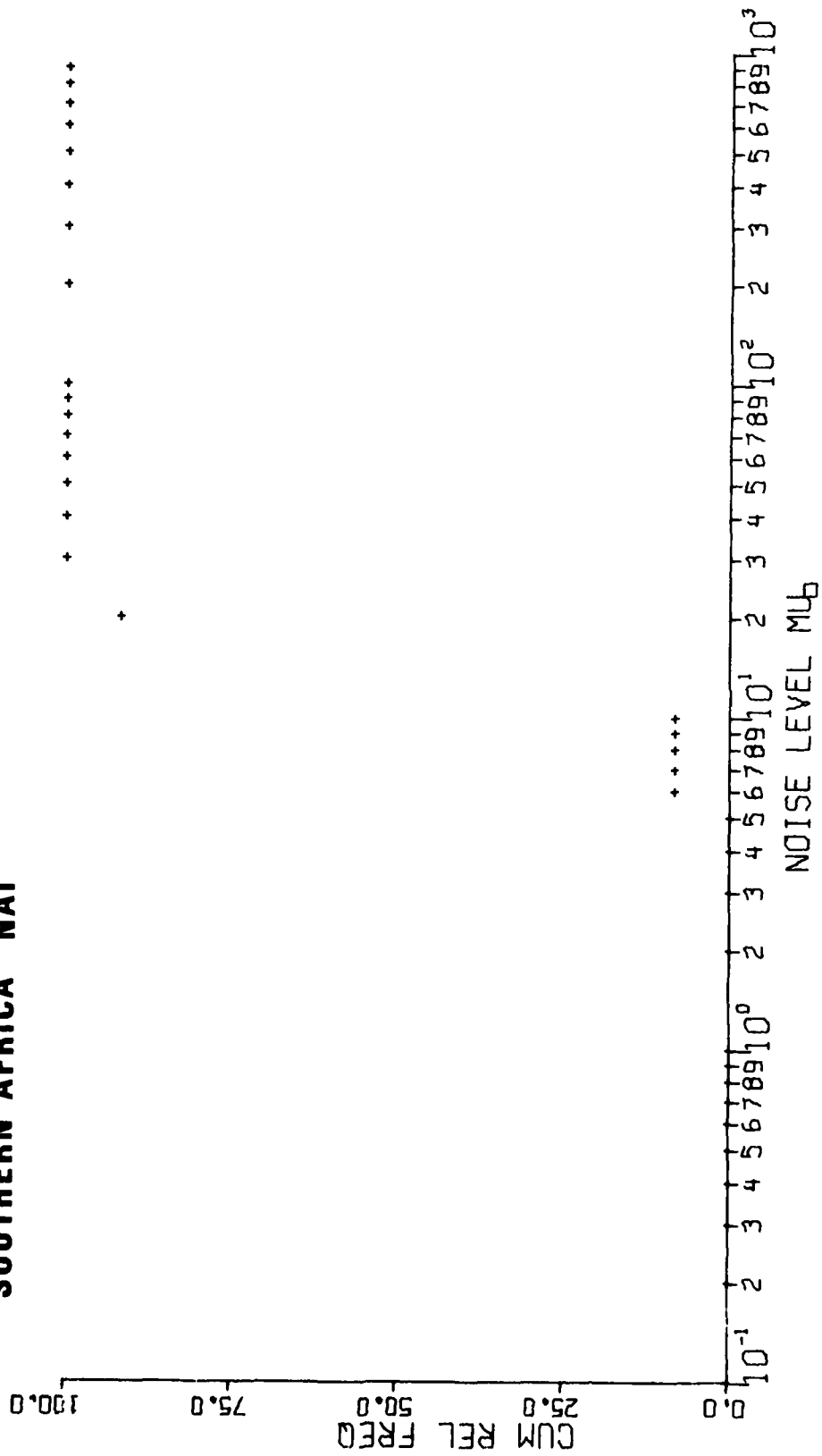
SOUTHERN AFRICA BUL



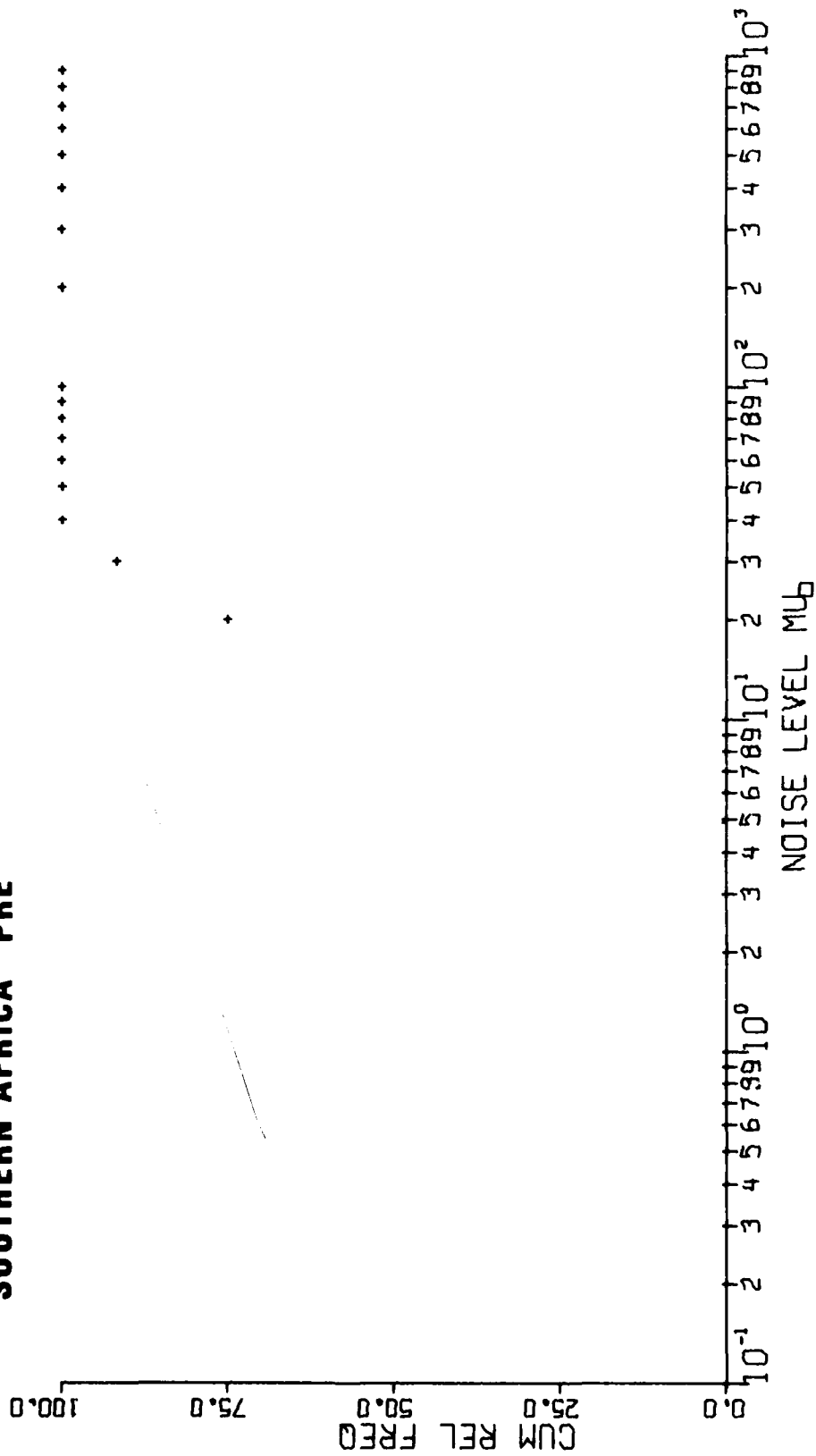
SOUTHERN AFRICA GRM



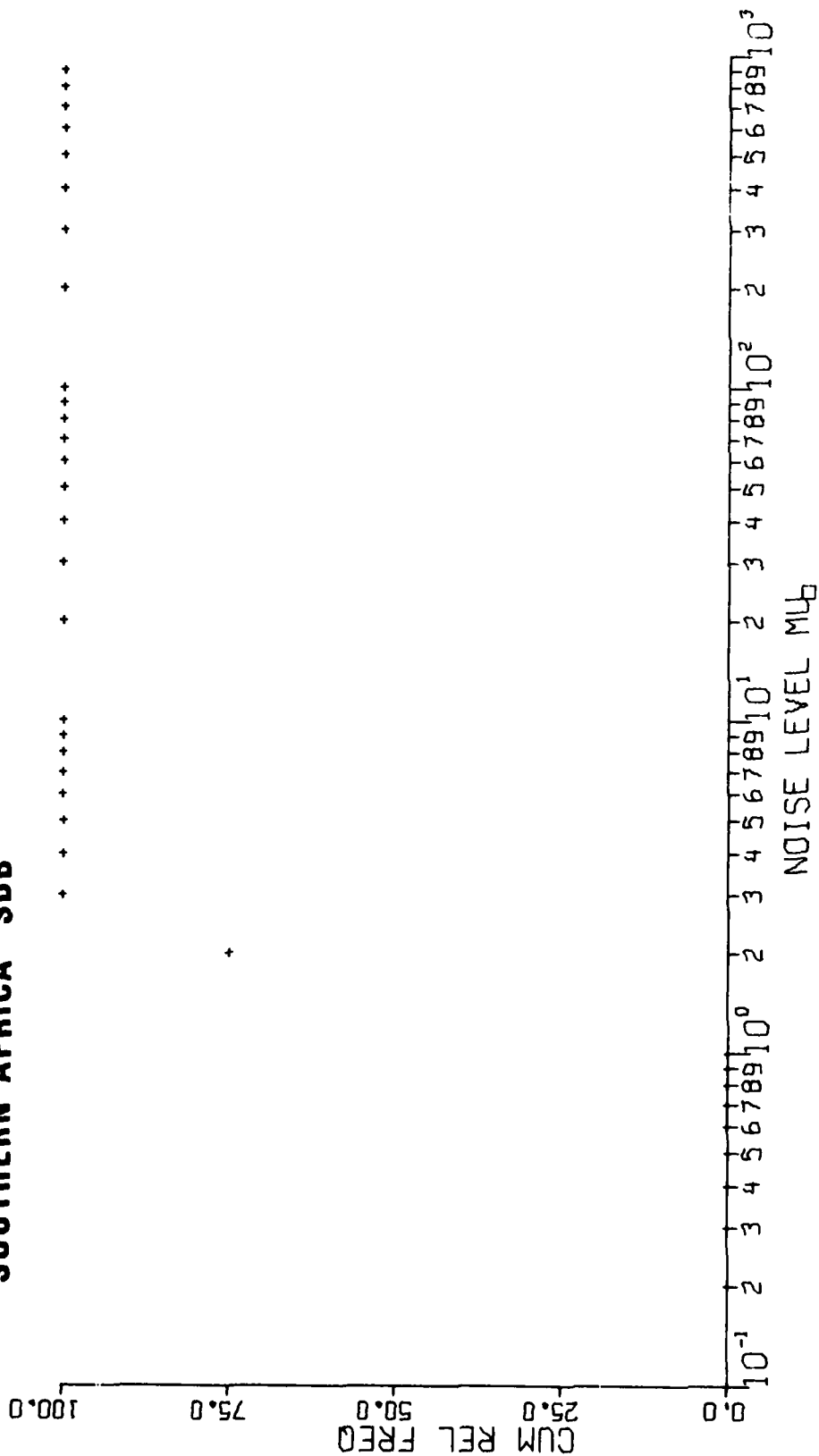
SOUTHERN AFRICA NAI



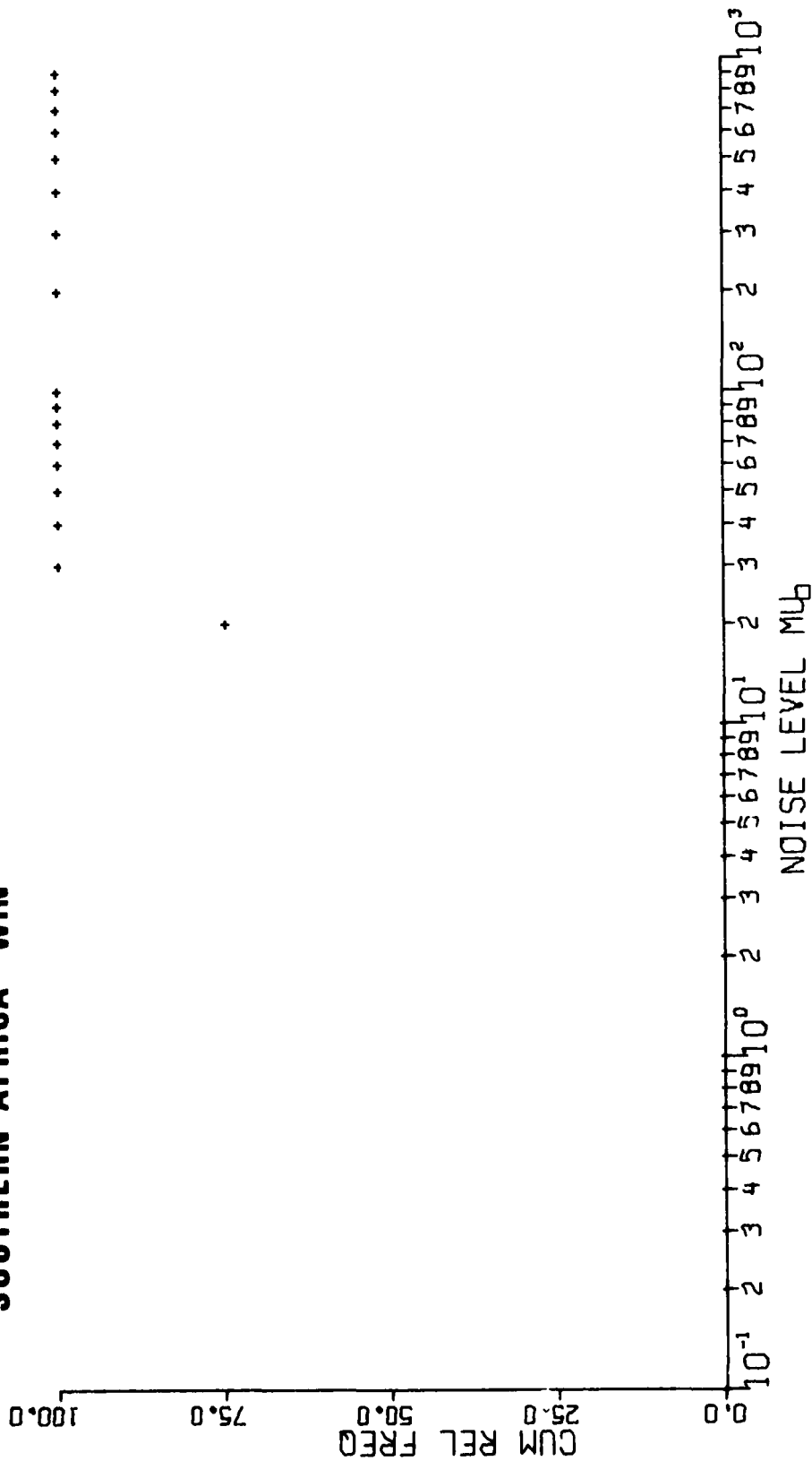
SOUTHERN AFRICA PRE



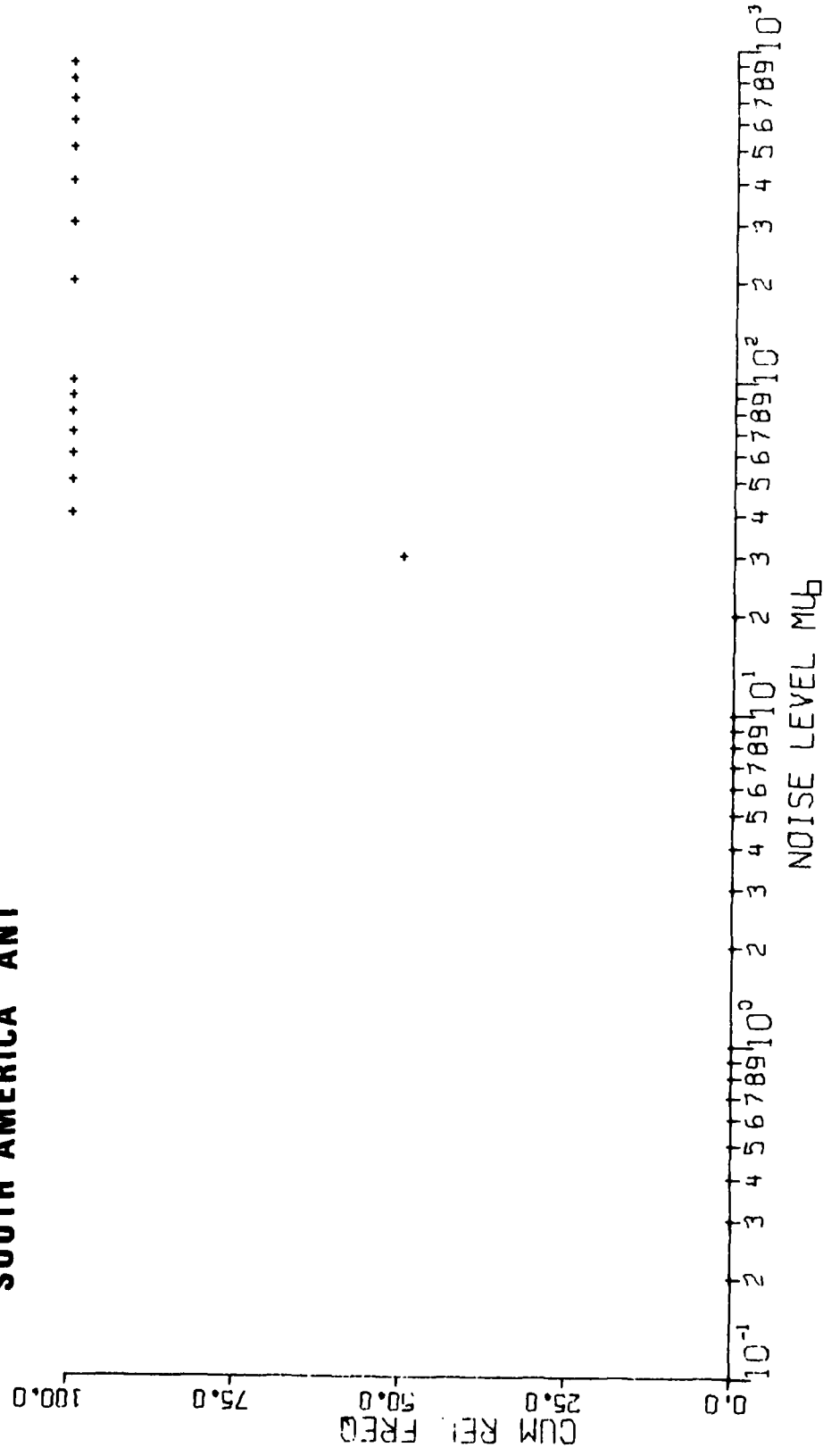
SOUTHERN AFRICA SDB



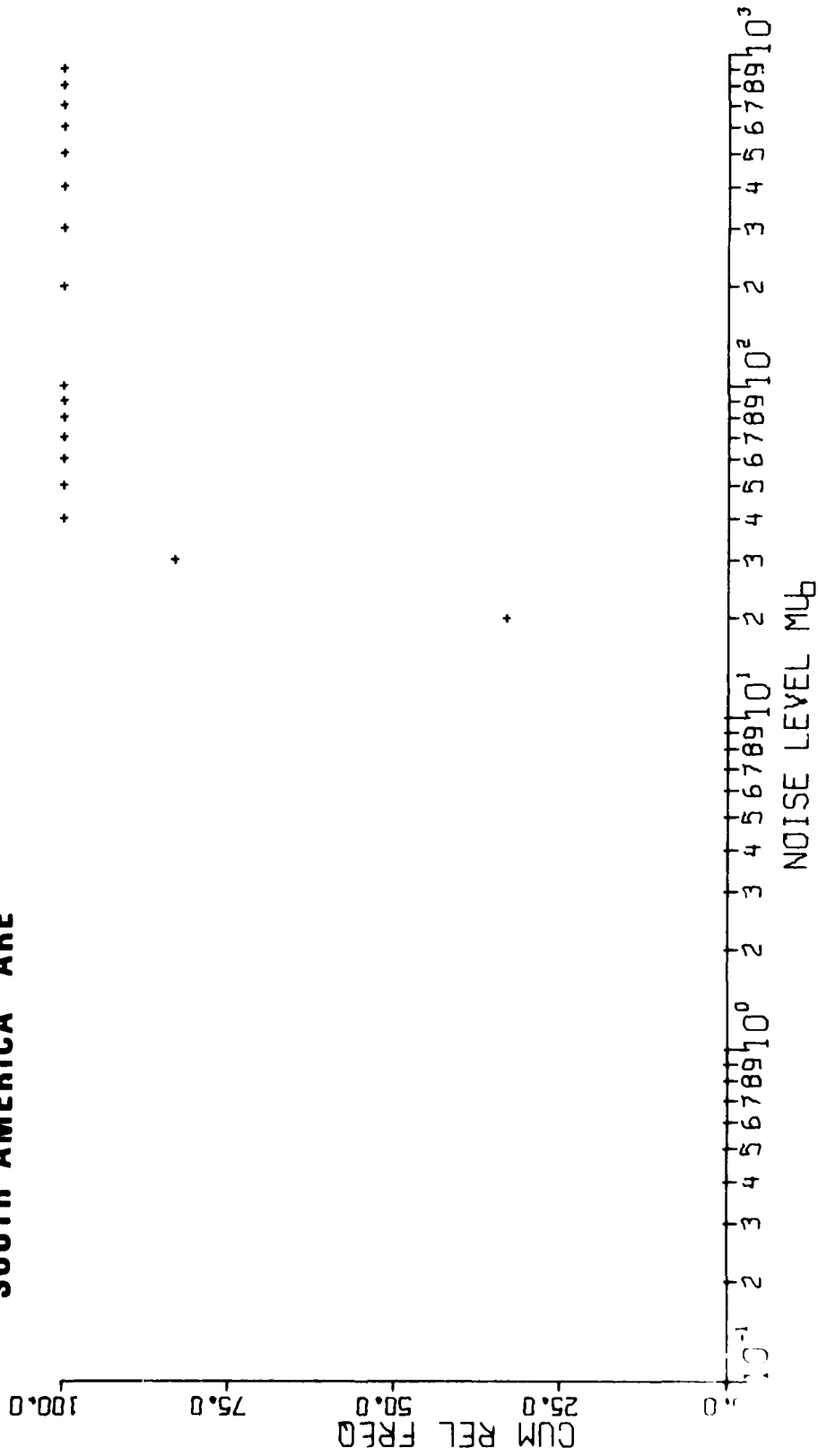
SOUTHERN AFRICA WIN



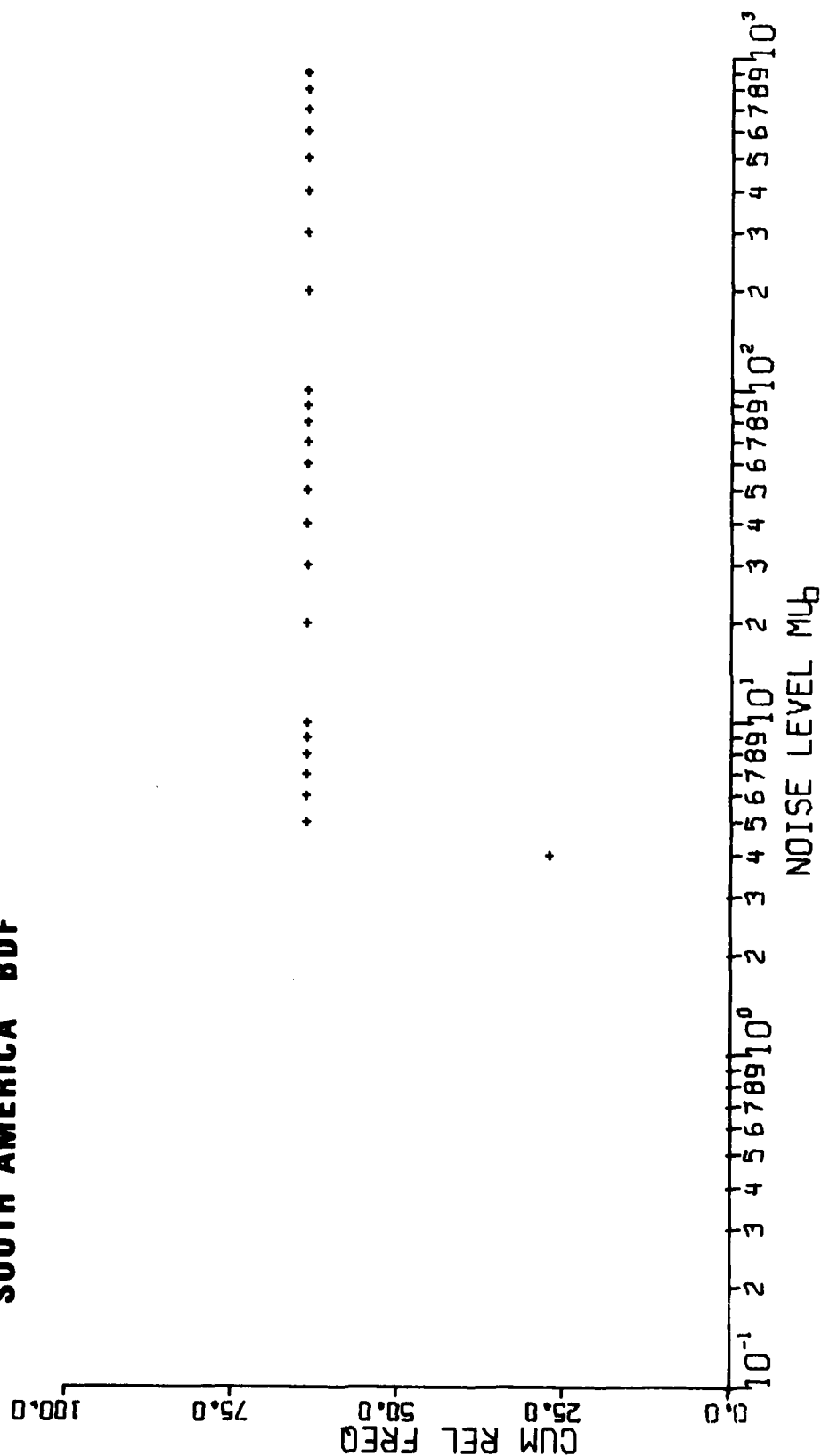
SOUTH AMERICA ANT



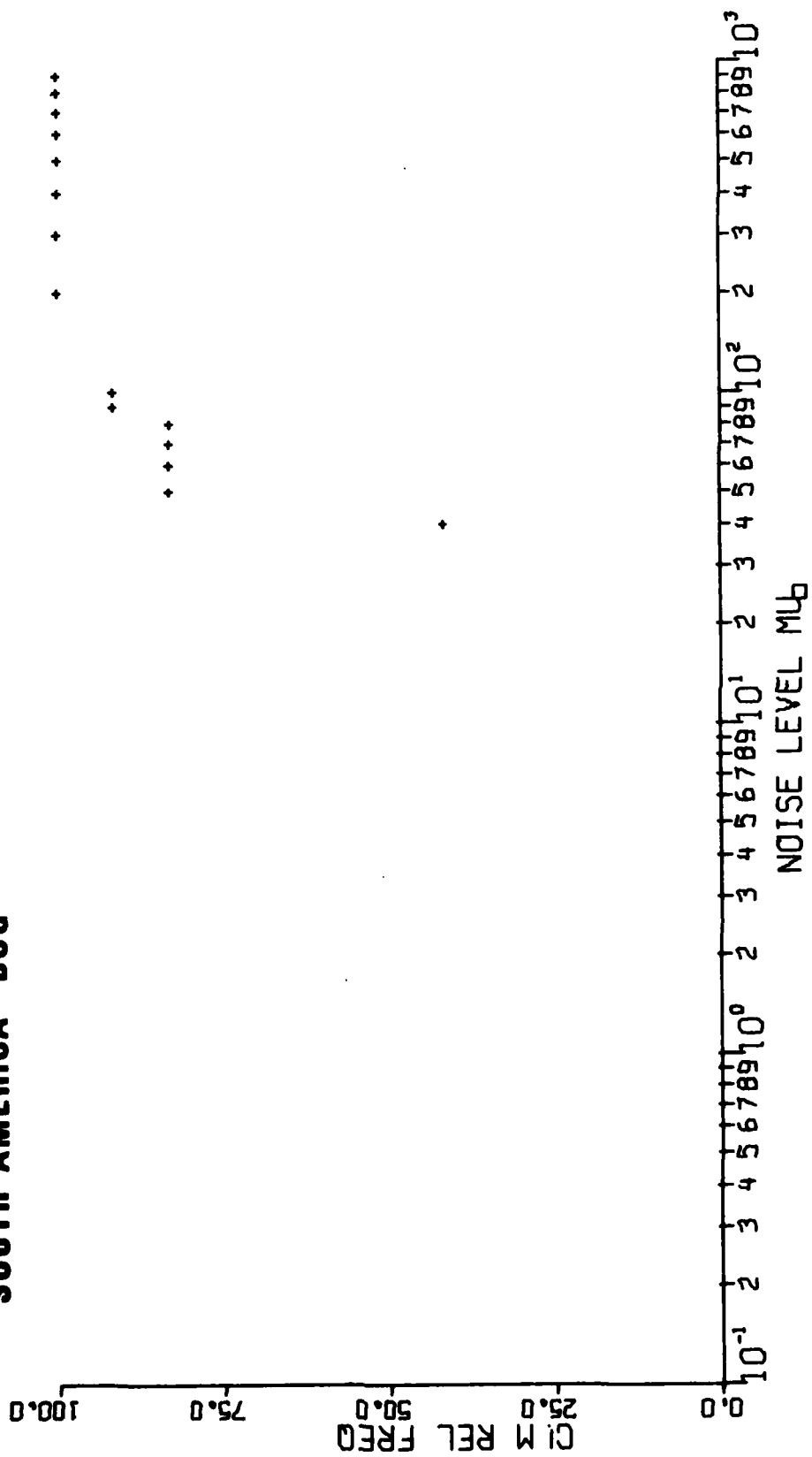
SOUTH AMERICA ARE



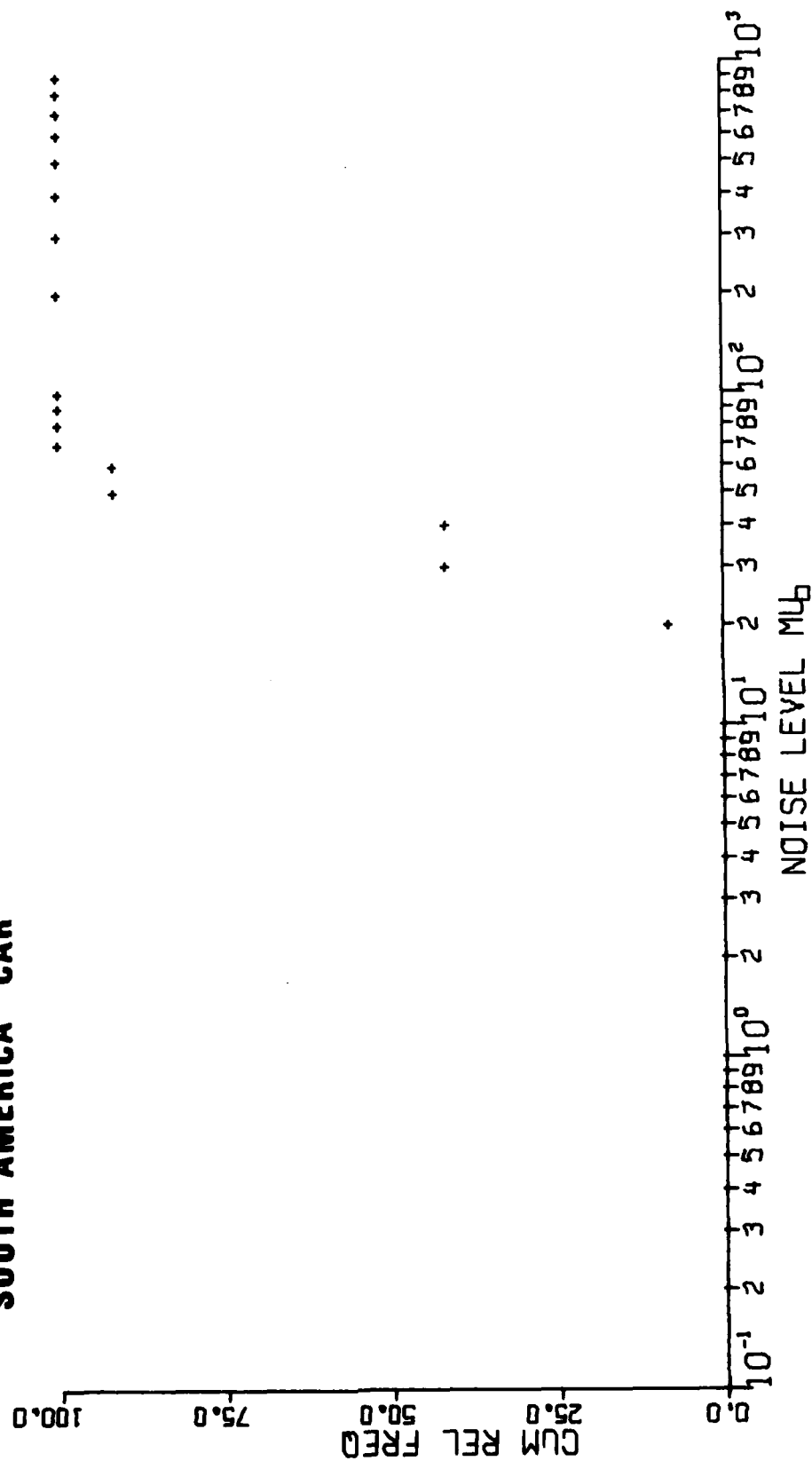
SOUTH AMERICA BDF



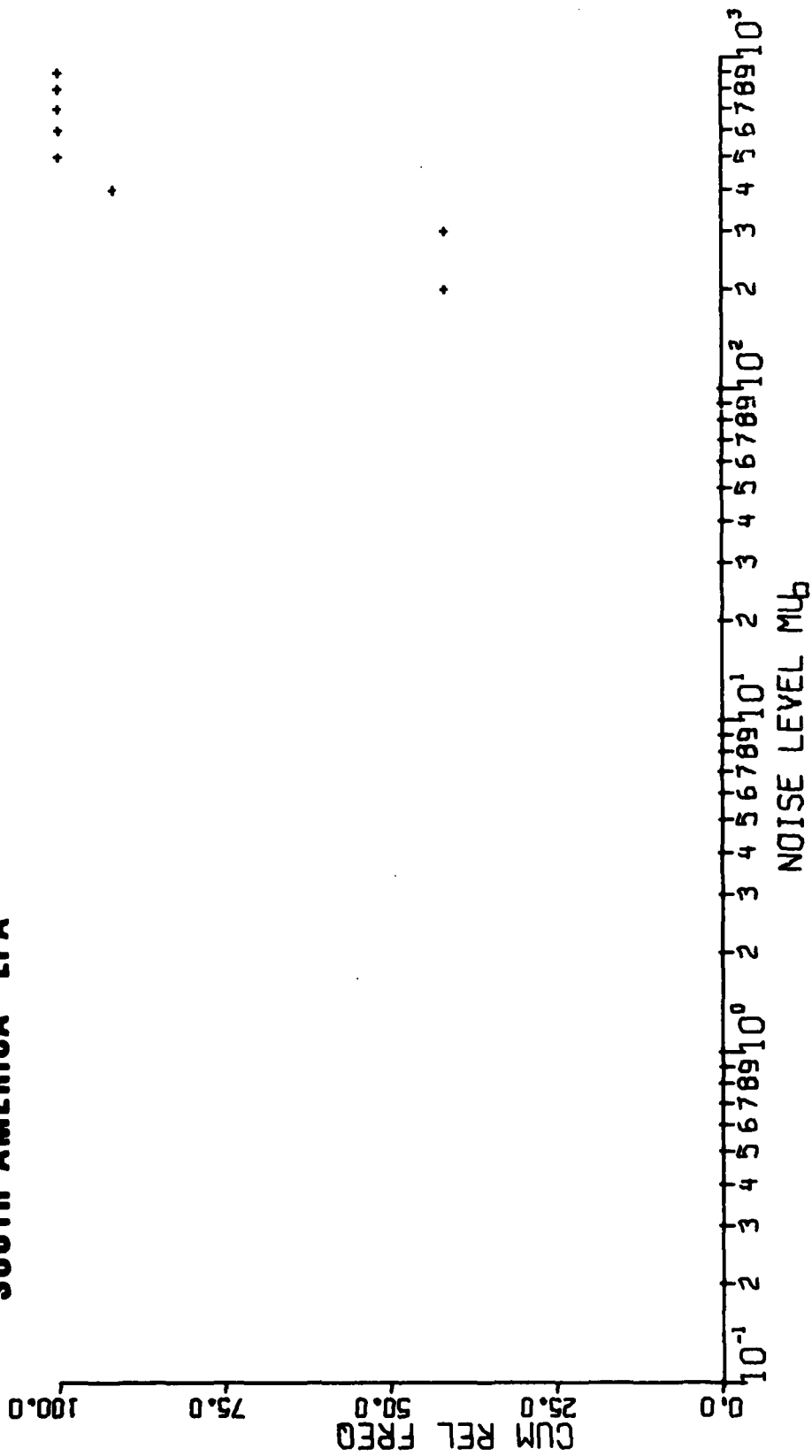
SOUTH AMERICA BOG



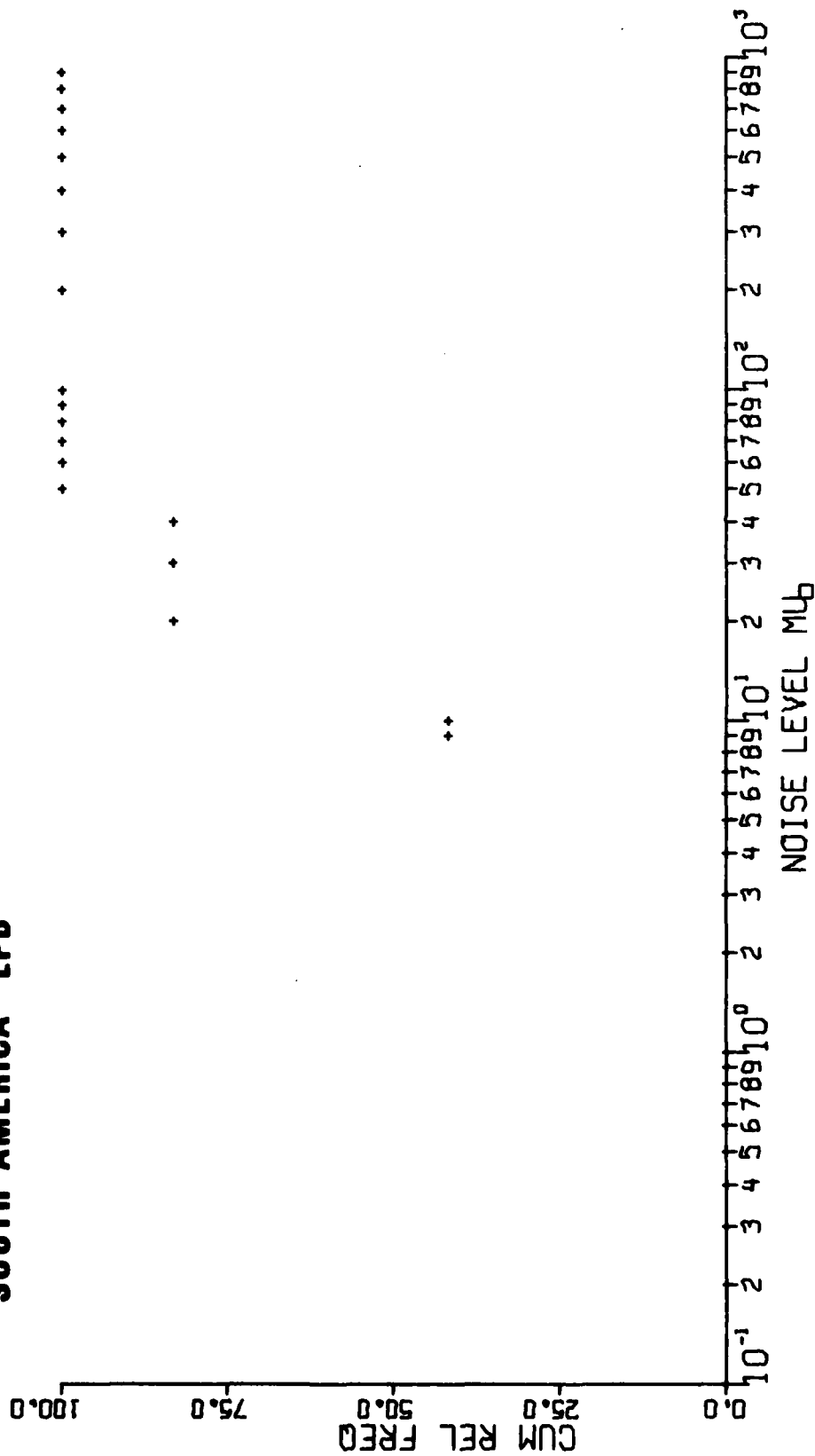
SOUTH AMERICA CAR



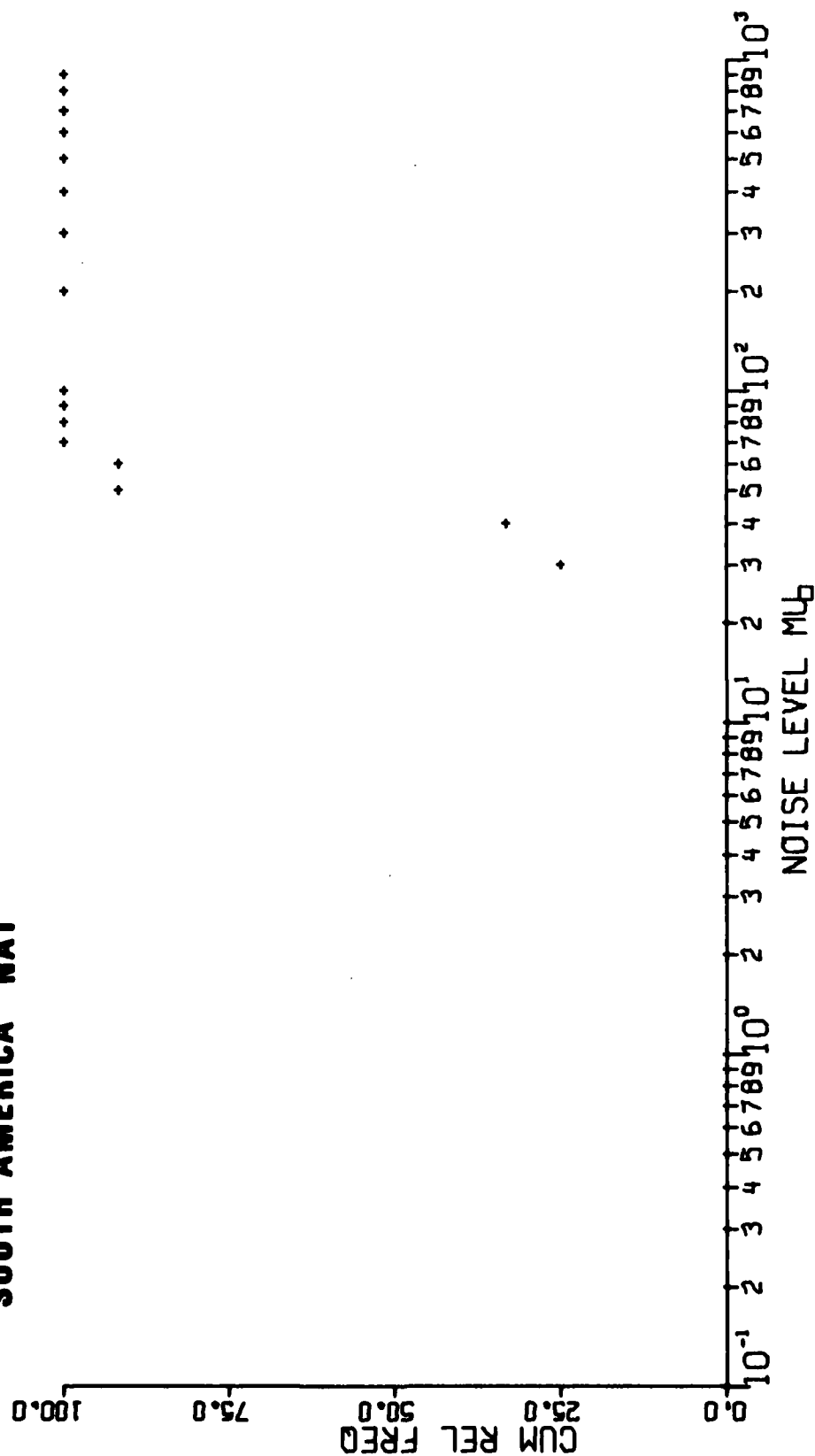
SOUTH AMERICA LPA



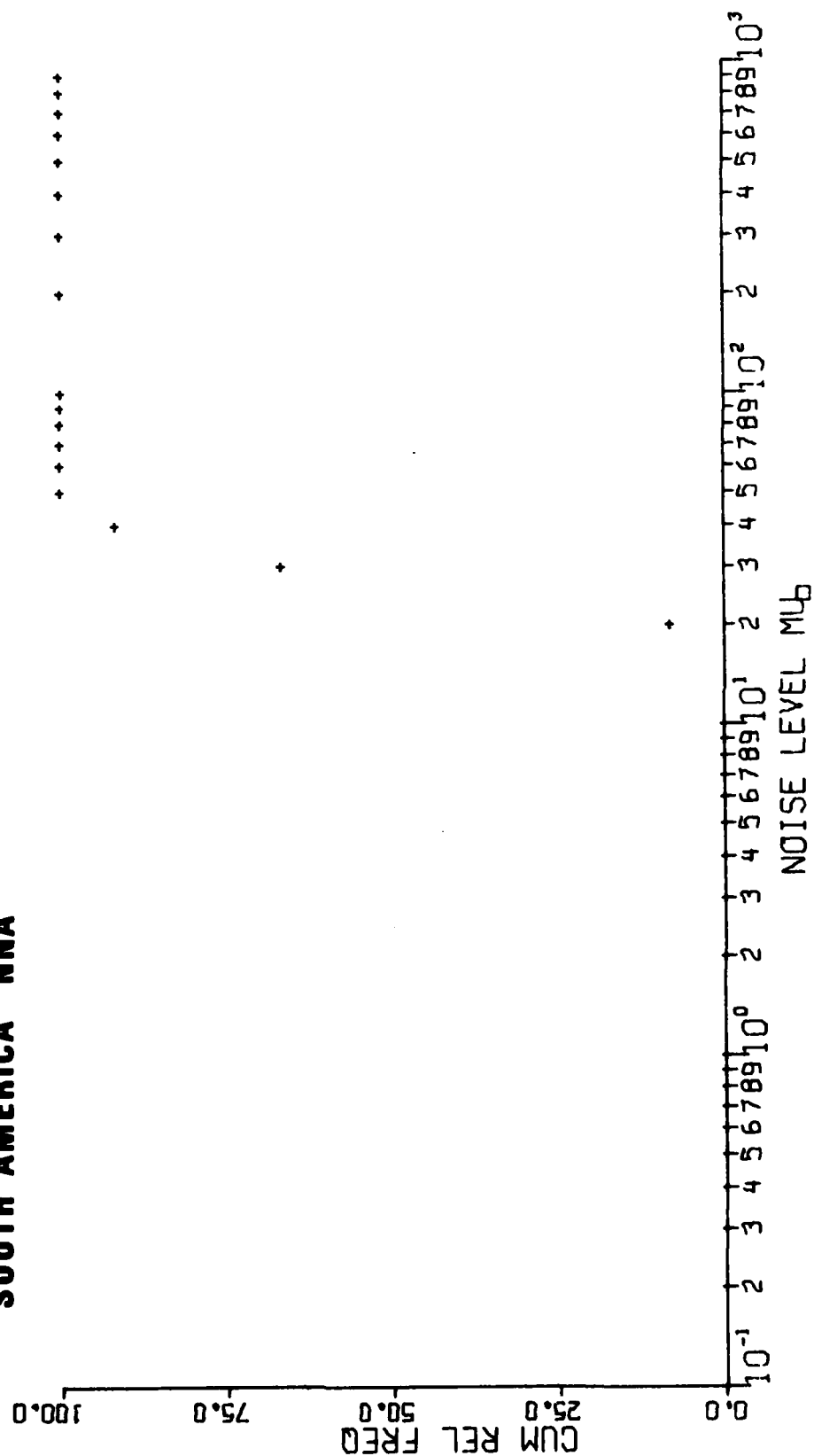
SOUTH AMERICA LPB



SOUTH AMERICA NAT



SOUTH AMERICA NNA



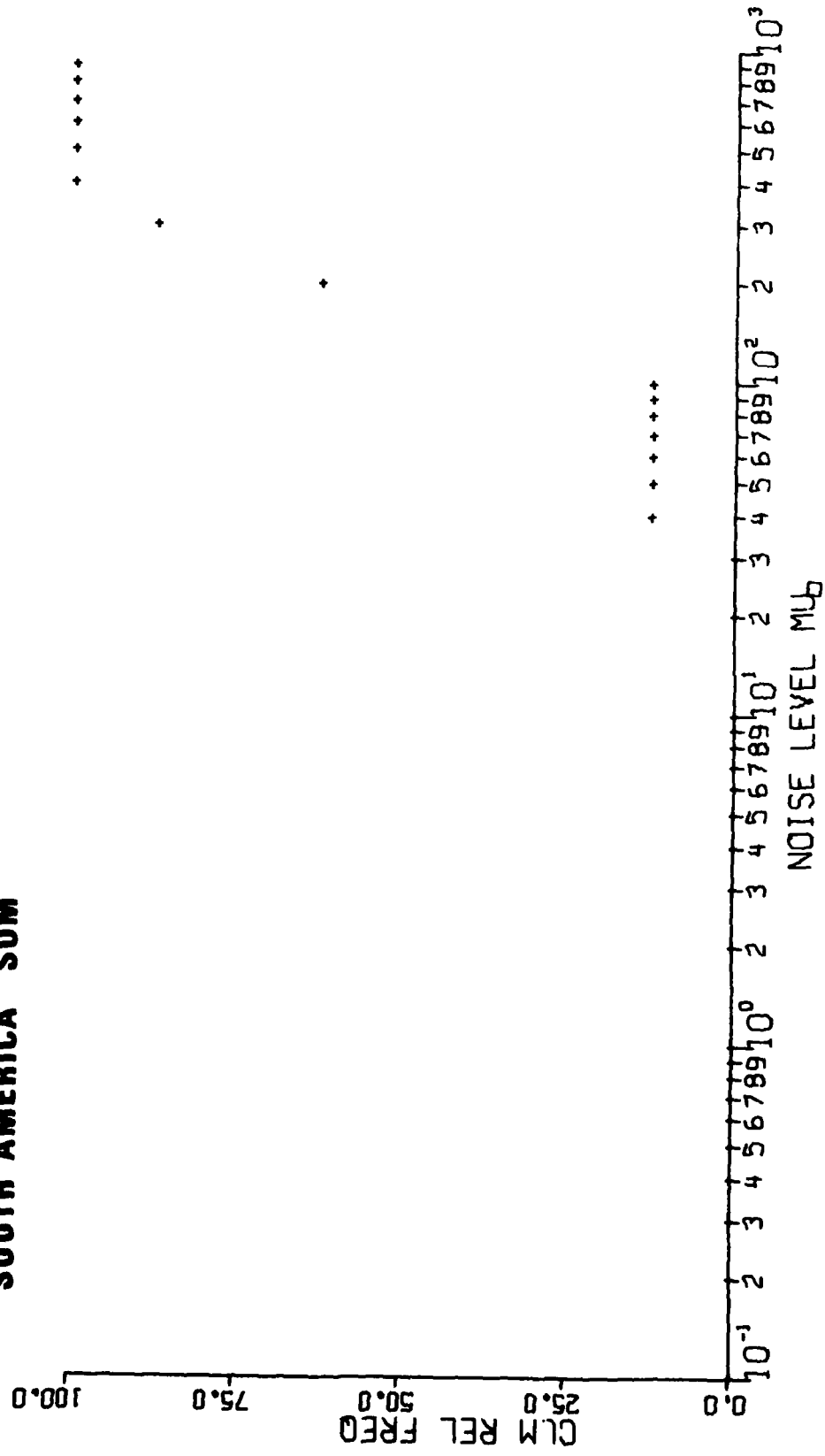
SOUTH AMERICA FEL

CUM REL FREQ

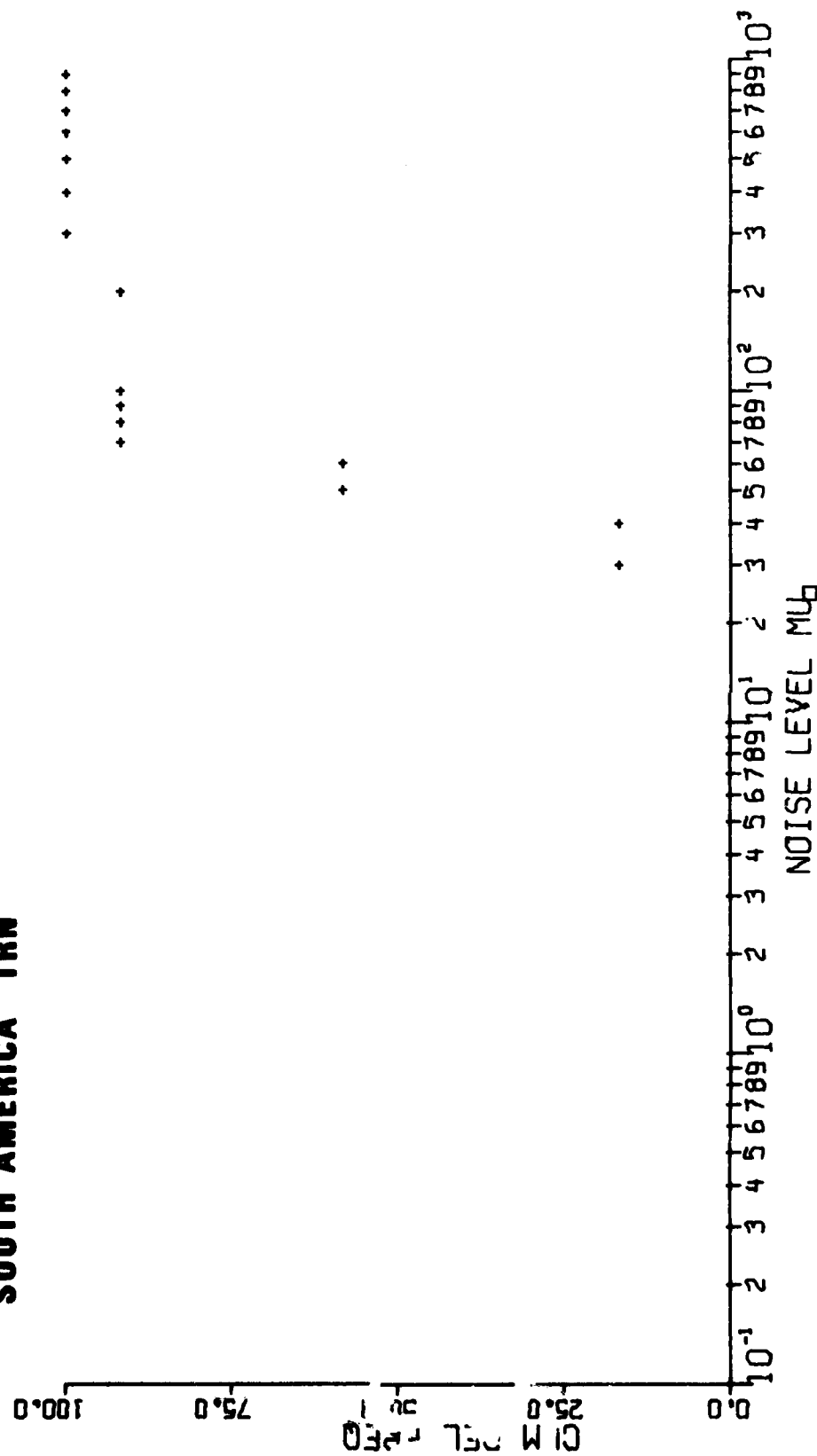
NOISE LEVEL μ_B

NOISE LEVEL μ_B	CUM REL FREQ (%)
10 ⁻¹	0.0
10 ⁰	0.0
10 ^{0.5}	0.0
10 ¹	0.0
10 ^{1.2}	10.0
10 ^{1.5}	60.0
10 ^{1.8}	80.0
10 ^{2.0}	100.0
10 ^{2.2}	100.0
10 ^{2.5}	100.0
10 ^{3.0}	100.0
10 ^{3.5}	100.0
10 ^{4.0}	100.0
10 ^{4.5}	100.0
10 ^{5.0}	100.0
10 ^{5.5}	100.0
10 ^{6.0}	100.0
10 ^{6.5}	100.0
10 ^{7.0}	100.0
10 ^{7.5}	100.0
10 ^{8.0}	100.0
10 ^{8.5}	100.0
10 ^{9.0}	100.0
10 ^{9.5}	100.0
10 ^{10.0}	100.0

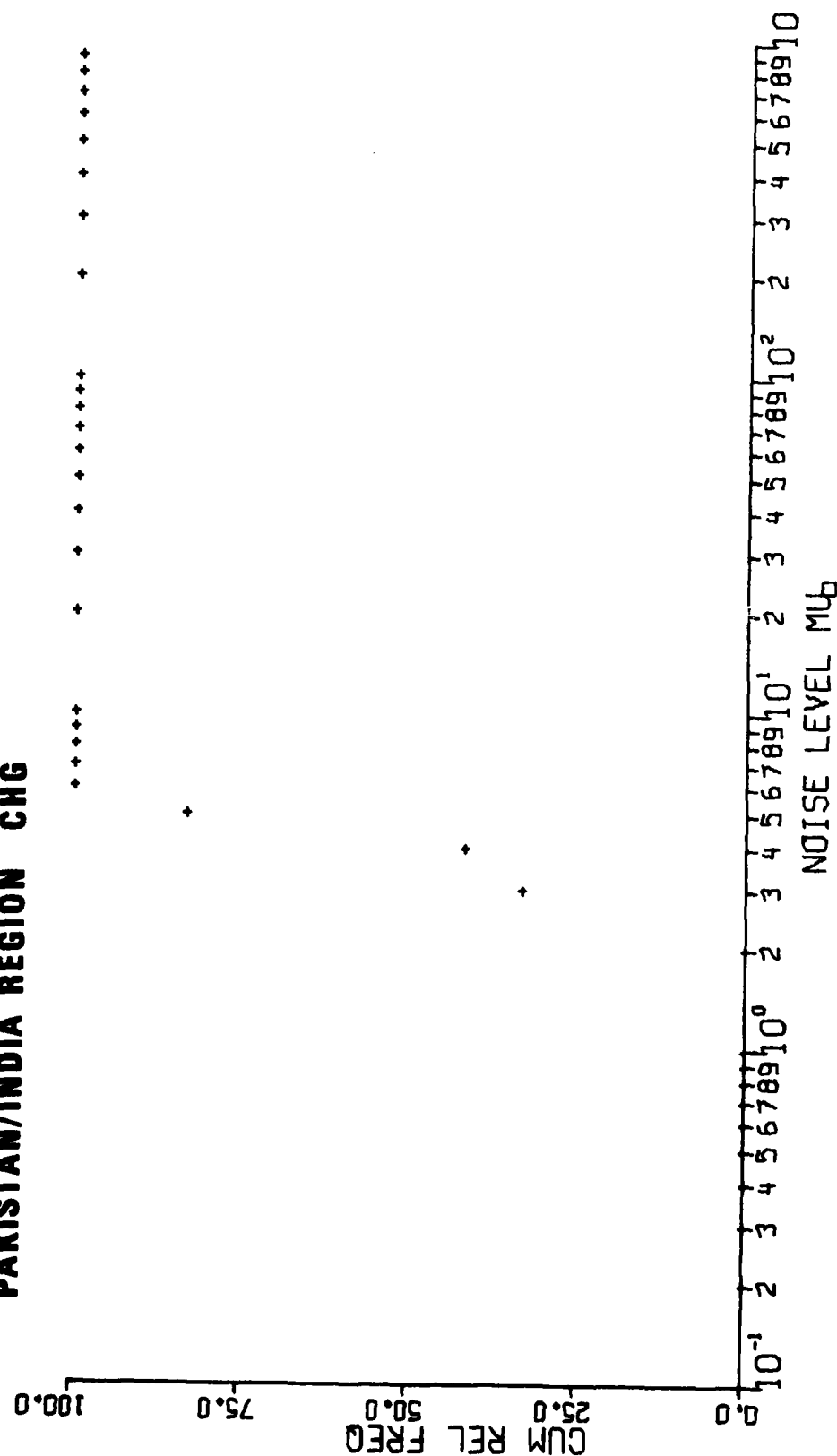
SOUTH AMERICA SOM



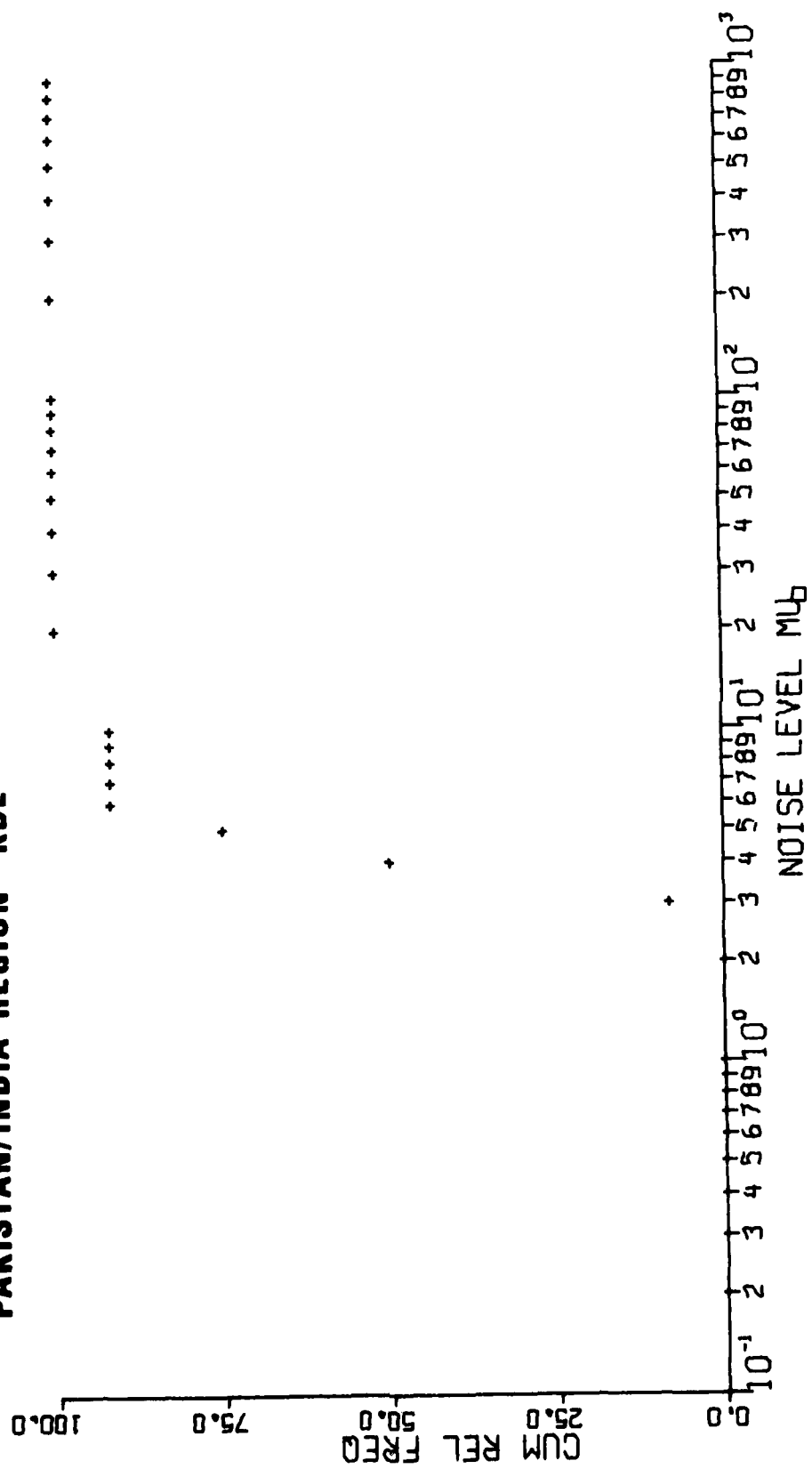
SOUTH AMERICA TRN



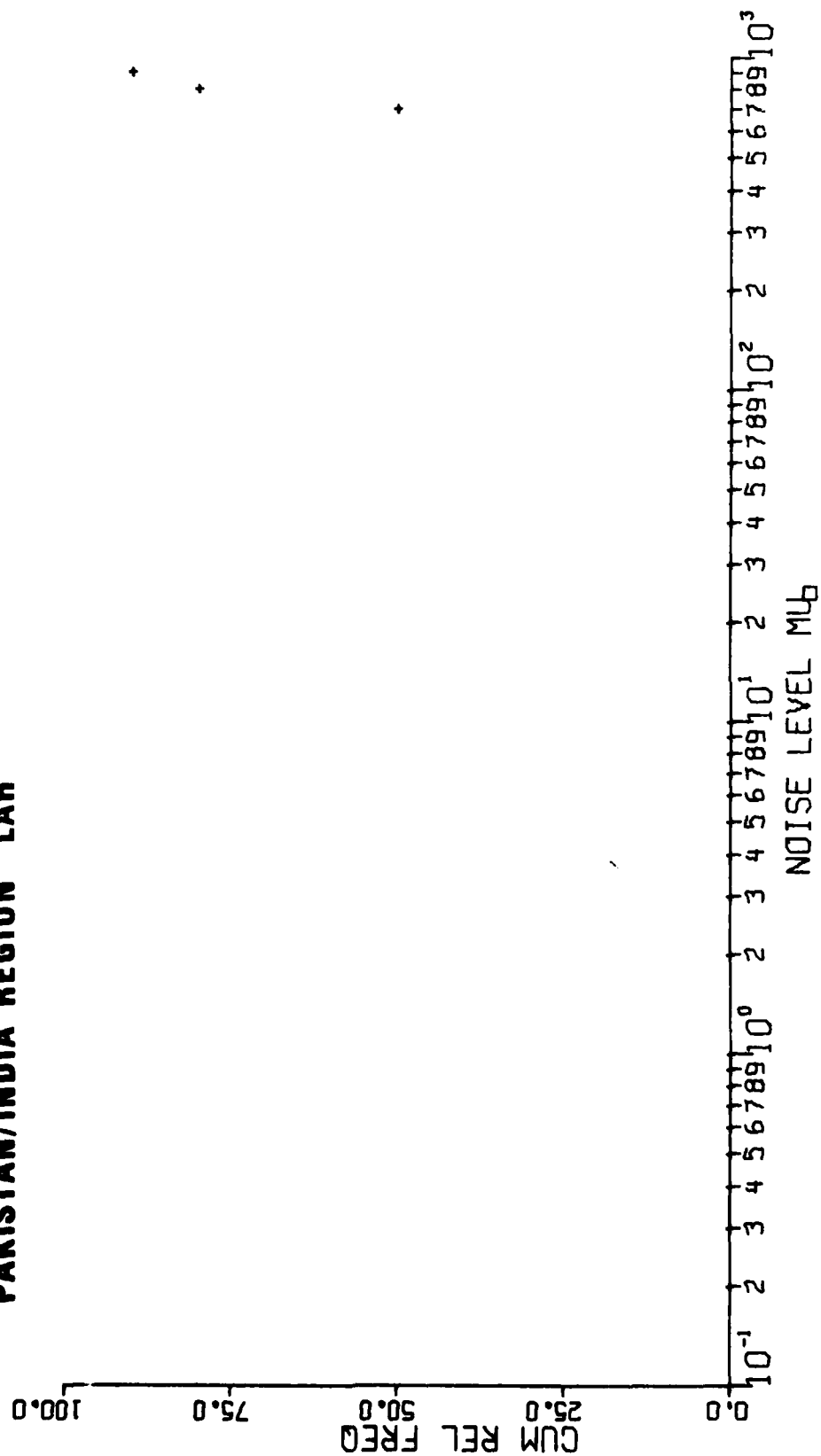
PAKISTAN/INDIA REGION CHG



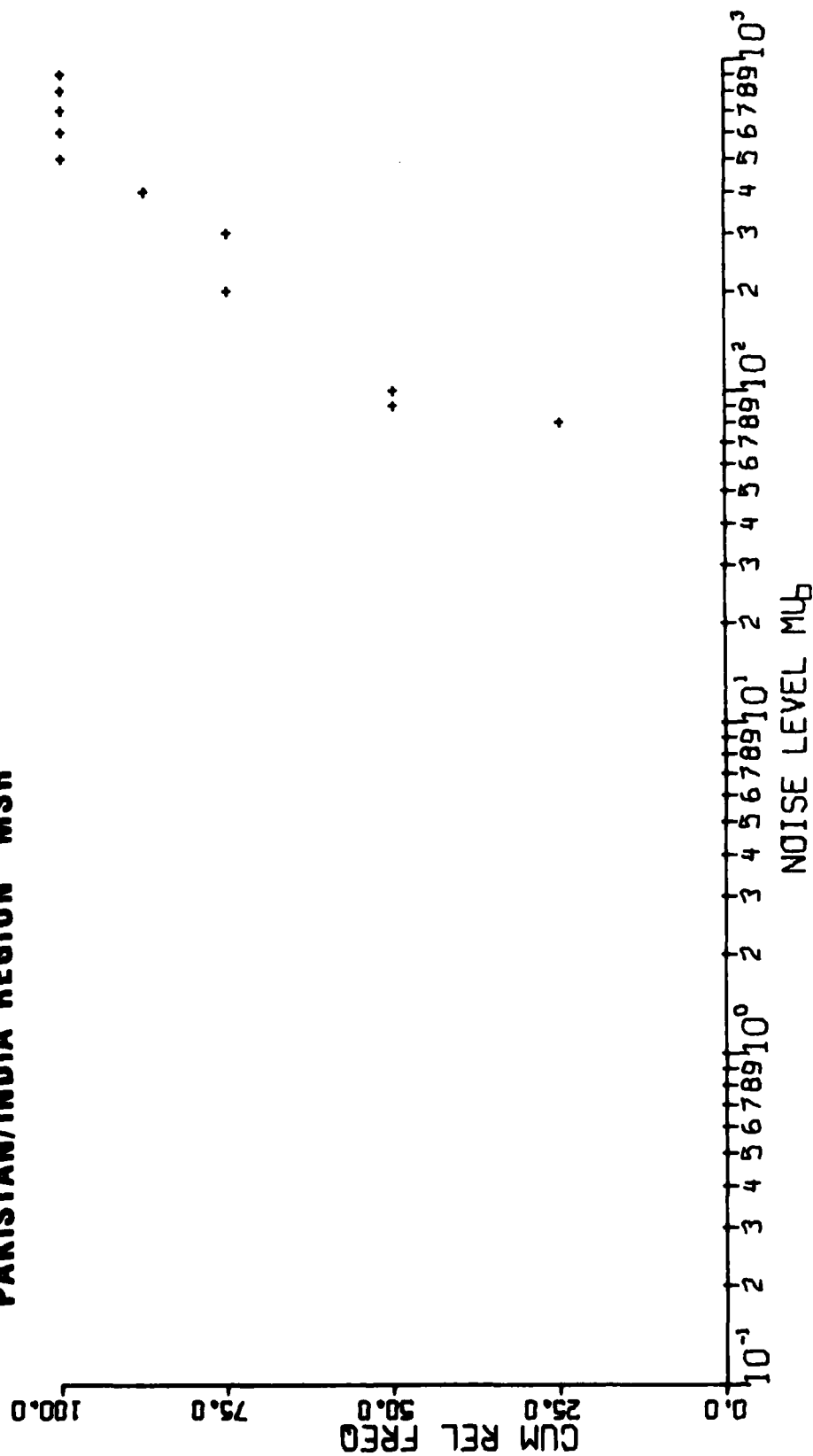
PAKISTAN/INDIA REGION KBL



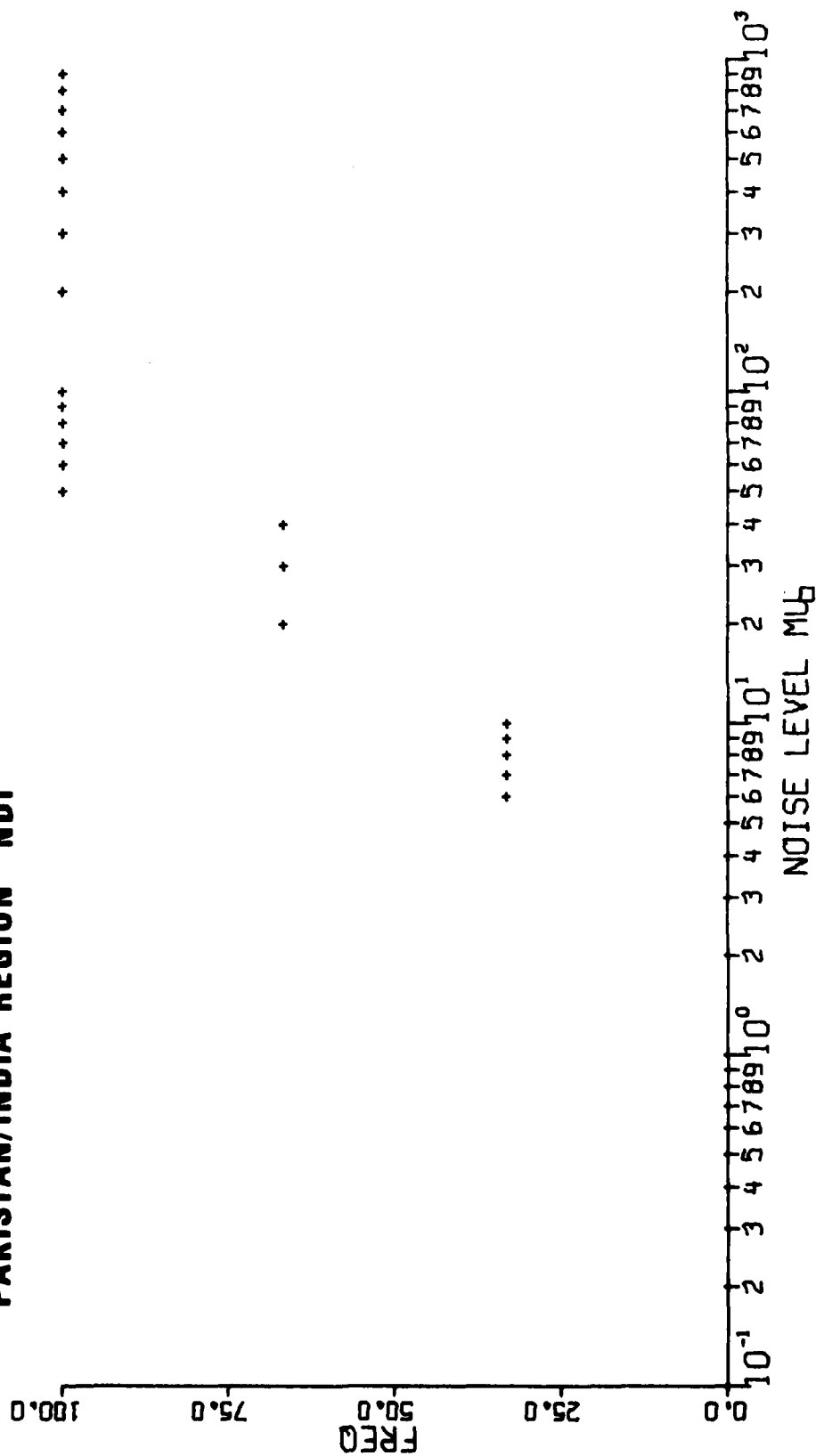
PAKISTAN/INDIA REGION LAH



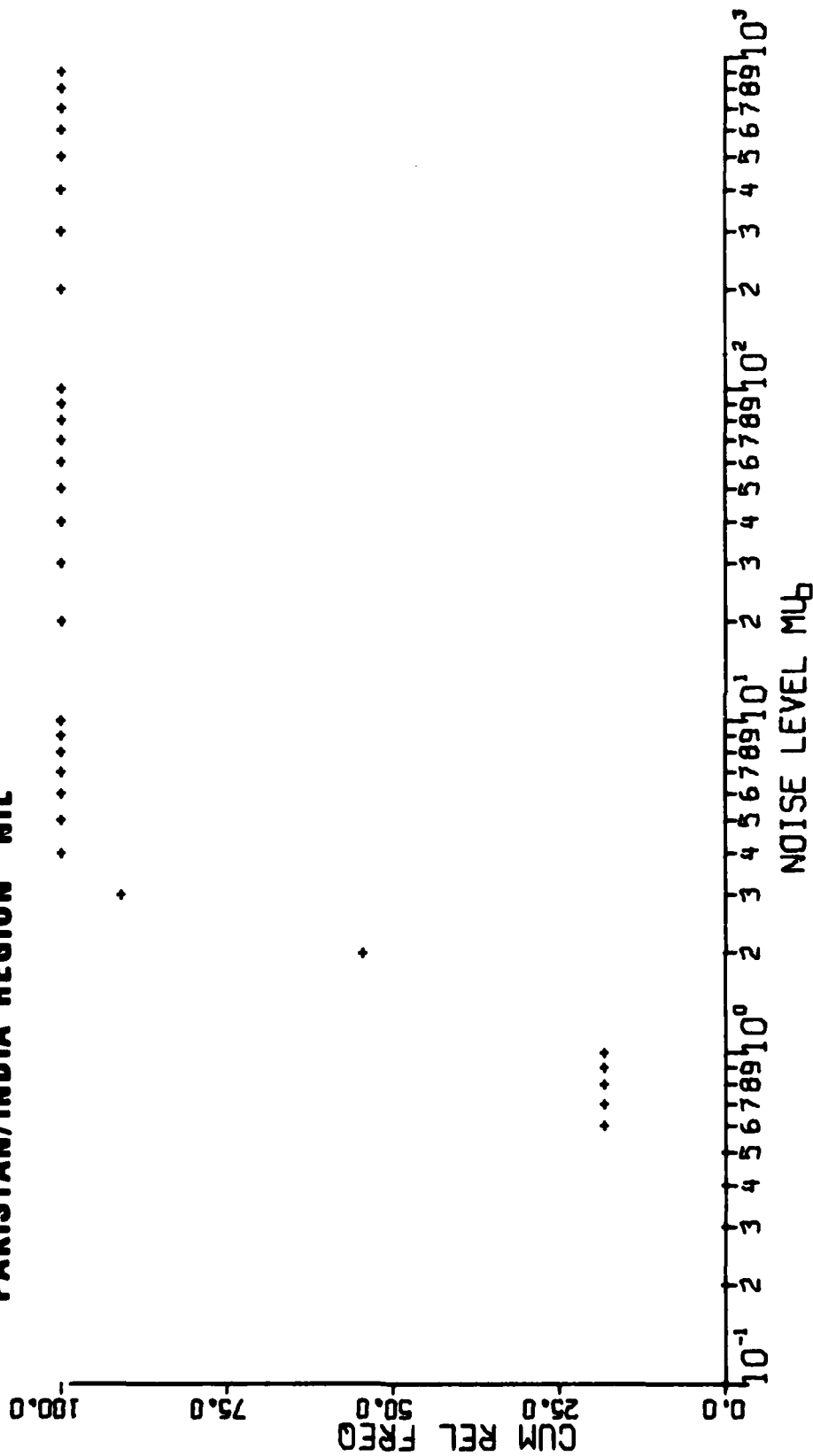
PAKISTAN/INDIA REGION MSH



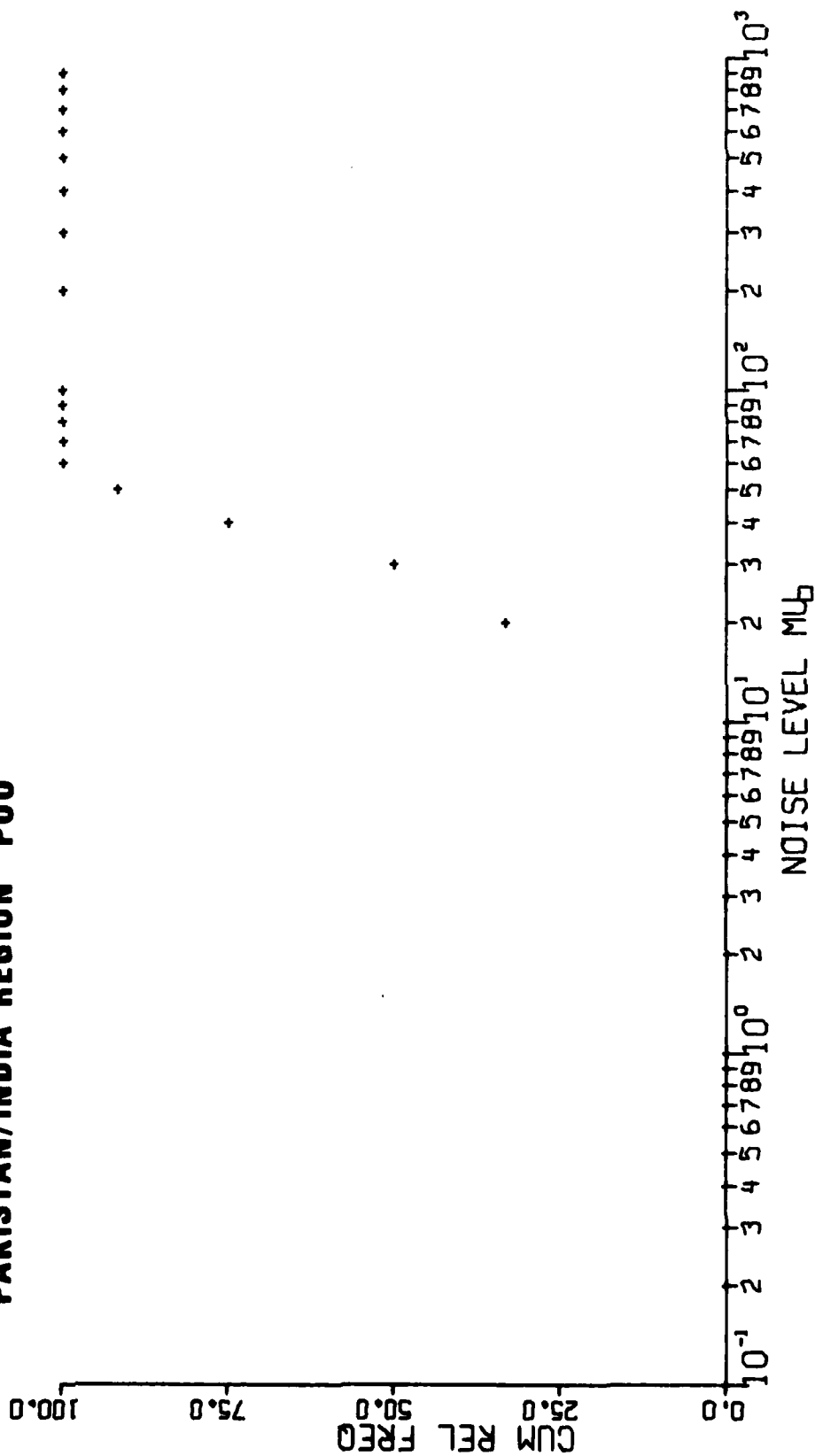
PAKISTAN/INDIA REGION NDI



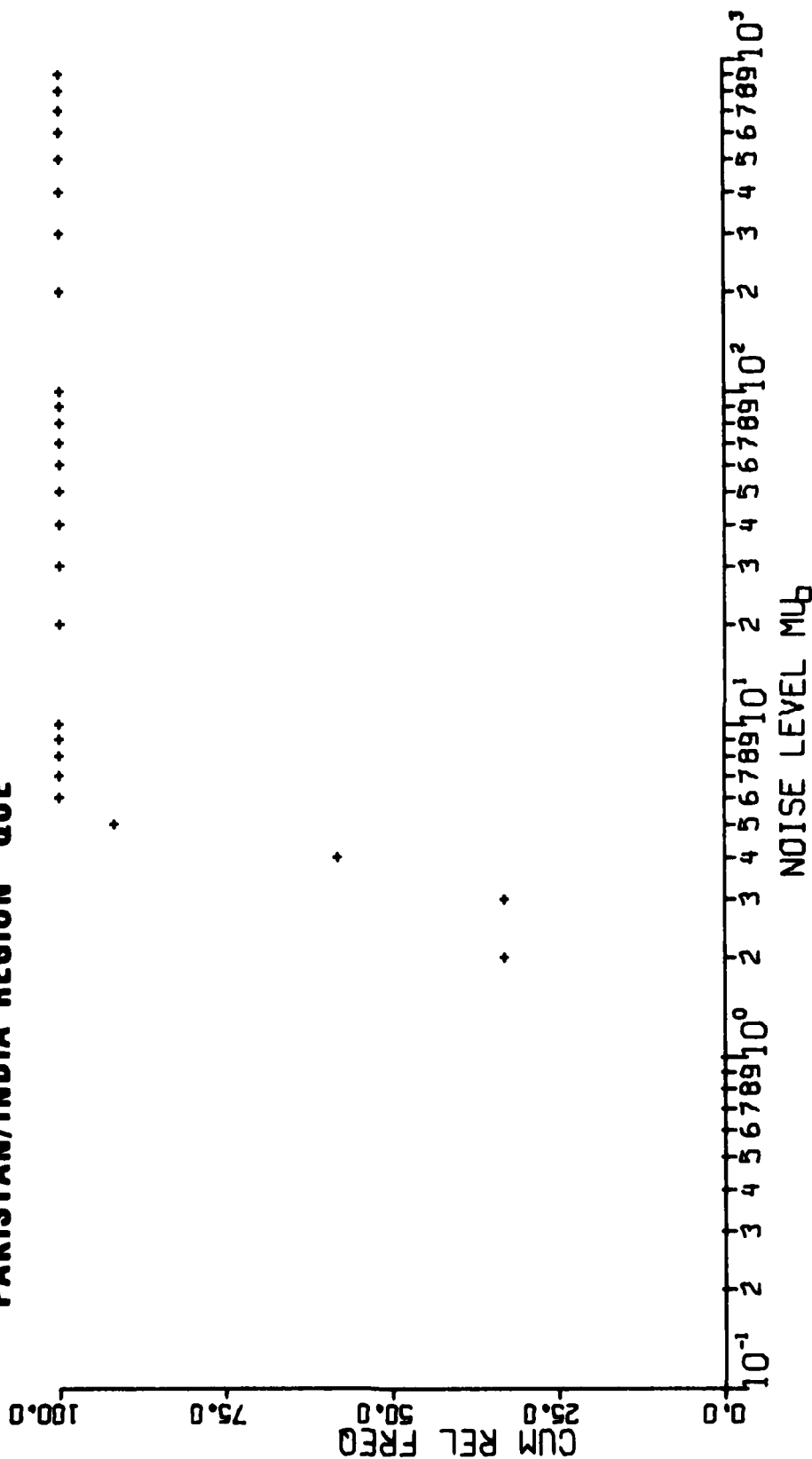
PAKISTAN/INDIA REGION NIL



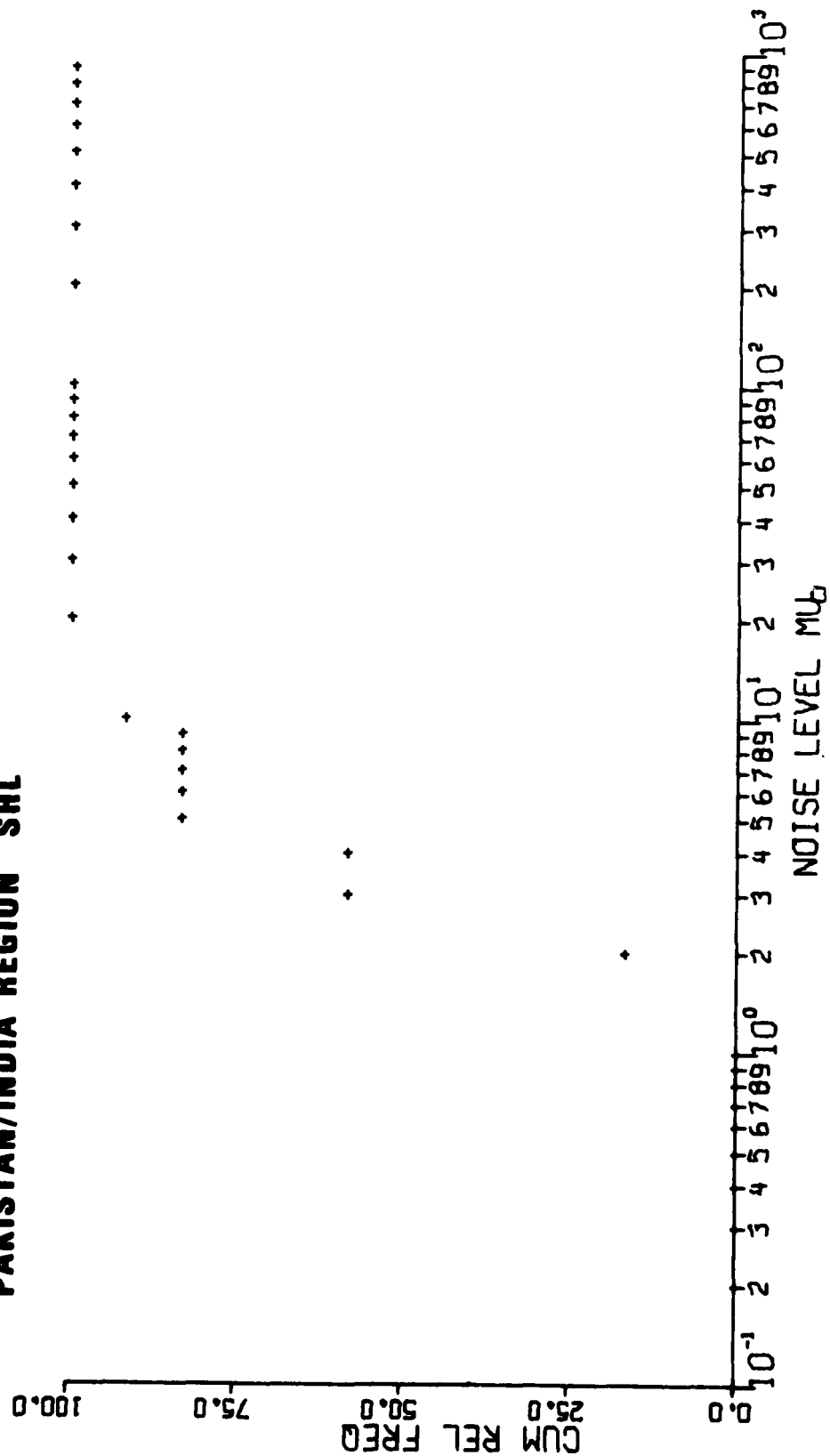
PAKISTAN/INDIA REGION P00



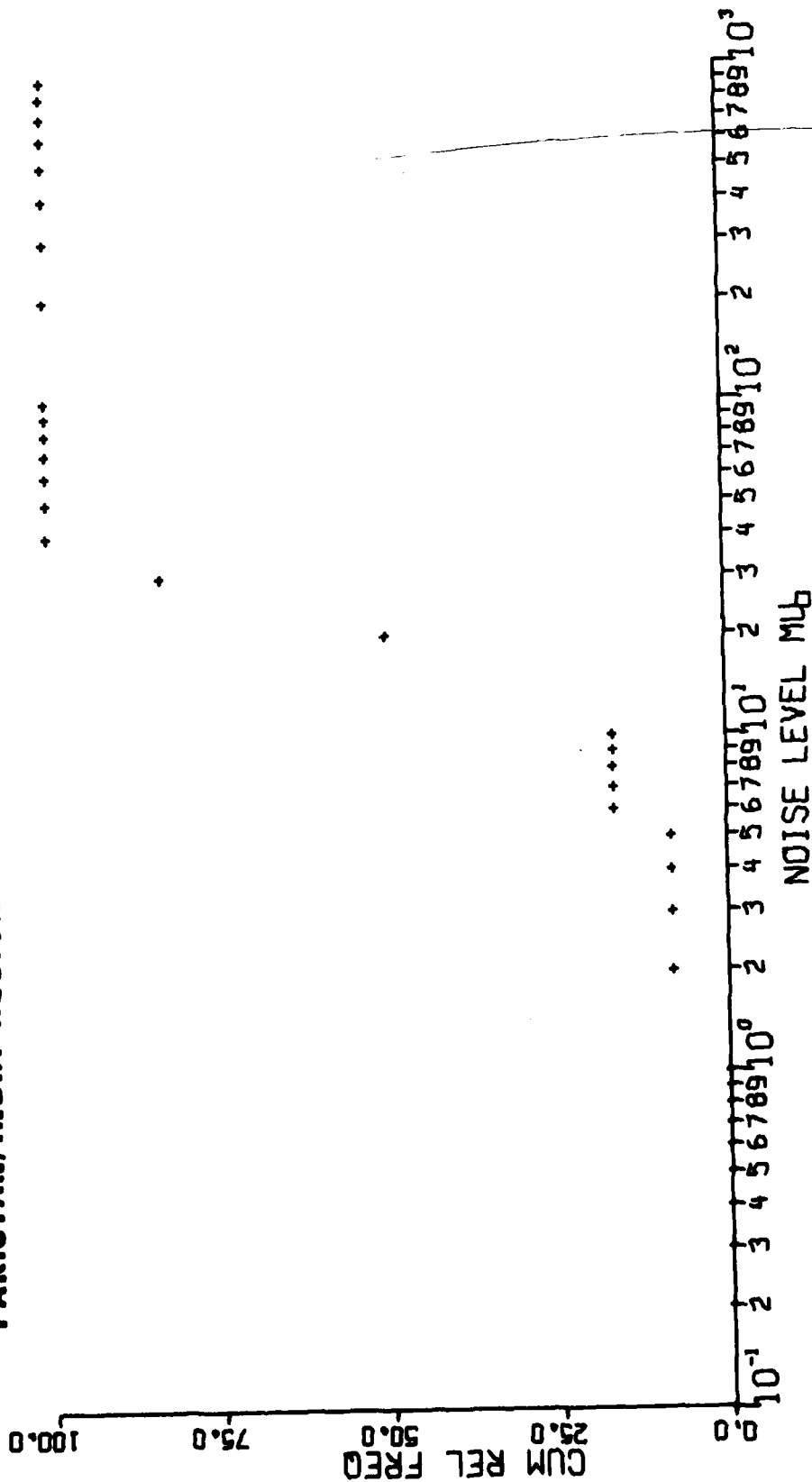
PAKISTAN/INDIA REGION QUE



PAKISTAN/INDIA REGION SHL



PAKISTAN/INDIA REGION SHI



NOISE LEVEL ML

CUM REL FREQ